Investigation of Probe Substrates to Assess Hepatic Transport Function

by

Brandon Swift

A dissertation submitted to the faculty of the University of North Carolina at Chapel Hill in partial fulfillment of the requirements for the degree of Doctor of Philosophy in the Eshelman School of Pharmacy

Chapel Hill

2009

Approved by:

Advisor: Kim L.R. Brouwer, Pharm.D., Ph.D.

Chair: Gary M. Pollack, Ph.D.

Reader: Roy Hawke, Pharm.D., Ph.D.

Reader: Dhiren Thakker, Ph.D.

Reader: Marijana Ivanovic, Ph.D.

Reader: Bert H. O'Neil, M.D.

ABSTRACT

Brandon Swift

Investigation of Probe Substrates to Assess Hepatic Transport Function

(Under the direction of Kim L.R. Brouwer, Pharm.D., Ph.D.)

The objective of this research project was to identify and characterize probe substrates for specific hepatic transport proteins. Identification of specific probe substrates for basolateral and canalicular transport proteins is necessary to elucidate mechanisms of hepatobiliary drug transport, phenotype for interindividual differences in transport protein function, and identify potential drug-drug interactions at the hepatic transport level. Three probe substrates were selected for investigation: fexofenadine, ^{99m}Technetium mebrofenin (^{99m}Tc-MEB), and ^{99m}Technetium sestamibi (^{99m}Tc-MIBI). Although fexofenadine has been touted as a P-gp specific probe substrate, pharmacokinetic modeling/siumulation of clinical data, sandwich-cultured human hepatocyte experiments and perfused liver studies in rats and mice demonstrated that fexofenadine is not a suitable probe for a specific transport protein due to compensatory efflux pathways. The hepatic uptake and excretion of ^{99m}Tc-MEB and ^{99m}Tc-MIBI have not been investigated fully despite their use as non-invasive probes to assess transport function. Therefore, suspended and sandwich-cultured rat and human hepatocytes were used to fully characterize the mechanisms of hepatic transport of ^{99m}Tc-MEB and ^{99m}Tc-MIBI. Then to validate the use of ^{99m}Tc-MEB and/or

^{99m}Tc-MIBI as probe substrates to predict the hepatic clearance of the anticancer agent, sorafenib studies were conducted to confirm similar mechanisms of hepatic uptake. Lastly, the pharmacokinetics and hepatic exposure of ^{99m}Tc-MIBI and ^{99m}Tc-MEB were compared in a patient with hepatocellular carcinoma and Child's Pugh B cirrhosis vs. healthy human volunteers. Pharmacokinetic models were constructed to describe the distribution and elimination of ^{99m}Tc-MEB and ^{99m}Tc-MIBI, to compare alterations in key rate constants representing hepatic uptake and efflux mechanisms secondary to disease. In conclusion, ^{99m}Tc-MEB and ^{99m}Tc-MIBI may be very useful phenotypic probes that are sensitive to changes in hepatic function associated with liver disease. The hepatic exposure to ^{99m}Tc-MIBI was decreased in the patient with hepatocellular carcinoma and cirrhosis compared to healthy volunteers, whereas the hepatic exposure of ^{99m}Tc-MEB was similar but the hepatic exposure profile was notably different with a lower maximum but more prolonged exposure. Collectively, the results of this research negate the use of fexofenadine as a probe for hepatic transport, but support the use of ^{99m}Tc-MEB and ^{99m}Tc-MIBI as probe substrates, which add the unique ability to quantify liver concentrations.

ACKNOWLEDGEMENTS

I want to thank Dr. Kim L. R. Brouwer for the opportunity to work on this exciting project and for guiding my personal and scientific development. Dr. Brouwer is the reason I considered graduate school and was a motivating factor in my progression as a student and Ph.D. candidate. I also want to thank all the members of my doctoral dissertation advisory committee who have been instrumental in the progression of this project: Dr. Gary M. Pollack who has been a wonderful chair of this committee, very supportive, always giving invaluable advice, and a great advocate; Dr. Marijana Invanovic who was always available, for her help in improving the hepatic scintigraphy methods and a few long days sitting in front of the computer staring at the Siemens software; Dr. Dhiren Thakker for his scientific advice and lectures in drug metabolism; Dr. Roy Hawke for always being available as a source of advice; and Dr. Bert O'Neil for allowing me to work with him on the clinical study even though we completed one subject successfully during my time here.

I am very grateful to those with whom I have spent time "in the trenches" – fellow lab mates Giulia Ghibellini, Amar Mehta, Dan Bow, Elaine Leslie, Jin Kyung Lee, Nathan Pfeifer, Brian Ferslew, Ahsan Rizwan, Zhixia "Grace" Yan, Tracy Marion, Kristina Wolf, Wei Yue, Maciej Zamek-Gliszczynski and Latoya

Poole, as well as fellow graduate students Rong Zhao, Jeannie Padowski, Will Proctor, and Shawn Watson. I am indebted to my friend Xianbin Tian with whom I had the pleasure of collaborating on our fexofenadine studies and our unforgettable trip to Fox Chase Cancer Center in Philadelphia, Pennsylvania. I would like to express my gratitude and appreciation to Drs. Gary Kruh and Martin Belinsky for their collaboration, hospitality at Fox Chase Cancer Center, and generosity in sharing their gene knockout mice. I also want to thank Elaine Kimple for her administrative support and making life at school and in the lab flow smoothly.

Most of all I am very grateful for the support of my wife Julie who sacrificed so much so that I could attain my goals. The next four years are hers while I attempt to manage the kids' day-to-day activities. I dedicate my work to my children, hoping that I have set a good example so they will have the same opportunities I have had to achieve success at the highest level.

TABLE OF CONTENTS

LIST OF TABLES

LIST OF FIGURES

CHAPTER 1

Introduction

Transport proteins are responsible for drug absorption, distribution and excretion. Transporters govern movement of endogenous compounds and xenobiotics across biological membranes to maintain cellular and physiologic solute concentrations and fluid balance, or to protect the body from dietary and environmental toxins. Most transport proteins are expressed in tissues with barrier functions such as the liver, kidney, intestine, placenta and brain, where they often play a key role in determining bioavailability, therapeutic efficacy and pharmacokinetics of drugs. Transport proteins are classified into two superfamilies, the adenosine triphosphate (ATP)-binding cassette (ABC) protein family and the solute carrier (SLC) protein family. ABC transport proteins function unidirectionally and actively efflux substrates directly utilizing the energy of ATP hydrolysis. The SLC family transporters are facilitated transporters, secondary or tertiaty active transporters, which function bidirectionally allowing drugs/molecules to move across cell membranes utilizing the electrochemical potential gradient or ion gradient, and thus do not directly consume any chemical energy. Proteins in the SLC and ABC familes often work in concert as a vectorial process to remove compounds from the blood and excrete them into bile or urine.

Transport proteins involved in drug disposition are referred to as drug transporters. Drug transporters play important roles in drug targeting, drug-drug interactions and drug-induced toxicity (1-6). Therefore, phenotyping drug transport function may be of importance in individualizing drug therapy. The first section of this chapter will provide an introduction to the transport proteins in both superfamilies; discussion will concentrate on the transport proteins that have the greatest potential

impact on clinical pharmacokinetics, efficacy and safety of drugs. Subsequently, probes that have been used to assess specific transport protein function will be discussed.

ABC Transport Proteins

Multidrug Resistance (MDR1) P-glycoprotein (P-gp)

P-gp was one of the first ABC proteins to be studied because of its role in the development of multidrug-resistance to chemotherapeutic agents. Like many other ABC proteins, P-gp comprises two membrane-bound domains, each made up of six transmembrane helices (7, 8). P-gp is encoded by the *ABCB1* gene, and is expressed at low levels in most tissues, but is found in much higher amounts at the apical surface of epithelial cells lining the colon, small intestine, pancreatic ductules, bile ductules (hepatocytes), kidney proximal tubules and the adrenal gland (9). Tissue localization suggests that P-gp plays a physiological role in the protection of susceptible organs such as the brain and testis from toxic xenobiotics, the secretion of metabolites and xenobiotics into bile, urine and the lumen of the gastrointestinal tract, and possibly the transport of hormones from the adrenal gland. P-gp represents the most widely studied ABC transport protein, and is responsible for the transport of predominantly bulky hydrophobic and cationic substrates including many chemotherapeutic agents, cardiac glycosides, cyclosporine A, and HIV-1 protease inhibitors.

Breast Cancer Resistance Protein (BCRP)

BCRP is encoded by the *ABCG2* gene. ABCG2 is considered a half-transporter that forms a homodimer in order to function, as opposed to other ABC half-transporters that engage in heterodimeric association to form a functional transporter such as ABCG5/ABCG8 (10). Little is known about the molecular mechanism(s) controlling expression; recent studies suggest that expression may be regulated by sex hormones or hypoxia (11-13). Localization of BCRP is very similar to P-gp; the highest expression of *ABCG2* mRNA is in placental tissue, with lower levels in brain, prostate, small intestine, testis, ovary, colon and liver (14, 15). BCRP was discovered based on its affinity to mitoxantrone and shares some substrate overlap with P-gp. BCRP also transports a variety of anticancer drugs such as SN-38, topotecan and doxorubicin (16-18). Other BCRP substrates include sulfate conjugates (19) the tyrosine kinase inhibitors (CI1033, gefitinib and imatinib (20-22)) and fluoroquinolone antibiotics (grepafloxacin, ulifloxacin, ciprofloxacin and ofloxacin (23)).

Multidrug Resistance Proteins (MRP)

There are 12 members of the ABCC family including nine MRPs, the cystic fibrosis transmembrane conductance regulator (CFTR), and the two sulfonyl-urea receptors SUR1 and SUR2. According to current topology prediction programs, ABCC proteins have two cytoplasmic nucleotide-binding domains and depending on the isoform, two or three membrane-spanning domains (24). The binding of ATP at the nucleotide-binding domains and subsequent ATP hydrolysis is required for MRP-mediated transport of

substances across the plasma membrane (1). MRP2 was first localized to the canalicular membrane of rat and human hepatocytes (25, 26). Since then, MRP2 also has been identified on the apical membrane of kidney proximal tubules, small intestine, colon, gallbladder, bronchi and placenta (27-29). The exclusive apical localization in these polarized cells underscores MRP2's role in the excretion and detoxification of endogenous and xenobiotic organic anions. MRP2 substrates include many endogenous compounds such as leukotriene C_4, as well as other glutathione, glucuronide, and sulfate conjugates of substrates such as S-glutathionyl 2,4-dinitrobenzene, mono- and bisglucuronosyl bilirubin, 17β-glucuronosyl estradiol and estrone 3-sulfate (30-33). The function and substrate specificity of MRP2 has been studied extensively by taking advantage of the naturally occurring Mrp2 deficient rats: Eisai hyperbilirubinemic (EHBR) rats and the CY/TR$^-$ mutant rats (25, 26, 34). Furthermore, these hereditary hyperbilirubinemic mutant rats helped to elucidate the upregulation of basolateral Mrp3, a compensatory mechanism that enables the excretion of Mrp2 substrates into the systemic circulation when Mrp2 function is compromised, thus avoiding excessive accumulation of organic anions in the hepatocytes (35, 36). A similar hereditary disorder has been discovered in humans; the absence of a functional *ABCC2* protein on the canalicular membrane leads to conjugated hyperbilirubinemia characteristic of Dubin-Johnson syndrome in humans (37-39). MRP3 is localized in the basolateral membrane of hepatocytes, cholangiocytes, and polarized cells from the gallbladder, colon, pancreas, spleen and adrenal cortex (35, 40-42). Hepatic MRP3 expression is inducible but appears to be

constitutive in other organs (42). Several hereditary and acquired liver disorders lead to increased *ABCC3* protein levels including Dubin-Johnson syndrome (35), progressive familial intrahepatic cholestasis type 3 (42), icteric primary biliary cirrhosis (43), and obstructive cholestasis (44).

SLC Transport Proteins

Organic Anion-Transporting Polypeptides (OATPs)

The OATPs are encoded by the *SLCO* genes that contain 12 transmembrane helices and are expressed in various epithelial cells. There are 11 human isoforms of which OATP1A2, OATP2A1, OATP2B1, OATP3A1 and OATP4A1 are expressed widely among human tissues while others appear to have tissue specific expression, such as OATP1B1 and OATP1B3 in liver, OATP4C1 in kidney and OATP6A1 in testes (45, 46). OATPs generally are considered to function in a bidirectional manner, as dictated by the solute gradient across the membrane. The mechanism of transport consists of anionic uptake into cells that is energized by countertransport with either bicarbonate (47) or reduced glutathione (48, 49). OATPs mediate the sodium-independent transport of a diverse range of amphiphilic organic compounds including bile acids, bilirubin, steroid conjugates, thyroid hormones, anionic peptides, and numerous drugs. Generally, substrates are negatively charged, but there are several examples of neutral (digoxin) and cationic (N-methylquinine) substrates. Several drug classes are susceptible to transport by OATPs including 3-hydroxy-3methylglutarylcoenzyme A (HMG-CoA) reductase inhibitors (statins),

angiotensin II receptor antagonists, angiotensin converting enzyme inhibitors and cardiac glycosides. Although a large number of OATPs have been identified, clinical relevance and drug-drug interactions related to OATPs have been noted primarily for OATP1A2, mediating intestinal absorption, and the liver-specific OATP1B1 and OATP1B3 isoforms, mediating hepatic uptake of drugs (50, 51). Furthermore, OATP1B1 and OATP1B3 have important physiological roles in the hepatic uptake of unconjugated and conjugated bilirubin (52, 53) and bile acid homeostasis based on direct transcriptional regulation by FXR (54) and down-regulation in expression levels during cholestatic disease (55). Both OATP1B1 and OATP1B3 have been shown to be affected by drugs such as rifampin (56, 57).

Organic Cation Transporters (OCTs)

Three OCT isoforms identified in humans are members of the SLC22A family of transporters. Transport of organic cations by the OCTs occurs by facilitated diffusion and is driven by the inside-negative membrane potential (58-60). OCT activity is insensitive to changes in the Na^+ gradient (61). The OCTs share common features such as structure and function, but there are important differences in tissue distribution. OCT1 is characterized as liver-specific, and is expressed predominantly in human liver with lower levels of expression in other tissues (62, 63). In contrast, OCT2 is expressed almost exclusively in kidney(62, 64). OCT3, also referred to as the extraneuronal monoamine transporter, has a broad tissue distribution with moderate levels of mRNA found in skeletal muscle,

prostate, adrenal gland, salivary gland and many other tissues (65). OCTs mediate the uptake of low molecular weight relatively hydrophilic organic cations (type I) such as the prototypical cations tetraethylammonium (TEA), the neurotoxin N-metyl-4-phenylpyridine (MPP^+) and the endogenous compound N-methylnicotinamide (NMN) (58, 66, 67). Drugs that are substrates of the OCTs include metformin, famotidine, and ranitidine (67-69). Most of the drug-drug interactions involving OCT proteins have been shown to occur for drugs predominantly excreted in urine by active renal secretion (70-72).

Organic Anion Transporters (OATs)

OATs are in the same SLC22A family as the organic cation transporters. Five human isoforms have been identified (OAT1, OAT2, OAT3, OAT4 and URAT1), which are located primarily in the kidneys (73). The uptake of organic anions is driven by the concentration gradient of intracellular dicarboxylates, such as α-ketoglutarate. The high concentration gradient of dicarboxylates is maintained by the sodium-dicarboxylate cotransporter, which in turn is driven by the inwardly directed sodium gradient across the basolateral membrane generated by Na^+/K^+-ATPase. Due to the high expression of the OATs in the kidneys, the majority of available data has been generated in the field of renal drug transport. However, OAT2 is expressed predominantly in the sinusoidal membrane of hepatocytes (74). The prototypical substrates of OATs are p-aminohippurate and estrone 3-sulfate, but OATs also transport a wide range of drugs including angiotensin converting enzyme inhibitors, loop and thiazide

diuretics, β-lactam antibiotics, methotrexate and nonsteroidal anti-inflammatory drugs (75).

Importance of Transport Protein Probe Substrates

Systemic concentrations typically correlate with drug efficacy and toxicity, and therapeutic concentration ranges have been established for a large number of drugs. However, significant interindividual variability in the concentration-response and/or concentration-toxicity relationships may exist for some drugs. Genetic polymorphisms and deficiencies in transport proteins are a well recognized source of variability resulting in altered pharmacokinetics and subsequent pharmacologic and toxicological effects of certain drugs (3). Recently, a high impact paper was published documenting that a common variant in *SLCO1B1*, the gene encoding OATP1B1, was strongly associated with increased risk of statin-induced myopathy (76). In addition to genetic polymorphisms, various disease states such as cholestasis and cirrhosis may modify transport protein expression and/or localization, thereby affecting the pharmacokinetics and/or pharmacodynamics of some drugs (77, 78). Therefore, utilizing a probe substrate to phenotype the functional changes in specific transport proteins due to genetics and/or disease state modifications would be useful in predicting the potential impact of alterations due to interindividual differences on the pharmacokinetics of drugs whose disposition is influenced by these specific proteins.

Probe substrates are also crucial for elucidating drug-drug interactions at the transport level, and would be useful for preventing potential adverse events in patient populations that require the use of many concomitantly administered drugs. A clinically important factor that may alter the efficacy and/or toxicity of a drug or endogenous compound is transporter-based drug interactions, which may result in inhibition, induction, or a mixed effect on the uptake and/or efflux of transport proteins (79). To date, many reviews have documented the considerable number of transporter-based clinically important drug interactions (6, 79-81). In fact, the US Food and Drug Administration (FDA) has issued a guidance on performing drug-drug interaction studies to determine P-gp inhibition *in vivo* (82). Probe substrates are an important tool that can be used to clarify the impact that a specific transport protein may have on a drug's disposition, interaction, efficacy and safety; information generated using probe substrates may lead to drug label changes that provide important mechanistic information useful for drug therapy. This same approach can be applied in the drug development or *in vitro* setting to facilitate evaluation of transport/interaction mechanisms for new drug candidates in which transport processes are relatively unknown. Utilizing a specific probe substrate in a cell-based, intact organ or *in vivo* model in the presence and absence of an investigational drug could aid in elucidating whether the investigational drug is an inhibitor, which often suggests the investigational drug is a substrate for that protein as well.

The aim of this review is to present an overview of potential probe substrates for use in humans *in vivo*. The use of imaging technologies to assess

tissue concentrations of probe substrates to elucidate transporter-based drug-drug interactions that may not be reflected by systemic concentrations will be highlighted. In addition, the challenges in identifying specific probe substrates and inhibitors will be discussed.

What Makes a Good Probe Substrate?

First and foremost, a probe substrate must be specific for a transport protein, and the pharmacokinetics of the probe substrate must be sensitive to functional changes in the transport protein. Ideally, a transporter probe substrate would display little or predictable metabolism. Furthermore, the probe would need to be safe for healthy human volunteer studies. Another important characteristic to consider is the disposition properties of the probe substrate. For instance, the clinical use of nitrofurantoin as a BCRP probe to assess BCRP-mediated biliary excretion is limited due to the fact that 30-60% of the parent compound undergoes renal elimination with extensive metabolism after oral administration (83). Other ideal characteristics include a short half-life allowing for a shorter sampling period and less laborious clinical study. Probes that are radiolabeled (gamma emitters or positron emitters) or fluorescent are useful for *in vivo* or *in vitro* studies due to the ease of bioanalytical quantitation. In addition to the obvious advantages from a bioanalysis standpoint, these probes may be capable of providing additional data that could not otherwise be obtained. For example, with the use of positron emission tomography (PET) and gamma scintigraphy, tissue concentrations of the probe can be obtained to assist in

elucidating the distribution of the radiolabeled probe and determining organ exposure.

Identification of specific probe substrates of transport proteins has proved to be difficult. There are many limitations including the broad and overlapping substrate specificity of the specific isoforms of each transport protein subfamily. Similarly, species differences in the transport proteins primarily involved in the disposition of some substrates require assessment of the function, or evaluation of drug interactions, in the appropriate species. This is the case for fexofenadine in which Mrp2 is primarily responsible for biliary excretion in mice whereas P-gp appears to play a more important role in rats (84, 85). Another difficulty is determining the exact mechanism of interaction in the vectorial transport of substrates in polarized cells when uptake and efflux processes are involved. For example, digoxin has been touted as a good P-gp probe substrate(82). However, an OATP-mediated interaction that inhibits the active uptake of digoxin into the hepatocytes or renal tubular cells before gaining access to P-gp could confound interpretation of data generated in a P-gp drug interaction study (86). There is also evidence for multiple binding sites for P-gp (87, 88) and MRP2/Mrp2 (89, 90); the binding of one compound may affect the binding of a second compound, regardless of whether the modulating compound is a substrate of that specific transport protein. A comparison can be made with cytochrome P450 (CYP) 3A4 and the need to use two compounds, midazolam and testosterone, as probe substrates for different binding sites to assess drug-drug interactions (51). Furthermore, drug-drug interactions may result in changes in concentration of the

substrate in a particular tissue without affecting the blood or plasma concentration of the substrate. For example, the P-gp inhibitor cyclosporine A significantly increased the distribution of verapamil, a P-gp probe substrate into the brain, without significantly affecting the plasma or blood concentration-time profile of verapamil (91). It is important to consider whether the clearance of a probe substrate reflects the function of a transport protein. For instance, a probe with a high hepatic extraction will have a hepatic clearance that is reflective of changes in blood flow; thus, it may not be an appropriate probe for a transport protein unless the probe is validated to confirm that it is sensitive to perturbation in function of the transport protein while accounting for differences in blood flow.

In vivo Probe Substrates

P-gp

P-gp is the most well known and widely studied transport protein. P-gp expression in organs of clearance such as the liver and kidneys, and barrier-forming tissues such as the gut and blood-brain barrier, may result in a significant contribution to the distribution and elimination of many drugs. Furthermore, similar to CYP3A, which metabolizes up to 50% of currently marketed drugs(92, 93), P-gp is able to transport a wide range of compounds with different chemical structures(94, 95). Despite the high expression at important epithelial and endothelial barrier-forming tissues, there are few clinically relevant drug-drug interactions attributed solely to P-gp. This may be due to the fact that many known P-gp substrates also are metabolized by CYPs, especially CYP3A4 (92).

For instance, when P-gp is inhibited in rat the metabolism of the dual CYP3A/P-gp substrates tacrolimus and digoxin were increased (96-98). Therefore, inhibition of P-gp leads to increased metabolism reducing any potential accumulation of the P-gp substrate.

Digoxin is the recommended probe in the US FDA draft guidance (http://www.fda.gov/cder/quidance/index/htm) for assessing P-gp inhibition. Digoxin is considered the gold standard P-gp probe because it is metabolically stable in humans (99, 100), and pharmacokinetic changes in absorption and clearance can be attributed primarily to modulation in P-gp function in the gut and kidney/liver, respectively(101, 102). In addition, many studies have assessed P-gp mediated drug-drug interactions using digoxin as the probe substrate(103). However, one limitation with digoxin is that close monitoring is required for untoward signs of digitalis-mediated toxicity due to the narrow therapeutic window of this drug; furthermore, concomitant administration of numerous drugs (e.g. quinidine, amiodarone, and verapamil) may lead to toxicity (104-106), and represents an important exclusion criteria. Another difficulty with digoxin is in separating interactions involving inhibition of P-gp function in the gut (105, 107) from those in the kidney and liver(108, 109). However, digoxin can be administered both intravenously and orally, allowing the impact of P-gp on digoxin bioavailability to be dissected from its impact on systemic or renal clearance. Lastly, digoxin is a good substrate of the basolateral uptake transport proteins OATP1B3 and OATP4C1 in the liver and kidney, respectively(110, 111). Thus, inhibition of digoxin transport might involve inhibition of uptake into the liver

and kidney, which has been shown with the specific P-gp/Bcrp inhibitor GF120918 *in vitro*(86), in addition to interactions at the level of P-gp mediated efflux.

One limitation with most probe drugs is that concentrations can only be measured in the systemic circulation *in vivo*. However, potential drug-drug interactions may result in tissue accumulation with minimal impact on systemic exposure. This has been demonstrated with the use of pharmacokinetic modeling of pravastatin(112) and fexofenadine(85) in humans. To overcome this problem, tissue concentrations should be determined in addition to blood concentrations with the use of imaging technologies such as single-photon computed tomography (SPECT), PET and magnetic resonance imaging (MRI).

One such example is ^{99m}Technetium (^{99m}Tc)-labeled sestamibi, a monovalent cation complex that is used commonly in nuclear medicine to assess myocardial perfusion; ^{99m}Tc-sestamibi distributes into the heart in proportion to blood flow and myocardial viability(113-115). ^{99m}Tc-sestamibi undergoes minimal metabolism in guinea pigs (116) and humans (Cardiolite package insert), and has been shown to be a substrate of P-gp both *in vitro (117, 118)* and *in vivo (119)*. Accumulation of ^{99m}Tc-sestamibi in cells is a function of free diffusion based on electrical potentials across the plasma and mitochondrial membranes, with localization in the mitochondria by electrostatic forces (120). Therefore, a drug-drug interaction with ^{99m}Tc-sestamibi would occur on the apical membrane as a result of P-gp modulation. A few studies have been published using ^{99m}Tc-sestamibi as a phenotypic probe demonstrating increased retention in the liver

and kidney in the presence of the specific P-gp inhibitors PSC833 and XR9576(121-123). In fact, 66 patients genotyped for the G2677T/A and C3435T single nucleotide polymorphisms (SNPs) in *ABCB1* exons 21 and 26, respectively, exhibited a significant reduction in the hepatic elimination rate constant of ^{99m}Tc-sestamibi(124). This suggests that ^{99m}Tc-sestamibi hepatic scintigraphy may provide a useful indicator of P-gp-mediated drug clearance. However, there is limited evidence *in vitro* and *in vivo* in rats that ^{99m}Tc-sestamibi is a substrate of Mrp1 and Mrp2(117, 125) but the overall significance in humans is unknown.

Another imaging agent utilized as a P-gp probe that has an advantage over ^{99m}Tc-sestamibi is the PET agent ^{11}C-verapamil, which has been used for quantitative dynamic imaging studies. Abundant data from *in vitro* and preclinical species studies have indicated that verapamil is a P-gp substrate(126-130); verapamil is also lipophilic so that it diffuses readily across the blood-brain barrier. Therefore, any possible interaction is most likely due to P-gp inhibition, and not by other uptake mechanisms. Working with a short-lived isotope such as ^{11}C has it advantages and disadvatages. One advantage is that only a tracer amount of drug is required, thus avoiding verapamil's pharmacologic effect and toxicity. The 20-min half-life represents an experimental challenge, but also allows for an ideal crossover study design, such as a protocol with a before and after transport protein modulator effect to assess a potential drug-drug interaction in which the subject serves as his/her own control. Verapamil is not an ideal probe due to extensive CYP3A-mediated metabolism in humans (131, 132)

generating the predominant metabolites norverapamil, D-620, and D-617 . However, norverapamil and D-620 would result in the loss of the ^{11}C label while D-617 and several other minor metabolites would retain the label contributing to the imaging (133). The majority of these unconjugated metabolites of verapamil have been shown to be substrates of P-gp and should mimic the disposition of ^{11}C-verapamil (91, 134). Sasongko et al., successfully demonstrated a modest inhibition of P-gp in humans at the blood brain barrier utilizing ^{11}C-verapamil PET imaging to quantify the AUC_{brain} to AUC_{blood} ratio in the absence and presence of cyclosporine without affecting metabolism or protein binding (91).

Other studies *in vitro* and in preclinical species have investigated the clinical use of the following PET tracers as P-gp probes: ^{11}C-colchicine (135), ^{11}C-daunorubicin (126), ^{18}F-fluorpaclitaxel (136), ^{11}C-carazolol (137), ^{18}F-fluorocarazolol (137), ^{11}C-carvedilol (138), ^{18}F-MPFF (137), ^{11}C-WAY100635 (137), ^{11}C-GR218231 (139), ^{11}C-TMSX (140), ^{11}C-MPDX (140), ^{11}C-flumazenil (140), ^{11}C-donepezil (140), ^{11}C-loperamide (141), and ^{11}C-carfentanyl (141).

Some lipophilic drugs that traverse the basolateral membrane by passive diffusion are good P-gp substrates as mentioned with ^{99m}Tc-sestamibi and ^{11}C-verapamil. Therefore, identifying such compounds would be ideal probe substrates for P-gp function, because they do not require uptake proteins to access the cell for subsequent efflux by P-gp. This typically is not the case with other efflux proteins discussed below. Although digoxin is the recommended and most widely used P-gp probe substrate, due to its safety profile and reliance on basolateral uptake transport proteins (OATPs), other substrates may be more

ideal P-gp probes. At one point, fexofenadine was considered an optimal replacement(142), but has since been shown to be a substrate of multiple transport proteins(84, 85, 143). Use of radiolabeled P-gp probes such as ^{99m}Tc-sestamibi and ^{11}C-verapamil allow for quantitation of tissue concentrations that are inaccessible with typical sampling, but are instrumental in demonstrating drug-drug interactions involving P-gp function at the canalicular membrane of hepatocytes in the liver, or the endothelial cells making up the blood brain barrier. More work is necessary to validate these and other radiolabeled probes.

BCRP

Bcrp expression and substrates are similar to P-gp, suggesting that this protein plays a similar role in drug absorption and disposition. However, this ABC half transporter is a relatively novel transporter, and its clinical relevance in drug absorption and elimination has not been characterized completely. The ideal BCRP-selective clinical probe substrate remains to be identified; many BCRP substrates lack a safety profile acceptable for use in healthy volunteer studies(6). There are several nonsynonymous SNPs in the human *ABCG2* gene that are associated with decreased BCRP function including C421A, C376T, G34A, T1291C and T623C; these may contribute to the intersubject variability observed for drugs that are BCRP substrates(144-148). The most widely studied SNP is C421A, which has been used to screen potential BCRP probe substrates.

Nitrofurantoin is a suitable Bcrp/BCRP substrate based on *in vitro* transport studies; nitrofurantoin is a substrate of mouse Bcrp and human BCRP in MDCKII cells (149), but not P-gp, MRP1 or MRP2 (149, 150). In addition, *in*

vivo pharmacokinetic studies have shown that Bcrp affects the absorption and biliary excretion of nitrofurantoin utilizing Bcrp-knockout mice, which exhibited a 4-fold higher plasma AUC after oral administration. After intravenous administration, the nitrofurantoin AUC was 2-fold higher, and biliary excretion decreased 48-fold in Bcrp-knockout compared to wild-type mice (149). BCRP/Bcrp is the primary transport protein responsible for the active secretion of nitrofurantoin into milk in mice and humans, and Bcrp limits the fetal distribution of substrates in pregnant mice (149, 151, 152). Nitrofurantoin is almost completely absorbed in humans, suggesting that BCRP efflux does not substantially influence intestinal absorption of this permeable compound(83). Nitrofurantoin elimination occurs primarily by renal (~30-60% unchanged) and biliary excretion, with some reductive metabolism by enzymes in human tissue and intestinal bacterial flora(83, 153). Nitrofurantoin exhibits a short half life in humans of ~46 – 58 min(83, 154). Recently, nitrofurantoin was assessed as a potential BCRP probe in healthy Chinese male subjects with the *ABCG2* polymorphism C421A, which is associated with reduced transport activity(154). Surprisingly, no significant differences in nitrofurantoin pharmacokinetics among the genotypic cohorts were observed. One explanation for this finding may be that the C421A polymorphism affects the pharmacokinetics of specific substrates, as is the case for topotecan and diflomotecan in which the plasma exposure increased only 1.4-fold for oral topotecan vs. 4-fold for intravenous diflomotecan(155, 156). Another explanation may be due to a smaller contribution of BCRP to the overall elimination of nitrofurantoin in humans *in vivo*

compared to *in vitro* experiments in human BCRP-transfected cell lines and *in vivo* rodent studies. These data suggested that nitrofurantoin is not a suitable clinical probe substrate for assessing BCRP activity.

Sulfasalazine is another probe that has been used clinically to phenotype BCRP function. The bioavailability of sulfasalazine is relatively low, with only one-quarter to one-third of the drug absorbed; extensive metabolism by intestinal bacteria results in the release of sulfapyridine and 5-aminosalicylate(157, 158). Less than 10% of the absorbed sulfasalzine dose is excreted unchanged in urine, with the remainder excreted unchanged in bile(157, 158). Therefore, sulfasalazine may be useful for assessing BCRP function in most tissues including the intestine. Importantly, the plasma AUC of sulfasalazine increased 111-fold in Bcrp-knockout compared to wild-type mice and was not significantly different in Mdr1a knockout mice, suggesting that sulfasalazine was sensitive and selective for Bcrp (159). Urquhart et al., demonstrated that sulfasalazine was a substrate of human BCRP in the Caco-2 system, and evaluated sulfasalazine as an *in vivo* probe in 17 healthy individuals with either the *ABCG2* genotypes 34GG/421CC (wild-type) or 34GG/421CA (variant SNP)(160). Remarkably, subjects with the 34GG/421CA genotype exhibited a 2.4-fold greater sulfasalazine AUC compared to subjects with the wild-type 34GG/421CC genotype after administration of a 1000 mg oral suspension(160).

Interestingly, rosuvastatin also has been used as a BCRP probe in subjects with the frequent *ABCG2* SNP C421A (161). Although rosuvastatin undergoes minimal metabolism via CYP2C9 (<10% of dose) (162, 163), it is a

substrate of multiple transport proteins including the OATPs, NTCP, P-gp and MRP2 (164, 165). Therefore, rosuvastatin relies on multiple mechanisms for clearance, suggesting that it would not be sensitive to modulation of a specific clearance pathway. Rosuvastatin, an HMG-CoA reductase inhibitor whose target site is the liver, is excreted extensively into bile with ~90% of the dose recovered in feces (76.8% unchanged); these characteristics suggest that rosuvastatin would be a good probe to assess hepatic transport protein function(162). After intravenous administration of rosuvastatin, renal and nonrenal (hepatic) clearance accounted for 28 and 72% of total systemic clearance, respectively (166). Zhang et al., evaluated the pharmacokinetics of rosuvastatin in individuals with the *ABCG2* C421A SNP, excluding those with the *SLCO1B1* 521T>C variant and *CYP2C9**1/*3, which would be expected to cause decreased hepatic uptake and metabolism, respectively. Their findings demonstrated that rosuvastatin disposition was significantly altered by the *ABCG2* C421A SNP (AUC was increased 80%; C_{max} was increased 90%; oral clearance was decreased 43%) after exclusion of individuals with the *SLCO1B1* T521C and *CYP2C9*3* SNPs to get a clear understanding of the impact of the BCRP (421C>A) genetic polymorphism on rosuvastatin disposition(161). This suggests rosuvastatin disposition is affected by BCRP function, but required the assessment of genetic polymorphisms in the OATP1B1 and CYP2C9 genes to be accounted for. Therefore, a drug-drug interaction study *in vivo* utilizing rosuvastatin as the phenotyping probe may be difficult to interpret because multiple mechanisms

may be involved in an interaction, including inhibition of uptake, metabolism and/or efflux.

One of the most widely studied BCRP substrates is the anticancer drug topotecan; a 2.2-fold increase in plasma AUC was reported in cancer patients when coadministered with the dual BCRP/P-gp inhibitor GF120918(167, 168). However, this interaction was not due solely to BCRP because topotecan is also a P-gp substrate(169, 170). Furthermore, topotecan cannot be administered to healthy humans due to its cytotoxic effects.

To date there are few candidate BCRP probe substrates identified, but sulfasalazine appears to be the most promising. Other than the extensive metabolism in the gut, sulfasalazine is amenable to assessing BCRP function in the kidneys and liver. Furthermore, a clinical study in 17 subjects demonstrated increased systemic exposure in patients expressing the variant SNP 421CA (160). The difficulty in identifying specific probes for efflux proteins is the substrate overlap with uptake transport proteins. This is one of the reasons that rosuvastatin is not an ideal BCRP probe. More work is necessary to identify and validate probes that are sensitive to changes in BCRP function.

MRP2

MRP2 mediates the efflux of many endogenous and xenobiotic organic anions including glutathione, glucuronide and sulfate conjugates. The localization in intestinal and renal epithelia, hepatocytes and in blood-tissue barriers signifies the importance of this efflux protein in drug absorption, distribution and elimination. The difficulty in identifying potential probes for

MRP2 function is that most substrates are likely substrates for the uptake proteins residing on the basolateral membrane (i.e. OATs and OATPs) of polarized cells in which MRP2 is localized on the apical membrane (i.e. renal tubular cells and hepatocytes). Furthermore, considerable substrate overlap between MRP2 and MRP3 exists. MRP3 is upregulated as a compensatory mechanism when MRP2 function is reduced in hepatocytes. Therefore, the combination of uptake and efflux in both directions makes it difficult to ascertain which protein the probe is assessing. For example, an increase in systemic exposure could be the result of either uptake inhibition, or MRP2 inhibition with increased MRP3 basolateral efflux. This complex scenario could be resolved with the use of a radiolabeled probe that enabled external quantitative imaging and direct measurement of increased tissue exposure due to decreased MRP2 efflux.

^{99m}Tc-Mebrofenin is a candidate for phentoyping MRP2 function *in vivo*. ^{99m}Tc-Mebrofenin is a substrate of OATP1B1, OATP1B3, MRP2 and MRP3 in transfected *Xenopus* oocytes and HEK293 cells (171). In fact, case reports have documented a failure to visualize the hepatobiliary tree after ^{99m}Tc-disofenin (DISIDA), the diisopropyl analog of acetanilidoiminodiacetic acid, when administered to patients with Dubin-Johnson syndrome (MRP2-deficient) (172, 173). ^{99m}Tc-HIDA, another analog of acetanilidoiminodiacetic acid, exhibited delayed biliary secretion in TR$^-$ rats (Mrp2-deficient) compared to wild-type rats, demonstrating the importance of Mrp2 in canalicular transport (125). A distinguishing feature of ^{99m}Tc-mebrofenin is that hepatic uptake is up to 2-fold

greater than its analogs when serum bilirubin levels are as high as 20 mg/dL, suggesting that hepatic uptake of ^{99m}Tc-mebrofenin would not be inhibited by other OATP substrates (174). ^{99m}Tc-mebrofenin is a high hepatic extraction drug, with more than 98% of an intravenous dose taken up by the liver; the hepatic excretion half-life is rapid (16 min) and only ~1.5% of the dose is recovered in urine after 24 hours in humans (174). Assuming well stirred conditions hepatic clearance would be limited by blood flow not uptake transport proteins (175) and the rapid excretion into bile (174) demonstrates the importance of MRP2-mediated biliary excretion compared to MRP3-mediated basolateral efflux. Therefore, ^{99m}Tc-mebrofenin is a potential hepatic probe of MRP2 and perhaps MRP3 in specific hereditary and acquired liver disorders including progressive familial intrahepatic cholestasis, cirrhosis and cholestasis (42-44).

Angiotensin II receptor antagonists such as olmesartan and valsartan are substrates of MRP2 (176-178). Olmesartan is not metabolized and hepatic clearance accounts for 60% of total clearance (179, 180). Olmesartan is taken up in hepatocytes equally by OATP1B1 and OATP1B3 as determined by the relative activity factor method; olmesartan is a substrate for MRP2, but not P-gp or BCRP (176, 177). In the kidney, olmesartan is a substrate of OAT1, OAT3, MRP2 and MRP4; however, the urinary excretion of olmesartan was unchanged in Mrp4-knockout compared to wild-type mice (176). Determining the rate-limiting step in hepatic and renal clearance of olmesartan would be important in establishing this drug as an MRP2 probe substrate. Valsartan undergoes a

minor degree of metabolism with 89% of the unchanged form circulating in plasma and 85% excreted into feces as the unchanged form after oral administration (181, 182). Similar to olmesartan, hepatic clearance of valsartan accounts for 70% of total clearance; valsartan is a substrate of OATP1B1, OATP1B3 and MRP2, but not P-gp or BCRP in transfected HEK293 and MDCKII cells (178). CYP2C9 is the only isoform involved in the 4-hydroxylation of valsartan; many prototypical inhibitors (i.e. furafylline, S(+)-mephenytoin, quinidine and troleandomycin) did not affect CYP2C9-mediated 4-hyroxylation of valsartan, thus plasma concentrations and systemic clearance would not be effectively altered with concomitant administration of CYP2C9 inhibitors(183). Both drugs, however, have not been established as clinical probes, or investigated in patients with genetic variants in the *ABCC2* gene which encodes for MRP2.

Another approach to phenotyping MRP2 function has been to take advantage of the role of MRP2 in the biliary clearance of phase II conjugates. For example, mycophenolate mofetil, an ester prodrug, is rapidly and extensively (95%) hydrolyzed by esterases to the active metabolite mycophenolic acid (184). Mycophenolic acid is conjugated by glucuronidation primarily in the liver by UGT1A9 and UGT2B7, but also by UGT1A8 in the gastrointestinal tract (185, 186). The glucuronide conjugates of mycophenolic acid are excreted into bile by MRP2 (187, 188), where they undergo bacterial deconjugation and extensive enterohepatic circulation, which accounts for 10 to 61% of the AUC of mycophenolic acid AUC (189); the phenolic glucuronide is preferentially excreted

in urine (190). Many studies have investigated the effect of *ABCC2* polymorphisms (C24T and G1249A) on the pharmacokinetics and pharmacodynamics of mycophenolic acid; however, the contribution of variants in the *SLCO1B3* and *UGT1A9* genes confound data interpretation (191-194). Overall, many mechanisms are involved in the clearance of mycophenolic acid, suggesting that the phenolic glucuronide may not be the best probe to assess MRP2 function.

Due to MRP2 localization on the apical membrane (i.e. renal tubular cells and hepatocytes), and the substrate overlap with many uptake proteins (i.e. OATs and OATPs), identifying specific probe substrates in which systemic concentrations are altered will be difficult. Currently there are no identified probes for this protein, and some that have promise (i.e. valsartan and olmesartan) always will be limited by the potential for multiple sites of interaction altering the probe substrate pharmacokinetics. For this reason ^{99m}Tc-mebrofenin is the most promising probe to assess hepatic MRP2 function due to its high hepatic extraction and the ability to directly assess systemic and tissue concentrations of this probe.

OATPs

Interest in the OATPs has increased in recent years due to the important role this subfamily of proteins plays in determining intestinal drug absorption, hepatic and renal clearance, and tissue distribution. Many OATPs share common substrates, but there are a few examples of clear differences in substrate specificity (*e.g.,* CCK-8 is a specific OATP1B3 subsrate(195)).

Isoform-specific substrates would be useful tools to define the contribution of specific OATP isoforms to drug disposition *in vitro* and *in vivo*.

Mechanisms of hepatic transport have been studied extensively for the statins, a class of compounds where the target organ is the liver. Except for pravastatin, most statins undergo negligible urinary excretion(196), and with the exception of pravastatin(197) and rosuvastatin(163, 198), most statins are metabolized by CYPs. Thus, many statins are susceptible to metabolism-mediated drug-drug interactions(196). Administration of potent CYP3A4, CYP2C9 and CYP2C19 inhibitors had no significant effects on the pharmacokinetics of pravastatin in healthy volunteers(199, 200). Transport pathways are particularly important for pravastatin clearance. However, pravastatin is a substrate of multiple transport proteins including BCRP, MRP2, BSEP, OATP1A2, OATP1B1, OATP2B1, and OAT3 (201-205). Despite multiple mechanisms of transport, pravastatin uptake is the rate-limiting step in the overall hepatic clearance of this statin in the rat (206, 207). Furthermore, pravastatin disposition has been studied in various ethnic groups and in patients exhibiting multiple genotypes. Ho et al. investigated the effects of polymorphisms in the hepatic drug uptake transport protein OATP1B1 (*SLCO1B1*), and the efflux proteins MRP2 (*ABCC2*), BSEP (*ABCB11*) and BCRP (*ABCG2*), following a single 40 mg oral dose of pravastatin in healthy European-Americans and African-Americans (208). The AUC and C_{max} were significantly higher in the subjects with the *SLCO1B1* T521C polymorphism while neither *ABCC2*, *ABCB11* or *ABCG2* genotypes were associated with differences in pravastatin

pharmacokinetics. Other studies using pravastatin as an *in vivo* probe for *SLCO1B1* activity have demonstrated altered pharmacokinetics in Japanese and European Caucasian individuals who possess variant *SLCO1B1* alleles *1b (A388G), *5 (T521C) and *15 (combination of *1b and *5) (209-211).

Rosuvastatin, another potential probe, is metabolically stable, but is a substrate for many hepatic uptake and efflux transport proteins including OATP1B1, OATP1B3, OATP1A2, OATP2B1, NTCP, P-gp and MRP2 (164, 165). As discussed above, rosuvastatin undergoes minimal metabolism. However, rosuvastatin relies on multiple transport proteins for clearance, suggesting that it would not be a good phenotypic probe specific for a given transport protein. Pharmacokinetic differences in rosuvastatin systemic exposure have been investigated in subjects with polymorphisms in the *SLCO1B1* gene. Following a 10 mg oral dose of rosuvastatin administered to 30 healthy Koreans, the AUC and C_{max} were significantly higher in the variant group *SLCO1B1**15 compared to the control *SLCO1B1**1a group (212). Similarly, 32 young healthy white volunteers of European descent genotyped for the *SLCO1B1* 521T>C exhibited an increase of 65 and 79% in AUC and C_{max}, respectively, compared to those with the CC genotype (213) following a 10 mg oral dose of rosuvastatin. Therefore, rosuvastatin disposition is sensitive to changes in OATP1B1 and BCRP function as a result of genetic polymorphism, but this drug is not the best probe due to the involvement of multiple transport mechanisms.

Pitavastatin is also taken up efficiently from the systemic circulation into hepatocytes by OATP1B1 and OATP1B3 (214); BCRP is involved in the biliary

excretion of pitavastatin(215). Unlike pravastatin and rosuvastatin, pitavastatin undergoes more extensive metabolism by CYP2C9 (216, 217), and glucuronidation by UGTs, that results in spontaneous lactonization by the elimination of the glucuronide moiety (218). The lactone form can be converted back to the parent drug by a reversible reaction(218). Two studies demonstrated that the *SLCO1B1**15 allele resulted in a significant increase in AUC and C_{max} of pitavastatin in Korean and Japanese healthy volunteers (219, 220). Furthermore, the nonsynonymous *ABCG2* variant C421A was not associated with altered pharmacokinetics of pitavastatin (220). Therefore, OATP1B1 is a determinant of pravastatin, pitavastatin and rosuvastatin hepatic uptake affecting their pharmacokinetic profiles in humans.

Fexofenadine is also a substrate of the OATPs, specifically OATP1B1, OATP1B3 and OATP1A2 in humans (221-224). However, much like other OATP substrates, fexofenadine is also a substrate of many efflux proteins such as P-gp, MRP2, MRP3, BSEP, and MATE1 (143, 222, 223, 225). Fexofenadine undergoes minimal metabolism (<10%) in humans (226-228) ; 12% of an oral dose is excreted into urine while the remainder of the bioavailable dose is excreted into bile (228). Therefore, fexofenadine relies on active transport as the major determinant for systemic clearance. Fexofenadine has been recommended as an *in vivo* probe substrate for P-gp interactions in the intestine (142), and many drug-drug and food-drug interaction studies in humans have been performed utilizing fexofenadine as a probe with various co-administered drugs, herbal supplements and food components (221, 226, 227, 229-233). However, the

mechanism(s) resulting in modulation of fexofenadine pharmacokinetics may not be straightforward. In fact, when fexofenadine is administered with known P-gp modulators such as diltiazem (233) or verapamil (234), or in individuals with P-gp polymorphisms (C3435T and G2677T) (230, 235, 236), no significant change in fexofenadine pharmacokinetics has been observed. However, significant changes in fexofenadine AUC have been reported in drug-drug interaction studies with known OATP modulators such as fruit juices (237), and in individuals with polymorphisms in the *SLCO1B1* gene (238), suggesting that fexofenadine may be more suitable for assessing OATP function. None the less fexofenadine is not an optimal probe due to the involvement of multiple transport proteins in uptake and excretion.

Most of the aforementioned compounds are primarily substrates of OATP1B1. The other liver-specific OATP isoform, OATP1B3, is involved predominantly in the hepatic uptake of telmisartan in humans. Ishiguro et al., did not observe significant uptake of telmisartan in OATP1B1 expressing HEK293 cells, but telmisartan displayed a high affinity for OATP1B3 with a K_m of 0.81 μM (239). Furthermore, 30 μM estrone-3-sulfate inhibited, the OATP substrate, estradiol 17β-D-glucuronide uptake, but did not inhibit the uptake of telmisartan in cyropreserved human hepatocytes(239). Telmisartan is a fairly lipophilic compound (log P 3.2) that is metabolized to an inactive acyl glucuronide by UGTs in the intestine and liver. The acyl glucuronide is excreted rapidly into bile and accounts for 10% of the circulating drug-related material 1 h after oral administration in humans. After intravenously and orally administered ^{14}C-

labeled mass balance studies, 98% of the telmisartan was recovered in feces, and less than 1% was recovered in urine (240, 241). One challenge in establishing an OATP1B3 probe is the lack of identified specific inhibitors *in vitro,* or especially *in vivo,* and the rare prevalence of functional polymorphisms in the *SLCO1B3* gene.

The difficulties in identifying OATP probe substrates are the overlapping specificity of the different isoforms and the involvement of efflux proteins. As mentioned above, statins distribute into the liver and may be useful for assessing OATP1B1 and OATP1B3 function. Although it appears that pravastatin is uptake rate-limited, as with all of the probe drugs discussed, many efflux proteins also are involved in pravastatin hepatobiliary disposition. Thus, assuming that alterations in the pharmacokinetics of the probe drug are due to decreased function of one specific transport protein may not be correct. Therefore, better probes need to be identified although currently, fexofenadine has been used extensively and may be suitable for assessing transport protein-mediated interactions in the intestine. With the improvement and increased availability of *in vitro* systems to study hepatic uptake, the differential involvement of OATP1B1 vs. OATP1B3 will continue to be elucidated and better probes will be identified.

OATs

The OAT family also facilitates the transport of anionic drugs. There are five functional human OAT transport proteins that have been identified. OAT1, OAT3, and OAT4 play a primary role in renal transport, whereas OAT2 is expressed significantly in the liver (242, 243). Studies on the OATs focus on

their involvement in the kidney because they are thought to play a minor role in the hepatic uptake of drugs. The potential for drug-drug interactions exists for drugs that are secreted actively by the OATs and whose renal clearance is a significant component of total clearance. For example, the decrease in renal excretion caused by probenecid co-administration with penicillins, cephalosporins and antivirals can be attributed, at least in part, to active tubular secretion via OATs (244-246). In general, the clinical significance of an OAT-mediated drug-drug interaction resulting in marked inhibition of active renal clearance has a very minimal impact on systemic exposure or AUC (247). An exception to this depends on the therapeutic margin of the OAT substrate of which the only clinically significant example is methotrexate when coadministered with other OAT inhibitors, probenecid and nonsteroidal anti-inflammatory drugs (248, 249). This may be due to the fact that renal elimination (a combination of glomerular filtration, active secretion, and in some cases reabsorption) typically accounts for 50% or less of total clearance, and therefore, other routes of clearance can compensate for reduced OAT function due to a genetic polymorphism or competitive inhibition (5, 79).

Tenofovir disoproxil fumarate is an oral prodrug which is converted rapidly to tenofovir monoester by esterases or chemical hydrolysis, and then to tenofovir by phosphodiesterases (250). Tenofovir is excreted primarily unchanged in urine, while biliary excretion of tenofovir is relatively low; tenofovir is not a substrate of CYP enzymes (251-253). Tenofovir undergoes renal elimination through a combination of glomerular filtration and active tubular secretion based

on the observation that renal clearance exceeds that of creatinine clearance in patients (254). Tenofovir is taken up with higher affinity for OAT1 than OAT3, and is not a substrate of OCT1 or OCT2 (255). On the apical membrane, tenofovir is excreted by MRP4, but not by P-gp or MRP2, as determined in multiple transfected systems (256). Data generated in TR^- (Mrp2-deficient) rats demonstrated that Mrp2 has a significant influence on tenofovir biliary excretion, but not on intestinal excretion in *in situ* efflux experiments (257). Two other nucleotide reverse transcriptase inhibitors, adefovir and cidofovir, also have been shown to be substrates of OAT1 and OAT3, but not OCT2 (255). Both drugs are actively secreted by the kidney (258, 259). Adefovir is a substrate of MRP2, MRP4 and MRP5 (260-262), but no interaction was reported with P-gp or MRP1 (263), and the absence of Mrp2 in TR^- rats did not affect renal clearance, suggesting that Mrp2 does not play a critical role in adefovir secretion (264). Overall, it appears that OAT1 and probably MRP4 play a significant role in the renal elimination of adeofovir, tenofovir and cidofovir, and OAT1 protein plays a critical role in mediating nephrotoxicity as a result of exposure of the renal tubular cells to clinical doses of adefovir and cidofovir (265). Of the twenty OAT1 SNPs identified in genomic DNA from African, Asian and Caucasian individuals, the R50H-OAT1 variant expressed in *xenopus* oocytes resulted in decreased adeofovir, tenofovir and cidofovir uptake (266). A separate study identified 12 coding region variants of OAT1; two of six non-synonymous variants were present at ≥ 1%. Only the OAT1-R454Q was non-functional to the prototypical substrates p-aminohippurate, ochratoxin A and methotrexate in *xenopus* oocytes.

However, in a small family-based clinical study, no significant decrease in the renal secretory clearance of adefovir was observed in family members heterozygous for OAT1-R454Q in comparison to the reference OAT1-454R, suggesting that coding region variants of OAT1 may not contribute substantially to interindividual differences in renal clearance of adefovir (267).

Ro 64-0802 is the active metabolite of oseltamivir, which is converted by carboxylesterase 1A1 in the liver and/or intestines (268). About 60-70% of an oral dose is excreted in urine as Ro 64-0802, and less than 5% as the prodrug (269). Less than 20% of an oral dose appears in feces as equal parts of Ro 64-0802 and oseltamivir (269). The renal clearance of Ro 64-0802 exceeds the glomerular filtration rate, and Ro- 64-0802 has been identified as a substrate of OAT1, OAT3 and MRP4 (270, 271). To investigate a potential transporter mediated drug-drug interaction in the renal secretion of Ro 64-0802, healthy volunteers were given 500 mg q.i.d. of probenecid starting 1 day before a single 150 mg oral dose of oseltamivir, which resulted in a 50% decrease in renal clearance and a 2.5-fold increase in the plasma AUC (270, 271). Probenecid is a general organic anion inhibitor, but also has been shown to inhibit P-gp, most of the MRPs and the OATs (272-276). Therefore, it is difficult to discern whether the decrease in renal clearance of Ro 64-0802 is due to inhibition of OAT-mediated uptake on the basolateral membrane, MRP-mediated excretion on the apical membrane, or a combination of both. The 2.5-fold increase in exposure (plasma AUC) is not clinically relevant due to the large safety margin (269, 277) of olsetamavir. Thus, olsetamavir is a relatively safe drug and may be used in

healthy volunteer studies as a probe in subjects expressing genetic variants resulting in increased or decreased OAT function.

More work is necessary to identify and validate probes of OAT function. Full characterization of the antiretrovirals tenofovir, adefovir and cidofovir, and the active metabolite of the antiviral oseltamivir, as probe substrates are necessary to understand the rate-limiting steps in renal clearance. However, Ro 64-0802 is the better choice at this point for further investigation due to its safer profile when compared to adefovir and cidofovir based on their dose-limiting toxicity of nephrotoxicity (278, 279).

OCTs

The OCTs are a family of transport proteins responsible for the uptake of organic cations in a variety of tissues. Thus far, thee human OCT isoforms have been extensively characterized (OCT1-3). Based on substrates and tissue distributions, OCT1, OCT2, and OCT3 are thought to play important roles in the biliary and renal excretion of organic cationic drugs and the distribution of these compounds in the liver, kidney, heart and brain (66).

Metformin, a very hydrophilic organic cation, is metabolically stable. Greater than 98% of the absorbed dose of metformin is excreted by the kidneys (280-282); approximately 20 to 30% of the dose is recovered in feces unchanged (283, 284). The renal clearance of metformin is much greater than the glomerular filtration rate, suggesting a significant contribution of tubular secretion (282). Metformin is a known substrate of OCT1, OCT2, OCT3, MATE1, and MATE2-K (69, 285-287) and the newly identified proton-coupled transporter,

plasma membrane monoamine transporter (PMAT) (288). Metformin is positively charged at physiologic pH and may be a good probe drug of organic cation transporters. Many studies have investigated the effects of genetic variation in OCTs on the pharmacokinetics of metformin. Shu et al., demonstrated that individuals carrying a reduced function *OCT1* allele (R61C, G401S, 420del, or G465R) had a higher plasma AUC, higher C_{max} and lower V/F compared to those carrying the OCT1-reference alleles after two oral doses of 850 and 1000 mg metformin (289). Human OCT1 is expressed primarily in the liver (62, 63); in *Oct1*-/- mice, the hepatic uptake of metformin is decreased compared to wild-type *Oct1*-/- mice (290). Therefore, the effects of *OCT1* genotype on metformin pharmacokinetics, as evidenced by the increased AUC, increased C_{max} and decreased volume of distribution, in the individuals carrying the reduced function alleles of *OCT1* may be explained by decreased hepatic uptake. The same group assessed changes in the renal clearance of metformin in Caucasian and African-American individuals with genetic variation in OCT2 (amino acid change A270S). The renal clearance and secretory clearance were significantly greater in individuals heterozygous for the variant allele (808G/T) of OCT2 than those homozygous for the reference allele (808G/G) (291). A separate study also examined genetic variants 596C>T, 620C>T, and 808G>T in the OCT2 gene, *SLC22A2*, which resulted in increased plasma concentrations and decreased renal clearance of metformin compared to the reference genotype (292). The discrepancy between the two studies with the 808G>T variant allele may be due to the small sample size of the second study and the fact that the reference

subjects did not have diabetes. The importance of OCT1 in the disposition of metformin is supported further by a study in 103 healthy male Caucasians; metformin renal clearance was significantly dependent on polymorphisms in OCT1, but not in OCT2, OCT3, OCTN1 and MATE1 (293). Cimetidine has been reported to significantly increase metformin plasma concentrations and reduce metformin renal clearance (72). The proposed mechanism of this interaction is inhibition of the organic cation transporters in the kidney; cimetidine is a substrate and inhibitor of OCT1 and OCT2 (64, 294). Recently, clinically relevant concentrations of cimetidine (1 μM) were shown to inhibit MATE1 on the apical membrane resulting in increased intracellular accumulation of metformin without affecting OCT2-mediated basolateral uptake in double transfected MDCKII cells (295). A clinical study investigated metformin renal clearance in 14 Chinese males with the 808G>T polymorphism of OCT2 in a crossover design in the presence and absence of cimetidine. The polymorphism significantly decreased metformin renal clearance by 26%. Inhibition by cimetidine was dependent on the genetic variant, resulting in a 42% decrease in metformin renal clearance in the reference allele subjects with a subsequent increase in plasma AUC. In contrast, cimetidine treatment significantly decreased renal and total clearance but did not significantly change metformin maximum concentration or plasma AUC in participants who were heterozygous for the OCT2 808G>T mutation (296). This may be due to increased metformin accumulation in renal epithelial cells, which may not be reflected by changes in the plasma concentration. This

hypothesis would support the notion that MATE plays an important role in the cimetidine-metformin interaction *in vivo*.

Therefore, metformin may not be an ideal probe for a specific organic cation transport protein due to changes in its pharmacokinetics associated with modulation of OCT1, OCT2 and MATE function, as demonstrated in the various clinical studies utilizing individuals with transport protein polymorphisms, and the possible cimetidine interaction with MATE on the apical membrane. What distinguishes metformin from other OCT substrates is that it is not a substrate for P-gp (297, 298). Based on its safety profile, high bioavailability, lack of metabolism, and extensive use in clinical studies, metformin may continue to be used as a general probe for OCT1 and OCT3 function in the liver, and OCT2 function in the kidney.

Conclusion

To date, there are not many probes suitable for clinical studies that are specific for a particular transport protein. The common difficulty is specificity, and the involvement of multiple transport proteins, oftentimes both uptake and efflux transporters, in polarized cells. This highlights the need to investigate transport mechanisms and potential drug-drug interactions in an isolated polarized *in vitro* system to help elucidate the *in vivo* handling of the probe. Radiolabeled probes are optimal due to their ability to provide direct, quantitative measures of exposure in multiple compartments, including those that are not routinely accessible. Additionally, radiolabeled probes may be useful for elucidating the precise protein affected if the probe is a substrate for an uptake and efflux

protein. Further investigations are necessary to identify and validate specific probes, which are needed to advance scientific knowledge in the field of drug transport.

Project Rational and Specific Aims

A review of the current literature clearly emphasizes the need for more thorough evaluation of three existing probes: fexofenadine, ^{99m}Tc-mebrofenin (^{99m}Tc-MEB) and ^{99m}Tc-sestamibi (^{99m}Tc-MIBI). Fexofenadine has been touted as a specific P-gp probe substrate (299). However, current literature suggests that other proteins are involved in the hepatic disposition of this compound. To date, many clinical studies have utilized fexofenadine as a probe substrate to assess P-gp activity and the inhibitory effects of various xenobiotics, herbal supplements, and food components on P-gp function (230, 232-234, 300). ^{99m}Tc-MEB and ^{99m}Tc-MIBI have been used as non-invasive probes to assess hepatic uptake and excretory function in humans and rodents (124, 301-303). However, the mechanisms of hepatic transport of ^{99m}Tc-MEB and ^{99m}Tc-MIBI have not been elucidated completely in intact hepatocytes and *in vivo*, especially in disease states such as cirrhosis and hepatocellular carcinoma, where hepatic transport protein function is altered. The anticancer agent sorafenib, a recently developed oral multikinase inhibitor, relies heavily on the liver for elimination in humans. The liver is the target site in the treatment of unresectable hepatocellular carcinoma. Many patients with cirrhosis and hepatocellular carcinoma have impaired hepatic function, which results in highly variable clearance of drugs including sorafenib. ^{99m}Tc-MEB and/or ^{99m}Tc-MIBI may be useful probe substrates to predict the hepatobiliary disposition of drugs that share similar mechanisms of hepatic transport to individualize dosing and explain the pharmacokinetic variability. Therefore, elucidating the mechanisms of hepatic

uptake and the extent of biliary excretion of sorafenib in humans is an important step in validating ^{99m}Tc-MEB and/or ^{99m}Tc-MIBI as probe substrates to predict the hepatic clearance of sorafenib.

Hypotheses:

The ***hypothesis of Aim #1*** is that fexofenadine is a substrate for multiple proteins on both the basolateral and canalicular membrane of hepatocytes in humans, rats and mice. Suggesting, fexofendine is not an optimal probe substrate for a specific hepatic transport protein due to compensatory transport processes that may be involved in the hepatic clearance of this drug. The ***hypothesis of Aim #2*** is that ^{99m}Tc-MEB is primarily a marker for OATP-mediated hepatic uptake and MRP2-mediated biliary excretion; ^{99m}Tc-MIBI is a marker for P-gp-mediated biliary excretion. Therefore, these diagnostic imaging agents may be used as specific probe substrate to phenotype these hepatic transport proteins clinically. The ***hypothesis of Aim #3*** is that the mechanisms of sorafenib hepatic disposition are similar to ^{99m}Tc-MEB and ^{99m}Tc-MIBI, making them ideal probe substrates to predict interindividual differences in hepatic clearance of sorafenib in patients with hepatocellular carcinoma and Child's B cirrhosis to explain the variability in the pharmacokinetics and clearance of sorafenib. Furthermore, ^{99m}Tc-MEB and ^{99m}Tc-MIBI can serve as tools to predict the locus and extent of modulation in hepatic transport due to disease states, genetics and/or drug interactions.

This dissertation addresses the following specific aims:

Aim #1. Determine whether fexofenadine is an optimal probe substrate for a specific transport protein by elucidating the transport proteins and species differences in transport proteins responsible for the hepatic excretion of fexofenadine (Chapters 2-3).

1.a. Develop a pharmacokinetic model to describe the disposition of fexofenadine in healthy human subjects, and conduct simulations to determine if fexofenadine systemic and/or hepatic concentrations are sensitive to the inhibition or induction of hepatic transport pathways.

1.b. Elucidate the involvement of P-gp in the biliary excretion of fexofenadine in humans using sandwich-cultured human hepatocytes and the P-gp inhibitor GF120918. Validate the results of the simulation studies in Aim #1.a by confirming changes in the systemic and hepatic compartment as a result of inhibition of fexofenadine biliary excretion.

1.c. Determine the canalicular transport protein(s) involved in the biliary excretion of fexofenadine using isolated perfused livers from Mrp2-deficient TR^- rats in combination with "specific" transport protein inhibitors (GF120918 and bosentan).

1.d. Define the role of basolateral and canalicular transport proteins in the overall hepatic disposition of fexofenadine using isolated perfused livers from transport protein-deficient mice.

Aim #2. Examine the mechanisms of hepatic uptake and excretion of ^{99m}Technetium mebrofenin (^{99m}Tc-MEB) and ^{99m}Technetium sestamibi (^{99m}Tc-MIBI) in intact hepatocytes, and the influence of altered hepatic transport protein function, on the hepatobiliary disposition of ^{99m}Tc-MEB and ^{99m}Tc-MIBI (Chapter 4).

2.a. Characterize ^{99m}Tc-MEB and ^{99m}Tc-MIBI uptake in suspended rat and human hepatocytes in the absence and presence of "specific" inhibitors of basolateral transport proteins.

2.b. Characterize ^{99m}Tc-MEB and ^{99m}Tc-MIBI hepatobiliary disposition in sandwich-cultured rat hepatocytes from wild-type (WT) wistar rats, TR^- rats,

and in the presence of “specific” transport protein inhibitors (*e.g.,* GF120918).

2.c. Characterize ^{99m}Tc-MEB and ^{99m}Tc-MIBI hepatobiliary disposition in sandwich-cultured human hepatocytes in the absence and presence of “specific” transport protein inhibitors (*e.g.,* GF120918 and MK-571).

Aim #3. Identify mechanisms of hepatic disposition of sorafenib in human hepatocytes, and evaluate ^{99m}Tc-MEB and ^{99m}Tc-MIBI as transport protein probe substrates to determine if their disposition is sensitive to changes in hepatic transport protein function as a result of hepatocellular carcinoma and cirrhosis (Chapters 5-6).

3.a. Investigate the hepatobiliary disposition of sorafenib in human hepatocytes.

3.b. Compare the pharmacokinetics and hepatic exposure of ^{99m}Tc-MEB and ^{99m}Tc-MIBI in a patient with hepatocellular carcinoma and Child’s Pugh B cirrhosis vs. healthy human volunteers.

References

1. A. Haimeur, G. Conseil, R. G. Deeley, and S. P. Cole. The MRP-related and BCRP/ABCG2 multidrug resistance proteins: biology, substrate specificity and regulation. *Curr Drug Metab* **5**: 21-53 (2004).

2. Y. Kato, H. Suzuki, and Y. Sugiyama. Toxicological implications of hepatobiliary transporters. *Toxicology* **181-182**: 287-90 (2002).

3. K. Maedaand Y. Sugiyama. Impact of genetic polymorphisms of transporters on the pharmacokinetic, pharmacodynamic and toxicological properties of anionic drugs. *Drug Metab Pharmacokinet* **23**: 223-35 (2008).

4. N. Mizuno, T. Niwa, Y. Yotsumoto, and Y. Sugiyama. Impact of drug transporter studies on drug discovery and development. *Pharmacol Rev* **55**: 425-61 (2003).

5. Y. Shitara, H. Sato, and Y. Sugiyama. Evaluation of drug-drug interaction in the hepatobiliary and renal transport of drugs. *Annu Rev Pharmacol Toxicol* **45**: 689-723 (2005).

6. C. Q. Xia, J. J. Yang, and L. S. Gan. Breast cancer resistance protein in pharmacokinetics and drug-drug interactions. *Expert Opin Drug Metab Toxicol* **1**: 595-611 (2005).

7. T. W. Looand D. M. Clarke. Membrane topology of a cysteine-less mutant of human P-glycoprotein. *J Biol Chem* **270**: 843-8 (1995).

8. L. Schmittand R. Tampe. Structure and mechanism of ABC transporters. *Curr Opin Struct Biol* **12**: 754-60 (2002).

9. F. Thiebaut, T. Tsuruo, H. Hamada, M. M. Gottesman, I. Pastan, and M. C. Willingham. Cellular localization of the multidrug-resistance gene product P-glycoprotein in normal human tissues. *Proc Natl Acad Sci U S A* **84**: 7735-8 (1987).

10. G. A. Graf, L. Yu, W. P. Li, R. Gerard, P. L. Tuma, J. C. Cohen, and H. H. Hobbs. ABCG5 and ABCG8 are obligate heterodimers for protein trafficking and biliary cholesterol excretion. *J Biol Chem* **278**: 48275-82 (2003).

11. P. L. Ee, S. Kamalakaran, D. Tonetti, X. He, D. D. Ross, and W. T. Beck. Identification of a novel estrogen response element in the breast cancer resistance protein (ABCG2) gene. *Cancer Res* **64**: 1247-51 (2004).

12. P. Krishnamurthy, D. D. Ross, T. Nakanishi, K. Bailey-Dell, S. Zhou, K. E. Mercer, B. Sarkadi, B. P. Sorrentino, and J. D. Schuetz. The stem cell

marker Bcrp/ABCG2 enhances hypoxic cell survival through interactions with heme. *J Biol Chem* **279**: 24218-25 (2004).

13. H. Wang, L. Zhou, A. Gupta, R. R. Vethanayagam, Y. Zhang, J. D. Unadkat, and Q. Mao. Regulation of BCRP/ABCG2 expression by progesterone and 17beta-estradiol in human placental BeWo cells. *Am J Physiol Endocrinol Metab* **290**: E798-807 (2006).

14. L. A. Doyle, W. Yang, L. V. Abruzzo, T. Krogmann, Y. Gao, A. K. Rishi, and D. D. Ross. A multidrug resistance transporter from human MCF-7 breast cancer cells. *Proc Natl Acad Sci U S A* **95**: 15665-70 (1998).

15. P. A. Fetsch, A. Abati, T. Litman, K. Morisaki, Y. Honjo, K. Mittal, and S. E. Bates. Localization of the ABCG2 mitoxantrone resistance-associated protein in normal tissues. *Cancer Lett* **235**: 84-92 (2006).

16. S. Kawabata, M. Oka, K. Shiozawa, K. Tsukamoto, K. Nakatomi, H. Soda, M. Fukuda, Y. Ikegami, K. Sugahara, Y. Yamada, S. Kamihira, L. A. Doyle, D. D. Ross, and S. Kohno. Breast cancer resistance protein directly confers SN-38 resistance of lung cancer cells. *Biochem Biophys Res Commun* **280**: 1216-23 (2001).

17. M. Maliepaard, M. A. van Gastelen, L. A. de Jong, D. Pluim, R. C. van Waardenburg, M. C. Ruevekamp-Helmers, B. G. Floot, and J. H. Schellens. Overexpression of the BCRP/MXR/ABCP gene in a topotecan-selected ovarian tumor cell line. *Cancer Res* **59**: 4559-63 (1999).

18. M. Nakagawa, E. Schneider, K. H. Dixon, J. Horton, K. Kelley, C. Morrow, and K. H. Cowan. Reduced intracellular drug accumulation in the absence of P-glycoprotein (mdr1) overexpression in mitoxantrone-resistant human MCF-7 breast cancer cells. *Cancer Res* **52**: 6175-81 (1992).

19. M. J. Zamek-Gliszczynski, K. Nezasa, X. Tian, J. C. Kalvass, N. J. Patel, T. J. Raub, and K. L. Brouwer. The important role of Bcrp (Abcg2) in the biliary excretion of sulfate and glucuronide metabolites of acetaminophen, 4-methylumbelliferone, and harmol in mice. *Mol Pharmacol* **70**: 2127-33 (2006).

20. H. Burger, H. van Tol, A. W. Boersma, M. Brok, E. A. Wiemer, G. Stoter, and K. Nooter. Imatinib mesylate (STI571) is a substrate for the breast cancer resistance protein (BCRP)/ABCG2 drug pump. *Blood* **104**: 2940-2 (2004).

21. N. B. Elkind, Z. Szentpetery, A. Apati, C. Ozvegy-Laczka, G. Varady, O. Ujhelly, K. Szabo, L. Homolya, A. Varadi, L. Buday, G. Keri, K. Nemet, and B. Sarkadi. Multidrug transporter ABCG2 prevents tumor cell death

induced by the epidermal growth factor receptor inhibitor Iressa (ZD1839, Gefitinib). *Cancer Res* **65**: 1770-7 (2005).

22. C. Erlichman, S. A. Boerner, C. G. Hallgren, R. Spieker, X. Y. Wang, C. D. James, G. L. Scheffer, M. Maliepaard, D. D. Ross, K. C. Bible, and S. H. Kaufmann. The HER tyrosine kinase inhibitor CI1033 enhances cytotoxicity of 7-ethyl-10-hydroxycamptothecin and topotecan by inhibiting breast cancer resistance protein-mediated drug efflux. *Cancer Res* **61**: 739-48 (2001).

23. T. Ando, H. Kusuhara, G. Merino, A. I. Alvarez, A. H. Schinkel, and Y. Sugiyama. Involvement of breast cancer resistance protein (ABCG2) in the biliary excretion mechanism of fluoroquinolones. *Drug Metab Dispos* **35**: 1873-9 (2007).

24. G. D. Kruh, H. Zeng, P. A. Rea, G. Liu, Z. S. Chen, K. Lee, and M. G. Belinsky. MRP subfamily transporters and resistance to anticancer agents. *J Bioenerg Biomembr* **33**: 493-501 (2001).

25. M. Buchler, J. Konig, M. Brom, J. Kartenbeck, H. Spring, T. Horie, and D. Keppler. cDNA cloning of the hepatocyte canalicular isoform of the multidrug resistance protein, cMrp, reveals a novel conjugate export pump deficient in hyperbilirubinemic mutant rats. *J Biol Chem* **271**: 15091-8 (1996).

26. D. Kepplerand J. Kartenbeck. The canalicular conjugate export pump encoded by the cmrp/cmoat gene. *Prog Liver Dis* **14**: 55-67 (1996).

27. T. P. Schaub, J. Kartenbeck, J. Konig, H. Spring, J. Dorsam, G. Staehler, S. Storkel, W. F. Thon, and D. Keppler. Expression of the MRP2 gene-encoded conjugate export pump in human kidney proximal tubules and in renal cell carcinoma. *J Am Soc Nephrol* **10**: 1159-69 (1999).

28. G. E. Sandusky, K. S. Mintze, S. E. Pratt, and A. H. Dantzig. Expression of multidrug resistance-associated protein 2 (MRP2) in normal human tissues and carcinomas using tissue microarrays. *Histopathology* **41**: 65-74 (2002).

29. H. E. Meyer zu Schwabedissen, G. Jedlitschky, M. Gratz, S. Haenisch, K. Linnemann, C. Fusch, I. Cascorbi, and H. K. Kroemer. Variable expression of MRP2 (ABCC2) in human placenta: influence of gestational age and cellular differentiation. *Drug Metab Dispos* **33**: 896-904 (2005).

30. Y. Cui, J. Konig, J. K. Buchholz, H. Spring, I. Leier, and D. Keppler. Drug resistance and ATP-dependent conjugate transport mediated by the apical multidrug resistance protein, MRP2, permanently expressed in human and canine cells. *Mol Pharmacol* **55**: 929-37 (1999).

31. R. Evers, M. Kool, L. van Deemter, H. Janssen, J. Calafat, L. C. Oomen, C. C. Paulusma, R. P. Oude Elferink, F. Baas, A. H. Schinkel, and P. Borst. Drug export activity of the human canalicular multispecific organic anion transporter in polarized kidney MDCK cells expressing cMOAT (MRP2) cDNA. *J Clin Invest* **101**: 1310-9 (1998).

32. T. Kamisako, I. Leier, Y. Cui, J. Konig, U. Buchholz, J. Hummel-Eisenbeiss, and D. Keppler. Transport of monoglucuronosyl and bisglucuronosyl bilirubin by recombinant human and rat multidrug resistance protein 2. *Hepatology* **30**: 485-90 (1999).

33. K. Kopplow, K. Letschert, J. Konig, B. Walter, and D. Keppler. Human hepatobiliary transport of organic anions analyzed by quadruple-transfected cells. *Mol Pharmacol* **68**: 1031-8 (2005).

34. C. C. Paulusma, P. J. Bosma, G. J. Zaman, C. T. Bakker, M. Otter, G. L. Scheffer, R. J. Scheper, P. Borst, and R. P. Oude Elferink. Congenital jaundice in rats with a mutation in a multidrug resistance-associated protein gene. *Science* **271**: 1126-8 (1996).

35. J. Konig, D. Rost, Y. Cui, and D. Keppler. Characterization of the human multidrug resistance protein isoform MRP3 localized to the basolateral hepatocyte membrane. *Hepatology* **29**: 1156-63 (1999).

36. M. Kuroda, Y. Kobayashi, Y. Tanaka, T. Itani, R. Mifuji, J. Araki, M. Kaito, and Y. Adachi. Increased hepatic and renal expressions of multidrug resistance-associated protein 3 in Eisai hyperbilirubinuria rats. *J Gastroenterol Hepatol* **19**: 146-53 (2004).

37. I. N. Dubinand F. B. Johnson. Chronic idiopathic jaundice with unidentified pigment in liver cells; a new clinicopathologic entity with a report of 12 cases. *Medicine (Baltimore)* **33**: 155-97 (1954).

38. H. Sprinzand R. S. Nelson. Persistent non-hemolytic hyperbilirubinemia associated with lipochrome-like pigment in liver cells: report of four cases. *Ann Intern Med* **41**: 952-62 (1954).

39. H. Tsujii, J. Konig, D. Rost, B. Stockel, U. Leuschner, and D. Keppler. Exon-intron organization of the human multidrug-resistance protein 2 (MRP2) gene mutated in Dubin-Johnson syndrome. *Gastroenterology* **117**: 653-60 (1999).

40. M. Kool, M. van der Linden, M. de Haas, G. L. Scheffer, J. M. de Vree, A. J. Smith, G. Jansen, G. J. Peters, N. Ponne, R. J. Scheper, R. P. Elferink, F. Baas, and P. Borst. MRP3, an organic anion transporter able to transport anti-cancer drugs. *Proc Natl Acad Sci U S A* **96**: 6914-9 (1999).

41. D. Rost, J. Konig, G. Weiss, E. Klar, W. Stremmel, and D. Keppler. Expression and localization of the multidrug resistance proteins MRP2 and MRP3 in human gallbladder epithelia. *Gastroenterology* **121**: 1203-8 (2001).

42. G. L. Scheffer, M. Kool, M. de Haas, J. M. de Vree, A. C. Pijnenborg, D. K. Bosman, R. P. Elferink, P. van der Valk, P. Borst, and R. J. Scheper. Tissue distribution and induction of human multidrug resistant protein 3. *Lab Invest* **82**: 193-201 (2002).

43. G. Zollner, P. Fickert, D. Silbert, A. Fuchsbichler, H. U. Marschall, K. Zatloukal, H. Denk, and M. Trauner. Adaptive changes in hepatobiliary transporter expression in primary biliary cirrhosis. *J Hepatol* **38**: 717-27 (2003).

44. J. Shoda, M. Kano, K. Oda, J. Kamiya, Y. Nimura, H. Suzuki, Y. Sugiyama, H. Miyazaki, T. Todoroki, S. Stengelin, W. Kramer, Y. Matsuzaki, and N. Tanaka. The expression levels of plasma membrane transporters in the cholestatic liver of patients undergoing biliary drainage and their association with the impairment of biliary secretory function. *Am J Gastroenterol* **96**: 3368-78 (2001).

45. B. Hagenbuchand C. Gui. Xenobiotic transporters of the human organic anion transporting polypeptides (OATP) family. *Xenobiotica* **38**: 778-801 (2008).

46. T. Mikkaichi, T. Suzuki, M. Tanemoto, S. Ito, and T. Abe. The organic anion transporter (OATP) family. *Drug Metab Pharmacokinet* **19**: 171-9 (2004).

47. L. M. Satlin, V. Amin, and A. W. Wolkoff. Organic anion transporting polypeptide mediates organic anion/HCO3- exchange. *J Biol Chem* **272**: 26340-5 (1997).

48. L. Li, T. K. Lee, P. J. Meier, and N. Ballatori. Identification of glutathione as a driving force and leukotriene C4 as a substrate for oatp1, the hepatic sinusoidal organic solute transporter. *J Biol Chem* **273**: 16184-91 (1998).

49. L. Li, P. J. Meier, and N. Ballatori. Oatp2 mediates bidirectional organic solute transport: a role for intracellular glutathione. *Mol Pharmacol* **58**: 335-40 (2000).

50. A. Ayrtonand P. Morgan. Role of transport proteins in drug absorption, distribution and excretion. *Xenobiotica* **31**: 469-97 (2001).

51. T. D. Bjornsson, J. T. Callaghan, H. J. Einolf, V. Fischer, L. Gan, S. Grimm, J. Kao, S. P. King, G. Miwa, L. Ni, G. Kumar, J. McLeod, R. S.

Obach, S. Roberts, A. Roe, A. Shah, F. Snikeris, J. T. Sullivan, D. Tweedie, J. M. Vega, J. Walsh, and S. A. Wrighton. The conduct of in vitro and in vivo drug-drug interaction studies: a Pharmaceutical Research and Manufacturers of America (PhRMA) perspective. *Drug Metab Dispos* **31**: 815-32 (2003).

52. O. Briz, M. A. Serrano, R. I. Maclas, J. Gonzalez-Gallego, and J. J. Marin. Role of organic anion-transporting polypeptides, OATP-A, OATP-C and OATP-8, in the human placenta-maternal liver tandem excretory pathway for foetal bilirubin. *Biochem J* **371**: 897-905 (2003).

53. Y. Cui, J. Konig, I. Leier, U. Buchholz, and D. Keppler. Hepatic uptake of bilirubin and its conjugates by the human organic anion transporter SLC21A6. *J Biol Chem* **276**: 9626-30 (2001).

54. D. Jung, M. Podvinec, U. A. Meyer, D. J. Mangelsdorf, M. Fried, P. J. Meier, and G. A. Kullak-Ublick. Human organic anion transporting polypeptide 8 promoter is transactivated by the farnesoid X receptor/bile acid receptor. *Gastroenterology* **122**: 1954-66 (2002).

55. G. Zollner, P. Fickert, R. Zenz, A. Fuchsbichler, C. Stumptner, L. Kenner, P. Ferenci, R. E. Stauber, G. J. Krejs, H. Denk, K. Zatloukal, and M. Trauner. Hepatobiliary transporter expression in percutaneous liver biopsies of patients with cholestatic liver diseases. *Hepatology* **33**: 633-46 (2001).

56. G. Acocella, F. B. Nicolis, and L. T. Tenconi. The effect of an intravenous infusion of rifamycin SV on the excretion of bilirubin, bromsulphalein, and indocyanine green in man. *Gastroenterology* **49**: 521-5 (1965).

57. S. D. Campbell, S. M. de Morais, and J. J. Xu. Inhibition of human organic anion transporting polypeptide OATP 1B1 as a mechanism of drug-induced hyperbilirubinemia. *Chem Biol Interact* **150**: 179-87 (2004).

58. M. J. Dresser, M. K. Leabman, and K. M. Giacomini. Transporters involved in the elimination of drugs in the kidney: organic anion transporters and organic cation transporters. *J Pharm Sci* **90**: 397-421 (2001).

59. H. Koepsell, V. Gorboulev, and P. Arndt. Molecular pharmacology of organic cation transporters in kidney. *J Membr Biol* **167**: 103-17 (1999).

60. S. H. Wright. Role of organic cation transporters in the renal handling of therapeutic agents and xenobiotics. *Toxicol Appl Pharmacol* **204**: 309-19 (2005).

61. H. Koepsell, B. M. Schmitt, and V. Gorboulev. Organic cation transporters. *Rev Physiol Biochem Pharmacol* **150**: 36-90 (2003).

62. V. Gorboulev, J. C. Ulzheimer, A. Akhoundova, I. Ulzheimer-Teuber, U. Karbach, S. Quester, C. Baumann, F. Lang, A. E. Busch, and H. Koepsell. Cloning and characterization of two human polyspecific organic cation transporters. *DNA Cell Biol* **16**: 871-81 (1997).

63. L. Zhang, M. J. Dresser, A. T. Gray, S. C. Yost, S. Terashita, and K. M. Giacomini. Cloning and functional expression of a human liver organic cation transporter. *Mol Pharmacol* **51**: 913-21 (1997).

64. Y. Urakami, M. Akazawa, H. Saito, M. Okuda, and K. Inui. cDNA cloning, functional characterization, and tissue distribution of an alternatively spliced variant of organic cation transporter hOCT2 predominantly expressed in the human kidney. *J Am Soc Nephrol* **13**: 1703-10 (2002).

65. S. Verhaagh, N. Schweifer, D. P. Barlow, and R. Zwart. Cloning of the mouse and human solute carrier 22a3 (Slc22a3/SLC22A3) identifies a conserved cluster of three organic cation transporters on mouse chromosome 17 and human 6q26-q27. *Genomics* **55**: 209-18 (1999).

66. J. W. Jonkerand A. H. Schinkel. Pharmacological and physiological functions of the polyspecific organic cation transporters: OCT1, 2, and 3 (SLC22A1-3). *J Pharmacol Exp Ther* **308**: 2-9 (2004).

67. H. Koepsell. Polyspecific organic cation transporters: their functions and interactions with drugs. *Trends Pharmacol Sci* **25**: 375-81 (2004).

68. D. L. Bourdet, J. B. Pritchard, and D. R. Thakker. Differential substrate and inhibitory activities of ranitidine and famotidine toward human organic cation transporter 1 (hOCT1; SLC22A1), hOCT2 (SLC22A2), and hOCT3 (SLC22A3). *J Pharmacol Exp Ther* **315**: 1288-97 (2005).

69. N. Kimura, S. Masuda, Y. Tanihara, H. Ueo, M. Okuda, T. Katsura, and K. Inui. Metformin is a superior substrate for renal organic cation transporter OCT2 rather than hepatic OCT1. *Drug Metab Pharmacokinet* **20**: 379-86 (2005).

70. S. Abel, D. J. Nichols, C. J. Brearley, and M. D. Eve. Effect of cimetidine and ranitidine on pharmacokinetics and pharmacodynamics of a single dose of dofetilide. *Br J Clin Pharmacol* **49**: 64-71 (2000).

71. B. Feng, R. S. Obach, A. H. Burstein, D. J. Clark, S. M. de Morais, and H. M. Faessel. Effect of human renal cationic transporter inhibition on the pharmacokinetics of varenicline, a new therapy for smoking cessation: an in vitro-in vivo study. *Clin Pharmacol Ther* **83**: 567-76 (2008).

72. A. Somogyi, C. Stockley, J. Keal, P. Rolan, and F. Bochner. Reduction of metformin renal tubular secretion by cimetidine in man. *Br J Clin Pharmacol* **23**: 545-51 (1987).

73. H. Koepselland H. Endou. The SLC22 drug transporter family. *Pflugers Arch* **447**: 666-76 (2004).

74. W. Sun, R. R. Wu, P. D. van Poelje, and M. D. Erion. Isolation of a family of organic anion transporters from human liver and kidney. *Biochem Biophys Res Commun* **283**: 417-22 (2001).

75. S. A. Eraly, K. T. Bush, R. V. Sampogna, V. Bhatnagar, and S. K. Nigam. The molecular pharmacology of organic anion transporters: from DNA to FDA? *Mol Pharmacol* **65**: 479-87 (2004).

76. E. Link, S. Parish, J. Armitage, L. Bowman, S. Heath, F. Matsuda, I. Gut, M. Lathrop, and R. Collins. SLCO1B1 variants and statin-induced myopathy--a genomewide study. *N Engl J Med* **359**: 789-99 (2008).

77. S. N. Barnes, L. M. Aleksunes, L. Augustine, G. L. Scheffer, M. J. Goedken, A. B. Jakowski, I. M. Pruimboom-Brees, N. J. Cherrington, and J. E. Manautou. Induction of hepatobiliary efflux transporters in acetaminophen-induced acute liver failure cases. *Drug Metab Dispos* **35**: 1963-9 (2007).

78. C. Pauli-Magnusand P. J. Meier. Hepatobiliary transporters and drug-induced cholestasis. *Hepatology* **44**: 778-87 (2006).

79. C. J. Endres, P. Hsiao, F. S. Chung, and J. D. Unadkat. The role of transporters in drug interactions. *Eur J Pharm Sci* **27**: 501-17 (2006).

80. M. Li, G. D. Anderson, and J. Wang. Drug-drug interactions involving membrane transporters in the human kidney. *Expert Opin Drug Metab Toxicol* **2**: 505-32 (2006).

81. S. Eyal, P. Hsiao, and J. D. Unadkat. Drug interactions at the blood-brain barrier: Fact or fantasy? *Pharmacol Ther* (2009).

82. L. Zhang, J. M. Strong, W. Qiu, L. J. Lesko, and S. M. Huang. Scientific perspectives on drug transporters and their role in drug interactionst. *Mol Pharm* **3**: 62-9 (2006).

83. B. Hoenerand S. E. Patterson. Nitrofurantoin disposition. *Clin Pharmacol Ther* **29**: 808-16 (1981).

84. X. Tian, M. J. Zamek-Gliszczynski, J. Li, A. S. Bridges, K. Nezasa, N. J. Patel, T. J. Raub, and K. L. Brouwer. Multidrug resistance-associated

protein 2 is primarily responsible for the biliary excretion of fexofenadine in mice. *Drug Metab Dispos* **36**: 61-4 (2008).

85. B. Swift, X. Tian, and K. L. Brouwer. Integration of preclinical and clinical data with pharmacokinetic modeling and simulation to evaluate fexofenadine as a probe for hepatobiliary transport function. *Pharm Res* **26**: 1942-51 (2009).

86. P. Acharya, M. P. O'Connor, J. W. Polli, A. Ayrton, H. Ellens, and J. Bentz. Kinetic identification of membrane transporters that assist P-glycoprotein-mediated transport of digoxin and loperamide through a confluent monolayer of MDCKII-hMDR1 cells. *Drug Metab Dispos* **36**: 452-60 (2008).

87. C. Martin, G. Berridge, C. F. Higgins, P. Mistry, P. Charlton, and R. Callaghan. Communication between multiple drug binding sites on P-glycoprotein. *Mol Pharmacol* **58**: 624-32 (2000).

88. A. B. Shapiro, K. Fox, P. Lam, and V. Ling. Stimulation of P-glycoprotein-mediated drug transport by prazosin and progesterone. Evidence for a third drug-binding site. *Eur J Biochem* **259**: 841-50 (1999).

89. K. Heredi-Szabo, H. Glavinas, E. Kis, D. Mehn, G. Bathori, Z. Veres, L. Kobori, O. von Richter, K. Jemnitz, and P. Krajcsi. Multidrug resistance protein 2-mediated estradiol-17beta-D-glucuronide transport potentiation: in vitro-in vivo correlation and species specificity. *Drug Metab Dispos* **37**: 794-801 (2009).

90. N. Zelcer, M. T. Huisman, G. Reid, P. Wielinga, P. Breedveld, A. Kuil, P. Knipscheer, J. H. Schellens, A. H. Schinkel, and P. Borst. Evidence for two interacting ligand binding sites in human multidrug resistance protein 2 (ATP binding cassette C2). *J Biol Chem* **278**: 23538-44 (2003).

91. L. Sasongko, J. M. Link, M. Muzi, D. A. Mankoff, X. Yang, A. C. Collier, S. C. Shoner, and J. D. Unadkat. Imaging P-glycoprotein transport activity at the human blood-brain barrier with positron emission tomography. *Clin Pharmacol Ther* **77**: 503-14 (2005).

92. C. L. Cummins, W. Jacobsen, and L. Z. Benet. Unmasking the dynamic interplay between intestinal P-glycoprotein and CYP3A4. *J Pharmacol Exp Ther* **300**: 1036-45 (2002).

93. R. B. Kim, C. Wandel, B. Leake, M. Cvetkovic, M. F. Fromm, P. J. Dempsey, M. M. Roden, F. Belas, A. K. Chaudhary, D. M. Roden, A. J. Wood, and G. R. Wilkinson. Interrelationship between substrates and inhibitors of human CYP3A and P-glycoprotein. *Pharm Res* **16**: 408-14 (1999).

94. C. Etievant, P. Schambel, Y. Guminski, J. M. Barret, T. Imbert, and B. T. Hill. Requirements for P-glycoprotein recognition based on structure-activity relationships in the podophyllotoxin series. *Anticancer Drug Des* **13**: 317-36 (1998).

95. A. Seelig. A general pattern for substrate recognition by P-glycoprotein. *Eur J Biochem* **251**: 252-61 (1998).

96. H. Jeongand W. L. Chiou. Role of P-glycoprotein in the hepatic metabolism of tacrolimus. *Xenobiotica* **36**: 1-13 (2006).

97. Y. Y. Lau, C. Y. Wu, H. Okochi, and L. Z. Benet. Ex situ inhibition of hepatic uptake and efflux significantly changes metabolism: hepatic enzyme-transporter interplay. *J Pharmacol Exp Ther* **308**: 1040-5 (2004).

98. C. Y. Wuand L. Z. Benet. Disposition of tacrolimus in isolated perfused rat liver: influence of troleandomycin, cyclosporine, and gg918. *Drug Metab Dispos* **31**: 1292-5 (2003).

99. P. H. Hinderlingand D. Hartmann. Pharmacokinetics of digoxin and main metabolites/derivatives in healthy humans. *Ther Drug Monit* **13**: 381-401 (1991).

100. B. Lacarelle, R. Rahmani, G. de Sousa, A. Durand, M. Placidi, and J. P. Cano. Metabolism of digoxin, digoxigenin digitoxosides and digoxigenin in human hepatocytes and liver microsomes. *Fundam Clin Pharmacol* **5**: 567-82 (1991).

101. M. E. Cavet, M. West, and N. L. Simmons. Transport and epithelial secretion of the cardiac glycoside, digoxin, by human intestinal epithelial (Caco-2) cells. *Br J Pharmacol* **118**: 1389-96 (1996).

102. K. M. Jalava, J. Partanen, and P. J. Neuvonen. Itraconazole decreases renal clearance of digoxin. *Ther Drug Monit* **19**: 609-13 (1997).

103. K. S. Fenner, M. D. Troutman, S. Kempshall, J. A. Cook, J. A. Ware, D. A. Smith, and C. A. Lee. Drug-drug interactions mediated through P-glycoprotein: clinical relevance and in vitro-in vivo correlation using digoxin as a probe drug. *Clin Pharmacol Ther* **85**: 173-81 (2009).

104. A. Hedman, B. Angelin, A. Arvidsson, O. Beck, R. Dahlqvist, B. Nilsson, M. Olsson, and K. Schenck-Gustafsson. Digoxin-verapamil interaction: reduction of biliary but not renal digoxin clearance in humans. *Clin Pharmacol Ther* **49**: 256-62 (1991).

105. K. E. Pedersen, B. D. Christiansen, N. A. Klitgaard, and F. Nielsen-Kudsk. Effect of quinidine on digoxin bioavailability. *Eur J Clin Pharmacol* **24**: 41-7 (1983).

106. H. Rameis. Quinidine-digoxin interaction: are the pharmacokinetics of both drugs altered? *Int J Clin Pharmacol Ther Toxicol* **23**: 145-53 (1985).

107. D. D. Brown, R. Spector, and R. P. Juhl. Drug interactions with digoxin. *Drugs* **20**: 198-206 (1980).

108. R. Ding, Y. Tayrouz, K. D. Riedel, J. Burhenne, J. Weiss, G. Mikus, and W. E. Haefeli. Substantial pharmacokinetic interaction between digoxin and ritonavir in healthy volunteers. *Clin Pharmacol Ther* **76**: 73-84 (2004).

109. G. Koren, C. Woodland, and S. Ito. Toxic digoxin-drug interactions: the major role of renal P-glycoprotein. *Vet Hum Toxicol* **40**: 45-6 (1998).

110. G. A. Kullak-Ublick, M. G. Ismair, B. Stieger, L. Landmann, R. Huber, F. Pizzagalli, K. Fattinger, P. J. Meier, and B. Hagenbuch. Organic anion-transporting polypeptide B (OATP-B) and its functional comparison with three other OATPs of human liver. *Gastroenterology* **120**: 525-33 (2001).

111. T. Mikkaichi, T. Suzuki, T. Onogawa, M. Tanemoto, H. Mizutamari, M. Okada, T. Chaki, S. Masuda, T. Tokui, N. Eto, M. Abe, F. Satoh, M. Unno, T. Hishinuma, K. Inui, S. Ito, J. Goto, and T. Abe. Isolation and characterization of a digoxin transporter and its rat homologue expressed in the kidney. *Proc Natl Acad Sci U S A* **101**: 3569-74 (2004).

112. T. Watanabe, H. Kusuhara, K. Maeda, Y. Shitara, and Y. Sugiyama. Physiologically based pharmacokinetic modeling to predict transporter-mediated clearance and distribution of pravastatin in humans. *J Pharmacol Exp Ther* **328**: 652-62 (2009).

113. G. A. Bellerand A. J. Sinusas. Experimental studies of the physiologic properties of technetium-99m isonitriles. *Am J Cardiol* **66**: 5E-8E (1990).

114. S. Mobasseriand R. C. Hendel. Cardiac imaging in women: use of radionuclide myocardial perfusion imaging and echocardiography for acute chest pain. *Cardiol Rev* **10**: 149-60 (2002).

115. G. C. Ravizzini, M. W. Hanson, L. K. Shaw, T. Z. Wong, R. J. Hagge, R. A. Pagnanelli, D. Jain, H. S. Lima, Jr., R. E. Coleman, and S. Borges-Neto. Efficiency comparison between 99m Tc-tetrofosmin and 99m Tc-sestamibi myocardial perfusion studies. *Nucl Med Commun* **23**: 203-8 (2002).

116. E. Barbarics, J. F. Kronauge, C. E. Costello, G. A. Janoki, B. L. Holman, A. Davison, and A. G. Jones. In vivo metabolism of the technetium isonitrile complex [Tc(2-ethoxy-2-methyl-1-isocyanopropane)6]+. *Nucl Med Biol* **21**: 583-91 (1994).

117. N. H. Hendrikse, E. J. Franssen, W. T. van der Graaf, C. Meijer, D. A. Piers, W. Vaalburg, and E. G. de Vries. 99mTc-sestamibi is a substrate for P-glycoprotein and the multidrug resistance-associated protein. *Br J Cancer* **77**: 353-8 (1998).

118. J. Vergote, J. L. Moretti, E. G. de Vries, and A. Garnier-Suillerot. Comparison of the kinetics of active efflux of 99mTc-MIBI in cells with P-glycoprotein-mediated and multidrug-resistance protein-associated multidrug-resistance phenotypes. *Eur J Biochem* **252**: 140-6 (1998).

119. B. Joseph, K. K. Bhargava, H. Malhi, M. L. Schilsky, D. Jain, C. J. Palestro, and S. Gupta. Sestamibi is a substrate for MDR1 and MDR2 P-glycoprotein genes. *Eur J Nucl Med Mol Imaging* **30**: 1024-31 (2003).

120. M. L. Chiu, J. F. Kronauge, and D. Piwnica-Worms. Effect of mitochondrial and plasma membrane potentials on accumulation of hexakis (2-methoxyisobutylisonitrile) technetium(I) in cultured mouse fibroblasts. *J Nucl Med* **31**: 1646-53 (1990).

121. M. Agrawal, J. Abraham, F. M. Balis, M. Edgerly, W. D. Stein, S. Bates, T. Fojo, and C. C. Chen. Increased 99mTc-sestamibi accumulation in normal liver and drug-resistant tumors after the administration of the glycoprotein inhibitor, XR9576. *Clin Cancer Res* **9**: 650-6 (2003).

122. C. C. Chen, B. Meadows, J. Regis, G. Kalafsky, T. Fojo, J. A. Carrasquillo, and S. E. Bates. Detection of in vivo P-glycoprotein inhibition by PSC 833 using Tc-99m sestamibi. *Clin Cancer Res* **3**: 545-52 (1997).

123. G. D. Luker, P. M. Fracasso, J. Dobkin, and D. Piwnica-Worms. Modulation of the multidrug resistance P-glycoprotein: detection with technetium-99m-sestamibi in vivo. *J Nucl Med* **38**: 369-72 (1997).

124. M. Wong, S. Evans, L. P. Rivory, J. M. Hoskins, G. J. Mann, D. Farlow, C. L. Clarke, R. L. Balleine, and H. Gurney. Hepatic technetium Tc 99m-labeled sestamibi elimination rate and ABCB1 (MDR1) genotype as indicators of ABCB1 (P-glycoprotein) activity in patients with cancer. *Clin Pharmacol Ther* **77**: 33-42 (2005).

125. N. H. Hendrikse, F. Kuipers, C. Meijer, R. Havinga, C. M. Bijleveld, W. T. van der Graaf, W. Vaalburg, and E. G. de Vries. In vivo imaging of hepatobiliary transport function mediated by multidrug resistance

associated protein and P-glycoprotein. *Cancer Chemother Pharmacol* **54**: 131-8 (2004).

126. N. H. Hendrikse, E. G. de Vries, L. Eriks-Fluks, W. T. van der Graaf, G. A. Hospers, A. T. Willemsen, W. Vaalburg, and E. J. Franssen. A new in vivo method to study P-glycoprotein transport in tumors and the blood-brain barrier. *Cancer Res* **59**: 2411-6 (1999).

127. N. H. Hendrikse, A. H. Schinkel, E. G. de Vries, E. Fluks, W. T. Van der Graaf, A. T. Willemsen, W. Vaalburg, and E. J. Franssen. Complete in vivo reversal of P-glycoprotein pump function in the blood-brain barrier visualized with positron emission tomography. *Br J Pharmacol* **124**: 1413-8 (1998).

128. Y. Adachi, H. Suzuki, and Y. Sugiyama. Quantitative evaluation of the function of small intestinal P-glycoprotein: comparative studies between in situ and in vitro. *Pharm Res* **20**: 1163-9 (2003).

129. J. Bart, A. T. Willemsen, H. J. Groen, W. T. van der Graaf, T. D. Wegman, W. Vaalburg, E. G. de Vries, and N. H. Hendrikse. Quantitative assessment of P-glycoprotein function in the rat blood-brain barrier by distribution volume of [11C]verapamil measured with PET. *Neuroimage* **20**: 1775-82 (2003).

130. C. Dagenais, J. Zong, J. Ducharme, and G. M. Pollack. Effect of mdr1a P-glycoprotein gene disruption, gender, and substrate concentration on brain uptake of selected compounds. *Pharm Res* **18**: 957-63 (2001).

131. M. Eichelbaum, M. Ende, G. Remberg, M. Schomerus, and H. J. Dengler. The metabolism of DL-[14C]verapamil in man. *Drug Metab Dispos* **7**: 145-8 (1979).

132. G. Mikus, M. Eichelbaum, C. Fischer, S. Gumulka, U. Klotz, and H. K. Kroemer. Interaction of verapamil and cimetidine: stereochemical aspects of drug metabolism, drug disposition and drug action. *J Pharmacol Exp Ther* **253**: 1042-8 (1990).

133. D. R. Abernethy, I. W. Wainer, and A. I. Anacleto. Verapamil metabolite exposure in older and younger men during steady-state oral verapamil administration. *Drug Metab Dispos* **28**: 760-5 (2000).

134. C. Pauli-Magnus, O. von Richter, O. Burk, A. Ziegler, T. Mettang, M. Eichelbaum, and M. F. Fromm. Characterization of the major metabolites of verapamil as substrates and inhibitors of P-glycoprotein. *J Pharmacol Exp Ther* **293**: 376-82 (2000).

135. A. Levchenko, B. M. Mehta, J. B. Lee, J. L. Humm, F. Augensen, O. Squire, P. J. Kothari, R. D. Finn, E. F. Leonard, and S. M. Larson. Evaluation of 11C-colchicine for PET imaging of multiple drug resistance. *J Nucl Med* **41**: 493-501 (2000).

136. A. Gangloff, W. A. Hsueh, A. L. Kesner, D. O. Kiesewetter, B. S. Pio, M. D. Pegram, M. Beryt, A. Townsend, J. Czernin, M. E. Phelps, and D. H. Silverman. Estimation of paclitaxel biodistribution and uptake in human-derived xenografts in vivo with (18)F-fluoropaclitaxel. *J Nucl Med* **46**: 1866-71 (2005).

137. P. H. Elsinga, N. H. Hendrikse, J. Bart, A. van Waarde, and W. Vaalburg. Positron emission tomography studies on binding of central nervous system drugs and P-glycoprotein function in the rodent brain. *Mol Imaging Biol* **7**: 37-44 (2005).

138. J. Bart, E. C. Dijkers, T. D. Wegman, E. G. de Vries, W. T. van der Graaf, H. J. Groen, W. Vaalburg, A. T. Willemsen, and N. H. Hendrikse. New positron emission tomography tracer [(11)C]carvedilol reveals P-glycoprotein modulation kinetics. *Br J Pharmacol* **145**: 1045-51 (2005).

139. E. F. de Vries, R. Kortekaas, A. van Waarde, D. Dijkstra, P. H. Elsinga, and W. Vaalburg. Synthesis and evaluation of dopamine D3 receptor antagonist 11C-GR218231 as PET tracer for P-glycoprotein. *J Nucl Med* **46**: 1384-92 (2005).

140. K. Ishiwata, K. Kawamura, K. Yanai, and N. H. Hendrikse. In vivo evaluation of P-glycoprotein modulation of 8 PET radioligands used clinically. *J Nucl Med* **48**: 81-7 (2007).

141. P. H. Elsinga, N. H. Hendrikse, J. Bart, W. Vaalburg, and A. van Waarde. PET Studies on P-glycoprotein function in the blood-brain barrier: how it affects uptake and binding of drugs within the CNS. *Curr Pharm Des* **10**: 1493-503 (2004).

142. G. T. Tucker, J. B. Houston, and S. M. Huang. Optimizing drug development: strategies to assess drug metabolism/transporter interaction potential--towards a consensus. *Br J Clin Pharmacol* **52**: 107-17 (2001).

143. S. Matsushima, K. Maeda, H. Hayashi, Y. Debori, A. H. Schinkel, J. D. Schuetz, H. Kusuhara, and Y. Sugiyama. Involvement of multiple efflux transporters in hepatic disposition of fexofenadine. *Mol Pharmacol* (2008).

144. Y. Imai, M. Nakane, K. Kage, S. Tsukahara, E. Ishikawa, T. Tsuruo, Y. Miki, and Y. Sugimoto. C421A polymorphism in the human breast cancer resistance protein gene is associated with low expression of Q141K protein and low-level drug resistance. *Mol Cancer Ther* **1**: 611-6 (2002).

145. C. Kondo, H. Suzuki, M. Itoda, S. Ozawa, J. Sawada, D. Kobayashi, I. Ieiri, K. Mine, K. Ohtsubo, and Y. Sugiyama. Functional analysis of SNPs variants of BCRP/ABCG2. *Pharm Res* **21**: 1895-903 (2004).

146. S. Mizuarai, N. Aozasa, and H. Kotani. Single nucleotide polymorphisms result in impaired membrane localization and reduced atpase activity in multidrug transporter ABCG2. *Int J Cancer* **109**: 238-46 (2004).

147. A. Tamura, K. Wakabayashi, Y. Onishi, M. Takeda, Y. Ikegami, S. Sawada, M. Tsuji, Y. Matsuda, and T. Ishikawa. Re-evaluation and functional classification of non-synonymous single nucleotide polymorphisms of the human ATP-binding cassette transporter ABCG2. *Cancer Sci* **98**: 231-9 (2007).

148. S. Yoshioka, K. Katayama, C. Okawa, S. Takahashi, S. Tsukahara, J. Mitsuhashi, and Y. Sugimoto. The identification of two germ-line mutations in the human breast cancer resistance protein gene that result in the expression of a low/non-functional protein. *Pharm Res* **24**: 1108-17 (2007).

149. G. Merino, J. W. Jonker, E. Wagenaar, A. E. van Herwaarden, and A. H. Schinkel. The breast cancer resistance protein (BCRP/ABCG2) affects pharmacokinetics, hepatobiliary excretion, and milk secretion of the antibiotic nitrofurantoin. *Mol Pharmacol* **67**: 1758-64 (2005).

150. X. Wangand M. E. Morris. Effects of the flavonoid chrysin on nitrofurantoin pharmacokinetics in rats: potential involvement of ABCG2. *Drug Metab Dispos* **35**: 268-74 (2007).

151. P. M. Gerk, R. J. Kuhn, N. S. Desai, and P. J. McNamara. Active transport of nitrofurantoin into human milk. *Pharmacotherapy* **21**: 669-75 (2001).

152. Y. Zhang, H. Wang, J. D. Unadkat, and Q. Mao. Breast cancer resistance protein 1 limits fetal distribution of nitrofurantoin in the pregnant mouse. *Drug Metab Dispos* **35**: 2154-8 (2007).

153. J. D. Conklin. The pharmacokinetics of nitrofurantoin and its related bioavailability. *Antibiot Chemother* **25**: 233-52 (1978).

154. K. K. Adkison, S. S. Vaidya, D. Y. Lee, S. H. Koo, L. Li, A. A. Mehta, A. S. Gross, J. W. Polli, Y. Lou, and E. J. Lee. The ABCG2 C421A polymorphism does not affect oral nitrofurantoin pharmacokinetics in healthy Chinese male subjects. *Br J Clin Pharmacol* **66**: 233-9 (2008).

155. A. Sparreboom, H. Gelderblom, S. Marsh, R. Ahluwalia, R. Obach, P. Principe, C. Twelves, J. Verweij, and H. L. McLeod. Diflomotecan

pharmacokinetics in relation to ABCG2 421C>A genotype. *Clin Pharmacol Ther* **76**: 38-44 (2004).

156. A. Sparreboom, W. J. Loos, H. Burger, T. M. Sissung, J. Verweij, W. D. Figg, K. Nooter, and H. Gelderblom. Effect of ABCG2 genotype on the oral bioavailability of topotecan. *Cancer Biol Ther* **4**: 650-8 (2005).

157. H. Schroderand D. E. Campbell. Absorption, metabolism, and excretion of salicylazosulfapyridine in man. *Clin Pharmacol Ther* **13**: 539-51 (1972).

158. K. M. Das, J. R. Chowdhury, B. Zapp, and J. W. Fara. Small bowel absorption of sulfasalazine and its hepatic metabolism in human beings, cats, and rats. *Gastroenterology* **77**: 280-4 (1979).

159. H. Zaher, A. A. Khan, J. Palandra, T. G. Brayman, L. Yu, and J. A. Ware. Breast cancer resistance protein (Bcrp/abcg2) is a major determinant of sulfasalazine absorption and elimination in the mouse. *Mol Pharm* **3**: 55-61 (2006).

160. B. L. Urquhart, J. A. Ware, R. G. Tirona, R. H. Ho, B. F. Leake, U. I. Schwarz, H. Zaher, J. Palandra, J. C. Gregor, G. K. Dresser, and R. B. Kim. Breast cancer resistance protein (ABCG2) and drug disposition: intestinal expression, polymorphisms and sulfasalazine as an in vivo probe. *Pharmacogenet Genomics* **18**: 439-48 (2008).

161. W. Zhang, B. N. Yu, Y. J. He, L. Fan, Q. Li, Z. Q. Liu, A. Wang, Y. L. Liu, Z. R. Tan, J. Fen, Y. F. Huang, and H. H. Zhou. Role of BCRP 421C>A polymorphism on rosuvastatin pharmacokinetics in healthy Chinese males. *Clin Chim Acta* **373**: 99-103 (2006).

162. P. D. Martin, M. J. Warwick, A. L. Dane, S. J. Hill, P. B. Giles, P. J. Phillips, and E. Lenz. Metabolism, excretion, and pharmacokinetics of rosuvastatin in healthy adult male volunteers. *Clin Ther* **25**: 2822-35 (2003).

163. A. D. McCormick, D. McKillop, C. J. Butters, G. S. Milles, T. Baba, A. Touchi, and Y. Yamaguchi. ZD4522-an HMG-CoA Reductase Inhibitor Free of Metabolically Mediated Drug Interactions: Metabolic Studies in Human In Vitro Systems. In J. o. C. Pharmacology (ed), *American College of Clinical Pharmacology*, Vol. 40 (J. o. C. Pharmacology, ed), Chicago, IL, 2000, pp. 1055.5.

164. S. Kitamura, K. Maeda, Y. Wang, and Y. Sugiyama. Involvement of multiple transporters in the hepatobiliary transport of rosuvastatin. *Drug Metab Dispos* **36**: 2014-23 (2008).

165. R. H. Ho, R. G. Tirona, B. F. Leake, H. Glaeser, W. Lee, C. J. Lemke, Y. Wang, and R. B. Kim. Drug and bile acid transporters in rosuvastatin hepatic uptake: function, expression, and pharmacogenetics. *Gastroenterology* **130**: 1793-806 (2006).

166. P. D. Martin, M. J. Warwick, A. L. Dane, C. Brindley, and T. Short. Absolute oral bioavailability of rosuvastatin in healthy white adult male volunteers. *Clin Ther* **25**: 2553-63 (2003).

167. C. M. Kruijtzer, J. H. Beijnen, H. Rosing, W. W. ten Bokkel Huinink, M. Schot, R. C. Jewell, E. M. Paul, and J. H. Schellens. Increased oral bioavailability of topotecan in combination with the breast cancer resistance protein and P-glycoprotein inhibitor GF120918. *J Clin Oncol* **20**: 2943-50 (2002).

168. C. M. Kruijtzer, J. H. Beijnen, and J. H. Schellens. Improvement of oral drug treatment by temporary inhibition of drug transporters and/or cytochrome P450 in the gastrointestinal tract and liver: an overview. *Oncologist* **7**: 516-30 (2002).

169. A. Collett, J. Tanianis-Hughes, D. Hallifax, and G. Warhurst. Predicting P-glycoprotein effects on oral absorption: correlation of transport in Caco-2 with drug pharmacokinetics in wild-type and mdr1a(-/-) mice in vivo. *Pharm Res* **21**: 819-26 (2004).

170. C. B. Hendricks, E. K. Rowinsky, L. B. Grochow, R. C. Donehower, and S. H. Kaufmann. Effect of P-glycoprotein expression on the accumulation and cytotoxicity of topotecan (SK&F 104864), a new camptothecin analogue. *Cancer Res* **52**: 2268-78 (1992).

171. G. Ghibellini, E. M. Leslie, G. M. Pollack, and K. L. Brouwer. Use of tc-99m mebrofenin as a clinical probe to assess altered hepatobiliary transport: integration of in vitro, pharmacokinetic modeling, and simulation studies. *Pharm Res* **25**: 1851-60 (2008).

172. T. Pinos, J. M. Constansa, A. Palacin, and C. Figueras. A new diagnostic approach to the Dubin-Johnson syndrome. *Am J Gastroenterol* **85**: 91-3 (1990).

173. T. Pinos, C. Figueras, and R. Herranz. Scintigraphic diagnosis of Dubin-Johnson syndrome: DISIDA is also useful. *Am J Gastroenterol* **86**: 1687-8 (1991).

174. G. T. Krishnamurthyand F. E. Turner. Pharmacokinetics and clinical application of technetium 99m-labeled hepatobiliary agents. *Semin Nucl Med* **20**: 130-49 (1990).

175. K. S. Pangand M. Rowland. Hepatic clearance of drugs. I. Theoretical considerations of a "well-stirred" model and a "parallel tube" model. Influence of hepatic blood flow, plasma and blood cell binding, and the hepatocellular enzymatic activity on hepatic drug clearance. *J Pharmacokinet Biopharm* **5**: 625-53 (1977).

176. A. Yamada, K. Maeda, E. Kamiyama, D. Sugiyama, T. Kondo, Y. Shiroyanagi, H. Nakazawa, T. Okano, M. Adachi, J. D. Schuetz, Y. Adachi, Z. Hu, H. Kusuhara, and Y. Sugiyama. Multiple human isoforms of drug transporters contribute to the hepatic and renal transport of olmesartan, a selective antagonist of the angiotensin II AT1-receptor. *Drug Metab Dispos* **35**: 2166-76 (2007).

177. R. Nakagomi-Hagihara, D. Nakai, K. Kawai, Y. Yoshigae, T. Tokui, T. Abe, and T. Ikeda. OATP1B1, OATP1B3, and mrp2 are involved in hepatobiliary transport of olmesartan, a novel angiotensin II blocker. *Drug Metab Dispos* **34**: 862-9 (2006).

178. W. Yamashiro, K. Maeda, M. Hirouchi, Y. Adachi, Z. Hu, and Y. Sugiyama. Involvement of transporters in the hepatic uptake and biliary excretion of valsartan, a selective antagonist of the angiotensin II AT1-receptor, in humans. *Drug Metab Dispos* **34**: 1247-54 (2006).

179. P. Laeis, K. Puchler, and W. Kirch. The pharmacokinetic and metabolic profile of olmesartan medoxomil limits the risk of clinically relevant drug interaction. *J Hypertens Suppl* **19**: S21-32 (2001).

180. L. R. Schwochoand H. N. Masonson. Pharmacokinetics of CS-866, a new angiotensin II receptor blocker, in healthy subjects. *J Clin Pharmacol* **41**: 515-27 (2001).

181. G. Flesch, P. Muller, and P. Lloyd. Absolute bioavailability and pharmacokinetics of valsartan, an angiotensin II receptor antagonist, in man. *Eur J Clin Pharmacol* **52**: 115-20 (1997).

182. F. Waldmeier, G. Flesch, P. Muller, T. Winkler, H. P. Kriemler, P. Buhlmayer, and M. De Gasparo. Pharmacokinetics, disposition and biotransformation of [14C]-radiolabelled valsartan in healthy male volunteers after a single oral dose. *Xenobiotica* **27**: 59-71 (1997).

183. A. Nakashima, H. Kawashita, N. Masuda, C. Saxer, M. Niina, Y. Nagae, and K. Iwasaki. Identification of cytochrome P450 forms involved in the 4-hydroxylation of valsartan, a potent and specific angiotensin II receptor antagonist, in human liver microsomes. *Xenobiotica* **35**: 589-602 (2005).

184. A. C. Allisonand E. M. Eugui. Mycophenolate mofetil and its mechanisms of action. *Immunopharmacology* **47**: 85-118 (2000).

185. K. Bowalgahaand J. O. Miners. The glucuronidation of mycophenolic acid by human liver, kidney and jejunum microsomes. *Br J Clin Pharmacol* **52**: 605-9 (2001).

186. N. Picard, D. Ratanasavanh, A. Premaud, Y. Le Meur, and P. Marquet. Identification of the UDP-glucuronosyltransferase isoforms involved in mycophenolic acid phase II metabolism. *Drug Metab Dispos* **33**: 139-46 (2005).

187. D. A. Hesselink, R. M. van Hest, R. A. Mathot, F. Bonthuis, W. Weimar, R. W. de Bruin, and T. van Gelder. Cyclosporine interacts with mycophenolic acid by inhibiting the multidrug resistance-associated protein 2. *Am J Transplant* **5**: 987-94 (2005).

188. M. Kobayashi, H. Saitoh, M. Kobayashi, K. Tadano, Y. Takahashi, and T. Hirano. Cyclosporin A, but not tacrolimus, inhibits the biliary excretion of mycophenolic acid glucuronide possibly mediated by multidrug resistance-associated protein 2 in rats. *J Pharmacol Exp Ther* **309**: 1029-35 (2004).

189. R. E. Bullingham, A. Nicholls, and M. Hale. Pharmacokinetics of mycophenolate mofetil (RS61443): a short review. *Transplant Proc* **28**: 925-9 (1996).

190. R. Bullingham, S. Monroe, A. Nicholls, and M. Hale. Pharmacokinetics and bioavailability of mycophenolate mofetil in healthy subjects after single-dose oral and intravenous administration. *J Clin Pharmacol* **36**: 315-24 (1996).

191. S. Baldelli, S. Merlini, N. Perico, A. Nicastri, M. Cortinovis, E. Gotti, G. Remuzzi, and D. Cattaneo. C-440T/T-331C polymorphisms in the UGT1A9 gene affect the pharmacokinetics of mycophenolic acid in kidney transplantation. *Pharmacogenomics* **8**: 1127-41 (2007).

192. M. Miura, S. Satoh, K. Inoue, H. Kagaya, M. Saito, T. Inoue, T. Suzuki, and T. Habuchi. Influence of SLCO1B1, 1B3, 2B1 and ABCC2 genetic polymorphisms on mycophenolic acid pharmacokinetics in Japanese renal transplant recipients. *Eur J Clin Pharmacol* **63**: 1161-9 (2007).

193. M. Naesens, D. R. Kuypers, K. Verbeke, and Y. Vanrenterghem. Multidrug resistance protein 2 genetic polymorphisms influence mycophenolic acid exposure in renal allograft recipients. *Transplantation* **82**: 1074-84 (2006).

194. W. X. Zhang, B. Chen, Z. Jin, Z. Yu, X. Wang, H. Chen, A. Mao, and W. Cai. Influence of uridine diphosphate (UDP)-glucuronosyltransferases and ABCC2 genetic polymorphisms on the pharmacokinetics of mycophenolic acid and its metabolites in Chinese renal transplant recipients. *Xenobiotica* **38**: 1422-36 (2008).

195. M. G. Ismair, B. Stieger, V. Cattori, B. Hagenbuch, M. Fried, P. J. Meier, and G. A. Kullak-Ublick. Hepatic uptake of cholecystokinin octapeptide by organic anion-transporting polypeptides OATP4 and OATP8 of rat and human liver. *Gastroenterology* **121**: 1185-90 (2001).

196. Y. Shitaraand Y. Sugiyama. Pharmacokinetic and pharmacodynamic alterations of 3-hydroxy-3-methylglutaryl coenzyme A (HMG-CoA) reductase inhibitors: drug-drug interactions and interindividual differences in transporter and metabolic enzyme functions. *Pharmacol Ther* **112**: 71-105 (2006).

197. T. Hatanaka. Clinical pharmacokinetics of pravastatin: mechanisms of pharmacokinetic events. *Clin Pharmacokinet* **39**: 397-412 (2000).

198. C. M. White. A review of the pharmacologic and pharmacokinetic aspects of rosuvastatin. *J Clin Pharmacol* **42**: 963-70 (2002).

199. T. Kantola, J. T. Backman, M. Niemi, K. T. Kivisto, and P. J. Neuvonen. Effect of fluconazole on plasma fluvastatin and pravastatin concentrations. *Eur J Clin Pharmacol* **56**: 225-9 (2000).

200. P. J. Neuvonen, T. Kantola, and K. T. Kivisto. Simvastatin but not pravastatin is very susceptible to interaction with the CYP3A4 inhibitor itraconazole. *Clin Pharmacol Ther* **63**: 332-41 (1998).

201. M. Hirano, K. Maeda, H. Hayashi, H. Kusuhara, and Y. Sugiyama. Bile salt export pump (BSEP/ABCB11) can transport a nonbile acid substrate, pravastatin. *J Pharmacol Exp Ther* **314**: 876-82 (2005).

202. S. Matsushima, K. Maeda, C. Kondo, M. Hirano, M. Sasaki, H. Suzuki, and Y. Sugiyama. Identification of the hepatic efflux transporters of organic anions using double-transfected Madin-Darby canine kidney II cells expressing human organic anion-transporting polypeptide 1B1 (OATP1B1)/multidrug resistance-associated protein 2, OATP1B1/multidrug resistance 1, and OATP1B1/breast cancer resistance protein. *J Pharmacol Exp Ther* **314**: 1059-67 (2005).

203. M. Hasegawa, H. Kusuhara, D. Sugiyama, K. Ito, S. Ueda, H. Endou, and Y. Sugiyama. Functional involvement of rat organic anion transporter 3 (rOat3; Slc22a8) in the renal uptake of organic anions. *J Pharmacol Exp Ther* **300**: 746-53 (2002).

204. B. Hsiang, Y. Zhu, Z. Wang, Y. Wu, V. Sasseville, W. P. Yang, and T. G. Kirchgessner. A novel human hepatic organic anion transporting polypeptide (OATP2). Identification of a liver-specific human organic anion transporting polypeptide and identification of rat and human

hydroxymethylglutaryl-CoA reductase inhibitor transporters. *J Biol Chem* **274**: 37161-8 (1999).

205. D. Kobayashi, T. Nozawa, K. Imai, J. Nezu, A. Tsuji, and I. Tamai. Involvement of human organic anion transporting polypeptide OATP-B (SLC21A9) in pH-dependent transport across intestinal apical membrane. *J Pharmacol Exp Ther* **306**: 703-8 (2003).

206. M. Yamazaki, S. Akiyama, R. Nishigaki, and Y. Sugiyama. Uptake is the rate-limiting step in the overall hepatic elimination of pravastatin at steady-state in rats. *Pharm Res* **13**: 1559-64 (1996).

207. M. Yamazaki, S. Akiyama, K. Ni'inuma, R. Nishigaki, and Y. Sugiyama. Biliary excretion of pravastatin in rats: contribution of the excretion pathway mediated by canalicular multispecific organic anion transporter. *Drug Metab Dispos* **25**: 1123-9 (1997).

208. R. H. Ho, L. Choi, W. Lee, G. Mayo, U. I. Schwarz, R. G. Tirona, D. G. Bailey, C. Michael Stein, and R. B. Kim. Effect of drug transporter genotypes on pravastatin disposition in European- and African-American participants. *Pharmacogenet Genomics* **17**: 647-56 (2007).

209. J. Mwinyi, A. Johne, S. Bauer, I. Roots, and T. Gerloff. Evidence for inverse effects of OATP-C (SLC21A6) 5 and 1b haplotypes on pravastatin kinetics. *Clin Pharmacol Ther* **75**: 415-21 (2004).

210. M. Niemi, E. Schaeffeler, T. Lang, M. F. Fromm, M. Neuvonen, C. Kyrklund, J. T. Backman, R. Kerb, M. Schwab, P. J. Neuvonen, M. Eichelbaum, and K. T. Kivisto. High plasma pravastatin concentrations are associated with single nucleotide polymorphisms and haplotypes of organic anion transporting polypeptide-C (OATP-C, SLCO1B1). *Pharmacogenetics* **14**: 429-40 (2004).

211. Y. Nishizato, I. Ieiri, H. Suzuki, M. Kimura, K. Kawabata, T. Hirota, H. Takane, S. Irie, H. Kusuhara, Y. Urasaki, A. Urae, S. Higuchi, K. Otsubo, and Y. Sugiyama. Polymorphisms of OATP-C (SLC21A6) and OAT3 (SLC22A8) genes: consequences for pravastatin pharmacokinetics. *Clin Pharmacol Ther* **73**: 554-65 (2003).

212. J. H. Choi, M. G. Lee, J. Y. Cho, J. E. Lee, K. H. Kim, and K. Park. Influence of OATP1B1 genotype on the pharmacokinetics of rosuvastatin in Koreans. *Clin Pharmacol Ther* **83**: 251-7 (2008).

213. M. K. Pasanen, H. Fredrikson, P. J. Neuvonen, and M. Niemi. Different effects of SLCO1B1 polymorphism on the pharmacokinetics of atorvastatin and rosuvastatin. *Clin Pharmacol Ther* **82**: 726-33 (2007).

214. M. Hirano, K. Maeda, Y. Shitara, and Y. Sugiyama. Contribution of OATP2 (OATP1B1) and OATP8 (OATP1B3) to the hepatic uptake of pitavastatin in humans. *J Pharmacol Exp Ther* **311**: 139-46 (2004).

215. M. Hirano, K. Maeda, S. Matsushima, Y. Nozaki, H. Kusuhara, and Y. Sugiyama. Involvement of BCRP (ABCG2) in the biliary excretion of pitavastatin. *Mol Pharmacol* **68**: 800-7 (2005).

216. H. Fujino, T. Saito, Y. Tsunenari, J. Kojima, and T. Sakaeda. Metabolic properties of the acid and lactone forms of HMG-CoA reductase inhibitors. *Xenobiotica* **34**: 961-71 (2004).

217. H. Fujino, I. Yamada, S. Shimada, T. Nagao, and M. Yoneda. Metabolic fate of pitavastatin (NK-104), a new inhibitor of 3-hydroxy-3-methyl-glutaryl coenzyme A reductase. Effects on drug-metabolizing systems in rats and humans. *Arzneimittelforschung* **52**: 745-53 (2002).

218. H. Fujino, I. Yamada, S. Shimada, M. Yoneda, and J. Kojima. Metabolic fate of pitavastatin, a new inhibitor of HMG-CoA reductase: human UDP-glucuronosyltransferase enzymes involved in lactonization. *Xenobiotica* **33**: 27-41 (2003).

219. J. Y. Chung, J. Y. Cho, K. S. Yu, J. R. Kim, D. S. Oh, H. R. Jung, K. S. Lim, K. H. Moon, S. G. Shin, and I. J. Jang. Effect of OATP1B1 (SLCO1B1) variant alleles on the pharmacokinetics of pitavastatin in healthy volunteers. *Clin Pharmacol Ther* **78**: 342-50 (2005).

220. I. Ieiri, S. Suwannakul, K. Maeda, H. Uchimaru, K. Hashimoto, M. Kimura, H. Fujino, M. Hirano, H. Kusuhara, S. Irie, S. Higuchi, and Y. Sugiyama. SLCO1B1 (OATP1B1, an uptake transporter) and ABCG2 (BCRP, an efflux transporter) variant alleles and pharmacokinetics of pitavastatin in healthy volunteers. *Clin Pharmacol Ther* **82**: 541-7 (2007).

221. H. Glaeser, D. G. Bailey, G. K. Dresser, J. C. Gregor, U. I. Schwarz, J. S. McGrath, E. Jolicoeur, W. Lee, B. F. Leake, R. G. Tirona, and R. B. Kim. Intestinal drug transporter expression and the impact of grapefruit juice in humans. *Clin Pharmacol Ther* **81**: 362-70 (2007).

222. M. Cvetkovic, B. Leake, M. F. Fromm, G. R. Wilkinson, and R. B. Kim. OATP and P-glycoprotein transporters mediate the cellular uptake and excretion of fexofenadine. *Drug Metab Dispos* **27**: 866-71 (1999).

223. S. Matsushima, K. Maeda, N. Ishiguro, T. Igarashi, and Y. Sugiyama. Investigation of the inhibitory effects of various drugs on the hepatic uptake of fexofenadine in humans. *Drug Metab Dispos* (2008).

224. M. Shimizu, K. Fuse, K. Okudaira, R. Nishigaki, K. Maeda, H. Kusuhara, and Y. Sugiyama. Contribution of OATP (organic anion-transporting polypeptide) family transporters to the hepatic uptake of fexofenadine in humans. *Drug Metab Dispos* **33**: 1477-81 (2005).

225. S. Matsushima, K. Maeda, K. Inoue, K. Y. Ohta, H. Yuasa, T. Kondo, H. Nakayama, S. Horita, H. Kusuhara, and Y. Sugiyama. The inhibition of human multidrug and toxin extrusion 1 is involved in the drug-drug interaction caused by cimetidine. *Drug Metab Dispos* **37**: 555-9 (2009).

226. M. A. Hamman, M. A. Bruce, B. D. Haehner-Daniels, and S. D. Hall. The effect of rifampin administration on the disposition of fexofenadine. *Clin Pharmacol Ther* **69**: 114-21 (2001).

227. G. L. Lemma, Z. Wang, M. A. Hamman, N. A. Zaheer, J. C. Gorski, and S. D. Hall. The effect of short- and long-term administration of verapamil on the disposition of cytochrome P450 3A and P-glycoprotein substrates. *Clin Pharmacol Ther* **79**: 218-30 (2006).

228. C. Lippert, Ling, J., Brown, P., Burmaster, S., Eller, M., Cheng, L., Thompson, R., and Weir, S. Mass Balance and Pharmacokinetics of MDL 16,455A in Healthy, Male Volunteers. *Pharmaceutical Research* **12**: S-390 (1995).

229. C. Banfield, S. Gupta, M. Marino, J. Lim, and M. Affrime. Grapefruit juice reduces the oral bioavailability of fexofenadine but not desloratadine. *Clin Pharmacokinet* **41**: 311-8 (2002).

230. J. H. Shon, Y. R. Yoon, W. S. Hong, P. M. Nguyen, S. S. Lee, Y. G. Choi, I. J. Cha, and J. G. Shin. Effect of itraconazole on the pharmacokinetics and pharmacodynamics of fexofenadine in relation to the MDR1 genetic polymorphism. *Clin Pharmacol Ther* **78**: 191-201 (2005).

231. S. Zhou, E. Chan, S. Q. Pan, M. Huang, and E. J. Lee. Pharmacokinetic interactions of drugs with St John's wort. *J Psychopharmacol* **18**: 262-76 (2004).

232. N. Yasui-Furukori, T. Uno, K. Sugawara, and T. Tateishi. Different effects of three transporting inhibitors, verapamil, cimetidine, and probenecid, on fexofenadine pharmacokinetics. *Clin Pharmacol Ther* **77**: 17-23 (2005).

233. M. Shimizu, T. Uno, K. Sugawara, and T. Tateishi. Effects of itraconazole and diltiazem on the pharmacokinetics of fexofenadine, a substrate of P-glycoprotein. *Br J Clin Pharmacol* **61**: 538-44 (2006).

234. C. Tannergren, N. Petri, L. Knutson, M. Hedeland, U. Bondesson, and H. Lennernas. Multiple transport mechanisms involved in the intestinal

absorption and first-pass extraction of fexofenadine. *Clin Pharmacol Ther* **74**: 423-36 (2003).

235. S. Drescher, E. Schaeffeler, M. Hitzl, U. Hofmann, M. Schwab, U. Brinkmann, M. Eichelbaum, and M. F. Fromm. MDR1 gene polymorphisms and disposition of the P-glycoprotein substrate fexofenadine. *Br J Clin Pharmacol* **53**: 526-34 (2002).

236. R. B. Kim, B. F. Leake, E. F. Choo, G. K. Dresser, S. V. Kubba, U. I. Schwarz, A. Taylor, H. G. Xie, J. McKinsey, S. Zhou, L. B. Lan, J. D. Schuetz, E. G. Schuetz, and G. R. Wilkinson. Identification of functionally variant MDR1 alleles among European Americans and African Americans. *Clin Pharmacol Ther* **70**: 189-99 (2001).

237. G. K. Dresser, D. G. Bailey, B. F. Leake, U. I. Schwarz, P. A. Dawson, D. J. Freeman, and R. B. Kim. Fruit juices inhibit organic anion transporting polypeptide-mediated drug uptake to decrease the oral availability of fexofenadine. *Clin Pharmacol Ther* **71**: 11-20 (2002).

238. M. Niemi, K. T. Kivisto, U. Hofmann, M. Schwab, M. Eichelbaum, and M. F. Fromm. Fexofenadine pharmacokinetics are associated with a polymorphism of the SLCO1B1 gene (encoding OATP1B1). *Br J Clin Pharmacol* **59**: 602-4 (2005).

239. N. Ishiguro, K. Maeda, W. Kishimoto, A. Saito, A. Harada, T. Ebner, W. Roth, T. Igarashi, and Y. Sugiyama. Predominant contribution of OATP1B3 to the hepatic uptake of telmisartan, an angiotensin II receptor antagonist, in humans. *Drug Metab Dispos* **34**: 1109-15 (2006).

240. J. Stangier, J. Schmid, D. Turck, H. Switek, A. Verhagen, P. A. Peeters, S. P. van Marle, W. J. Tamminga, F. A. Sollie, and J. H. Jonkman. Absorption, metabolism, and excretion of intravenously and orally administered [14C]telmisartan in healthy volunteers. *J Clin Pharmacol* **40**: 1312-22 (2000).

241. J. Stangier, C. A. Su, G. Schondorfer, and W. Roth. Pharmacokinetics and safety of intravenous and oral telmisartan 20 mg and 120 mg in subjects with hepatic impairment compared with healthy volunteers. *J Clin Pharmacol* **40**: 1355-64 (2000).

242. H. Miyazaki, T. Sekine, and H. Endou. The multispecific organic anion transporter family: properties and pharmacological significance. *Trends Pharmacol Sci* **25**: 654-62 (2004).

243. C. Srimaroeng, J. L. Perry, and J. B. Pritchard. Physiology, structure, and regulation of the cloned organic anion transporters. *Xenobiotica* **38**: 889-935 (2008).

244. P. de Miranda, S. S. Good, R. Yarchoan, R. V. Thomas, M. R. Blum, C. E. Myers, and S. Broder. Alteration of zidovudine pharmacokinetics by probenecid in patients with AIDS or AIDS-related complex. *Clin Pharmacol Ther* **46**: 494-500 (1989).

245. J. W. Massarella, L. A. Nazareno, S. Passe, and B. Min. The effect of probenecid on the pharmacokinetics of zalcitabine in HIV-positive patients. *Pharm Res* **13**: 449-52 (1996).

246. A. Somogyi. Renal transport of drugs: specificity and molecular mechanisms. *Clin Exp Pharmacol Physiol* **23**: 986-9 (1996).

247. A. Ayrtonand P. Morgan. Role of transport proteins in drug discovery and development: a pharmaceutical perspective. *Xenobiotica* **38**: 676-708 (2008).

248. Y. Nozaki, H. Kusuhara, T. Kondo, M. Iwaki, Y. Shiroyanagi, H. Nakayama, S. Horita, H. Nakazawa, T. Okano, and Y. Sugiyama. Species difference in the inhibitory effect of nonsteroidal anti-inflammatory drugs on the uptake of methotrexate by human kidney slices. *J Pharmacol Exp Ther* **322**: 1162-70 (2007).

249. Y. Uwai, H. Saito, and K. Inui. Interaction between methotrexate and nonsteroidal anti-inflammatory drugs in organic anion transporter. *Eur J Pharmacol* **409**: 31-6 (2000).

250. L. Naesens, N. Bischofberger, P. Augustijns, P. Annaert, G. Van den Mooter, M. N. Arimilli, C. U. Kim, and E. De Clercq. Antiretroviral efficacy and pharmacokinetics of oral bis(isopropyloxycarbonyloxymethyl)-9-(2-phosphonylmethoxypropyl)adenine in mice. *Antimicrob Agents Chemother* **42**: 1568-73 (1998).

251. K. C. Cundy, C. Sueoka, G. R. Lynch, L. Griffin, W. A. Lee, and J. P. Shaw. Pharmacokinetics and bioavailability of the anti-human immunodeficiency virus nucleotide analog 9-[(R)-2-(phosphonomethoxy)propyl]adenine (PMPA) in dogs. *Antimicrob Agents Chemother* **42**: 687-90 (1998).

252. J. E. Gallantand S. Deresinski. Tenofovir disoproxil fumarate. *Clin Infect Dis* **37**: 944-50 (2003).

253. B. P. Kearney, J. F. Flaherty, and J. Shah. Tenofovir disoproxil fumarate: clinical pharmacology and pharmacokinetics. *Clin Pharmacokinet* **43**: 595-612 (2004).

254. P. Barditch-Crovo, S. G. Deeks, A. Collier, S. Safrin, D. F. Coakley, M. Miller, B. P. Kearney, R. L. Coleman, P. D. Lamy, J. O. Kahn, I.

McGowan, and P. S. Lietman. Phase i/ii trial of the pharmacokinetics, safety, and antiretroviral activity of tenofovir disoproxil fumarate in human immunodeficiency virus-infected adults. *Antimicrob Agents Chemother* **45**: 2733-9 (2001).

255. Y. Uwai, H. Ida, Y. Tsuji, T. Katsura, and K. Inui. Renal transport of adefovir, cidofovir, and tenofovir by SLC22A family members (hOAT1, hOAT3, and hOCT2). *Pharm Res* **24**: 811-5 (2007).

256. A. S. Ray, T. Cihlar, K. L. Robinson, L. Tong, J. E. Vela, M. D. Fuller, L. M. Wieman, E. J. Eisenberg, and G. R. Rhodes. Mechanism of active renal tubular efflux of tenofovir. *Antimicrob Agents Chemother* **50**: 3297-304 (2006).

257. R. Mallants, K. Van Oosterwyck, L. Van Vaeck, R. Mols, E. De Clercq, and P. Augustijns. Multidrug resistance-associated protein 2 (MRP2) affects hepatobiliary elimination but not the intestinal disposition of tenofovir disoproxil fumarate and its metabolites. *Xenobiotica* **35**: 1055-66 (2005).

258. K. C. Cundy, P. Barditch-Crovo, R. E. Walker, A. C. Collier, D. Ebeling, J. Toole, and H. S. Jaffe. Clinical pharmacokinetics of adefovir in human immunodeficiency virus type 1-infected patients. *Antimicrob Agents Chemother* **39**: 2401-5 (1995).

259. K. C. Cundy, B. G. Petty, J. Flaherty, P. E. Fisher, M. A. Polis, M. Wachsman, P. S. Lietman, J. P. Lalezari, M. J. Hitchcock, and H. S. Jaffe. Clinical pharmacokinetics of cidofovir in human immunodeficiency virus-infected patients. *Antimicrob Agents Chemother* **39**: 1247-52 (1995).

260. A. Katiyar, S. Yadav, P. G. Smirniotis, and N. G. Pinto. Synthesis of ordered large pore SBA-15 spherical particles for adsorption of biomolecules. *J Chromatogr A* **1122**: 13-20 (2006).

261. D. S. Miller. Nucleoside phosphonate interactions with multiple organic anion transporters in renal proximal tubule. *J Pharmacol Exp Ther* **299**: 567-74 (2001).

262. G. Reid, P. Wielinga, N. Zelcer, M. De Haas, L. Van Deemter, J. Wijnholds, J. Balzarini, and P. Borst. Characterization of the transport of nucleoside analog drugs by the human multidrug resistance proteins MRP4 and MRP5. *Mol Pharmacol* **63**: 1094-103 (2003).

263. S. Dallas, L. Schlichter, and R. Bendayan. Multidrug resistance protein (MRP) 4- and MRP 5-mediated efflux of 9-(2-phosphonylmethoxyethyl)adenine by microglia. *J Pharmacol Exp Ther* **309**: 1221-9 (2004).

264. A. Servais, P. Lechat, N. Zahr, S. Urien, G. Aymard, M. C. Jaudon, G. Deray, and C. Isnard Bagnis. Tubular transporters and clearance of adefovir. *Eur J Pharmacol* **540**: 168-74 (2006).

265. E. S. Ho, D. C. Lin, D. B. Mendel, and T. Cihlar. Cytotoxicity of antiviral nucleotides adefovir and cidofovir is induced by the expression of human renal organic anion transporter 1. *J Am Soc Nephrol* **11**: 383-93 (2000).

266. K. Bleasby, L. A. Hall, J. L. Perry, H. W. Mohrenweiser, and J. B. Pritchard. Functional consequences of single nucleotide polymorphisms in the human organic anion transporter hOAT1 (SLC22A6). *J Pharmacol Exp Ther* **314**: 923-31 (2005).

267. T. Fujita, C. Brown, E. J. Carlson, T. Taylor, M. de la Cruz, S. J. Johns, D. Stryke, M. Kawamoto, K. Fujita, R. Castro, C. W. Chen, E. T. Lin, C. M. Brett, E. G. Burchard, T. E. Ferrin, C. C. Huang, M. K. Leabman, and K. M. Giacomini. Functional analysis of polymorphisms in the organic anion transporter, SLC22A6 (OAT1). *Pharmacogenet Genomics* **15**: 201-9 (2005).

268. D. Shi, J. Yang, D. Yang, E. L. LeCluyse, C. Black, L. You, F. Akhlaghi, and B. Yan. Anti-influenza prodrug oseltamivir is activated by carboxylesterase human carboxylesterase 1, and the activation is inhibited by antiplatelet agent clopidogrel. *J Pharmacol Exp Ther* **319**: 1477-84 (2006).

269. G. He, J. Massarella, and P. Ward. Clinical pharmacokinetics of the prodrug oseltamivir and its active metabolite Ro 64-0802. *Clin Pharmacokinet* **37**: 471-84 (1999).

270. G. Hill, T. Cihlar, C. Oo, E. S. Ho, K. Prior, H. Wiltshire, J. Barrett, B. Liu, and P. Ward. The anti-influenza drug oseltamivir exhibits low potential to induce pharmacokinetic drug interactions via renal secretion-correlation of in vivo and in vitro studies. *Drug Metab Dispos* **30**: 13-9 (2002).

271. A. Ose, M. Ito, H. Kusuhara, K. Yamatsugu, M. Kanai, M. Shibasaki, M. Hosokawa, J. D. Schuetz, and Y. Sugiyama. Limited brain distribution of [3R,4R,5S]-4-acetamido-5-amino-3-(1-ethylpropoxy)-1-cyclohexene-1-carboxyl ate phosphate (Ro 64-0802), a pharmacologically active form of oseltamivir, by active efflux across the blood-brain barrier mediated by organic anion transporter 3 (Oat3/Slc22a8) and multidrug resistance-associated protein 4 (Mrp4/Abcc4). *Drug Metab Dispos* **37**: 315-21 (2009).

272. A. Enomoto, M. Takeda, M. Shimoda, S. Narikawa, Y. Kobayashi, Y. Kobayashi, T. Yamamoto, T. Sekine, S. H. Cha, T. Niwa, and H. Endou.

Interaction of human organic anion transporters 2 and 4 with organic anion transport inhibitors. *J Pharmacol Exp Ther* **301**: 797-802 (2002).

273. A. S. Mulato, E. S. Ho, and T. Cihlar. Nonsteroidal anti-inflammatory drugs efficiently reduce the transport and cytotoxicity of adefovir mediated by the human renal organic anion transporter 1. *J Pharmacol Exp Ther* **295**: 10-5 (2000).

274. M. Rius, A. T. Nies, J. Hummel-Eisenbeiss, G. Jedlitschky, and D. Keppler. Cotransport of reduced glutathione with bile salts by MRP4 (ABCC4) localized to the basolateral hepatocyte membrane. *Hepatology* **38**: 374-84 (2003).

275. M. Takeda, S. Narikawa, M. Hosoyamada, S. H. Cha, T. Sekine, and H. Endou. Characterization of organic anion transport inhibitors using cells stably expressing human organic anion transporters. *Eur J Pharmacol* **419**: 113-20 (2001).

276. H. Zeng, Z. S. Chen, M. G. Belinsky, P. A. Rea, and G. D. Kruh. Transport of methotrexate (MTX) and folates by multidrug resistance protein (MRP) 3 and MRP1: effect of polyglutamylation on MTX transport. *Cancer Res* **61**: 7225-32 (2001).

277. C. Oo, J. Barrett, G. Hill, J. Mann, A. Dorr, R. Dutkowski, and P. Ward. Pharmacokinetics and dosage recommendations for an oseltamivir oral suspension for the treatment of influenza in children. *Paediatr Drugs* **3**: 229-36 (2001).

278. J. P. Lalezari, R. J. Stagg, B. D. Kuppermann, G. N. Holland, F. Kramer, D. V. Ives, M. Youle, M. R. Robinson, W. L. Drew, and H. S. Jaffe. Intravenous cidofovir for peripheral cytomegalovirus retinitis in patients with AIDS. A randomized, controlled trial. *Ann Intern Med* **126**: 257-63 (1997).

279. E. J. Fisher, K. Chaloner, D. L. Cohn, L. B. Grant, B. Alston, C. L. Brosgart, B. Schmetter, W. M. El-Sadr, and J. Sampson. The safety and efficacy of adefovir dipivoxil in patients with advanced HIV disease: a randomized, placebo-controlled trial. *Aids* **15**: 1695-700 (2001).

280. R. Beckmann. [Absorption, distribution in the organism and elimination of metformin]. *Diabetologia* **5**: 318-24 (1969).

281. P. J. Pentikainen, P. J. Neuvonen, and A. Penttila. Pharmacokinetics of metformin after intravenous and oral administration to man. *Eur J Clin Pharmacol* **16**: 195-202 (1979).

282. A. J. Scheen. Clinical pharmacokinetics of metformin. *Clin Pharmacokinet* **30**: 359-71 (1996).

283. G. T. Tucker, C. Casey, P. J. Phillips, H. Connor, J. D. Ward, and H. F. Woods. Metformin kinetics in healthy subjects and in patients with diabetes mellitus. *Br J Clin Pharmacol* **12**: 235-46 (1981).

284. N. Vidon, S. Chaussade, M. Noel, C. Franchisseur, B. Huchet, and J. J. Bernier. Metformin in the digestive tract. *Diabetes Res Clin Pract* **4**: 223-9 (1988).

285. Y. Tanihara, S. Masuda, T. Sato, T. Katsura, O. Ogawa, and K. Inui. Substrate specificity of MATE1 and MATE2-K, human multidrug and toxin extrusions/H(+)-organic cation antiporters. *Biochem Pharmacol* **74**: 359-71 (2007).

286. N. Kimura, M. Okuda, and K. Inui. Metformin transport by renal basolateral organic cation transporter hOCT2. *Pharm Res* **22**: 255-9 (2005).

287. A. T. Nies, H. Koepsell, S. Winter, O. Burk, K. Klein, R. Kerb, U. M. Zanger, D. Keppler, M. Schwab, and E. Schaeffeler. Expression of organic cation transporters OCT1 (SLC22A1) and OCT3 (SLC22A3) is affected by genetic factors and cholestasis in human liver. *Hepatology* **50**: 1227-40 (2009).

288. M. Zhou, L. Xia, and J. Wang. Metformin transport by a newly cloned proton-stimulated organic cation transporter (plasma membrane monoamine transporter) expressed in human intestine. *Drug Metab Dispos* **35**: 1956-62 (2007).

289. Y. Shu, C. Brown, R. A. Castro, R. J. Shi, E. T. Lin, R. P. Owen, S. A. Sheardown, L. Yue, E. G. Burchard, C. M. Brett, and K. M. Giacomini. Effect of genetic variation in the organic cation transporter 1, OCT1, on metformin pharmacokinetics. *Clin Pharmacol Ther* **83**: 273-80 (2008).

290. D. S. Wang, J. W. Jonker, Y. Kato, H. Kusuhara, A. H. Schinkel, and Y. Sugiyama. Involvement of organic cation transporter 1 in hepatic and intestinal distribution of metformin. *J Pharmacol Exp Ther* **302**: 510-5 (2002).

291. Y. Chen, S. Li, C. Brown, S. Cheatham, R. A. Castro, M. K. Leabman, T. J. Urban, L. Chen, S. W. Yee, J. H. Choi, Y. Huang, C. M. Brett, E. G. Burchard, and K. M. Giacomini. Effect of genetic variation in the organic cation transporter 2 on the renal elimination of metformin. *Pharmacogenet Genomics* **19**: 497-504 (2009).

292. I. S. Song, H. J. Shin, E. J. Shim, I. S. Jung, W. Y. Kim, J. H. Shon, and J. G. Shin. Genetic variants of the organic cation transporter 2 influence the disposition of metformin. *Clin Pharmacol Ther* **84**: 559-62 (2008).

293. M. V. Tzvetkov, S. V. Vormfelde, D. Balen, I. Meineke, T. Schmidt, D. Sehrt, I. Sabolic, H. Koepsell, and J. Brockmoller. The Effects of Genetic Polymorphisms in the Organic Cation Transporters OCT1, OCT2, and OCT3 on the Renal Clearance of Metformin. *Clin Pharmacol Ther* (2009).

294. L. Zhang, M. E. Schaner, and K. M. Giacomini. Functional characterization of an organic cation transporter (hOCT1) in a transiently transfected human cell line (HeLa). *J Pharmacol Exp Ther* **286**: 354-61 (1998).

295. M. Tsuda, T. Terada, M. Ueba, T. Sato, S. Masuda, T. Katsura, and K. Inui. Involvement of human multidrug and toxin extrusion 1 in the drug interaction between cimetidine and metformin in renal epithelial cells. *J Pharmacol Exp Ther* **329**: 185-91 (2009).

296. Z. J. Wang, O. Q. Yin, B. Tomlinson, and M. S. Chow. OCT2 polymorphisms and in-vivo renal functional consequence: studies with metformin and cimetidine. *Pharmacogenet Genomics* **18**: 637-45 (2008).

297. N. N. Song, Q. S. Li, and C. X. Liu. Intestinal permeability of metformin using single-pass intestinal perfusion in rats. *World J Gastroenterol* **12**: 4064-70 (2006).

298. W. R. Proctor, D. L. Bourdet, and D. R. Thakker. Mechanisms underlying saturable intestinal absorption of metformin. *Drug Metab Dispos* **36**: 1650-8 (2008).

299. G. T. Tucker, J. B. Houston, and S. M. Huang. Optimizing drug development: strategies to assess drug metabolism/transporter interaction potential--toward a consensus. *Pharm Res* **18**: 1071-80 (2001).

300. Z. Wang, M. A. Hamman, S. M. Huang, L. J. Lesko, and S. D. Hall. Effect of St John's wort on the pharmacokinetics of fexofenadine. *Clin Pharmacol Ther* **71**: 414-20 (2002).

301. R. L. Vetelainen, R. J. Bennink, K. de Bruin, A. van Vliet, and T. M. van Gulik. Hepatobiliary function assessed by 99mTc-mebrofenin cholescintigraphy in the evaluation of severity of steatosis in a rat model. *Eur J Nucl Med Mol Imaging* **33**: 1107-14 (2006).

302. M. Wong, R. L. Balleine, E. Y. Blair, A. J. McLachlan, S. P. Ackland, M. B. Garg, S. Evans, D. Farlow, M. Collins, L. P. Rivory, J. M. Hoskins, G. J. Mann, C. L. Clarke, and H. Gurney. Predictors of vinorelbine

pharmacokinetics and pharmacodynamics in patients with cancer. *J Clin Oncol* **24**: 2448-55 (2006).

303. M. Michael, M. Thompson, R. J. Hicks, P. L. Mitchell, A. Ellis, A. D. Milner, J. Di Iulio, A. M. Scott, V. Gurtler, J. M. Hoskins, S. J. Clarke, N. C. Tebbut, K. Foo, M. Jefford, and J. R. Zalcberg. Relationship of hepatic functional imaging to irinotecan pharmacokinetics and genetic parameters of drug elimination. *J Clin Oncol* **24**: 4228-35 (2006).

TABLE 1: Clinical Transport Protein Probes

Protein	Probe	Established No (n=1) Moderately (n=3-5 studies) Yes (n=>5 studies)	Advantages	Limitations
P-gp	Digoxin	Yes (FDA recommended)	Well established Oral and I.V. doses No metabolism	OATP substrate, Narrow therapeutic window
	^{99m}Tc-Sestamibi	Moderately	Radiolabeled No metabolism No uptake protein interaction	Contribution of MRPs unknown
	^{11}C-Verapamil	No	Radiolabeled Assess P-gp at the BBB No uptake protein interaction	CYP3A-mediated metabolism
BCRP	Sulfasalazine	No		Low F due to extensive metabolism in the gut
MRP2	^{99m}Tc-Mebrofenin	No	Radiolabeled No metabolism	Hepatic MRP2 only Substrate of OATPs but high hepatic E
OATP1B1	Pravastatin	Yes	Minimal metabolism Uptake rate-limited	Substrate of other OATPs and efflux proteins Higher degree of urinary excretion compared to other statins
	Rosuvastatin	No	Minimal metabolism	Substrate of many other transport proteins including OATPs Possible BCRP probe
	Pitavastatin	No		Substrate of many other

				transport proteins Extensive metabolism
	Fexofenadine	Yes	Safe Minimal Metabolism	Often used as a P-gp probe Substrate of many other transport proteins
OATP1B3	Telmisartan	No	OATP1B3 specific	Metabolized by UGTs to an acyl glucuronide
OAT	Tenofovir	No		Substrate of Efflux Proteins Prodrug requires metabolism
	Ro 64-0802, active metabolite of Oseltamivir	No	Safe	Substrate of Efflux Proteins Prodrug requires metabolism Needs further transport characterization
OCT	Metformin	Yes	Safe Minimal Metabolism Not a P-gp substrate	Substrate of efflux proteins Not isoform specific

CHAPTER 2

Integration of Preclinical and Clinical Data with Pharmacokinetic Modeling and Simulation to Evaluate Fexofenadine as a Probe for Hepatobiliary Transport Function

This chapter is published in Pharmaceutical Research 2009 Aug;26(8):1942-51,

Abstract

The suitability of fexofenadine as a probe substrate to assess hepatobiliary transport function in humans was evaluated by pharmacokinetic modeling/simulation and *in vitro/in situ* studies using chemical modulators. Simulations based on a pharmacokinetic model developed to describe fexofenadine disposition in humans were conducted to examine the impact of altered hepatobiliary transport on fexofenadine disposition. The effect of GF120918 on fexofenadine disposition was evaluated in human sandwich-cultured hepatocytes (SCH). Additionally, the effect of GF120918, bosentan, and taurocholate on fexofenadine disposition in perfused livers from TR^- Wistar rats was examined. Based on modeling/simulation, fexofenadine systemic exposure was most sensitive to changes in the hepatic uptake rate constant, and did not reflect changes in hepatic exposure due to altered hepatic efflux. GF120918 did not impair fexofenadine biliary excretion in human SCH. GF120918 coadministration significantly decreased $Cl'_{biliary}$ to 27.5% of control in perfused rat livers. Simulations were in agreement with perfused liver data which predicted changes in fexofenadine systemic exposure primarily due to altered hepatic uptake. Fexofenadine is not a suitable probe to assess hepatic efflux function based on systemic concentrations. GF120918-sensitive protein(s) mediate fexofenadine biliary excretion in rat liver, whereas in human hepatocytes multiple efflux proteins are involved in fexofenadine hepatobiliary disposition.

Introduction

Fexofenadine is an orally administered nonsedating H_1-receptor antagonist commonly used in the treatment of allergic rhinitis and chronic urticaria. Fexofenadine has a low passive membrane permeability with reported Papp values in the absorptive direction of 0.17×10^6 to 0.27×10^6 cm/s determined in the Caco-2 model (1). Furthermore, the effective jejunal permeability in healthy human volunteers also was very low when fexofenadine was administered alone and with verapamil using jejunal single-pass perfusion ($0.06 \times 10^{-4} \pm 0.07 \times 10^{-4}$ and $0.04 \times 10^{-4} \pm 0.07 \times 10^{-4}$ cm/s, respectively)(2, 3). The primary elimination pathway of fexofenadine in humans is biliary excretion of the unchanged drug (4). Tahara et al. demonstrated that biliary clearance accounts for ~56-72% and 40% of total body clearance in mice and rats, respectively (5). Therefore, fexofenadine relies on active hepatic transport as one of the determinants for systemic clearance.

Identifying the degree and importance of drug-drug interactions in the human liver is very challenging because the bile and liver compartments are not readily accessible due to the anatomy of the human hepatobiliary tract. The absolute oral bioavailability of fexofenadine was reported to be 33% (product information, Hoechst Marion, Roussel, Laval, Quebec, Canada), with 12% of the total administered dose recovered in urine (4). Therefore, two-thirds of the bioavailable dose of fexofenadine is presumed to be excreted in bile, underscoring the importance of this excretory route to overall systemic clearance. Fexofenadine has been used extensively as an *in vivo* probe substrate to assess P-glycoprotein/multidrug resistance protein 1 (P-gp/MDR1) activity; altered systemic concentrations and overall exposure have been reported due to perturbations in P-gp efflux in the intestine (6-9). The contribution of P-gp to

fexofenadine hepatobiliary transport, or the degree of interaction with hepatic P-gp, are poorly understood in humans.

The organic anion transporting polypeptides (OATPs), specifically OATP1B1, OATP1B3 and OATP1A2 in humans, and Oatp1a1, Oatp1a4, and Oatp1b2 in rats, have been implicated in the cellular uptake of fexofenadine (8, 10-12). *In vitro* studies demonstrated that P-gp mediated the cellular efflux of fexofenadine (10). Thus, fexofenadine has been recommended as an *in vivo* probe substrate for P-gp interactions in the intestine (13). In fact many drug-drug and food-drug interaction studies in humans utilizing fexofenadine as a probe substrate for P-gp activity have been performed with various co-administered drugs, herbal supplements and food components (6-9, 14-17). Although P-gp plays a role in limiting intestinal absorption and blood-brain barrier penetration of fexofenadine (5, 10), multiple transport mechanisms are involved in the biliary excretion of fexofenadine (18, 19).

In mice fexofenadine is excreted into bile predominantly by multidrug resistance-associated protein 2 (Mrp2), and to a minor extent by P-gp and other yet unidentified mechanisms (18). The mechanisms of biliary excretion of fexofenadine *in vivo* in rats and humans have not been elucidated. However, the biliary excretion rate and intrinsic biliary clearance of fexofenadine in naturally occurring Mrp2-deficient TR^- rats and Eisai hyperbilirubinemic rats (EHBR) were unchanged compared to wild-type rats (5, 18). In the present studies, the role of other canalicular transport proteins including the bile salt export pump (Bsep) and P-gp in fexofenadine biliary clearance was investigated in rat perfused livers.

Bsep is primarily involved in the biliary excretion of bile acids (20), but also is capable of transporting some xenobiotics including vinblastine, pravastatin and

fexofenadine in transfected expression systems (19, 21, 22). P-gp serves an important barrier function and is responsible for biliary excretion of bulky hydrophobic and cationic substrates, including many chemotherapeutic agents, cardiac glycosides, cyclosporin A, HIV protease inhibitors, and fexofenadine, as mentioned above (23). Breast cancer resistance protein (Bcrp) transports sulfated steroids and many anticancer agents in addition to some organic anions and cations (24-26). Fexofenadine does not appear to be a BCRP/Bcrp substrate based on the results of studies utilizing Bcrp knockout mice and MDCKII cells transfected with human BCRP (5, 19).

The objective of the present study was to examine the suitability of fexofenadine as a probe substrate for altered hepatobiliary transport in humans. A pharmacokinetic model was developed to describe the disposition of fexofenadine in healthy human subjects, and simulations were conducted to examine the effect of inhibition or induction of hepatic transport processes on fexofenadine disposition. The findings from compartmental modeling and simulation were tested using chemical modulators of hepatic transport proteins. The effect of GF120918, a human P-gp and BCRP inhibitor, was assessed in human sandwich-cultured hepatocytes (SCH). In addition, livers from Mrp2-deficient TR^- rats were perfused *in situ* in a single-pass manner in the presence and absence of the Bsep inhibitor bosentan (27), and GF120918 to examine the impact of modulation of uptake and efflux proteins on fexofendadine hepatobiliary disposition. Furthermore, the taurocholate infusion in perfused livers was withheld to perturb trafficking of ATP-binding cassette (ABC) transport proteins to the canalicular membrane (28, 29) in order to assess the contribution of impaired biliary excretion to fexofenadine disposition.

Material and Methods

Materials. Dulbecco's modified Eagle's medium (DMEM), insulin, MEM non-essential amino acids solution (100x), L-glutamine, insulin and penicillin G-streptomycin solution were purchased from Invitrogen (Carlsbad, CA). Collagenase (type 4), fetal bovine serum (FBS), fexofenadine, cetirizine, sodium taurocholate, digoxin, Triton X-100, dexamethasone, methanol, Krebs-Henseleit buffer packs (K-3753) and Hanks' balanced salt solution (HBSS) modified with (H-1387) or without (H-4891) calcium chloride were obtained from Sigma-Aldrich (St. Louis, MO). BioCoat™ collagen I plates, Matrigel™ basement membrane matrix, and ITS+™ (insulin/transferrin/selenium) culture supplement were purchased from BD Biosciences Discovery Labware (Bedford, MA). [^{3}H]-taurocholate (5 Ci/mmol, >97% purity) and [^{3}H]-digoxin (40 Ci/mmol, >97% purity) were obtained from PerkinElmer Life and Analytical Sciences (Boston, MA). Bio-Safe II™ liquid scintillation cocktail was obtained from Research Products International (Mt. Prospect, IL). Centrifree® micropartition devices were obtained from Millipore (Billerica, MA). Bicinchoninic acid (BCA) protein assay reagents and BSA for the protein assay standard were purchased from Pierce Chemical Co. (Rockford, IL). N-(4-[2-(1,2,3,4-tetrahydro-6,7-dimethoxy-2-isoquinolinyl)ethyl]-phenyl)-9,10-dihydro-5-methoxy-9-oxo-4-acridine carboxamide (GF120918) was a gift from GlaxoSmithKline (Research Triangle Park, NC). All other chemicals and reagents were of analytical grade and available from commercial sources.

Pharmacokinetic Modeling

Mean fexofenadine plasma concentrations and urinary excretion rate data were estimated from previously published data in healthy human subjects after a single oral dose of 120 mg (9). Cumulative mass in bile after 48 hours was estimated based on the

assumption that bioavailability of oral fexofenadine was 33% (product information, Hoechst Marion, Roussel, Laval, Quebec, Canada), of which approximately one-third of the 120 mg dose was excreted into urine (30), and two-thirds was excreted into bile. To achieve model parsimony, the bioavailability of fexofendine was fixed at the aforementioned literature value (33%). The adoption of fixed bioavailability accounted for the first-pass extraction of fexofenadine; the remaining fixed fraction of the dose was assumed to be absorbed directly into the systemic compartment. This assumption was supported by the fact that fexofenadine exhibited a low hepatic uptake clearance. A number of different compartmental models were developed (including a peripheral compartment in addition to the liver compartment, with elimination from the peripheral, central and/or liver compartments) using the concentration- and mass-time profiles. Differential equations describing the disposition of fexofenadine in the compartments were fit simultaneously to plasma, urine and bile profiles using nonlinear least-squares regression (WinNonlin v. 4.1 Pharsight Corporation, Mountain View, CA). The final parameter estimates were selected after fitting the model to the data using different sets of initial values combined with a broad range of lower and upper bounds to avoid convergence at a local minimum. The goodness of fit was based on Akaike's Information Criterion, the residual sum of squares, coefficients of variation on the parameter estimates, the condition number, and visual inspection of the residual plots and of model fitting to the concentration- and mass-time profiles. Due to the disparity in the number of data points for the mass in bile and the urinary excretion rate data compared with the plasma concentration data, a weighting scheme was used to account for the relative contribution of each data set to the overall number of data points. Each data point was assigned a weight of $\frac{1}{y} \times (1-n)$, where n is the fraction of the total number of data

points that support a particular sample matrix. The optimal model that best described the data is shown in Figure 2.1. This model included a compartment depicting the systemic circulation described by the plasma concentration-time profile after absorption, represented by a first-order rate constant K_{absorb}, from the gut compartment. A first-order rate constant, K_{12}, governed fexofenadine uptake from the central compartment into a peripheral compartment, representing the liver. K_{21} represented a first-order rate constant for hepatic basolateral efflux; K_{bile} and K_{urine} represented biliary and urinary excretion rate constants, respectively. The following differential equations described fexofenadine disposition in healthy human subjects:

$$\frac{dX_{gut}}{dt} = -K_{absorb} \times X_{gut} \qquad X^0_{gut} = X_{oral\ dose} \times 0.33$$

$$\frac{dC_C}{dt} = K_{absorb} \times X_{gut} \times \frac{1}{V_c} - K_{12} \times C_c + K_{21} \times X_{liver} \times \frac{1}{V_c} - K_{urine} \times C_c \qquad C^0_C = 0$$

$$\frac{dX_{liver}}{dt} = K_{12} \times C_C \times V_C - K_{21} \times X_{liver} - K_{bile} \times X_{liver} \qquad X^0_{liver} = 0$$

$$\frac{dX_{bile}}{dt} = K_{bile} \times X_{liver} \qquad X^0_{bile} = 0$$

$$\frac{dX_{urine}}{dt} = K_{urine} \times C_c \times V_c \qquad X^0_{urine} = 0$$

Pharmacokinetic Simulations

The contribution of each parameter in this compartment model to the overall disposition of fexofenadine was assessed through a series of simulation experiments. Each parameter was varied sequentially from the baseline value by either increasing (i.e. induction) or decreasing (i.e. inhibition) the parameter estimate by 50%, 100% or 300%.

The concentration-, mass- and excretion rate-time profiles were simulated using WinNonlin v.4.1, and the area under the curve (AUC) for the plasma concentration-time and hepatic mass-time profiles were calculated utilizing a standard noncompartmental approach.

Isolation and *In Vitro* Culture of Primary Human Hepatocytes

Human liver tissue was obtained by qualified medical staff from the University of North Carolina, School of Medicine, as waste from surgical resection. Written informed consent was obtained from patients before undergoing hepatic surgery. IRB approval was obtained for the collection of human liver tissue. Hepatocytes were isolated by a modification of the two-step collagenase perfusion, as described previously (31). Cell viability, determined by trypan blue exclusion, was >88%. Hepatocytes were seeded (~1.5 x 10^6 cells/well) in 6-well BioCoat™ plates in DMEM without phenol red supplemented with 2 mM L-glutamine, 1% (v/v) MEM non-essential amino acids, 100 units penicillin G sodium, 100 µg streptomycin sulfate, 1 µM dexamethasone, 5% (v/v) FBS, and 10 µM insulin (day 0 of culture), and allowed to attach for 2-6 h in a humidified incubator (95% O_2, 5% CO_2) at 37°C. After cell attachment, culture plates were swirled gently and the culture medium was replaced with the same medium. Cells were overlaid 16-24 h (day 1 of culture) after seeding with ice-cold Matrigel™ basement membrane matrix (0.25 mg/mL) in 2 mL/well cold serum-free DMEM containing 2 mM L-glutamine, 1% (v/v) MEM non-essential amino acids, 100 units penicillin G sodium, 100 µg streptomycin sulfate, 0.1 µM dexamethasone, and 1% (v/v) ITS+™. The culture medium was changed every 24 h until experiments were performed on day 9-10 of culture.

Accumulation Experiments

The method to determine substrate accumulation in SCH has been described previously (32). Briefly, hepatocytes were rinsed twice with 2 mL warm HBSS containing Ca^{2+} (standard buffer) or Ca^{2+}-free HBSS and incubated with 2 mL of the same buffer for 10 min at 37°C (to maintain tight junction integrity and bile canalicular networks, or disrupt tight junctions and open bile canalicular networks, respectively). The buffer was removed, and the cells were incubated for 10 min at 37°C with 1.5 mL of [^{3}H]-taurocholate (1 μM), [^{3}H]-digoxin (1 μM) in the presence and absence of 2 μM GF120918, or for 30 min with fexofenadine (5 μM) in the presence and absence of 2 μM GF120918 in standard buffer. Hepatocytes were rinsed vigorously three times with 2 mL ice-cold standard buffer following the incubation. Taurocholate- and digoxin-treated hepatocytes were lysed with 1 mL 0.5% (v/v) Triton X-100 in phosphate-buffered saline by placing plates on an orbital shaker for a minimum of 20 min at room temperature. Substrate uptake was corrected for nonspecific binding by subtracting uptake on blank six-well Biocoat™ plates overlaid with Matrigel™. Data were normalized to protein concentration in each well, determined in duplicate aliquots using BCA protein assay reagent kit (Pierce) as instructed by the manufacturer. BSA, as supplied by the manufacturer, was used as a standard (0.2 – 1 mg/mL). Due to incompatability of the protein assay with methanol, the average protein concentration for standard HBSS or Ca^{2+}-free HBSS incubations in the same liver preparation was used to normalize fexofenadine content. The [^{3}H]-taurocholate and [^{3}H]-digoxin samples were analyzed by liquid scintillation spectroscopy in a Packard Tri-Carb scintillation counter (PerkinElmer Life and Analytical Sciences). Fexofenadine-treated hepatocytes were lysed with 1 mL 70% (v/v) ice-cold methanol/water and stored at -80ºC until analysis. The cells were scraped off the plates and centrifuged at 10,000 g for 5 min before analysis by LC/MS/MS.

Animals

Male Mrp2-deficient TR^- rats bred at the University of North Carolina (212–341 g; breeding stock obtained from Dr. Mary Vore, University of Kentucky, Lexington, KY) were used for perfused liver studies. Rats had free access to water and food prior to surgery. All animal procedures complied with the guidelines of the Institutional Animal Care and Use Committee (University of North Carolina, Chapel Hill, NC).

In Situ Liver Perfusion

All experimental procedures were performed under full anesthesia induced with ketamine/xylazine (140/8 mg/kg i.p.). The liver perfusion procedure was modified slightly from the previous report of Tian et al (2008). Briefly, the common bile duct was cannulated with polyethylene PE-10 tubing (Becton Dickinson, Parsippany, NJ). The portal vein was cannulated with a 16-gauge catheter (B. Braun Medical Inc., Bethlehem, PA), the abdominal vena cava below the liver was severed immediately by incision, and the inferior vena cava above the liver was cannulated with a 14-gauge catheter. Subsequently, the inferior vena cava was ligated between the liver and kidney to direct all perfusate outflow through the cannulated inferior vena cava above the liver. The liver was perfused in a single-pass manner (30 ml/min with fexofenadine-free, continually oxygenated, Krebs-Henseleit buffer in the presence of 5 μM taurocholate, unless otherwise indicated) for an equilibration period of ~15 min. Following the pre-perfusion period to allow for equilibration of temperature (37ºC) and bile flow, the liver was perfused for 60 min with buffer containing 5 μM taurocholate, unless otherwise indicated, and 0.5 μM fexofenadine alone, or with 2 μM GF120918 or 5 μM bosentan. Bile and outflow perfusate were collected in 10-min intervals *in toto*, and livers were isolated at

the end of perfusion and stored at -80ºC until analysis. Perfusion pressure and bile flow were used to assess liver viability (33).

Determination of Protein Binding

Livers were thawed and homogenenized in three volumes (v/w) of 0.1 M phosphate buffer (pH 7.4). Liver homogenate samples (500 µL) were placed in Centrifree® micropartition devices and centrifuged at 1000 g at 4°C for 10 min to pass ~10% of the original volume through the filter. The absence-of-protein condition was used to assess non-specific binding. Samples were obtained from above (total concentration in the presence of protein) and below (unbound concentration) the filter, and analyzed by liquid chromatography with detection by tandem mass spectrometry (LC/MS/MS).

Analytical Methods

Bile, outflow perfusate, liver homogenate, ultracentrifugation filtrate and human SCH lysates were analyzed by LC/MS/MS (Applied Biosystems API 4000 triple quadrupole with TurboIonSpray interface, MDS Sciex, Concord, ON, Canada). Fexofenadine and cetirizine (internal standard) were eluted from an Aquasil C18 column (5µm, 50mm x 2.1mm, Thermo-Electron, Waltham, MA) using a mobile phase gradient at a flow rate of 0.75 mL/min (A: 0.1% formic acid in water, B: 0.1% formic acid in methanol); 0-0.8 min hold at 10% B, 0.8-3.5 min linear increase to 85% B, 3.5-4.0 min hold at 85% B, 4.0-4.5 min return to 10% B, 4.5-5 min hold at 10% B (Shimazdu solvent delivery system, Columbia, MD). Fexofenadine and the internal standard, cetirizine, were detected in positive ion mode using multiple reaction monitoring: fexofenadine, 502.3 $\rightarrow$ 466.4 m/z; cetirizine, 389.0 $\rightarrow$ 201.0 m/z. Fexofenadine was quantified with seven point standard curves prepared in the appropriate matrix, and coefficients of variation were <14%.

Data Analysis

For SCH studies, the biliary excretion index (BEI, %) and *in vitro* biliary clearance ($Cl_{biliary}$, mL/min/kg) were calculated using B-CLEAR® technology [Qualyst, Inc., Raleigh, NC; (32)]:

$$BEI = \frac{Accumulation_{Cells+Bile} - Accumulation_{Cells}}{Accumulation_{Cells+Bile}} \times 100 \quad (1)$$

where substrate accumulation in the cells + bile compartments was determined in hepatocytes preincubated in standard buffer; cellular accumulation of substrate was determined in hepatocytes preincubated with Ca^{2+}-free HBSS.

$$\text{in vitro } Cl_{biliary} = \frac{Accumulation_{Cells+Bile} - Accumulation_{Cells}}{AUC_{0-T}} \quad (2)$$

where AUC_{0-T} represents the product of the incubation time (T) and the initial concentration in the medium. *In vitro* $Cl_{biliary}$ values were scaled per kilogram body weight using 1 mg protein/1.5 x 10^6 cells (the typical value obtained in all preparations), 107 x 10^6 hepatocytes/g of human liver tissue (34), and 25.7 g of liver tissue per kg of body weight (35).

Steady-state fexofenadine concentrations were defined as the average perfusate concentration during the 50- to 60-min interval based on experiments performed by Tian et al. (18) in which outflow fexofenadine concentrations reached a plateau after 50 min of infusion in *in situ* single-pass perfused rat liver studies. The hepatic extraction ratio was calculated as the ratio of the difference between steady-state inflow and outflow fexofenadine concentrations and the steady-state inflow concentration. Unbound intrinsic biliary clearance ($Cl'_{biliary}$) was calculated as the ratio of the fexofenadine biliary excretion rate and the unbound liver concentration ($C_{liver,unbound}$).

All data were reported as mean ± SD (n = 3-4 per group). Statistical significance was assessed by one-way analysis of variance (ANOVA) with Dunnett's *post*-hoc test. In all cases, $p < 0.05$ was considered to be statistically significant.

Results

Pharmacokinetic Modeling and Simulation of Data from Healthy Human Subjects

The model scheme depicted in Fig. 2.1 best described the fexofenadine plasma concentration vs. time and urinary excretion rate vs. time data obtained from a previously published study (9), as shown in Fig. 2.2. Parameter estimates for fexofenadine disposition based on the human data are reported in Table 2.1. The ratio of the biliary (K_{bile}) and basolateral (K_{21}) efflux rate constants was 5.6, suggesting that once in the liver, the predominant process that determines fexofenadine disposition is excretion into bile.

To assess the influence of alterations in hepatic uptake (K_{12}) or excretion (K_{21}, K_{bile}) on fexofenadine systemic and hepatic exposure, simulations were performed using the parameter estimates in Table 2.1. Based on these simulations, a 50%, 100% and 300% change in the hepatic uptake rate constant (K_{12}) resulted in a 18% or greater difference in the systemic exposure of fexofenadine, determined as the AUC of the plasma concentration-time profile (Fig. 2.3.A). Similar changes in the basolateral efflux rate constant (K_{21}), and biliary excretion rate constant (K_{bile}), resulted in less than a 7% change in the systemic AUC, except for the 300% increase in basolateral efflux, which increased the systemic AUC ~14%. Importantly, hepatic exposure, determined as the AUC of the hepatic mass-time profile, was sensitive to changes in the hepatic uptake rate constant (K_{12}) as well as the biliary excretion rate constant (K_{bile}). A 50%, 100% and 300% change in K_{12} resulted in a 12–16%, 26–30% and 39–46% change, respectively in hepatic exposure. In contrast to systemic exposure, perturbations in K_{bile} produced at least a 18% difference in hepatic exposure for all simulations. Alterations in

the basolateral efflux rate constant (K_{21}) resulted in negligible changes in hepatic exposure of fexofenadine.

Biliary Excretion of Fexofenadine in Human Sandwich-Cultured Hepatocytes

The *in vitro* biliary excretion of [^{3}H]taurocholate, [^{3}H]digoxin and fexofenadine was measured in human SCH from two unrelated donors. Cellular accumulation of the model bile acid [^{3}H]taurocholate (73.8 and 57.8 pmol/mg protein) and BEI [58.1 and 52.4 %, (Table 2.2)] were consistent with previous data generated in this model system. As a positive control, the P-gp substrate [^{3}H]digoxin was evaluated in the presence and absence of GF120918. Cellular accumulation of [^{3}H]digoxin was increased slightly by GF120918 for one liver (21.0 vs. 29.9 pmol/mg protein); the BEI and *in vitro* biliary clearance of [^{3}H]digoxin were abolished completely by GF120918 in both livers (Table 2.2). Fexofenadine cellular accumulation increased slightly in the presence of GF120918 in both livers (66.2 vs. 93.2 and 62.5 vs. 65.1 pmol/mg protein), but fexofenadine BEI and *in vitro* biliary clearance were not decreased by GF120918 in human SCH. Both, BEI and *in vitro* biliary clearance values were decreased in hepatocytes from the second liver donor compared to the first for all three compounds, suggesting decreased development of the bile canalicular networks and/or canalicular protein function in this liver donor.

Fexofenadine Recovery in Perfused Livers from TR$^-$ Rats

Bile flow rates (mean ± SD) in TR$^-$ rat livers perfused with 5 μM taurocholate and 0.5 μM fexofenadine (control) or in combination with either 2 μM GF120918 or 5 μM bosentan, were 0.54 ± 0.04, 0.52 ± 0.02 and 0.60 ± 0.05 μL/min/g liver, respectively. Compared to control values, bile flow rates in livers from TR$^-$ rats perfused without 5 μM

taurocholate were decreased ~50% to 0.28 ± 0.03 µL/min/g liver. Bile flow in each group was stable during the 60-min perfusion period (Fig. 2.4.A). The total recovery of fexofenadine at the end of the perfusion period, as a percentage of the total infused dose, was 86 ± 16% in control, 77 ± 9% without taurocholate, 75 ± 4% with GF120918, and 81 ± 9% with bosentan.

Fexofenadine concentrations in outflow perfusate are presented in Fig. 2.4.B (mean ± SD). Outflow perfusate concentrations at the end of the infusion were significantly increased in the presence of GF120918 (171.5 ± 58.8 pmol/mL) and bosentan (209.0 ± 19.4 pmol/mL), compared to control (92.3 ± 29.4 pmol/mL); GF120918 and bosentan significantly decreased the extraction ratio of fexofenadine (Fig. 2.4.B; Table 2.3)]. The biliary excretion rate of fexofenadine was decreased ~38% when taurocholate was withheld from the inflow perfusate; coadministration of GF120918 and bosentan decreased the fexofenadine biliary excretion rate ~75% and ~35%, respectively (Fig. 2.4.C; Table 2.3). Unbound fexofenadine concentrations in livers were not significantly different among the treatment groups, although unbound liver concentrations tended to be higher in the presence of GF120918. Bosentan significantly decreased the ratio of fexofenadine unbound liver concentrations to outflow perfusate concentrations, consistent with inhibition of fexofenadine partitioning from perfusate to liver. Fexofenadine $CL'_{biliary}$ was only significantly decreased in the presence of GF120918.

Discussion

To evaluate the utility of fexofenadine as a probe substrate for hepatobiliary transport function, pharmacokinetic modeling and simulation studies based on previously published data were utilized to examine the impact of hepatic transport modulation on the systemic and hepatic exposure of fexofenadine in humans. Furthermore, modeling and simulation of fexofenadine data in humans was supported by *in vitro* studies in human SCH and perfused rat livers using various chemical modulators of hepatic transport proteins.

The pharmacokinetic model adequately described the mean fexofenadine plasma concentrations, urinary excretion rate and estimated cumulative mass in bile data after a 120 mg oral dose (Fig. 2.2); low variability was associated with the parameter estimates (Table 2.1). Although the predominant process determining the systemic clearance of fexofenadine in humans appears to be hepatic uptake based on the parameter estimates governing fexofenadine disposition (Table 2.1), the hepatic uptake clearance of fexofenadine is low [K_{12} x V_c = 6.92 L/h] relative to hepatic blood flow in humans ~87 L/h (35) .

To examine the sensitivity of systemic and hepatic exposure to changes in hepatic uptake and efflux processes in humans, a simulation approach was utilized, and the rate constants representing the active transport processes governing hepatic uptake and efflux were modulated in a systematic manner. The results indicated that the central compartment, representing the systemic circulation, is most sensitive to changes in the hepatic uptake rate constant, rather than the basolateral efflux rate constant, or the biliary excretion rate constant (Fig. 2.3). This finding is supported by the absence of drug-drug interactions (defined as a significant change in fexofenadine

pharmacokinetics) when fexofenadine is administered with known P-gp modulators such as diltiazem (9) or verapamil (3), or in individuals with P-gp polymorphisms (C3435T and G2677T) (14, 36, 37). Furthermore, simulations are consistent with drug-drug interaction studies with known OATP modulators such as fruit juices (30), and in individuals with polymorphisms of the *SLCO1B1* gene (38), where significant changes in fexofenadine AUC have been reported. In contrast, simulations revealed that hepatic fexofenadine exposure in humans was sensitive to alterations in either the hepatic uptake rate constant or the biliary excretion rate constant. Most importantly, the marked increase in fexofenadine hepatic exposure due to modulation of K_{bile} was not reflected by changes in the systemic concentration-time profile in humans (Fig. 2.3). This demonstrates the difficulty in assessing hepatic exposure by only measuring systemic concentrations of a substrate like fexofenadine. In humans, multiple transport proteins appear to be involved in fexofenadine biliary excretion, thus, the suitability of this substrate as a probe to assess altered hepatic excretion in humans is limited. However, based on perfused rat liver data, the GF120918-sensitive component of biliary excretion plays a predominant role in canalicular transport in rats; inhibition of fexofenadine biliary excretion resulted in increased perfusate concentrations. These data underscore the importance of species differences in hepatobiliary drug transport, and the important role that compensatory transport proteins may play in determining the systemic and/or hepatic exposure of a substrate when hepatic transport processes are modulated. Furthermore, as depicted in Figure 2.3, significant interactions in hepatic excretion of a drug that displays hepatobiliary disposition characteristics similar to fexofenadine may not be reflected by changes in the plasma concentration-time profile.

To investigate the changes in systemic and hepatic exposure after inhibition of fexofenadine biliary excretion, and examine the involvement of P-gp in the biliary

excretion of fexofenadine in humans, studies were performed in human SCH using the inhibitor GF120918. The possible involvement of BCRP was ruled out based on previously published data generated in MDCKII cells transfected with human BCRP demonstrating that BCRP does not transport fexofenadine (19). OATP and P-gp function were assessed by the probe substrate [^{3}H]digoxin as a positive control. Intracellular accumulation and BEI values of [^{3}H]digoxin were comparable to previously reported data (39, 40). GF120918 (2 μM), used previously to inhibit P-gp in rat SCH (39), completely abolished the BEI and *in vitro* $Cl_{biliary}$ of [^{3}H]digoxin in human SCH (Table 2.2). Fexofenadine exhibited a low BEI and *in vitro* $Cl_{biliary}$ which was marginally affected by GF120918. The trend towards increased hepatocellular accumulation of fexofenadine in the presence of GF120918 (Table 2.2) is in agreement with the pharmacokinetic simulations which predicted that hepatic accumulation would increase when the biliary excretion rate constant was decreased (Fig. 2.3.B). However the possibility that GF120918-mediated inhibition of basolateral efflux results in increased hepatocellular accumulation of fexofenadine cannot be ruled out. These data suggest that GF120918-sensitive protein(s) (presumably P-gp) play a minor role in fexofenadine biliary excretion in human hepatocytes. Quite possibly, other canalicular transport proteins fully compensate when GF120918-sensitive protein(s) is/are inhibited. Fexofenadine is a known substrate for human MRP2 and BSEP based on previously published studies using MDCKII and HEK293 transfected cells (11, 19). These data imply that fexofenadine would not be a suitable probe substrate in humans to assess altered biliary excretion associated with a specific canalicular transport process.

Due to the limited availability of human hepatocytes, the lack of specific MRP2 inhibitors that would not affect OATP-mediated fexofenadine uptake, and the multiplicity of efflux transport proteins involved in fexofenadine hepatobiliary disposition in humans

(19, 41), further investigations were conducted in rat perfused livers. Previous studies demonstrated that the biliary excretion and intrinsic biliary clearance of fexofenadine were not significantly different in wild-type and Mrp2-deficient rats (5, 18). Therefore, TR^- rats were employed in the present studies to rule out any compensatory role of Mrp2 in the biliary excretion of fexofenadine. Co-infusion of fexofenadine and GF120918 resulted in a significant decrease in both the biliary excretion rate and the intrinsic biliary clearance of fexofenadine (Fig. 2.4.C; Table 2.3). Fexofenadine is a substrate of the basolateral efflux protein Mrp3 (19, 41), which is upregulated 7-fold in TR^- rats (42) and may explain the significant increase in outflow perfusate concentrations of fexofenadine in the presence of GF120918. This observation is supported by simulations examining the impact of induction of the basolateral efflux rate constant (K_{21}) on fexofenadine disposition, which resulted in noticeable changes in the plasma AUC (Fig 2.3.A). Although fexofenadine liver concentrations tended to be higher when biliary excretion was inhibited by GF120918 in perfused TR^- rat livers, as predicted in humans based on the pharmacokinetic simulations, differences failed to reach statistical significance. This apparent discrepancy could be due to species differences in the role of basolateral efflux proteins in fexofenadine hepatobiliary disposition. In humans, perturbations in biliary excretion only affected hepatic exposure; basolateral efflux was such a minor pathway that systemic exposure was not influenced by changes in biliary excretion. Basolateral efflux may play a more important role in systemic exposure of fexofenadine in the rat based on the present data, and also in the mouse as reported previously using Mrp2 knock-out mice (19, 41).

Fexofenadine is not a substrate of human or mouse BCRP/Bcrp based on previously published data generated in MDCKII cells transfected with human BCRP, or in Bcrp knockout mice (5, 19). Therefore, the predominant pathway for excretion of

fexofenadine into rat bile is likely P-gp, in contrast to the mouse in which Mrp2 plays the greatest role (18). This is supported by Milne et al., who demonstrated that the P-gp inhibitor erythromycin decreased cumulative recovery of fexofenadine in bile, and slightly increased hepatic accumulation and the perfusate AUC of fexofenadine in rat isolated perfused livers (43). Interestingly, mass balance data reported by these investigators indicated that 50% of the fexofenadine dose remained in the liver at the end of perfusion. Our studies revealed that ~40% of the fexofenadine dose was retained within the rat liver at the end of perfusion. As previously suggested, the liver may act as a reversible binding or sequestration site as well as an elimination organ for fexofenadine (3).

Withholding taurocholate from the perfusion buffer resulted in a significant decrease in the biliary excretion rate of fexofenadine (Fig. 2.4.C; Table 2.3). Hepatic fexofenadine concentrations were similar to control livers perfused with fexofenadine and taurocholate. The significant decrease in the biliary excretion of fexofenadine may be due to reduced canalicular localization of Bsep and other ABC transport proteins that mediate fexofenadine biliary excretion, causing a modest shift in the route of fexofenadine excretion to perfusate. Treatment of rats *in vivo* with taurocholate has been shown to modestly increase canalicular ABC transport protein expression on the hepatocyte canalicular membrane within minutes (28, 29).

Fexofenadine has been shown to be a substrate of human and rat BSEP/Bsep using *in vitro* transfected systems (19). Therefore, bosentan, a known inhibitor of Bsep (27), was concurrently infused into the perfusate. Although bosentan was expected to decrease fexofenadine biliary excretion, only a 35% decrease in the biliary excretion rate was noted (Table 2.3). Interestingly, bosentan significantly decreased the extraction ratio and partitioning of fexofenadine from perfusate to liver (Table 2.3). These results may

be due to bosentan-mediated inhibition of fexofenadine hepatic uptake, and/or to increased basolateral efflux as a result of inhibition of fexofenadine biliary excretion; either scenario would result in significantly increased fexofenadine perfusate concentrations (Fig. 2.4.B; Table 2.3). Bosentan is a substrate of all three Oatp isoforms in the rat liver [Oatp1a1, 1a4 and 1b2; (44)] which are responsible for fexofenadine hepatic uptake (8). Furthermore, bosentan (100 μM) competitively inhibited (by ~40%) the transport of model probes of the human OATP1B1, 1B3 and 2B1 isoforms in transfected CHO cell lines (45). Interestingly, the simulations of impaired hepatic uptake of fexofenadine in humans agreed with the results from perfused rat liver studies: perfusate (a surrogate for plasma) concentrations significantly increased in the presence of bosentan (Fig. 2.4.B).

Conclusion

In summary, pharmacokinetic modeling and simulation studies revealed that fexofenadine in humans is not an optimal probe for any specific hepatic efflux transport protein due to compensatory hepatic transport mechanisms. Systemic fexofenadine concentrations are most sensitive to changes in fexofenadine hepatic uptake. Increased or decreased hepatocyte concentrations as a result of impaired or induced biliary or hepatic basolateral efflux, respectively, associated with drug-drug interactions or genetic mutations, has minimal impact on systemic exposure. Furthermore, pharmacokinetic modeling and simulation studies were in good agreement with preclinical data that predicted changes in systemic and liver exposure due to inhibition of hepatic uptake. Studies in perfused livers from TR^- rats demonstrated that fexofenadine biliary excretion is mediated primarily by a GF120918-sensitive (presumably P-gp) mechanism. In contrast, either P-gp plays a minor role in fexofenadine biliary excretion in human

hepatocytes, or other canalicular transport proteins fully compensate when P-gp is inhibited.

List of Nonstandard Abbreviations:

SCH, sandwich-cultured hepatocytes, OATP, organic anion transporting polypeptide; MDR1, multidrug resistance protein 1; P-gp, P-glycoprotein; Mrp, multidrug resistance-associated protein; TR^-, Mrp2-deficient Wistar rat; EHBR, Eisai hyperbilirubinemic rats; Bsep, bile salt export pump; Bcrp, breast cancer resistance protein; WT, wild-type Wistar rat; GF120918, N-(4-[2-(1,2,3,4-tetrahydro-6,7-dimethoxy-2-isoquinolinyl)ethyl]-phenyl)-9,10-dihydro-5-methoxy-9-oxo-4-acridine carboxamide; ABC, ATP-binding cassette; DMEM, Dulbecco's modified Eagle's medium; FBS, Fetal bovine serum; HBSS, Hanks' balanced salt solution; BCA, Bicinchoninic acid; LC/MS/MS**,** liquid chromatography with detection by tandem mass spectrometry; AUC, area under the curve; ABC, ATP binding cassette

Acknowledgment

The authors would like to thank Arlene S. Bridges, Ph. D. for her analytical support, and Yiwei Rong, for her technical expertise in the isolation of human hepatocytes. This research was supported by a grant from the National Institutes of Health (R01 GM41935). Brandon Swift is supported by an Eli Lilly predoctoral fellowship.

References

1. N. Petri, C. Tannergren, D. Rungstad, and H. Lennernas. Transport characteristics of fexofenadine in the Caco-2 cell model. *Pharm Res* **21**: 1398-404 (2004).

2. C. Tannergren, T. Knutson, L. Knutson, and H. Lennernas. The effect of ketoconazole on the in vivo intestinal permeability of fexofenadine using a regional perfusion technique. *Br J Clin Pharmacol* **55**: 182-90 (2003).

3. C. Tannergren, N. Petri, L. Knutson, M. Hedeland, U. Bondesson, and H. Lennernas. Multiple transport mechanisms involved in the intestinal absorption and first-pass extraction of fexofenadine. *Clin Pharmacol Ther* **74**: 423-36 (2003).

4. C. Lippert, Ling, J., Brown, P., Burmaster, S., Eller, M., Cheng, L., Thompson, R., and Weir, S. Mass Balance and Pharmacokinetics of MDL 16,455A in Healthy, Male Volunteers. *Pharmaceutical Research* **12**: S-390 (1995).

5. H. Tahara, H. Kusuhara, E. Fuse, and Y. Sugiyama. P-glycoprotein plays a major role in the efflux of fexofenadine in the small intestine and blood-brain barrier, but only a limited role in its biliary excretion. *Drug Metab Dispos* **33**: 963-8 (2005).

6. M. A. Hamman, M. A. Bruce, B. D. Haehner-Daniels, and S. D. Hall. The effect of rifampin administration on the disposition of fexofenadine. *Clin Pharmacol Ther* **69**: 114-21 (2001).

7. C. Banfield, S. Gupta, M. Marino, J. Lim, and M. Affrime. Grapefruit juice reduces the oral bioavailability of fexofenadine but not desloratadine. *Clin Pharmacokinet* **41**: 311-8 (2002).

8. H. Glaeser, D. G. Bailey, G. K. Dresser, J. C. Gregor, U. I. Schwarz, J. S. McGrath, E. Jolicoeur, W. Lee, B. F. Leake, R. G. Tirona, and R. B. Kim. Intestinal drug transporter expression and the impact of grapefruit juice in humans. *Clin Pharmacol Ther* **81**: 362-70 (2007).

9. M. Shimizu, T. Uno, K. Sugawara, and T. Tateishi. Effects of itraconazole and diltiazem on the pharmacokinetics of fexofenadine, a substrate of P-glycoprotein. *Br J Clin Pharmacol* **61**: 538-44 (2006).

10. M. Cvetkovic, B. Leake, M. F. Fromm, G. R. Wilkinson, and R. B. Kim. OATP and P-glycoprotein transporters mediate the cellular uptake and excretion of fexofenadine. *Drug Metab Dispos* **27**: 866-71 (1999).

11. S. Matsushima, K. Maeda, N. Ishiguro, T. Igarashi, and Y. Sugiyama. Investigation of the inhibitory effects of various drugs on the hepatic uptake of fexofenadine in humans. *Drug Metab Dispos* (2008).

12. M. Shimizu, K. Fuse, K. Okudaira, R. Nishigaki, K. Maeda, H. Kusuhara, and Y. Sugiyama. Contribution of OATP (organic anion-transporting polypeptide) family transporters to the hepatic uptake of fexofenadine in humans. *Drug Metab Dispos* **33**: 1477-81 (2005).

13. G. T. Tucker, J. B. Houston, and S. M. Huang. Optimizing drug development: strategies to assess drug metabolism/transporter interaction potential--towards a consensus. *Br J Clin Pharmacol* **52**: 107-17 (2001).

14. J. H. Shon, Y. R. Yoon, W. S. Hong, P. M. Nguyen, S. S. Lee, Y. G. Choi, I. J. Cha, and J. G. Shin. Effect of itraconazole on the pharmacokinetics and pharmacodynamics of fexofenadine in relation to the MDR1 genetic polymorphism. *Clin Pharmacol Ther* **78**: 191-201 (2005).

15. S. Zhou, E. Chan, S. Q. Pan, M. Huang, and E. J. Lee. Pharmacokinetic interactions of drugs with St John's wort. *J Psychopharmacol* **18**: 262-76 (2004).

16. G. L. Lemma, Z. Wang, M. A. Hamman, N. A. Zaheer, J. C. Gorski, and S. D. Hall. The effect of short- and long-term administration of verapamil on the disposition of cytochrome P450 3A and P-glycoprotein substrates. *Clin Pharmacol Ther* **79**: 218-30 (2006).

17. N. Yasui-Furukori, T. Uno, K. Sugawara, and T. Tateishi. Different effects of three transporting inhibitors, verapamil, cimetidine, and probenecid, on fexofenadine pharmacokinetics. *Clin Pharmacol Ther* **77**: 17-23 (2005).

18. X. Tian, M. J. Zamek-Gliszczynski, J. Li, A. S. Bridges, K. Nezasa, N. J. Patel, T. J. Raub, and K. L. Brouwer. Multidrug resistance-associated protein 2 is primarily responsible for the biliary excretion of fexofenadine in mice. *Drug Metab Dispos* **36**: 61-4 (2008).

19. S. Matsushima, K. Maeda, H. Hayashi, Y. Debori, A. H. Schinkel, J. D. Schuetz, H. Kusuhara, and Y. Sugiyama. Involvement of multiple efflux transporters in hepatic disposition of fexofenadine. *Mol Pharmacol* (2008).

20. J. A. Byrne, S. S. Strautnieks, G. Mieli-Vergani, C. F. Higgins, K. J. Linton, and R. J. Thompson. The human bile salt export pump: characterization of substrate specificity and identification of inhibitors. *Gastroenterology* **123**: 1649-58 (2002).

21. M. Hirano, K. Maeda, H. Hayashi, H. Kusuhara, and Y. Sugiyama. Bile salt export pump (BSEP/ABCB11) can transport a nonbile acid substrate, pravastatin. *J Pharmacol Exp Ther* **314**: 876-82 (2005).

22. V. Lecureur, D. Sun, P. Hargrove, E. G. Schuetz, R. B. Kim, L. B. Lan, and J. D. Schuetz. Cloning and expression of murine sister of P-glycoprotein reveals a more discriminating transporter than MDR1/P-glycoprotein. *Mol Pharmacol* **57**: 24-35 (2000).

23. U. Hoffmannand H. K. Kroemer. The ABC transporters MDR1 and MRP2: multiple functions in disposition of xenobiotics and drug resistance. *Drug Metab Rev* **36**: 669-701 (2004).

24. S. Kawabata, M. Oka, K. Shiozawa, K. Tsukamoto, K. Nakatomi, H. Soda, M. Fukuda, Y. Ikegami, K. Sugahara, Y. Yamada, S. Kamihira, L. A. Doyle, D. D. Ross, and S. Kohno. Breast cancer resistance protein directly confers SN-38 resistance of lung cancer cells. *Biochem Biophys Res Commun* **280**: 1216-23 (2001).

25. M. Suzuki, H. Suzuki, Y. Sugimoto, and Y. Sugiyama. ABCG2 transports sulfated conjugates of steroids and xenobiotics. *J Biol Chem* **278**: 22644-9 (2003).

26. G. Merino, J. W. Jonker, E. Wagenaar, A. E. van Herwaarden, and A. H. Schinkel. The breast cancer resistance protein (BCRP/ABCG2) affects pharmacokinetics, hepatobiliary excretion, and milk secretion of the antibiotic nitrofurantoin. *Mol Pharmacol* **67**: 1758-64 (2005).

27. K. Fattinger, C. Funk, M. Pantze, C. Weber, J. Reichen, B. Stieger, and P. J. Meier. The endothelin antagonist bosentan inhibits the canalicular bile salt export pump: a potential mechanism for hepatic adverse reactions. *Clin Pharmacol Ther* **69**: 223-31 (2001).

28. Z. C. Gatmaitan, A. T. Nies, and I. M. Arias. Regulation and translocation of ATP-dependent apical membrane proteins in rat liver. *Am J Physiol* **272**: G1041-9 (1997).

29. H. Kipp, N. Pichetshote, and I. M. Arias. Transporters on demand: intrahepatic pools of canalicular ATP binding cassette transporters in rat liver. *J Biol Chem* **276**: 7218-24 (2001).

30. G. K. Dresser, D. G. Bailey, B. F. Leake, U. I. Schwarz, P. A. Dawson, D. J. Freeman, and R. B. Kim. Fruit juices inhibit organic anion transporting polypeptide-mediated drug uptake to decrease the oral availability of fexofenadine. *Clin Pharmacol Ther* **71**: 11-20 (2002).

31. E. L. LeCluyse, P. L. Bullock, A. Parkinson, and J. H. Hochman. Cultured rat hepatocytes. *Pharm Biotechnol* **8**: 121-59 (1996).

32. X. Liu, E. L. LeCluyse, K. R. Brouwer, L. S. Gan, J. J. Lemasters, B. Stieger, P. J. Meier, and K. L. Brouwer. Biliary excretion in primary rat hepatocytes cultured in a collagen-sandwich configuration. *Am J Physiol* **277**: G12-21 (1999).

33. P. Chandra, B. M. Johnson, P. Zhang, G. M. Pollack, and K. L. Brouwer. Modulation of hepatic canalicular or basolateral transport proteins alters hepatobiliary disposition of a model organic anion in the isolated perfused rat liver. *Drug Metab Dispos* **33**: 1238-43 (2005).

34. Z. E. Wilson, A. Rostami-Hodjegan, J. L. Burn, A. Tooley, J. Boyle, S. W. Ellis, and G. T. Tucker. Inter-individual variability in levels of human microsomal protein and hepatocellularity per gram of liver. *Br J Clin Pharmacol* **56**: 433-40 (2003).

35. B. Daviesand T. Morris. Physiological parameters in laboratory animals and humans. *Pharm Res* **10**: 1093-5 (1993).

36. S. Drescher, E. Schaeffeler, M. Hitzl, U. Hofmann, M. Schwab, U. Brinkmann, M. Eichelbaum, and M. F. Fromm. MDR1 gene polymorphisms and disposition of the P-glycoprotein substrate fexofenadine. *Br J Clin Pharmacol* **53**: 526-34 (2002).

37. R. B. Kim, B. F. Leake, E. F. Choo, G. K. Dresser, S. V. Kubba, U. I. Schwarz, A. Taylor, H. G. Xie, J. McKinsey, S. Zhou, L. B. Lan, J. D. Schuetz, E. G. Schuetz, and G. R. Wilkinson. Identification of functionally variant MDR1 alleles among European Americans and African Americans. *Clin Pharmacol Ther* **70**: 189-99 (2001).

38. M. Niemi, K. T. Kivisto, U. Hofmann, M. Schwab, M. Eichelbaum, and M. F. Fromm. Fexofenadine pharmacokinetics are associated with a polymorphism of the SLCO1B1 gene (encoding OATP1B1). *Br J Clin Pharmacol* **59**: 602-4 (2005).

39. P. P. Annaert, R. Z. Turncliff, C. L. Booth, D. R. Thakker, and K. L.R. Brouwer. P-glycoprotein-mediated in vitro biliary excretion in sandwich-cultured rat hepatocytes. *Drug Metab Dispos* **29**: 1277-83 (2001).

40. Y. A. Bi, D. Kazolias, and D. B. Duignan. Use of cryopreserved human hepatocytes in sandwich culture to measure hepatobiliary transport. *Drug Metab Dispos* **34**: 1658-65 (2006).

41. X. Tian, B. Swift, M. J. Zamek-Gliszczynski, M. G. Belinsky, G. D. Kruh, and K. L.R. Brouwer. Impact of basolateral multidrug resistance-associated protein

(Mrp) 3 and Mrp4 on the hepatobiliary disposition of fexofenadine in perfused mouse livers. *Drug Metab Dispos* **36**: 911-5 (2008).

42. H. Xiong, K. C. Turner, E. S. Ward, P. L. Jansen, and K. L. Brouwer. Altered hepatobiliary disposition of acetaminophen glucuronide in isolated perfused livers from multidrug resistance-associated protein 2-deficient TR(-) rats. *J Pharmacol Exp Ther* **295**: 512-8 (2000).

43. R. W. Milne, L. A. Larsen, K. L. Jorgensen, J. Bastlund, G. R. Stretch, and A. M. Evans. Hepatic disposition of fexofenadine: influence of the transport inhibitors erythromycin and dibromosulphothalein. *Pharm Res* **17**: 1511-5 (2000).

44. A. Treiber, R. Schneiter, S. Delahaye, and M. Clozel. Inhibition of organic anion transporting polypeptide-mediated hepatic uptake is the major determinant in the pharmacokinetic interaction between bosentan and cyclosporin A in the rat. *J Pharmacol Exp Ther* **308**: 1121-9 (2004).

45. A. Treiber, R. Schneiter, S. Hausler, and B. Stieger. Bosentan is a substrate of human OATP1B1 and OATP1B3: inhibition of hepatic uptake as the common mechanism of its interactions with cyclosporin A, rifampicin, and sildenafil. *Drug Metab Dispos* **35**: 1400-7 (2007).

Legend to Figures

Figure 2.1. Model scheme depicting fexofenadine disposition in healthy humans. X_{gut} represents the amount of fexofenadine in the gut after an oral dose; K_{absorb} represents the first–order absorption rate constant; C_C represents the concentration of fexofenadine in the central compartment (systemic circulation) with volume V_C; K_{12} represents the first–order rate constant for hepatic uptake; K_{21} represents the first-order rate constant for hepatic basolateral efflux; X_{liver} represents the amount of fexofenadine in the liver; K_{bile} represents the first–order rate constant for biliary excretion; X_{bile} represents the amount of fexofenadine in bile; K_{urine} represents the first–order rate constant for urinary excretion; X_{urine} represents the amount of fexofenadine in urine.

Figure 2.2. Mean fexofenadine disposition in healthy humans. The curves represent the best fit of the pharmacokinetic model based on the scheme depicted in Fig. I to the data obtained from Shimizu et al. (9). The plasma concentration-time profile (♦; solid line) and urinary excretion rate-time profile (▲; dashed line) are plotted on log-linear scale. Symbols represent actual data points while lines represent the best fit of the model to the data.

Figure 2.3. Simulated percentage change from baseline in the AUC of the (A) plasma concentration-time profile, predictive of systemic exposure, and (B) hepatic mass-time profile, predictive of hepatic exposure, associated with perturbations in the hepatic uptake rate constant (K_{12}; *solid bars*), basolateral efflux rate constant (K_{21}; *hatched bars*) and biliary excretion rate constant (K_{bile}; *open bars*).

Figure 2.4. Data generated in perfused livers from Mrp2-deficient TR^- rats. **(A)** Bile flow rates, **(B)** Fexofenadine concentrations in outflow perfusate, and **(C)** Biliary excretion rates of fexofenadine in livers perfused with 0.5 μM fexofenadine (●), 0.5 μM fexofenadine without 5 μM taurocholate (□), 0.5 μM fexofenadine + GF120918 (Δ), and 0.5 μM fexofenadine + bosentan (◊). Perfusate buffer contained 5 μM taurocholate, unless otherwise noted. Data represent mean ± SD (n-3-4 per group).

Table 2.1 Pharmacokinetic parameters governing fexofenadine disposition in healthy humans estimated using nonlinear regression analysis based on the compartmental model scheme depicted in Fig. 3.1. Parameter estimates and coefficients of variation were generated based on mean data (n=8 healthy subjects) from a previously published report (6).

Parameters	Estimate	CV (%)
K_{absorb} (h^{-1})	1.67	23.0
V_c (L)	55.8	7.71
K_{12} (h^{-1})	0.124	11.0
K_{21} (h^{-1})	0.00788	49.7
K_{bile} (h^{-1})	0.0438	11.1
K_{urine} (h^{-1})	0.0689	10.1

Table 2.2. Accumulation, BEI and *in vitro* $Cl_{biliary}$ of [^{3}H]Taurocholate, [^{3}H]Digoxin and Fexofenadine in human SCH. SCH were incubated with 1 µM [^{3}H]taurocholate (10 min), 1 µM [^{3}H]digoxin (10 min) or 5 µM fexofenadine (30 min) in the presence and absence of 2 µM GF120918. Results are presented as representative data from triplicate experiments from two livers. The incubation time (t) is indicated in parentheses.

Substrate	Accumulation Cells + Bile (pmol/mg)	Accumulation Cells (pmol/mg)	BEI %	*in vitro* $Cl_{biliary}$ (mL/min/kg)
[^{3}H]Taurocholate (t=10 min)	176 ± 5	73.8 ± 2.3	58.1	18.7
	121 ± 11	57.8 ± 5.5	52.4	11.6
[^{3}H]Digoxin (t=10 min)	28.1 ± 1.6	21.0 ± 1.3	25.0	1.29
	26.9 ± 1.5	25.1 ± 2.4	6.76	0.33
[^{3}H]Digoxin + 2 µM GF120918 (t=10 min)	26.2 ± 0.9	29.9 ± 1.6	0	0
	23.4 ± 2.3	25.2 ± 1.6	0	0
Fexofenadine (t=30 min)	78.8 ± 8.2	66.2 ± 3.7	16.0	0.15
	66.3 ± 19.1	62.5 ± 4.3	5.79	0.05
Fexofenadine + 2 µM GF120918 (t=30 min)	112 ± 6	93.2 ± 9.7	16.8	0.23
	73.2 ± 3.8	65.1 ± 2.3	11.0	0.10

Table 2.3 Fexofenadine disposition in single-pass perfused TR^- rat livers. Mean ± SD (n = 3-4 per group). * p< 0.05 fexofenadine ± modulator vs. fexofenadine alone. # Total concentration determined based on 50–60-min collection interval. Perfusate buffer contained 5 μM taurocholate, unless otherwise noted.

	0.5 μM Fexofenadine	**0.5 μM Fexofenadine without TC**	**0.5 μM Fexofenadine + 2 μM GF120918**	**0.5 μM Fexofenadine + 5 μM Bosentan**
$C_{ss,out}$ (pmol/mL) #	92.3 ± 29.4	135 ± 21	172 ± 59*	209 ± 19*
C_{liver} (pmol/mL)	7295 ± 786	7156 ± 1529	8159 ± 720	5561 ± 873
$C_{liver, unbound}$ (pmol/mL)	1389 ± 196	1282 ± 142	1631 ± 620	1235 ± 369
$C_{liver, unbound}$ / $C_{ss,out}$	16.2 ± 5.4	9.53± 0.46	10.8 ± 6.0	6.05 ± 2.34*
Extraction Ratio	0.82 ± 0.06	0.73 ± 0.04	0.66 ± 0.12*	0.58± 0.04*
Biliary Excretion Rate (pmol/min/g liver)	218 ± 66	136 ± 34*	55.6 ± 6.4*	142 ± 29
$Cl'_{biliary}$ (mL/h/g liver)	8.57 ± 2.00	6.56 ± 2.27	2.36 ± 1.12*	7.52 ± 2.78

Figure 2.1

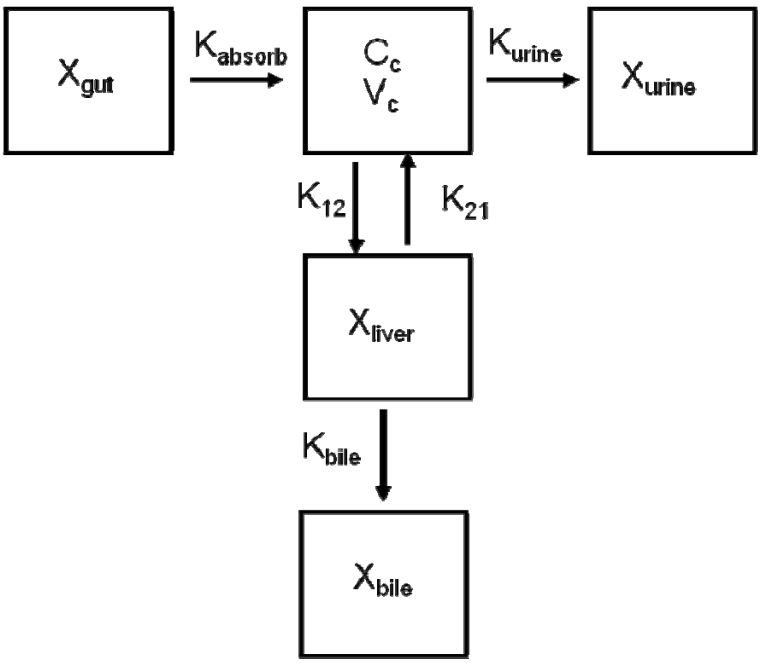

Figure 2.2

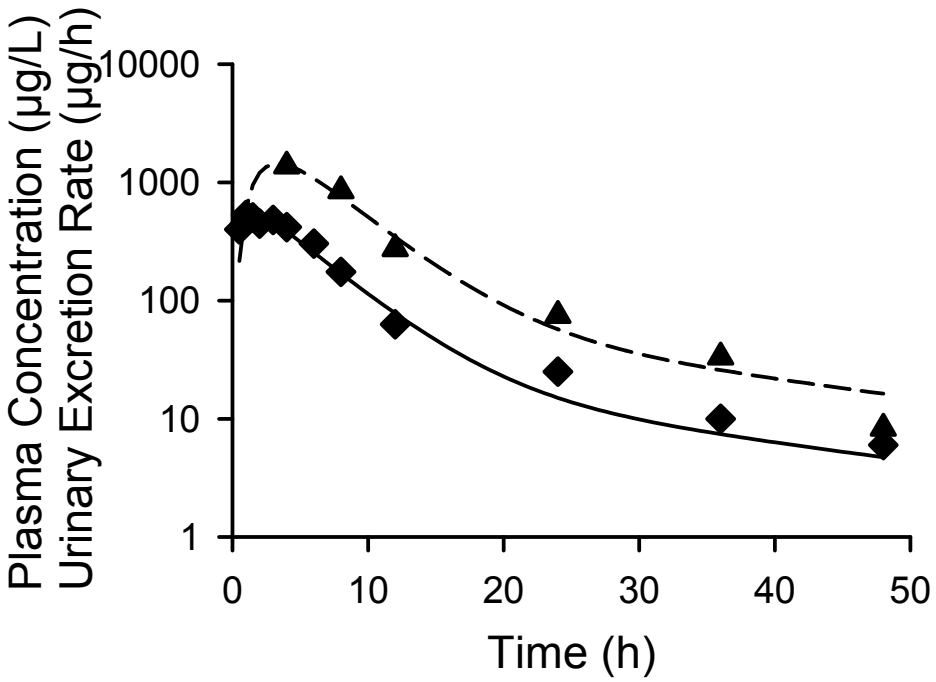
Plasma Concentration (µg/L)
Urinary Excretion Rate (µg/h)
10000
1000
100
10
1
0
10
20
30
40
50
Time (h)

Figure 2.3

(A)

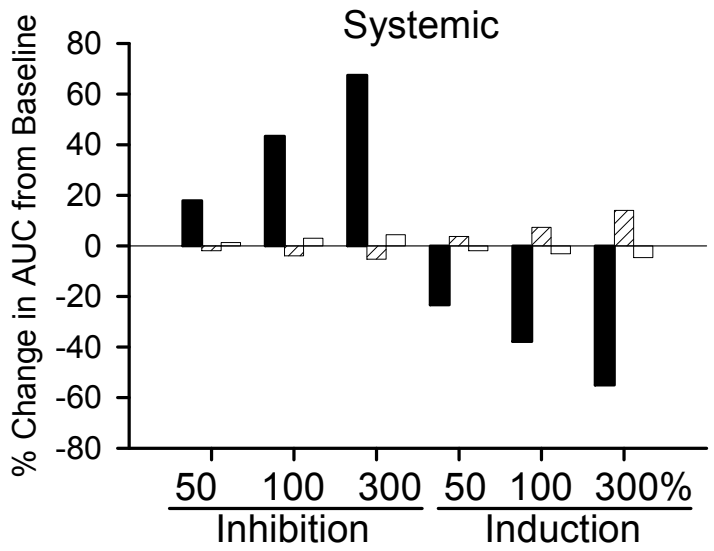
Systemic
% Change in AUC from Baseline
80
60
40
20
0
-20
-40
-60
-80
50
100
300
50
100
300%
Inhibition
Induction

(B)

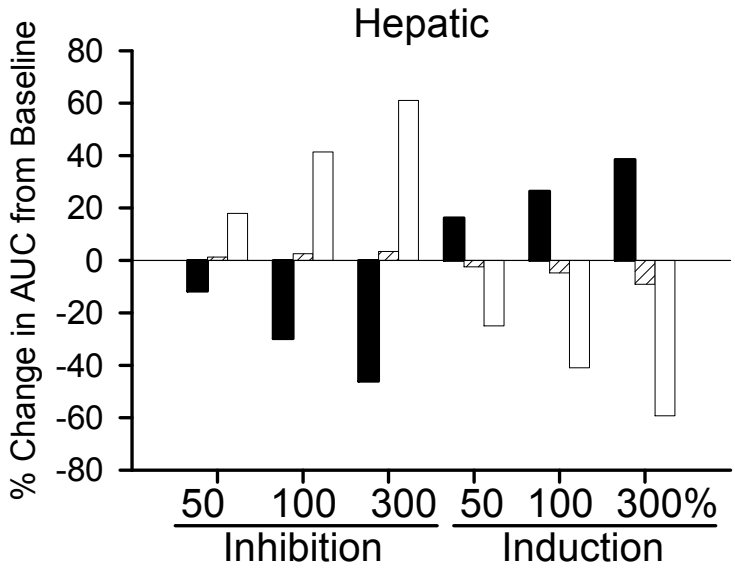
Hepatic
% Change in AUC from Baseline
80
60
40
20
0
-20
-40
-60
-80
50
100
300
50
100
300%
Inhibition
Induction

Figure 2.4

(A)

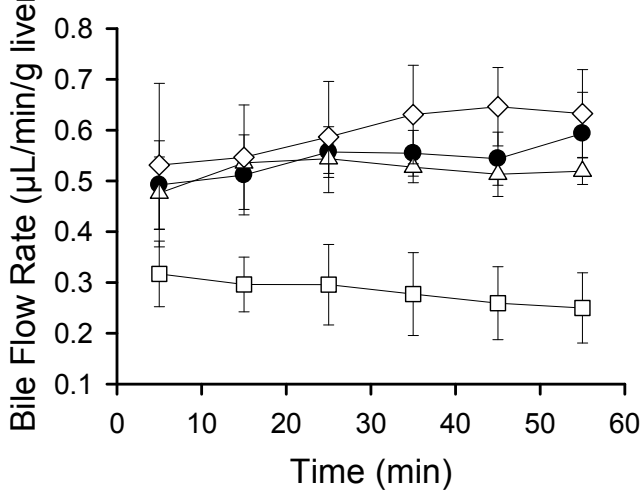

(B)

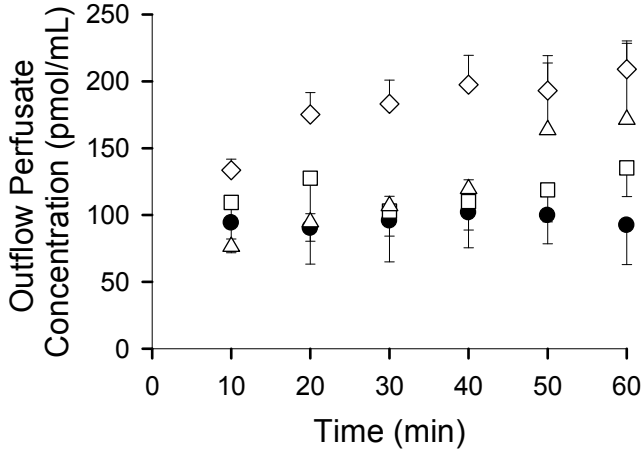

(C)

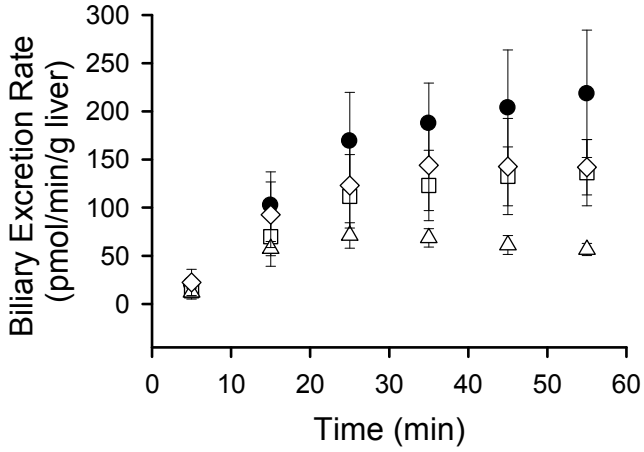

CHAPTER 3

Impact of Basolateral Mrp3 (Abcc3) and Mrp4 (Abcc4) on the Hepatobiliary Disposition of Fexofenadine in Perfused Mouse Livers

This chapter is published in Drug Metabolism and Disposition 2008 May; 36(5):911-5,

Abstract

The disposition of fexofenadine, a commonly-used antihistamine drug, is governed primarily by active transport. Biliary excretion of the parent compound is the major route of systemic clearance. Previous studies demonstrated that fexofenadine hepatic uptake is mediated by organic anion transporting polypeptides. Recently, we showed that in mice fexofenadine is excreted into bile primarily by Mrp2 (Abcc2). In the present study, the role of Mrp3 (Abcc3) and Mrp4 (Abcc4) in the hepatobiliary disposition of fexofenadine was examined in knockout mice using *in situ* liver perfusion. Compared to wild-type mice, basolateral excretion of fexofenadine was impaired resulting in a ~50% decrease in perfusate recovery in *Abcc3(-/-)* mice*;* in contrast, fexofenadine hepatobiliary disposition was unaltered in *Abcc4(-/-)* mice. As expected, in *Abcc2(-/-)* mice, fexofenadine was redirected from the canalicular to the basolateral membrane for excretion. In *Abcc2(-/-)/Abcc3(-/-)* double knock-out mice, fexofenadine biliary excretion was impaired, but perfusate recovery was similar to wild-type mice, and more than 2-fold higher than in *Abcc3(-/-)* mice, presumably due to compensatory basolateral transport mechanism(s). These results demonstrate that multiple transport proteins are involved in the hepatobiliary disposition of fexofenadine. In addition to Mrp2 and Mrp3, other transport proteins play an important role in the biliary and hepatic basolateral excretion of this zwitterionic drug.

Introduction

Fexofenadine is an H1 receptor antagonist commonly used in the treatment of seasonal allergies and chronic urticaria. The intestinal absorption of fexofenadine is mediated by organic anion transporting polypeptides (Oatps), a process that is counteracted by P-glycoprotein-mediated efflux (Cvetkovic et al., 1999). Metabolism accounts for less than 5% of total fexofenadine clearance in humans, and the oral and intravenous exposure of fexofenadine in rats is not altered by the pan-cytochrome P450 mechanism-based inactivator, aminobenzotriazole (Strelevitz et al., 2005). However, specific information regarding fexofenadine metabolism in mice is not available. Biliary excretion of unchanged fexofenadine is the primary route of systemic clearance (Tahara et al., 2005). Although fexofenadine intestinal absorption and blood-brain barrier penetration are limited by P-glycoprotein (Cvetkovic et al., 1999; Tahara et al., 2005), the biliary excretion of fexofenadine is mediated by multiple transport mechanisms (Tian et al., 2008). The unusual dispositional properties of fexofenadine, i.e. low metabolism and extensive transport, have led to its use as a probe for the analysis of both Oatp and P-glycoprotein modulation by various co-administered drugs and herbal products (Banfield et al., 2002; Zhou et al., 2004; Shon et al., 2005; Lemma et al., 2006).

Following uptake from sinusoidal blood into the hepatocyte, drugs and derived metabolites, may undergo excretion across the canalicular membrane into bile or across the basolateral membrane into blood. For example, carboxydichlorofluorescein is taken up into hepatocytes via basolateral Oatps, and is subsequently excreted unchanged into bile by multidrug resistance-associated protein (Mrp) 2 and also undergoes basolateral export into blood by Mrp3 (Zamek-Gliszczynski et al., 2003; Nezasa et al., 2006). Similarly, glucuronide conjugates of acetaminophen and morphine also are subject to

bidirectional excretion into bile and blood by Mrp2 and Mrp3, respectively (Xiong 2000, 2002, van de Wetering 2007, Zelcer 2005). Basolateral Mrp3 is similar to canalicular Mrp2 in terms of amino acid sequence, membrane topology, and substrate specificity (Konig et al., 1999; Ogawa et al., 2000). Mrp3 is highly upregulated in obstructive cholestasis (e.g. bile duct ligation) and hereditary conjugated hyperbilirubinemia in rats and humans (e.g. Mrp2-deficient animals, Dubin-Johnson patients), acting as an overflow pump for hepatic excretion of Mrp2 substrates and conjugated bile acids when biliary excretion is impaired (Hirohashi et al., 1998; Konig 1999). Although expression levels of Mrp3 protein are relatively high in mice, a 2-fold up-regulation of Mrp3 protein is still observed in Mrp2-knockout mice (Nezasa et al., 2005). Based upon recent findings that the biliary excretion of fexofenadine is mediated in part by Mrp2 in mice (Tian et al., 2008), we hypothesized that fexofenadine may also undergo hepatic basolateral excretion via Mrp3. In addition to Mrp3, Mrp4 functions as an excretory mechanism on the hepatic basolateral membrane (Rius et al., 2003). Limited evidence of functional overlap between Mrp3 and Mrp4 exists. For example, both Mrp3 and Mrp4 are upregulated in response to obstructive cholestasis (Hirohashi et al., 1998; Denk et al., 2004). Furthermore, both Mrp3 and Mrp4 mediate the hepatic basolateral excretion of the sulfate metabolites of acetaminophen, 4-methylumbelliferone, and harmol in mice (Zamek-Gliszczynski et al., 2006). While these features suggest that Mrp3 and Mrp4 may be involved in the hepatic basolateral excretion of fexofenadine, the extent to which these pumps function in this capacity has not been investigated.

Studies outlined in this manuscript tested the hypothesis that fexofenadine undergoes basolateral excretion from the liver via Mrp3 and Mrp4. Perfused livers from relevant transporter-gene knockout mice were utilized to examine the role of Mrp2, Mrp3 and Mrp4 in the hepatobiliary disposition of fexofenadine. Furthermore, the combined

role of Mrp2 and Mrp3 in the overall hepatic excretion of this zwitterion was studied in livers from *Abcc2(-/-)/Abcc3(-/-)* double-knockout mice. The data presented herein demonstrate the importance of Mrp2 and Mrp3 in the biliary and hepatic basolateral excretion, respectively, of fexofenadine in mice.

Material and Methods

Chemicals. Fexofenadine, cetirizine, taurocholate, and Krebs-Henseleit buffer packets were purchased from Sigma Chemical Co. (St. Louis, MO). All other chemicals were of reagent grade and were readily available from commercial sources.

Animals. Male C57BL/6 wild-type (WT) (age-matched heterozygotes), *Abcc2(-/-)*, *Abcc3(-/-)*, *Abcc2(-/-)/Abcc3(-/-)*, *and Abcc4(-/-)* mice (23-31g) were generated as described previously (Belinsky et al., 2005; Belinsky et al., 2007). *Abcc2(-/-)* mice have been generated recently by gene-targeting methods in the laboratory of Dr. Gary Kruh (unpublished). *Abcc2(-/-), Abcc3(-/-)* and *Abcc4(-/-)* mice employed in this study were derived from mixed 129/C57BL/6 animals and were backcrossed to C57BL/6 for eight generations. *Abcc2(-/-)* and *Abcc3(-/-)* mice on the C57BL/6 background were used to breed the *Abcc2(-/-)/Abcc3(-/-)* mice. Mice were maintained on a 12-h light/dark cycle with free access to water and rodent chow. Experiments were performed at Fox Chase Cancer Center and approved by their Institutional Animal Care and Use Committee.

In Situ Liver Perfusion. All experimental procedures were performed under full anesthesia induced with ketamine/xylazine (140/8 mg/kg i.p.). The liver perfusion procedure was modified slightly from the previous report of Tian et al (2007). Briefly, the common bile duct was ligated above the duodenum to prevent bile from entering the intestine, and the gallbladder was cannulated with PE-10 tubing (Becton Dickinson, Parsippany, NJ). The portal vein was cannulated with a 20-gauge catheter (B. Braun Medical Inc., Bethlehem, PA), the abdominal vena cava below the liver was severed immediately by incision, and the inferior vena cava above the liver was cannulated with a 20-gauge catheter. The liver was perfused (5 ml/min with fexofenadine-free continually oxygenated Krebs-Henseleit buffer containing 5 μM taurocholate) for an equilibration

period of approximately 15 min. Subsequently, the inferior vena cava was ligated between the liver and kidney to direct all perfusate outflow through the cannulated inferior vena cava above the liver. Following the pre-perfusion period to allow for equilibration of temperature and bile flow, the liver was perfused for 30 min with buffer containing 0.5 μM fexofenadine, followed by a washout with fexofenadine-free buffer for 45 min. Bile was collected in 7-min intervals; outflow perfusate was collected at designated time points *in toto*. Perfusion pressure and bile flow were monitored to assess liver viability (Chandra et al., 2005).

Analytical Methods. Bile and outflow perfusate samples were analyzed by liquid chromatography with detection by tandem mass spectrometry (Applied Biosystems API 4000 triple quadrupole with TurboIonSpray interface, MDS Sciex, Concord, ON, Canada). Fexofenadine and cetirizine (internal standard) were eluted from an Aquasil C18 column (5μm, 50mm x 2.1mm, Thermo-Electron, Waltham, MA) using a mobile phase gradient (A: 0.1% formic acid in water, B: 0.1% formic acid in methanol); 0-0.8 min hold at 10% B, 0.8-3.5 min linear increase to 85% B, 3.5-4.0 min hold at 85% B, 4.0-4.5 min return to 10% B, 4.5-5 min hold at 10% B; flow rate was 0.75 mL/min (Shimazdu solvent delivery system, Columbia, MD). Fexofenadine and the internal standard, cetirizine, were detected in positive ion mode using multiple reaction monitoring: fexofenadine: 502.3 $\rightarrow$ 466.4 m/z, cetirizine: 389.0 $\rightarrow$ 201.0 m/z. Fexofenadine was quantified with standard curves prepared in the appropriate matrix.

Data Analysis. All data were reported as mean ± SD (n = 3-4, per group). Statistical significance was assessed by one-way analysis of variance (ANOVA) with Tukey's *post*-hoc test. In cases where the normality test failed, data were log-transformed prior to statistical analysis. In all cases, $p < 0.05$ was considered to be statistically significant.

Results

Body weight, liver weight, and bile flow. Body weight was comparable between WT and knockout mice (Table 3.1). Liver weight (normalized for body weight) was significantly increased (~30%) in *Abcc2(-/-)* and (~46%) in *Abcc2(-/-)/Abcc3(-/-)* relative to WT mice. *Abcc3(-/-)* and *Abcc4(-/-)* mouse liver weights were comparable to WT controls (Table 3.1). The bile flow rate was decreased ~30% in *Abcc2(-/-)* and *Abcc2(-/-)/Abcc3(-/-)* mouse livers relative to WT, but was normal in livers from *Abcc3(-/-)* and *Abcc4(-/-)* mice (Table 3.1).

Recovery of fexofenadine in outflow perfusate. Fexofenadine concentrations in outflow perfusate from WT and knockout mouse livers are presented in Figure 3.1. For clarity, only mean data are plotted; standard deviations were within ~50% of the mean data. The total recovery of fexofenadine at the end of the washout period as a percentage of the infused dose was 73 ± 10% in WT, 62 ± 30% in *Abcc3(-/-),* 68 ± 9% in *Abcc4(-/-),* 77 ± 12% in *Abcc2(-/-)*, and 71 ± 15% in *Abcc2(-/-)/Abcc3(-/-)* mouse livers. In order to quantify the impact of Mrp3 and Mrp4 genetic ablation on the basolateral efflux of fexofenadine from the liver, fexofenadine recovery in perfusate during the washout phase was expressed as a percentage of liver fexofenadine content at the end of the infusion (determined as the difference between infused dose and the cumulative mass of fexofenadine excreted in outflow perfusate and bile through 30 min; Table 3.2). The fraction of fexofenadine excreted into outflow perfusate was significantly decreased (~50%) in livers from *Abcc3(-/-)* mice; in contrast, significantly increased perfusate recovery (~60%) was noted in *Abcc2(-/-)* relative to WT mouse livers. Interestingly, perfusate recovery of fexofenadine in livers from *Abcc2(-/-)/Abcc3(-/-)* mice was similar to WT control livers. In contrast to livers from *Abcc3(-/-)* mice, perfusate recovery of fexofenadine in livers from *Abcc4(-/-)* mice was unchanged.

Recovery of fexofenadine in bile. Fexofenadine biliary excretion rates and cumulative biliary excretion in livers from WT and knockout mice are presented in Figures 3.2A and B, respectively; standard deviations were within ~50% of the mean data and are not included in the figures for clarity. The biliary recovery of fexofenadine was not significantly different in *Abcc3(-/-)* and *Abcc4(-/-)* mouse livers relative to WT controls (Figure 3.2B; Table 3.2). Fexofenadine biliary excretion rates and cumulative biliary excretion were significantly decreased in livers from *Abcc2(-/-)* and *Abcc2(-/-)/Abcc3(-/-)* mice (Figure 3.2). The biliary recovery of fexofenadine during the washout phase, normalized for liver content of fexofenadine at the end of the infusion, was ~61% and ~53% lower in *Abcc2(-/-)* and *Abcc2(-/-)/Abcc3(-/-)* relative to WT mouse livers, respectively (Table 3.2). Interestingly, liver fexofenadine concentrations at the end of the washout period were not altered in *Abcc3(-/-), Abcc4(-/-)* and *Abcc2(-/-)/Abcc3(-/-)* mice (Table 3.2). However, consistent with our previous report (Tian et al., 2008), liver fexofenadine concentrations decreased ~2-fold in *Abcc2(-/-)* mice after the washout phase (Table 3.2).

Discussion

Previous studies utilizing transporter gene knockout mice identified Mrp2 as the predominant protein responsible for fexofenadine biliary excretion (Tian et al., 2008). In contrast, fexofenadine biliary excretion was not impaired in mice lacking the breast cancer resistance protein or P-glycoprotein (Tahara et al., 2005). In agreement with previous work, Mrp2 was responsible for ~60% of fexofenadine biliary excretion in the current study. However, the present data also establish the importance of Mrp3 in the hepatic basolateral excretion of fexofenadine. Approximately 50% of fexofenadine basolateral excretion may be attributed to Mrp3-mediated transport when outflow perfusate concentrations are in the range of 300 ng/ml based on the 2-fold decrease in perfusate recovery of fexofenadine in livers from *Abcc3(-/-)* mice. These data highlight the functional interplay between Mrp2 and Mrp3 in fexofenadine hepatobiliary disposition. However, the basolateral excretion of fexofenadine in *Abcc2(-/-)/Abcc3(-/-)* mice was not impaired. Fexofenadine concentrations in *Abcc3(-/-)* and *Abcc2(-/-)/Abcc3(-/-)* mouse livers were similar to those in WT mouse livers. Mechanism(s) responsible for the Mrp2- and Mrp3-independent component of fexofenadine hepatobiliary clearance remain to be elucidated.

Mrp2 plays a critical role as an organic anion excretory system in liver detoxification. Unlike human MRP3, MRP2 protein is highly expressed in humans under normal conditions (Stöckel et al., 2000). Protein expression of Mrp3, the“Mrp2 backup system”, is increased markedly in rats and humans that are deficient in Mrp2 (Hirohashi et al., 1998; Konig et al., 1999; Xiong et al., 2002). Mrp3 constitutive expression levels in mice are already high, but in Mrp2-knockout mice, Mrp3 is further upregulated (Nezasa et al., 2006). In contrast, this functional compensation is not reciprocal in mouse liver;

the absence of Mrp3 does not result in a notable upregulation of Mrp2 protein or function in mouse liver, as demonstrated by this and other studies (Belinsky et al., 2005; Zamek-Gliszczynski et al., 2006). This suggests that hepatic protection mechanisms other than Mrp2-mediated biliary excretion exist in mice when Mrp3 function is ablated. Mrp4 is another efflux transport protein located on the hepatic basolateral membrane (Rius et al., 2003). Limited evidence of functional overlap between Mrp3 and Mrp4 (Hirohashi et al 1999; Denk et al., 2004; Zamek-Gliszczynski et al., 2006) prompted the exploration of fexofenadine disposition in livers from *Abcc4(-/-)* mice. Interestingly, fexofenadine basolateral excretion was not affected by the absence of Mrp4. The impact of genetic ablation of Mrp4 has been associated with impaired Sulfotransferase 2a1 expression and function (Assem et al., 2004), but an appreciable effect on the function or expression of other hepatic transport proteins has not been observed (Assem et al., 2004; Mennone et al., 2006; Zamek-Gliszczynski et al., 2006). Whether Mrp4 serves as the backup system for Mrp3-mediated fexofenadine basolateral excretion requires further investigation.

The existence of multiple transport and backup transport systems on both the basolateral and canalicular membranes complicates the extrapolation of transport studies from single-knockout to double-knockout animals (van de Wetering et al., 2007). The biliary and basolateral excretion of the Mrp2 and Mrp3 substrate, morphine-3-glucuronide in *Abcc2(-/-)/Abcc3(-/-)* mice following morphine administration was severely impaired, resulting in considerable hepatic accumulation of the glucuronide metabolite. However, residual plasma concentrations of morphine-3-glucuronide in *Abcc2(-/-)/Abcc3(-/-*) mice were substantial, and the concentrations of morphine-3-glucuronide were similar between *Abcc2(-/-)/Abcc3(-/-)* and WT mice 24 hrs post morphine administration, which resulted in near-normal urinary excretion of morphine-3-

glucuronide, suggesting that a low-capacity backup transport system was present for the basolateral excretion of morphine-3-glucuronide into plasma in *Abcc2(-/-)/Abcc3(-/-)* mice (van de Wetering et al., 2007). In the present study, fexofenadine biliary excretion in livers from *Abcc2(-/-)/Abcc3(-/-)* mice was impaired to the same extent as in mice only lacking Mrp2; fexofenadine basolateral excretion in livers from these double-knockout mice was similar to WT mice, and was more than two-fold higher than in Mrp3 single-knockout mice. The unchanged liver concentrations of fexofenadine in *Abcc3(-/-)* mice, and considerable basolateral excretion of fexofenadine in the livers of *Abcc2(-/-)/Abcc3(-/-)* mice, are consistent with the hypothesis that additional clearance mechanisms compensate for the loss of Mrp3 function. Basolateral Mrps (other than Mrp3), the bidirectional organic anion transport proteins, or other basolateral export proteins may contribute to increased basolateral clearance of fexofenadine in *Abcc2(-/-)/Abcc3(-/-)* mouse livers. The possibility of altered fexofenadine metabolism in *Abcc3(-/-)* and *Abcc2(-/-)/Abcc3(-/-)* mouse livers cannot be ruled out because no detailed information on fexofenadine metabolism in mouse livers has been published.

In summary, fexofenadine is taken up into the hepatocyte and undergoes biliary as well as basolateral excretion. Using perfused livers from relevant transporter gene knockout mice, Mrp2 and Mrp3 were identified as important transport proteins mediating fexofenadine biliary and hepatic basolateral excretion, respectively. Mrp4 did not appear to contribute to hepatic basolateral excretion of this zwitterionic drug in the intact mouse liver in the presence of Mrp3 and/or Mrp2 proteins. Mechanism(s) responsible for the residual, Mrp2- and Mrp3-independent, biliary and basolateral excretion of fexofenadine remain to be elucidated. Once again, this study exemplified the importance of using physiologically relevant systems such as the intact liver to evaluate the contributions of hepatic transport proteins in drug pharmacokinetic studies.

Acknowledgment

The authors would like to thank Arlene S. Bridges, Ph. D. for her analytical support and Peijin Zhang, Ph. D. for helpful scientific discussions. This work was supported by the National Institutes of Health (GM41935 to K.L.R.B. and CA73728 to G.D.K.) and by the National Cancer Institute (Core Grant CA06927 to Fox Chase Cancer Center).

References

Assem M, Schuetz EG, Leggas M, Sun D, Yasuda K, Reid G, Zelcer N, Adachi M, Strom S, Evans RM, Moore DD, Borst P and Schuetz JD (2004) Interactions between hepatic Mrp4 and Sult2a as revealed by the constitutive androstane receptor and Mrp4 knockout mice. *J Biol Chem* **279:**22250-22257.

Banfield C, Gupta S, Marino M, Lim J and Affrime M (2002) Grapefruit juice reduces the oral bioavailability of fexofenadine but not desloratadine. *Clin Pharmacokinet* **41:**311-318.

Belinsky MG, Dawson PA, Shchaveleva I, Bain LJ, Wang R, Ling V, Chen ZS, Grinberg A, Westphal H, Klein-Szanto A, Lerro A and Kruh GD (2005) Analysis of the in vivo functions of Mrp3. *Mol Pharmacol* **68:**160-168.

Belinsky MG, Guo P, Lee K, Zhou F, Kotova E, Grinberg A, Westphal H, Shchaveleva I, Klein-Szanto A, Gallo JM, Kruh GD (2007) Multidrug resistance protein 4 protects bone marrow, thymus, spleen, and intestine from nucleotide analogue-induced damage. *Cancer Res* **67**:262-268.

Chandra P, Johnson BM, Zhang P, Pollack GM, Brouwer KL (2005) Modulation of hepatic canalicular or basolateral transport proteins alters hepatobiliary disposition of a model organic anion in the isolated perfused rat liver. Drug Metab Dispos **33**:1238-43.

Cvetkovic M, Leake B, Fromm MF, Wilkinson GR and Kim RB (1999) OATP and P-glycoprotein transporters mediate the cellular uptake and excretion of fexofenadine. *Drug Metab Dispos* **27:**866-871.

Denk GU, Soroka CJ, Takeyama Y, Chen WS, Schuetz JD and Boyer JL (2004) Multidrug resistance-associated protein 4 is up-regulated in liver but down-regulated in kidney in obstructive cholestasis in the rat. *J Hepatol* **40:**585-591.

Hirohashi T, Suzuki H, Ito K, Ogawa K, Kume K, Shimizu T and Sugiyama Y (1998) Hepatic expression of multidrug resistance-associated protein-like proteins maintained in eisai hyperbilirubinemic rats. *Mol Pharmacol* **53:**1068-1075.

Hirohashi T, Suzuki H and Sugiyama Y (1999) Characterization of the transport properties of cloned rat multidrug resistance-associated protein 3 (MRP3). *J Biol Chem* **274:**15181-15185.

Konig J, Rost D, Cui Y and Keppler D (1999) Characterization of the human multidrug resistance protein isoform MRP3 localized to the basolateral hepatocyte membrane. *Hepatology* **29:**1156-1163.

Lemma GL, Wang Z, Hamman MA, Zaheer NA, Gorski JC and Hall SD (2006) The effect of short- and long-term administration of verapamil on the disposition of cytochrome P450 3A and P-glycoprotein substrates. *Clin Pharmacol Ther* **79:**218-230.

Mennone A, Soroka CJ, Cai SY, Harry K, Adachi M, Hagey L, Schuetz JD and Boyer JL (2006) Mrp4-/- mice have an impaired cytoprotective response in obstructive cholestasis. *Hepatology* **43:**1013-1021.

Nezasa K, Tian X, Zamek-Gliszczynski MJ, Patel NJ, Raub TJ and Brouwer KL (2006) Altered hepatobiliary disposition of 5 (and 6)-carboxy-2',7'-dichlorofluorescein in Abcg2 (Bcrp1) and Abcc2 (Mrp2) knockout mice. *Drug Metab Dispos* **34:**718-723.

Ogawa K, Suzuki H, Hirohashi T, Ishikawa T, Meier PJ, Hirose K, Akizawa T, Yoshioka M and Sugiyama Y (2000) Characterization of inducible nature of MRP3 in rat liver. *Am J Physiol Gastrointest Liver Physiol* **278:**G438-446.

Rius M, Nies AT, Hummel-Eisenbeiss J, Jedlitschky G and Keppler D (2003) Cotransport of reduced glutathione with bile salts by MRP4 (ABCC4) localized to the basolateral hepatocyte membrane. *Hepatology* **38:**374-384.

Shon JH, Yoon YR, Hong WS, Nguyen PM, Lee SS, Choi YG, Cha IJ and Shin JG (2005) Effect of itraconazole on the pharmacokinetics and pharmacodynamics of fexofenadine in relation to the MDR1 genetic polymorphism. *Clin Pharmacol Ther* **78:**191-201.

Stöckel B, König J, Nies AT, Cui Y, Brom M, Keppler D. 2000. Characterization of the 5'-flanking region of the human multidrug resistance protein 2 (MRP2) gene and its regulation in comparison with the multidrug resistance protein 3 (MRP3) gene.Eur J Biochem. **267**:1347-58.

Strelevitz TJ, Foti RS and Fisher MB (2006) In vivo use of the P450 inactivator 1-aminobenzotriazole in the rat: varied dosing route to elucidate gut and liver contributions to first-pass and systemic clearance. *J Pharm Sci* **95:**1334-1341.

Tahara H, Kusuhara H, Fuse E and Sugiyama Y (2005) P-glycoprotein plays a major role in the efflux of fexofenadine in the small intestine and blood-brain barrier, but only a limited role in its biliary excretion. *Drug Metab Dispos* **33:**963-968.

Tian X, Li J, Zamek-Gliszczynski MJ, Bridges AS, Zhang P, Patel NJ, Raub TJ, Pollack GM, Brouwer KL (2007) Roles of P-glycoprotein, Bcrp, and Mrp2 in biliary excretion of spiramycin in mice. Antimicrob Agents Chemother. **51**:3230-4.

Tian X, Zamek-Gliszczynski MJ, Li J, Bridges AS, Nezasa K, Patel NJ, Raub TJ and Brouwer KL (2008) Multidrug Resistance-Associated Protein 2 (Mrp2) is Primarily Responsible for the Biliary Excretion of Fexofenadine (FEX) in Mice. *Drug Metab Dispos,* 36:61-4.

van de Wetering K, Zelcer N, Kuil A, Feddema W, Hillebrand M, Vlaming ML, Schinkel AH, Beijnen JH and Borst P (2007) Multidrug resistance protein 2 and 3 provide alternative routes for hepatic excretion of morphine-glucuronides. *Mol Pharmacol*. **72**:387-94.

Xiong H, Suzuki H, Sugiyama Y, Meier PJ, Pollack GM and Brouwer KL (2002) Mechanisms of impaired biliary excretion of acetaminophen glucuronide after acute phenobarbital treatment or phenobarbital pretreatment. *Drug Metab Dispos* **30:**962-969.

Xiong H, Turner KC, Ward ES, Jansen PL and Brouwer KL (2000) Altered hepatobiliary disposition of acetaminophen glucuronide in isolated perfused livers from multidrug resistance-associated protein 2-deficient TR(-) rats. *J Pharmacol Exp Ther* **295:**512-518.

Zamek-Gliszczynski MJ, Nezasa K, Tian X, Bridges AS, Lee K, Belinsky MG, Kruh GD and Brouwer KL (2006) Evaluation of the role of multidrug resistance-associated protein (Mrp) 3 and Mrp4 in hepatic basolateral excretion of sulfate and glucuronide metabolites of acetaminophen, 4-methylumbelliferone, and harmol in Abcc3-/- and Abcc4-/- mice. *J Pharmacol Exp Ther* **319:**1485-1491.

Zamek-Gliszczynski MJ, Xiong H, Patel NJ, Turncliff RZ, Pollack GM and Brouwer KL (2003) Pharmacokinetics of 5 (and 6)-carboxy-2',7'-dichlorofluorescein and its diacetate promoiety in the liver. *J Pharmacol Exp Ther* **304:**801-809.

Zelcer N, van de Wetering K, Hillebrand M, Sarton E, Kuil A, Wielinga PR, Tephly T, Dahan A, Beijnen JH and Borst P (2005) Mice lacking multidrug resistance protein 3 show altered morphine pharmacokinetics and morphine-6-glucuronide antinociception. *Proc Natl Acad Sci U S A* **102:**7274-7279.

Zhou S, Chan E, Pan SQ, Huang M and Lee EJ (2004) Pharmacokinetic interactions of drugs with St John's wort. *J Psychopharmacol* **18:**262-276.

Figure Legends

Figure 3.1. Fexofenadine concentrations in outflow perfusate from wild-type C57BL/6 (●), *Abcc3*$^{-/-}$ (Δ), *Abcc4*$^{-/-}$ (∇), *Abcc2*$^{-/-}$ (□), and *Abcc2*$^{-/-}$/*Abcc3*$^{-/-}$ (◊) mouse livers (mean data are plotted; n = 3-4 per group). Livers were perfused (5 ml/min) with fexofenadine (0.5 μM) for 30 min followed by a 45-min washout phase.

Figure 3.2. Biliary excretion rate (A) and cumulative biliary excretion (B) of fexofenadine in perfused livers from wild-type C57BL/6 (●), *Abcc3*$^{-/-}$ (Δ), *Abcc4*$^{-/-}$ (∇), *Abcc2*$^{-/-}$ (□), and *Abcc2*$^{-/-}$/*Abcc3*$^{-/-}$ (◊) mice (mean data are plotted; n = 3-4 per group). Livers were perfused (5 ml/min) with fexofenadine (0.5 μM) for 30 min followed by a 45-min washout phase.

Table 3.1. Body weight, liver weight normalized for body weight, and bile flow rate in wild-type and transporter gene knockout mice. Mean ± SD (n = 3-4 per group). * p< 0.05 knockout vs. wild type.

Mice	Body Weight (g)	Liver Weight / Body Weight	Bile Flow Rate (µL/min/g liver)
Wild-Type	27.5 ± 1.4	0.041 ± 0.006	1.3 ± 0.3
Abcc3(-/-)	27.9 ± 3.1	0.043 ± 0.001	1.3 ± 0.2
Abcc4(-/-)	26.1 ± 2.4	0.041 ± 0.005	1.3 ± 0.4
Abcc2(-/-)	29.4 ± 1.9	0.053 ± 0.001 *	0.87 ± 0.02 *
Abcc2(-/-)/Abcc3(-/-)	27.7 ± 1.5	0.060 ± 0.002 *	0.85 ± 0.15 *

Table 3.2. Recovery of fexofenadine in perfusate and bile during the washout phase of mouse liver perfusions, and liver concentrations after the washout phase. Values are expressed as percentage of fexofenadine liver content after the 30-min infusion. Mean ± SD (n = 3-4 per group). * p< 0.05 knockout vs. wild type.

Mice	**Biliary Recovery (% liver content at 30 min)**	**Recovery in Perfusate (% liver content at 30 min)**	**Liver Concentration (ng/g liver)**
Wild-Type	15.3 ± 3.8	25.8 ± 4.1	1500 ± 330
Abcc3(-/-)	13.5 ± 6.1	12.7 ± 6.1*	1500 ± 500
Abcc4(-/-)	12.3 ± 3.3	26.2 ± 7.6	1300 ± 420
Abcc2(-/-)	5.9 ± 3.4*	42.0 ± 2.7 *	850 ± 400
Abcc2(-/-)/ Abcc3(-/-)	7.1 ± 2.9 *	28.6 ± 12.3	1600 ± 420

Figure 3.1

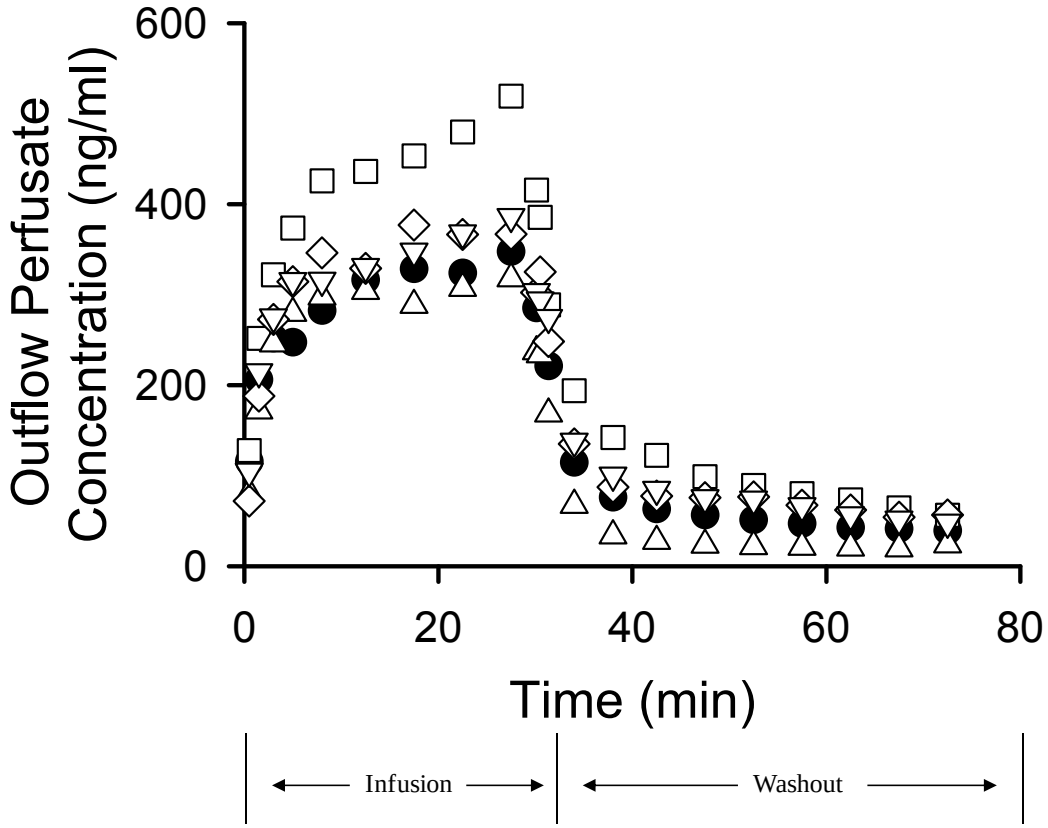
Outflow Perfusate Concentration (ng/ml)
600
400
200
0
0
20
40
60
80
Time (min)
Infusion
Washout

Figure 3.2

(A)

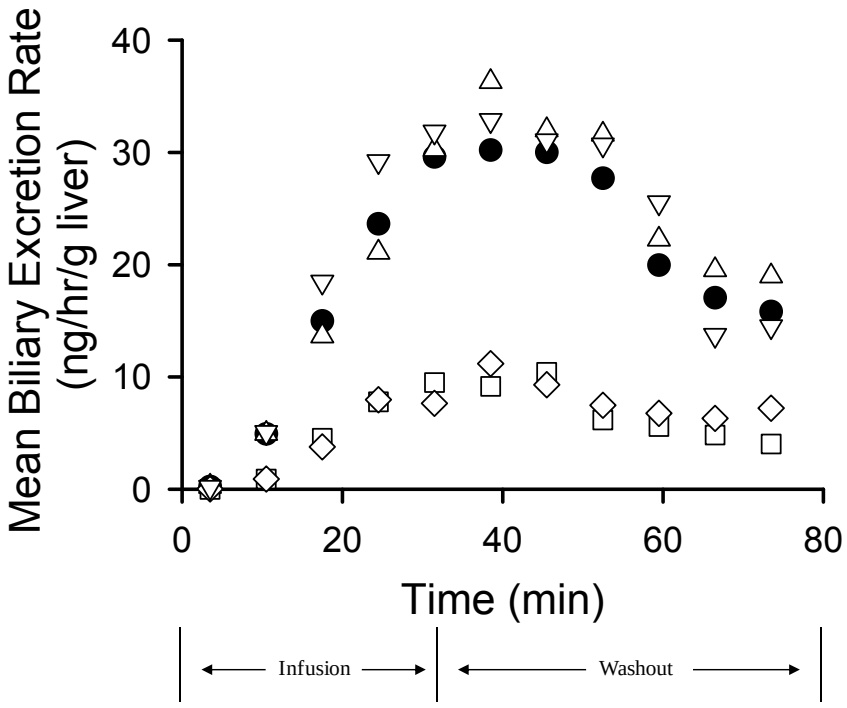
Mean Biliary Excretion Rate
(ng/hr/g liver)
40
30
20
10
0
0
20
40
60
80
Time (min)
Infusion
Washout

(B)

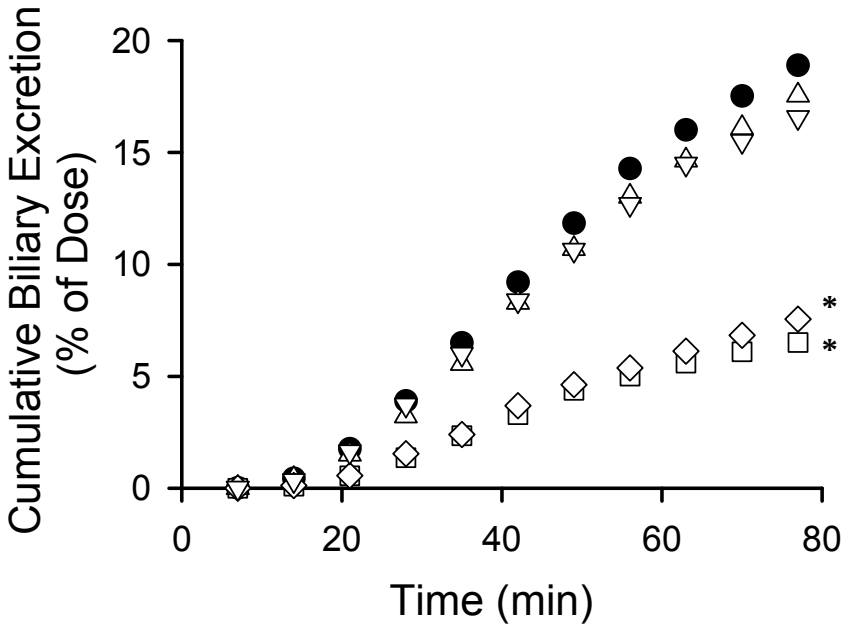
Cumulative Biliary Excretion
(% of Dose)
20
15
10
5
0
0
20
40
60
80
Time (min)
*
*

CHAPTER 4

Evaluation of ^{99m}Technetium-Mebrofenin and ^{99m}Technetium-Sestamibi as Specific Probes for Hepatic Transport Protein Function in Rat and Human Hepatocytes

This chapter will be submitted to Journal of Nuclear Medicine and is formatted in the style of the journal.

Abstract

The present study characterized the transport proteins involved in uptake and excretion of ^{99m}Tc-MEB and ^{99m}Tc-MIBI, and the preferential route of efflux (canalicular vs. basolateral), in rat and human hepatocytes. Initial ^{99m}Tc-MEB uptake was reduced to 20.7 and 35.4% of control in the presence of the general Oatp/OATP inhibitor rifamycin SV in rat and human suspended hepatocytes, respectively. Initial ^{99m}Tc-MIBI uptake in suspended rat hepatocytes was not influenced by inhibitors or replacement of sodium with choline. ^{99m}Tc-MEB canalicular efflux was decreased 6.6-fold and 30% in the presence of MK571 (100μM) in rat and human SCH, and completely ablated in Mrp2-deficient TR$^-$ SCH, suggesting that ^{99m}Tc-MEB hepatic uptake is predominantly Oatp-mediated with biliary excretion by Mrp2. ^{99m}Tc-MEB efflux in human SCH was predominantly canalicular (45.8±8.6%), and ~3-fold greater than in rat SCH. ^{99m}Tc-MEB basolateral efflux in human (16.7±0.6%) and rat (25.0±6.7%) SCH was similar. ^{99m}Tc-^{99m}Tc-MIBI canalicular efflux was similar in human and rat SCH, but basolateral efflux was 37% greater in human compared to rat SCH. ^{99m}Tc-MIBI cellular accumulation, biliary excretion index (BEI) and *in vitro* biliary clearance ($Cl_{biliary}$) in rat SCH were unaffected by Bcrp knockdown (siBcrp). ^{99m}Tc-MIBI BEI and *in vitro* $Cl_{biliary}$ were ablated by GF120918 (2μM) in siBcrp SCH. ^{99m}Tc-MIBI hepatic uptake appears to occur by passive diffusion with biliary excretion mediated by P-gp. The SCH model is a useful system to investigate the influence of factors (*e.g.,* species differences, drug interactions)

that may alter the route and/or extent of basolateral and canalicular efflux of substrates from hepatocytes.

Introduction

Probe substrates are used to obtain an *in vivo* phenotypic measure of specific biotransformation or transport pathways in preclinical or clinical species. Ideally, a transport probe substrate would be specific for a single transport protein, relatively safe for healthy human volunteer studies and metabolically stable. There are currently very few identified transport probe substrates suitable for clinical use. Digoxin has been recommended as a multidrug resistance P-glycoprotein (P-gp) probe in the FDA guidance (http://www.fda.gov/Cder/drug/drugInteractions/default.htm), however, digoxin also is transported by organic anion transporting polypeptide 1B3, 4C1 (OATP1B3 and OATP4C1) and recent publications have investigated other potential probe substrates for breast cancer resistance protein (BCRP) including sulfasalazine (Urquhart et al., 2008), nitrofurantoin (Adkison et al., 2008) and rosuvastatin (Zhang et al., 2006). ^{99m}Technetium-mebrofenin (^{99m}Tc-MEB) and ^{99m}Technetium-sestamibi (^{99m}Tc-MIBI) are candidate probe substrates for multidrug resistance associated protein 2 (MRP2) and P-gp, respectively.

^{99m}Tc-MEB is the ^{99m}Tc-labeled trimethylbromo analogue of acetanilidoiminodiacetic acid (BRIDA) derivative commonly used in nuclear medicine for hepatobiliary scintigraphy. This compound belongs to a class of agents that couples a lidocaine-like structure, resulting in high liver extraction, with ^{99m}technetium, which is ideal for gamma scintigraphy (Krishnamurthy and Turner, 1990). ^{99m}Tc-MEB commonly is used to evaluate the presence of gallbladder dysfunction (Doo et al., 1991), although several investigators have

proposed other uses, including preoperative assessment of liver function (Erdogan et al., 2004), evaluation of hepatocyte viability *in vivo* (Gencoglu et al., 2002; Koruk et al., 2003), and detection of genetic diseases that could affect biliary excretion (Bujanover et al., 1983; Pinos et al., 1990). Several analogs of ^{99m}Tc-MEB have been developed, all of which are anions at physiologic pH and bind to albumin to varying degrees, depending on their lipophilicity (Nunn et al., 1983). Several hepatic transport proteins involved in the hepatobiliary disposition of ^{99m}Tc-MEB were characterized recently by Ghibellini et al., who demonstrated that ^{99m}Tc-MEB is a substrate of OATP1B1, OATP1B3, MRP2 and MRP3 in expressed systems (Ghibellini et al., 2008). ^{99m}Tc-MEB exhibited increased and prolonged hepatic exposure measured by gamma scintigraphy in Mrp2-deficient TR$^-$ rats compared to wild-type rats, suggesting that Mrp2 is involved in canalicular transport (Bhargava et al., 2009). Furthermore, case reports have documented a failure to visualize the hepatobiliary tree after administration of ^{99m}Tc-disofenin (DISIDA), the diisopropyl analogue of acetanilidoiminodiacetic acid, when administered to patients with Dubin-Johnson syndrome (MRP2-deficiency) (Pinos et al., 1990). More than 98% of a ^{99m}Tc-MEB dose is taken up by the liver; the hepatic excretion half-life of ^{99m}Tc-MEB is rapid (16 min) and ~1.5% of the dose was recovered in urine after 24 hours in humans (Krishnamurthy and Turner, 1990).

^{99m}Tc-MIBI a monovalent cation complex of ^{99m}Tc (^{99m}Tc-2-methoxyisobutylisonitrile), is used clinically to assess myocardial perfusion; ^{99m}Tc-MIBI distributes into the heart in proportion to blood flow and myocardial

viability (Beller and Sinusas, 1990; Mobasseri and Hendel, 2002; Ravizzini et al., 2002). Accumulation of ^{99m}Tc-MIBI in cells is a function of free diffusion based on electrical potentials across the plasma and mitochondrial membranes, with localization in the mitochondria by electrostatic forces (Chiu et al., 1990). Decreased uptake of ^{99m}Tc-MIBI in resistant cells also has been attributed to a lower membrane potential and reduced mitochondrial density (Piwnica-Worms et al., 1993). Several groups have used ^{99m}Tc-MIBI as a functional P-gp probe substrate in rodents and humans (Chen et al., 1997; Luker et al., 1997; Slapak et al., 2001; Wong et al., 2005). Further investigations using cancer cells in culture revealed that ^{99m}Tc-MIBI is a MRP1 substrate (Hendrikse et al., 1998; Chen et al., 2000; Perek et al., 2000). In TR$^-$ rats, ^{99m}Tc-MIBI cumulative recovery in bile and liver activity profiles based on *in vivo* imaging were similar compared to wild-type rats, suggesting that Mrp2 is not involved, or other mechanisms compensate for impaired hepatic excretion (Hendrikse et al., 2004). ^{99m}Tc-MIBI clearance in humans is similarly distributed between renal elimination and feces mediated by biliary excretion and possible contribution by intestinal secretion [Cardiolite® package insert (Ghibellini et al., 2008)].

^{99m}Tc-MIBI and analogs of ^{99m}Tc-MEB have been used as probe substrates to assess interindividual variation in hepatic drug handling and function (Wong et al., 2005; Michael et al., 2006; Wong et al., 2006). ^{99m}Tc-MIBI has been used to phenotype P-gp function with the P-gp inhibitors PSC833 and LY335979 resulting in prolonged hepatic exposure (Chen et al., 1997; Luker et al., 1997; Slapak et al., 2001). Alterations in ^{99m}Tc-MIBI pharmacokinetics were

assessed in a cohort of cancer patients with common single nucleotide polymorphisms (SNPs) in *ABCB1* exons 12 (C1236T) and 26 (C3435T) resulting in a significantly decreased elimination rate constant (Wong et al., 2005). However, the mechanisms of hepatic transport have not been fully investigated, including potential compensatory proteins involved in hepatobiliary disposition. The purpose of the current study was to characterize the mechanisms of uptake and excretion of ^{99m}Tc-MEB and ^{99m}Tc-MIBI in rat and human hepatocytes. The processes involved in hepatic uptake, basolateral efflux and canalicular excretion are too complicated to be completely elucidated *in vivo*. Therefore, suspended hepatocytes were used to investigate uptake mechanisms because of the loss of cell polarity after isolation (Groothuis et al., 1981; Oude Elferink et al., 1995). While sandwich-cultured hepatocytes (SCH) were used to elucidate the hepatobiliary disposition of ^{99m}Tc-MEB and ^{99m}Tc-MIBI (Liu et al., 1999a; Liu et al., 1999b). TR$^-$ rats serve as a useful tool to examine altered hepatobiliary disposition in response to impaired Mrp2 function, and facilitate the identification of compensatory basolateral and apical efflux mechanisms involved in ^{99m}Tc-MEB hepatobiliary disposition.

Material and Methods

Materials. Dulbecco's modified Eagle's medium (DMEM), insulin, MEM non-essential amino acids solution (100x), L-glutamine, insulin and penicillin G-streptomycin solution were purchased from Invitrogen (Carlsbad, CA). Estradiol-17-β-D-glucuronide (E217G), para-aminohippuric acid sodium salt (PAH), tetraethylammonium (TEA), rifamycin SV, glycyrrhizic acid, clonidine, desipramine, ketoprofen, fetal bovine serum (FBS), Triton X-100, dexamethasone, and Hanks' balanced salt solution (HBSS) modified with (H-1387) or without (H-4891) calcium chloride were obtained from Sigma-Aldrich (St. Louis, MO). Collagenase (type 1) was obtained from Worthington Biochemical Corporation (Freehold, NJ). BioCoat™ collagen I plates, Matrigel™ basement membrane matrix, and ITS+™ (insulin/transferrin/selenium) culture supplement were purchased from BD Biosciences Discovery Labware (Bedford, MA). Bicinchoninic acid (BCA) protein assay reagents and BSA for the protein assay standard were purchased from Pierce Chemical Co. (Rockford, IL). ^{99m}Tc-MEB and ^{99m}Tc-MIBI were purchased as sterile doses on the day of the experiment from Cardinal Health Nuclear Pharmacy (Research Triangle Park, NC). Ultima Gold™ XR scintillation cocktail, ^{3}H-PAH (3.28 Ci/mmol) and ^{3}H-E217G (45.8 Ci/mmol) were purchased from Perkin Elmer Life Sciences (Boston, MA). ^{14}C-TEA (55mCi/mmol) was purchased from American Radiolabeled Chemicals. MK-571 sodium salt was purchased from Cayman Chemical Co (Ann Arbor, MI). N-(4-[2-(1,2,3,4-tetrahydro-6,7-dimethoxy-2-isoquinolinyl)ethyl]-phenyl)-9,10-dihydro-5-methoxy-9-oxo-4-acridine carboxamide (GF120918) was

a gift from GlaxoSmithKline (Research Triangle Park, NC). All other chemicals and reagents were of analytical grade and available from commercial sources.

Animals. Male Wistar wild-type (WT) rats (201-312 g) from Charles River Laboratories, Inc. and Mrp2-deficient TR^- rats bred at the University of North Carolina (228–306 g; breeding stock obtained from Dr. Mary Vore, University of Kentucky, Lexington, KY) were used for sandwich-cultured hepatocyte studies. All animals acclimated for one week before experiments. Rats were housed in an alternating 12-h light and dark cycle with free access to water and food prior to surgery. All animal procedures complied with the guidelines of the Institutional Animal Care and Use Committee (University of North Carolina, Chapel Hill, NC).

Suspended Hepatocyte Isolation/Uptake Studies.

Rat hepatocytes were isolated by a two-step collagenase perfusion method as described previously (LeCluyse et al., 1996). Viability, as determined by trypan blue exclusion, was 90 to 95% (mean = 92%). CellzDirect, Life Technologies (RTP, NC) kindly provided freshly isolated human hepatocytes in suspension. Hepatocyte donors included a 60 yr old female Caucasian, and 63 and 69 yr old male Caucasians, with no recent history of smoking or alcohol use. Hepatocyte viability, as determined by trypan blue exclusion, was 90, 86 and 89%, respectively. Cells were suspended in cold modified Hank's buffer with 10 mM Tris/5 mM glucose (pH = 7.4) or Na^+-free choline buffer (10 mM Tris, 5 mM glucose, 5.4 mM KCl, 1.8 mM $CaCl_2$, 0.9 mM $MgSO_4$, 10 mM HEPES and 137 mM choline; pH = 7.4) and stored on ice prior to conducting uptake studies

(Leslie et al., 2007). Isolated hepatocytes were suspended at 1 x 10^6 cells/ml in the same buffer, placed on ice, and used immediately in experiments. Hepatocyte suspensions (4 ml; n = 3 – 6 livers, in duplicate or triplicate) were preincubated in bottom inverted Erlenmeyer flasks at 37˚C for 5 min; 0.1% DMSO or chemical inhibitor was added 1 min before, followed by ^{99m}Tc-MEB (0.5 µCi/ml), ^{99m}Tc-MIBI (0.5 µCi/ml), ^{3}H-E217G (1 µM, 60 nCi/mL), ^{14}C-TEA (20 µM, 60 nCi/mL) or ^{3}H-PAH (0.2, 1 or 20 µM, 60 nCi/mL). The following concentrations of inhibitors were selected based upon reported affinities for the given active transport processes: 20 µM rifamycin SV (Oatp1a1, Oatp1a4, OATP1B1, OATP1B3, and OATP2B1 inhibitor), 20 µM glycyrrhizic acid (Oatp1a1, 1a4 and 1b2 inhibitor), 200 µM clonidine [organic cation transporter (Oct1) inhibitor], 10 µM desipramine (Oct1 and 3 inhibitor), 5 µM decynium 22 (OCT inhibitor), 10 µM ketoprofen [organic anion transporter 2 (Oat2) inhibitor]. Aliquots (100 µL) of the suspension were removed at timed intervals (up to 5 min), placed in 0.4-ml polyethylene tubes and centrifuged immediately through a top layer of silicone oil:mineral oil (82:18, v/v; 100 µL) and a bottom layer of 3M KOH (50 µL). ^{99m}Tc-MEB and ^{99m}Tc-MIBI in the cell pellet and supernatant were analyzed using a sodium iodide well counter and corrected for decay (^{99m}Tc $t_{1/2}$=6.01 hr). ^{3}H-E217G, ^{14}C-TEA or ^{3}H-PAH were analyzed by liquid scintillation counting. Adherent fluid volume was estimated with ^{14}C-inulin as previously described (Baur et al., 1975). Protein concentrations for individual hepatocyte suspensions were determined with the BCA protein assay reagent kit (Pierce) as

instructed by the manufacturer. BSA, as supplied by the manufacturer, was used as a standard (0.2 – 1 mg/mL).

Sandwich-Cultured Hepatocyte Studies.

CellzDirect, Life Technologies (RTP, NC) provided human hepatocytes plated on six-well Biocoat™ plates and overlaid with Matrigel™. Hepatocyte donors were a 56 and 64 yr old female Caucasian with no history of smoking or alcohol use. Rat hepatocytes (>88% viability) were seeded [~1.5 x 10^6 cells/well (TR^-) or 1.75 x 10^6 cells/well (WT)] in 6-well BioCoat™ plates in DMEM without phenol red supplemented with 2 mM L-glutamine, 1% (v/v) MEM non-essential amino acids, 100 units penicillin G sodium, 100 µg streptomycin sulfate, 1 µM dexamethasone, 5% (v/v) FBS, and 10 µM insulin (day 0 of culture), and allowed to attach for 2-6 h in a humidified incubator (95% O_2, 5% CO_2) at 37°C. After cell attachment, culture plates were swirled gently and the culture medium was replaced with the same medium. Cells were overlaid 16-24 h (day 1 of culture) after seeding with ice-cold Matrigel™ basement membrane matrix (0.25 mg/mL) in 2 mL/well cold serum-free DMEM containing 2 mM L-glutamine, 1% (v/v) MEM non-essential amino acids, 100 units penicillin G sodium, 100 µg streptomycin sulfate, 0.1 µM dexamethasone, and 1% (v/v) ITS+™. The culture medium was changed every 24 h until experiments were performed on day 4 of culture.

Efflux Studies.

On day 4, efflux experiments were performed as previously described (Liu et al., 1999a) with modifications. Briefly, hepatocytes were rinsed with 2 mL warm standard buffer and incubated with 1.5 mL of ^{99m}Tc-MEB or ^{99m}Tc-MIBI (5 μCi/ml) in standard HBSS for 20 min in a humidified incubator (95% O_2, 5% CO_2) at 37°C. Subsequently, hepatocytes were rinsed vigorously twice with 2 mL warm standard HBSS or Ca^{2+}-free HBSS (to maintain or disrupt tight junctions, respectively), and incubated with 1.5 mL of the same buffer supplemented with chemical inhibitors (100 μM MK571 or 20 μM GF120918) or vehicle control (0.6% dimethyl sulfoxide) for 20 min at 37°C. The amount of ^{99m}Tc-MEB or ^{99m}Tc-MIBI in the efflux buffer was sampled at 20 min and medium was aspirated. Hepatocytes were lysed as detailed above. Data were normalized to protein concentration in each well, determined in duplicate aliquots using the BCA protein assay reagent kit with BSA as a standard, as described previously. Samples were analyzed using a gamma counter and corrected for decay.

The amount of substrate was measured in the medium at 20 min and in the lysed SCH at the end of the efflux phase. The extent of basolateral and canalicular efflux was determined based on the following equations and normalized to the total substrate mass preloaded in the hepatocytes, which was determined as the sum of the substrate mass in the efflux medium and in the hepatocyte lysate at the end of the efflux phase:

$$\mathrm{Basolateral\,Efflux} = \mathrm{Total\,Mass\,in\,Efflux\,Medium}_{\mathrm{Standard\,HBSS}}$$

$$\text{Apical Efflux} = \text{Total Mass in Efflux Medium}_{Ca^{2+}\text{ - free HBSS}} - \text{Total Mass in Efflux Medium}_{\text{Standard HBSS}}$$

Accumulation Studies.

The method to determine substrate accumulation in the bile canalicular networks of SCH has been described previously (Liu et al., 1999a; Wolf et al., 2008). Cells were incubated for 10 min at 37°C with 1.5 mL of ^{99m}Tc-MIBI (0.5 µCi/ml) with or without RNAi knockdown of Bcrp, and in the presence and absence of 2µM GF120918 in standard buffer. Substrate uptake was corrected for nonspecific binding by subtracting uptake on blank six-well Biocoat™ plates overlaid with Matrigel™. Hepatocytes were lysed as detailed above and data were normalized to protein concentration in each well, as described above.

The biliary excretion index (BEI, %) was calculated using B-CLEAR® technology [Qualyst, Inc., Raleigh, NC; (Liu et al., 1999a)]:

$$\text{BEI} = \frac{\text{Accumulation}_{\text{Cells+Bile}} - \text{Accumulation}_{\text{Cells}}}{\text{Accumulation}_{\text{Cells+Bile}}} \times 100$$

where substrate accumulation in the cells+bile compartments was determined in hepatocytes preincubated in standard buffer; cellular accumulation of substrate was determined in hepatocytes preincubated with Ca^{2+}-free HBSS.

$$\textit{in vitro}\ CL_{biliary} = \frac{Accumulation_{Cells+Bile} - Accumulation_{Cells}}{AUC_{0-T}}$$

where $AUC_{0\text{-}T}$ represents the product of the incubation time (T) and the initial concentration in the medium. *In vitro* $CL_{biliary}$ values were scaled per kilogram body weight assuming the following: 200 mg protein/g rat liver tissue and 40 g rat liver tissue/kg body weight (Seglen, 1976).

RNAi knockdown of Bcrp.

The methods for packaging of recombinant siRNA-expressing adenoviral vectors and infection of sandwich-cultured hepatoctyes have been described previously (Yue et al., 2009). Briefly, after seeding hepatocytes on Biocoat™ plates and changing seeding medium, cells were infected overnight with a non-target siRNA (siNT), or siRNA sequences targeting the rat Bcrp gene at positions 288-306 (siBcrp) at a multiplicity of infection of 20. Approximately 24 h after-seeding, cells were overlaid and cultured as described above. Knockdown of Bcrp was confirmed by western blot analysis and determination of the biliary clearance of nitrofurantoin using LC/MS/MS analysis, as detailed previously (Yue et al., 2009).

Immunoblots.

Cells were washed once with HBSS, and resuspended in lysis buffer consisting of 1% SDS, 1 mM EDTA and Complete protease inhibitor cocktail tablets (Roche

Diagnostics, Mannheim, Germany). Protein concentrations were determined by the BCA assay. Whole-cell lysates (30-40 μg) were resolved on NuPAGE 4 to 20% Bis-Tris gel (Invitrogen Corp, Carlsbad, CA) and the proteins were transferred to polyvinylidene difluoride (PVDF) membranes. After blocking in 5% milk-Tris-buffered saline with Tween 20 (TBST) for 30 min, blots were incubated overnight at 4°C with the following antibodies: Bcrp (BXP-53, Alexis Biochemicals, San Diego, CA) and β-actin (C4, Chemicon, San Francisco, CA). After incubation with HRP-conjugated secondary antibody, signals were detected by chemiluminescent substrate Supersignal West Dura (Pierce, Rockford, IL) with a Bio-Rad VersaDoc imaging system; densitometry analysis was performed using Quantity One v4.1 software (Bio-Rad Laboratories, Hercules, CA).

Results.

Uptake of ^{99m}Tc-MEB, ^{99m}Tc-MIBI, ^{3}H-E217G, and ^{14}C-TEA in Suspended Rat and Human Hepatocytes. Preliminary experiments in suspended rat hepatocytes sampling over 60 min indicated that the linear range of uptake was 2.5, 1.5, 2.5, and 5 min for ^{99m}Tc-MIBI, ^{99m}Tc-MEB, ^{3}H-E217G, and ^{14}C-TEA, respectively. Therefore, subsequent experiments were conducted up to the respective times to evaluate the initial uptake rate of each substrate. The Oct/OCT inhibitors clonidine, desipramine and decynium 22, and the Oat/OAT inhibitor ketoprofen, and the absence of sodium (substitution with choline-based buffer to rule out the involvement of Ntcp/NTCP) had marginal effects on the initial uptake of ^{99m}Tc-MEB in WT rat and human hepatocytes compared to control (Fig. 4.1A and 4.2A). Initial ^{99m}Tc-MEB uptake was reduced to 20.7 and 35.4% of control in the presence of the Oatp/OATP inhibitor rifamycin SV in WT rat and human hepatocytes, respectively (Fig. 4.1A and 4.2A). In WT rat hepatocytes, the Oatp inhibitor glycyrrhizic acid reduced ^{99m}Tc-MEB initial uptake to 39.5% of control (Fig. 4.1A). Initial ^{99m}Tc-MIBI uptake in suspended WT rat hepatocytes was not influenced by inhibitors or replacement of sodium with choline in the uptake buffer; all values were within 10% of control (Fig. 4.1B).

In order to confirm the specificity of the selected inhibitors, transport of probe substrates was assessed in the presence of each inhibitor. ^{3}H-E217G, ^{14}C-TEA, and ^{3}H-PAH were selected based on their selective affinities for the Oatps/OATPs, Octs/OCTs and Oats/OATs, respectively. As expected, initial

hepatocyte uptake of the Oatp probe substrate ^{3}H-E217G was inhibited to 15.5 and 23.8% of control in the presence of rifamycin SV and glycyrrhizic acid, respectively, in suspended WT rat hepatoyctes (Fig. 4.1C), and 51.5% of control in the presence of rifamycin SV in suspended human hepatocytes (Fig. 4.2B). All other inhibitors had marginal effects on ^{3}H-E217G uptake in both WT rat and human suspended hepatocytes (Fig. 4.1C and 4.2B). Initial uptake of the Oct probe substrate ^{14}C-TEA was inhibited to 23.7% and 25.6% of control in the presence of clonidine and desipramine, respectively, in suspended rat hepatocytes (Fig. 4.1D), and 54.2% of control in the presence of decynium 22 (Fig. 4.2C) in suspended human hepatocytes. Interestingly, the Oatp1a1, Oatp1a4 and Oatp1b2 inhibitor glycyrrhizic acid reduced ^{14}C-TEA uptake by 62.1% compared to control in suspended rat hepatocytes (Fig. 4.1D). The uptake of 20 μM ^{3}H-PAH over 60 min was marginally greater than background, which was attributed primarily to nonspecific binding to the hepatocytes. ^{3}H-PAH uptake was not significantly influenced by the presence of 50 μM MK571 in the incubation medium (a known Mrp inhibitor added to inhibit potential basolateral efflux; data not shown).

Hepatobiliary Disposition of ^{99m}Tc-MEB in Rat and Human Sandwich-Cultured Hepatocytes

^{99m}Tc-MEB canalicular efflux was slightly lower than basolateral efflux over 20 min in SCH from WT rats (15.3 ± 5.7% vs. 25.0 ± 6.7 of total preloaded mass). In contrast, in human SCH ^{99m}Tc-MEB canalicular efflux was greater than

basolateral efflux (45.8 ± 8.6% vs. 16.7 ± 0.6% of total preloaded mass). ^{99m}Tc-MEB canalicular efflux was ~3-fold greater in human compared to rat SCH, while basolateral efflux in human SCH was slightly lower than in rat SCH (Fig. 4.3A). ^{99m}Tc-MEB basolateral efflux tended to be higher in TR$^-$ SCH (31.8 ± 6.2 % of total preloaded mass) relative to WT values, while canalicular efflux of ^{99m}Tc-MEB in TR$^-$ SCH was negligible (Fig. 4.3A). MK571 (100 μM) decreased ^{99m}Tc-MEB canalicular efflux 665% in rat SCH and 30% in human SCH (Fig. 4.3A), but increased ^{99m}Tc-MEB basolateral efflux 136% in rat SCH and 240% in human SCH (Fig. 4.3A). ^{99m}Tc-MEB hepatocellular content (cell only) at the end of the 20-min efflux phase was slightly greater in rat SCH (58.7 ± 7.2%) compared to human SCH (37.6 ± 8.0%) (Fig. 4.3B), consistent with the species differences observed in the total efflux of ^{99m}Tc-MEB in rat (40.3 ± 5.4%) and human (62.4 ± 8.0%) SCH.

Hepatobiliary Disposition of ^{99m}Tc-MIBI in Rat and Human Sandwich-Cultured Hepatocytes.

^{99m}Tc-MIBI basolateral efflux was greater than canalicular efflux over 20 min in SCH from WT rats (40.5 ± 7.6 vs. 23.6 ± 3.4% of total preloaded mass), TR$^-$ rats (39.4 ± 7.1 vs. 30.9 ± 2.1% of total preloaded mass), and humans (64.0 ± 4.2 vs. 25.4 ± 6.0% of total preloaded mass) (Fig. 4.4A). ^{99m}Tc-MIBI canalicular efflux was similar between human and WT rat SCH, but basolateral efflux was 37% greater in human compared to WT rat SCH (Fig. 4.4A). ^{99m}Tc-MIBI basolateral efflux was similar in SCH from TR$^-$ and WT rats; likewise, canalicular efflux of

^{99m}Tc-MIBI was not altered in SCH from TR$^-$ compared to WT rats (Fig. 4.4A). GW918 (20 μM) decreased ^{99m}Tc-MIBI canalicular efflux 1.5-fold in rat SCH and 2.1-fold in human SCH. Interestingly, GW918 also decreased ^{99m}Tc-MIBI basolateral efflux in rat and human SCH (~2.3- and ~2.9-fold, respectively) (Fig. 4.4A). Hepatocellular content of ^{99m}Tc-MIBI at the end of the 20-min efflux phase was greater in rat SCH compared to human SCH (34.0 ± 4.3 vs. 10.6 ± 1.8 % of total preloaded mass; Fig. 4.4B), consistent with greater total efflux of ^{99m}Tc-MIBI in human (89.4 ± 1.8%) compared to rat (64.0 ± 8.2%) SCH using the 20-min efflux study design.

Using the 10-min accumulation study design, ^{99m}Tc-MIBI accumulation in cells+bile and cells was determined in rat SCH; BEI and *in vitro* $Cl_{biliary}$ values were 18.8% and 4.07 mL/min/kg, respectively. To examine whether Bcrp and/or P-gp were responsible for the biliary excretion of ^{99m}Tc-MIBI in rat SCH, 10-min accumulation studies were conducted. ^{99m}Tc-MIBI BEI (26.6 and 36.0%) and *in vitro* $Cl_{biliary}$ (8.08 and 9.73 mL/min/kg) in day 4 WT rat SCH were marginally increased by infection with adenoviral vectors expressing a non-target control (siNT) or short hairpin RNA targeting rat Bcrp (siBcrp), respectively (Fig. 4.5A). ^{99m}Tc-MIBI BEI and *in vitro* $Cl_{biliary}$ were ablated in the presence of 2μM GW918 in siNT- and siBcrp-infected SCH, which resulted in a ~2-fold increase in hepatocellular accumulation (cells only) of ^{99m}Tc-MIBI (Fig. 4.5A). As shown in Figure 4.5B, in day 4 rat SCH, protein levels of Bcrp (normalized by β-actin) in siBcrp-infected cells were ~20% of those in control (siNT-infected) cells. No significant differences in nitrofurantoin cellular accumulation, BEI, or *in vitro*

$Cl_{biliary}$ in noninfected or control siNT-infected rat SCH were noted (Fig. 4.5C). As expected, the cellular accumulation of nitrofurantoin, a Bcrp substrate, was increased due to the ~6-fold decrease in BEI in siBcrp-infected cells compared to control (siNT-infected) cells.

Discussion.

The utility of ^{99m}Tc-MEB and ^{99m}Tc-MIBI as probe substrates for phenotyping the function of specific hepatic transport proteins was confirmed using well established *in vitro* methods. Suspended hepatocytes and SCH were utilized from rats and humans to characterize hepatic uptake and efflux mechanisms in combination with the use of "specific" chemical inhibitors to examine the impact of hepatic transport modulation on the disposition of ^{99m}Tc-MEB and ^{99m}Tc-MIBI.

Two inhibitors were selected to encompass all Oatp/OATP isoforms reported to be expressed in rat and human liver. Rifamycin SV inhibits Oatp1a1 and 1a4 (Fattinger et al., 2000) and all of the relevant human isoforms expressed in the liver (OATP1A2, OATP1B1, OATP1B3 and OATP2B1) (Vavricka et al., 2002); glycyrrhzic acid inhibits Oatp1b2, OATP1B1 and OATP1B3 (Ismair et al., 2003). Octs were inhibited by clonidine (Martel et al., 1996), desipramine (Grundemann et al., 1994) and decynium 22 (Hayer-Zillgen et al., 2002), and Oat function was inhibited with ketoprofen (Morita et al., 2001; Ohtsuki et al., 2002). To assess sodium-dependent transport by the sodium taurocholate co-transporting polypeptide (Ntcp), choline-based buffer was substituted for sodium-based buffer in suspended hepatocytes.

Probe substrates were evaluated in the presence and absence of the panel of inhibitors to confirm the specificity of the selected inhibitors. The use of ^{3}H-E217G as a model Oatp/OATP probe substrate is well established (Brock and

Vore, 1984; Shitara et al., 2003). ^{3}H-E217G initial uptake was decreased significantly only by the Oatp/OATP inhibitors rifamycin SV and glycyrrhzic acid (Fig. 4.1C and 4.2B), which supports the use of these compounds as broad (not specific for any given isoform) Oatp/OATP inhibitors, and confirms that the other inhibitors used in this study did not interfere with the uptake of this model substrate. Oct/OCT function in the presence of the panel of inhibitors was assessed with the probe substrate ^{14}C-TEA, which has reported K_m values for Oct1 ranging from 35 to 251 μM (Grundemann et al., 1994; Busch et al., 1996; Chen and Nelson, 2000). As expected, the Oct/OCT inhibitors (clonidine, desipramine, and decynium 22) significantly reduced the initial uptake of ^{14}C-TEA (Fig. 4.1D and 4.2C). Unexpectedly, the Oatp/OATP inhibitor glyzyrrhizic acid significantly decreased ^{14}C-TEA initial uptake to 37.9% of control, suggesting that this inhibitor is not specific for Oatp isoforms because TEA is not a substrate of the Oatps expressed in the rat liver (Cattori et al., 2001). Rifamycin SV and ketoprofen had no effect on ^{14}C-TEA, supporting the hypothesis that these inhibitors may be specific for Oatps/OATPs and Oat2/OAT2, respectively. Lastly, the function of Oat2/OAT2 (Simonson et al., 1994; Hilgendorf et al., 2007), was assessed with the model Oat/OAT substrate ^{3}H-PAH (Sekine et al., 1998; Kobayashi et al., 2005). ^{3}H-PAH is not a substrate for Oatp1a1, Oatp1a4 or Oatp1b2 individually expressed in *Xenopus laevis* oocytes (Cattori et al., 2001). However, incubation of freshly isolated rat and human hepatocytes with 0.2, 1 or 20 μM ^{3}H-PAH over 60 min in the absence and presence of 50 μM MK571, co-administered to inhibit potential basolateral efflux, resulted in no measurable

increase in activity above background. Carrier-mediated retrieval of human OAT1 expressed in *Xenopus* oocytes and HEK293 cells from the cell membrane results in decreased function (Wolff et al., 2003). These findings suggest that Oat2/OAT2 may not be properly localized to assess transport function in freshly isolated rat and human hepatocytes.

Based on the specificity of the chosen inhibitors, ^{99m}Tc-MEB and ^{99m}Tc-MIBI hepatic uptake were examined. ^{99m}Tc-MEB initial uptake was sodium-independent, and was only affected by the Oatp/OATP inhibitors, rifamycin SV and glycyrrhizic acid (Fig. 4.1A and 4.2A). These data support the hypothesis that MEB uptake is predominantly mediated by Oatps/OATPs in rat and human hepatocytes, and is in agreement with data demonstrating ^{99m}Tc-MEB is a substrate of OATP1B1 and OATP1B3 in HEK293 overexpressing cells (Ghibellini et al., 2008). Bilirubin (20 μM), an Oatp substrate, inhibited ^{99m}Tc-MEB initial uptake in plated rat hepatocytes by ~30% (Lan et al., 1988).

^{99m}Tc-MIBI initial uptake was not influenced by inhibitors or the absence of sodium in the uptake buffer (Fig. 4.1B), suggesting that an active transport process is not involved in ^{99m}Tc-MIBI hepatic uptake at these low concentrations. Concentrations of ^{99m}Tc-MIBI were increased (5 - 200 μCi/mL) to saturate a possible active transport process but partitioning of ^{99m}Tc-MIBI into hepatocytes was linear at designated time points collected for 60 min. These findings are consistent with previous reports that MIBI uptake is a function of free diffusion based on electrical potentials across the plasma and mitochondrial membranes,

with localization in the mitochondria by electrostatic forces (Chiu et al., 1990; Delmon-Moingeon et al., 1990). Therefore, ^{99m}Tc-MIBI uptake experiments were not conducted in human hepatocytes to conserve this limited resource.

Further studies were undertaken to examine the efflux processes involved in ^{99m}Tc-MEB hepatic disposition. Remarkably, the canalicular efflux of ^{99m}Tc-MEB was ~3-fold greater in human compared to WT rat SCH, whereas the basolateral efflux was comparable (Fig. 4.3A). This cannot be attributed to differences in the absolute amount of Mrp2/MRP2 protein primarily responsible for biliary excretion of ^{99m}Tc-MEB, but could be explained by affinity differences. Based on work by Li et al., total Mrp2/MRP2 protein was not significantly different in day 4 rat and day 7 human SCH (~4 fmol/μg protein) utilizing a quantitative LC-MS/MS analysis (Li et al., 2009). ^{99m}Tc-MEB total efflux also was greater in human compared to rat SCH due to this increased canalicular efflux (Fig. 4.3A). ^{99m}Tc-MEB canalicular efflux was completely ablated in TR$^-$ rat SCH. The Mrp2 inhibitor MK571 decreased ^{99m}Tc-MEB canalicular efflux ~6.7-fold in rat SCH, but only 30% in human SCH (Fig. 4.3A). This apparent discrepancy could be due to limitations in the experimental design of the efflux experiments. For example, during the preloading phase, ^{99m}Tc-MEB accumulates in the canalicular networks and may not be completely washed away before initiating the efflux phase or rapid canalicular excretion of ^{99m}Tc-MEB may occur before MK571 had time to access the hepatocyte and reach the site of MRP2 inhibition, especially in human SCH. Overall, MK571 inhibition and the absence of ^{99m}Tc-MEB in the bile canalicular networks of TR$^-$ rat SCH support the hypothesis that ^{99m}Tc-MEB is a

specific Mrp2 probe substrate, consistent with other reports documenting increased hepatic exposure of ^{99m}Tc-MEB in TR$^-$ rats (Bhargava et al., 2009), and decreased biliary excretion in patients with Dubin-Johnson syndrome (MRP2-deficiency) administered ^{99m}Tc-MEB analogs (Pinos et al., 1990). ^{99m}Tc-MEB basolateral efflux was increased in TR$^-$ sandwich-cultured rat hepatocytes compared to WT, and in the presence of MK571 (Fig. 4.3A), while intracellular accumulation of ^{99m}Tc-MEB was unchanged (Fig. 4.3B). These important findings suggest that this probe can be redirected from biliary excretion to basolateral efflux. This increase in basolateral efflux also could be due, in part, to inhibition of ^{99m}Tc-MEB hepatic re-uptake, because MK571 has been shown to inhibit OATP1B3 with a reported K_i of 0.6 μM (Letschert et al., 2005).

Further studies were conducted to investigate the efflux processes involved in ^{99m}Tc-MIBI hepatic disposition. The absence of Mrp2 based on efflux studies in sandwich-cultured TR$^-$ rat hepatocytes did not alter basolateral or canalicular efflux, suggesting that either Mrp2 is not involved, or other proteins (e.g. P-gp) are able to fully compensate (Fig.4.4A). In TR$^-$ rats, ^{99m}Tc-MIBI hepatic scintigraphy and biliary excretion were unchanged compared to WT control rats (Hendrikse et al., 2004). ^{99m}Tc-MIBI efflux was assessed in the presence of 20 μM GW918, a concentration 10-fold greater than previously used to inhibit P-gp in rat SCH (Annaert et al., 2001). This concentration was selected based on studies in cancer cell lines expressing multidrug resistance transport proteins (P-gp and Bcrp) demonstrating GW918 is a more potent inhibitor of P-gp

than Bcrp by an order of magnitude or more (de Bruin et al., 1999), and the use of 10 μM GW918 in isolated perfused rat livers to impair Bcrp-mediated biliary excretion of 4-methylumbelliferyl sulfate generated in the hepatocyte (Zamek-Gliszczynski et al., 2006). As expected, ^{99m}Tc-MIBI canalicular efflux was GW918 sensitive, consistent with a role for P-gp and/or Bcrp in ^{99m}Tc-MIBI biliary excretion. Surprisingly, ^{99m}Tc-MIBI basolateral efflux was GW918 sensitive, suggesting involvement of an active transport process. Recently, GW918 was demonstrated to inhibit MRP4 in inside-out membrane vesicles prepared from transiently transfected HEK293 cells (Lee, 2009). Hepatocellular accumulation of ^{99m}Tc-MIBI increased in the presence of GW918 (Fig. 4.4B) due to decreased basolateral and canalicular efflux of MIBI (Fig. 4.4A).

In order to further investigate the transport processes involved in ^{99m}Tc-MIBI biliary excretion, accumulation studies were conducted in rat SCH. The involvement of Bcrp in the biliary excretion of ^{99m}Tc-MIBI was assessed with the use of RNAi knockdown of Bcrp, as confirmed by immunoblot (Fig. 4.5B) and significantly impaired biliary excretion of the rat Bcrp probe susbstrate nitrofurantoin (Fig. 4.5C). This approach using adenoviral vectors expressing a non-target control (siNT) and short hairpin RNA targeting Bcrp (siBcrp) has been shown to efficiently and specifically knock down Bcrp in sandwich-cultured rat hepatocytes (Yue et al., 2009). Bcrp knockdown did not affect ^{99m}Tc-MIBI cellular accumulation, biliary excretion or *in vitro* biliary clearance (Fig. 4.5A). This finding was consistent with data generated in the cancer cell lines SIM1 and MCF-7, and their BCRP overexpressing derivative cells (Chen et al., 2000).

^{99m}Tc-MIBI biliary excretion was inhibited completely by 2μM GW918 (Fig. 4.5A), used previously to inhibit P-gp in rat SCH (Annaert et al., 2001). Cellular accumulation also increased in the presence of GW918 (Fig. 4.5A), suggesting that P-gp is the primary protein responsible for the biliary excretion of ^{99m}Tc-MIBI. These findings are in agreement with reduced ^{99m}Tc-MIBI biliary elimination and/or increased retention of ^{99m}Tc-MIBI in the liver determined by hepatic scintigraphy in humans with single nucleotide polymorphisms in the *ABCB1* gene resulting in decreased P-gp function (Wong et al., 2005), and in cancer patients administered MIBI and the P-gp inhibitor PSC833 (Chen et al., 1997) (Luker et al., 1997).

Remarkable species differences existed in the fraction of canalicular vs. basolateral efflux of ^{99m}Tc-MEB in rats (38.0% and 62.0%, respectively) and humans (73.3% and 26.7%, respectively; Fig. 4.3A), suggesting that biliary excretion would be the preferential route of hepatic elimination of this probe in humans. This finding is consistent with *in vivo* data from healthy human subjects indicating that ~84% of a 2.3 μCi dose of intravenously administered ^{99m}Tc-MEB was recovered in bile (Ghibellini et al., 2004). In contrast, the fraction of canalicular vs. basolateral efflux of ^{99m}Tc-MIBI in rats (36.8% and 63.2%, respectively) and humans (28.3% and 71.7%, respectively; Fig. 4.4A), basolateral excretion of ^{99m}Tc-MIBI appears to be the preferential route of hepatic elimination of this probe in both rats and humans. This finding is consistent with biliary recovery of ~22% of a 3.1 μCi dose of intraveneously administered ^{99m}Tc-MIBI in healthy human subjects (Ghibellini et al., 2007). Overall the efflux method

is useful for examining the preferential route of hepatic efflux (canalicular vs. basolateral) and elucidating species differences in hepatic efflux.

In summary, the hepatic uptake of ^{99m}Tc-MIBI appears to occur by passive diffusion; ^{99m}Tc-MIBI biliary excretion is mediated by P-gp. ^{99m}Tc-MEB hepatic uptake is predominantly Oatp-mediated with biliary excretion by Mrp2. Remarkable species differences exist between rat and human in the total efflux and route of efflux for ^{99m}Tc-MEB. Preloading SCH and measurement of efflux over 20 min in SCH is a useful approach to investigate the route of hepatic excretion (basolateral vs. canalicular), species differences in basolateral and canalicular efflux, and compensatory changes in canalicular and basolateral efflux due to impaired transport function associated with drug interactions, disease state alterations or genetic variation.

Acknowledgment.

This research was supported by a grant from the National Institutes of Health (R01GM41935). Brandon Swift is supported by an Eli Lilly and Company predoctoral fellowship. The authors would like to thank Wei Yue, Ph.D., for providing the adenoviral vector packaged RNAi to knockdown BCRP in SCH, Arlene S. Bridges, Ph. D., for her analytical support, Yiwei Rong, for her technical expertise in the isolation of rat hepatocytes, and CellzDirect, Life Technologies, for kindly providing freshly isolated suspended and sandwich-cultured human hepatocytes.

References.

Adkison KK, Vaidya SS, Lee DY, Koo SH, Li L, Mehta AA, Gross AS, Polli JW, Lou Y and Lee EJ (2008) The ABCG2 C421A polymorphism does not affect oral nitrofurantoin pharmacokinetics in healthy Chinese male subjects. *Br J Clin Pharmacol* **66**:233-239.

Annaert PP, Turncliff RZ, Booth CL, Thakker DR and Brouwer KL (2001) P-glycoprotein-mediated in vitro biliary excretion in sandwich-cultured rat hepatocytes. *Drug Metab Dispos* **29**:1277-1283.

Baur H, Kasperek S and Pfaff E (1975) Criteria of viability of isolated liver cells. *Hoppe Seylers Z Physiol Chem* **356**:827-838.

Beller GA and Sinusas AJ (1990) Experimental studies of the physiologic properties of technetium-99m isonitriles. *Am J Cardiol* **66**:5E-8E.

Bhargava KK, Joseph B, Ananthanarayanan M, Balasubramaniyan N, Tronco GG, Palestro CJ and Gupta S (2009) Adenosine triphosphate-binding cassette subfamily C member 2 is the major transporter of the hepatobiliary imaging agent (99m)Tc-mebrofenin. *J Nucl Med* **50**:1140-1146.

Brock WJ and Vore M (1984) Characterization of uptake of steroid glucuronides into isolated male and female rat hepatocytes. *J Pharmacol Exp Ther* **229**:175-181.

Bujanover Y, Bar-Meir S, Hayman I and Baron J (1983) 99mTc-HIDA cholescintigraphy in children with Dubin-Johnson syndrome. *J Pediatr Gastroenterol Nutr* **2**:311-312.

Busch AE, Quester S, Ulzheimer JC, Waldegger S, Gorboulev V, Arndt P, Lang F and Koepsell H (1996) Electrogenic properties and substrate specificity of the polyspecific rat cation transporter rOCT1. *J Biol Chem* **271**:32599-32604.

Cattori V, van Montfoort JE, Stieger B, Landmann L, Meijer DK, Winterhalter KH, Meier PJ and Hagenbuch B (2001) Localization of organic anion transporting polypeptide 4 (Oatp4) in rat liver and comparison of its substrate specificity with Oatp1, Oatp2 and Oatp3. *Pflugers Arch* **443**:188-195.

Chen CC, Meadows B, Regis J, Kalafsky G, Fojo T, Carrasquillo JA and Bates SE (1997) Detection of in vivo P-glycoprotein inhibition by PSC 833 using Tc-99m sestamibi. *Clin Cancer Res* **3**:545-552.

Chen R and Nelson JA (2000) Role of organic cation transporters in the renal secretion of nucleosides. *Biochem Pharmacol* **60**:215-219.

Chen WS, Luker KE, Dahlheimer JL, Pica CM, Luker GD and Piwnica-Worms D (2000) Effects of MDR1 and MDR3 P-glycoproteins, MRP1, and BCRP/MXR/ABCP on the transport of (99m)Tc-tetrofosmin. *Biochem Pharmacol* **60**:413-426.

Chiu ML, Kronauge JF and Piwnica-Worms D (1990) Effect of mitochondrial and plasma membrane potentials on accumulation of hexakis (2-methoxyisobutylisonitrile) technetium(I) in cultured mouse fibroblasts. *J Nucl Med* **31**:1646-1653.

de Bruin M, Miyake K, Litman T, Robey R and Bates SE (1999) Reversal of resistance by GF120918 in cell lines expressing the ABC half-transporter, MXR. *Cancer Lett* **146**:117-126.

Delmon-Moingeon LI, Piwnica-Worms D, Van den Abbeele AD, Holman BL, Davison A and Jones AG (1990) Uptake of the cation hexakis(2-methoxyisobutylisonitrile)-technetium-99m by human carcinoma cell lines in vitro. *Cancer Res* **50**:2198-2202.

Doo E, Krishnamurthy GT, Eklem MJ, Gilbert S and Brown PH (1991) Quantification of hepatobiliary function as an integral part of imaging with technetium-99m-mebrofenin in health and disease. *J Nucl Med* **32**:48-57.

Erdogan D, Heijnen BH, Bennink RJ, Kok M, Dinant S, Straatsburg IH, Gouma DJ and van Gulik TM (2004) Preoperative assessment of liver function: a comparison of 99mTc-Mebrofenin scintigraphy with indocyanine green clearance test. *Liver Int* **24**:117-123.

Fattinger K, Cattori V, Hagenbuch B, Meier PJ and Stieger B (2000) Rifamycin SV and rifampicin exhibit differential inhibition of the hepatic rat organic anion transporting polypeptides, Oatp1 and Oatp2. *Hepatology* **32**:82-86.

Gencoglu E, Karakayali H, Moray G, Aktas A and Haberal M (2002) Evaluation of pediatric liver transplant recipients using quantitative hepatobiliary scintigraphy. *Transplant Proc* **34**:2160-2162.

Ghibellini G, Johnson BM, Kowalsky RJ, Heizer WD and Brouwer KL (2004) A novel method for the determination of biliary clearance in humans. *Aaps J* **6**:e33.

Ghibellini G, Leslie EM, Pollack GM and Brouwer KL (2008) Use of tc-99m mebrofenin as a clinical probe to assess altered hepatobiliary transport: integration of in vitro, pharmacokinetic modeling, and simulation studies. *Pharm Res* **25**:1851-1860.

Ghibellini G, Vasist LS, Leslie EM, Heizer WD, Kowalsky RJ, Calvo BF and Brouwer KL (2007) In vitro-in vivo correlation of hepatobiliary drug clearance in humans. *Clin Pharmacol Ther* **81**:406-413.

Groothuis GM, Hulstaert CE, Kalicharan D and Hardonk MJ (1981) Plasma membrane specialization and intracellular polarity of freshly isolated rat hepatocytes. *Eur J Cell Biol* **26**:43-51.

Grundemann D, Gorboulev V, Gambaryan S, Veyhl M and Koepsell H (1994) Drug excretion mediated by a new prototype of polyspecific transporter. *Nature* **372**:549-552.

Hayer-Zillgen M, Bruss M and Bonisch H (2002) Expression and pharmacological profile of the human organic cation transporters hOCT1, hOCT2 and hOCT3. *Br J Pharmacol* **136**:829-836.

Hendrikse NH, Franssen EJ, van der Graaf WT, Meijer C, Piers DA, Vaalburg W and de Vries EG (1998) 99mTc-sestamibi is a substrate for P-glycoprotein and the multidrug resistance-associated protein. *Br J Cancer* **77**:353-358.

Hendrikse NH, Kuipers F, Meijer C, Havinga R, Bijleveld CM, van der Graaf WT, Vaalburg W and de Vries EG (2004) In vivo imaging of hepatobiliary transport function mediated by multidrug resistance associated protein and P-glycoprotein. *Cancer Chemother Pharmacol* **54**:131-138.

Hilgendorf C, Ahlin G, Seithel A, Artursson P, Ungell AL and Karlsson J (2007) Expression of thirty-six drug transporter genes in human intestine, liver, kidney, and organotypic cell lines. *Drug Metab Dispos* **35**:1333-1340.

Ismair MG, Stanca C, Ha HR, Renner EL, Meier PJ and Kullak-Ublick GA (2003) Interactions of glycyrrhizin with organic anion transporting polypeptides of rat and human liver. *Hepatol Res* **26**:343-347.

Kobayashi Y, Ohshiro N, Sakai R, Ohbayashi M, Kohyama N and Yamamoto T (2005) Transport mechanism and substrate specificity of human organic anion transporter 2 (hOat2 [SLC22A7]). *J Pharm Pharmacol* **57**:573-578.

Koruk M, Ozkilic S, Savas MC, Celen Z, Kadayifci A and Ozkilic C (2003) Evaluation of hepatic functions and biliary dynamics in patients with liver cirrhosis by quantitative scintigraphy. *Hepatogastroenterology* **50**:1803-1805.

Krishnamurthy GT and Turner FE (1990) Pharmacokinetics and clinical application of technetium 99m-labeled hepatobiliary agents. *Semin Nucl Med* **20**:130-149.

Lan JA, Chervu LR, Johansen KL and Wolkoff AW (1988) Uptake of technetium 99m hepatobiliary imaging agents by cultured rat hepatocytes. *Gastroenterology* **95**:1625-1631.

LeCluyse EL, Bullock PL, Parkinson A and Hochman JH (1996) Cultured rat hepatocytes. *Pharm Biotechnol* **8**:121-159.

Lee JK (2009) Role of Hepatic Transport Proteins in Drug Disposition and Drug-Induced Liver Injury, in *School of Pharmacy* p 257, University of North Carolina at Chapel Hill, Chapel Hill.

Leslie EM, Watkins PB, Kim RB and Brouwer KL (2007) Differential inhibition of rat and human Na+-dependent taurocholate cotransporting polypeptide (NTCP/SLC10A1)by bosentan: a mechanism for species differences in hepatotoxicity. *J Pharmacol Exp Ther* **321**:1170-1178.

Letschert K, Komatsu M, Hummel-Eisenbeiss J and Keppler D (2005) Vectorial transport of the peptide CCK-8 by double-transfected MDCKII cells stably expressing the organic anion transporter OATP1B3 (OATP8) and the export pump ABCC2. *J Pharmacol Exp Ther* **313**:549-556.

Li N, Bi YA, Duignan DB and Lai Y (2009) Quantitative expression profile of hepatobiliary transporters in sandwich cultured rat and human hepatocytes. *Mol Pharm* **6**:1180-1189.

Liu X, LeCluyse EL, Brouwer KR, Gan LS, Lemasters JJ, Stieger B, Meier PJ and Brouwer KL (1999a) Biliary excretion in primary rat hepatocytes cultured in a collagen-sandwich configuration. *Am J Physiol* **277**:G12-21.

Liu X, LeCluyse EL, Brouwer KR, Lightfoot RM, Lee JI and Brouwer KL (1999b) Use of Ca2+ modulation to evaluate biliary excretion in sandwich-cultured rat hepatocytes. *J Pharmacol Exp Ther* **289**:1592-1599.

Luker GD, Fracasso PM, Dobkin J and Piwnica-Worms D (1997) Modulation of the multidrug resistance P-glycoprotein: detection with technetium-99m-sestamibi in vivo. *J Nucl Med* **38**:369-372.

Martel F, Vetter T, Russ H, Grundemann D, Azevedo I, Koepsell H and Schomig E (1996) Transport of small organic cations in the rat liver. The role of the organic cation transporter OCT1. *Naunyn Schmiedebergs Arch Pharmacol* **354**:320-326.

Michael M, Thompson M, Hicks RJ, Mitchell PL, Ellis A, Milner AD, Di Iulio J, Scott AM, Gurtler V, Hoskins JM, Clarke SJ, Tebbut NC, Foo K, Jefford M and Zalcberg JR (2006) Relationship of hepatic functional imaging to irinotecan pharmacokinetics and genetic parameters of drug elimination. *J Clin Oncol* **24**:4228-4235.

Mobasseri S and Hendel RC (2002) Cardiac imaging in women: use of radionuclide myocardial perfusion imaging and echocardiography for acute chest pain. *Cardiol Rev* **10**:149-160.

Morita N, Kusuhara H, Sekine T, Endou H and Sugiyama Y (2001) Functional characterization of rat organic anion transporter 2 in LLC-PK1 cells. *J Pharmacol Exp Ther* **298**:1179-1184.

Nunn AD, Loberg MD and Conley RA (1983) A structure-distribution-relationship approach leading to the development of Tc-99m mebrofenin: an improved cholescintigraphic agent. *J Nucl Med* **24**:423-430.

Ohtsuki S, Asaba H, Takanaga H, Deguchi T, Hosoya K, Otagiri M and Terasaki T (2002) Role of blood-brain barrier organic anion transporter 3 (OAT3) in the efflux of indoxyl sulfate, a uremic toxin: its involvement in neurotransmitter metabolite clearance from the brain. *J Neurochem* **83**:57-66.

Oude Elferink RP, Meijer DK, Kuipers F, Jansen PL, Groen AK and Groothuis GM (1995) Hepatobiliary secretion of organic compounds; molecular mechanisms of membrane transport. *Biochim Biophys Acta* **1241**:215-268.

Perek N, Prevot N, Koumanov F, Frere D, Sabido O, Beauchesne P and Dubois F (2000) Involvement of the glutathione S-conjugate compounds and the MRP protein in Tc-99m-tetrofosmin and Tc-99m-sestamibi uptake in glioma cell lines. *Nucl Med Biol* **27**:299-307.

Pinos T, Constansa JM, Palacin A and Figueras C (1990) A new diagnostic approach to the Dubin-Johnson syndrome. *Am J Gastroenterol* **85**:91-93.

Piwnica-Worms D, Chiu ML, Budding M, Kronauge JF, Kramer RA and Croop JM (1993) Functional imaging of multidrug-resistant P-glycoprotein with an organotechnetium complex. *Cancer Res* **53**:977-984.

Ravizzini GC, Hanson MW, Shaw LK, Wong TZ, Hagge RJ, Pagnanelli RA, Jain D, Lima HS, Jr., Coleman RE and Borges-Neto S (2002) Efficiency comparison between 99m Tc-tetrofosmin and 99m Tc-sestamibi myocardial perfusion studies. *Nucl Med Commun* **23**:203-208.

Seglen PO (1976) Preparation of isolated rat liver cells. *Methods Cell Biol* **13**:29-83.

Sekine T, Cha SH, Tsuda M, Apiwattanakul N, Nakajima N, Kanai Y and Endou H (1998) Identification of multispecific organic anion transporter 2 expressed predominantly in the liver. *FEBS Lett* **429**:179-182.

Shitara Y, Li AP, Kato Y, Lu C, Ito K, Itoh T and Sugiyama Y (2003) Function of uptake transporters for taurocholate and estradiol 17beta-D-glucuronide in cryopreserved human hepatocytes. *Drug Metab Pharmacokinet* **18**:33-41.

Simonson GD, Vincent AC, Roberg KJ, Huang Y and Iwanij V (1994) Molecular cloning and characterization of a novel liver-specific transport protein. *J Cell Sci* **107 (Pt 4)**:1065-1072.

Slapak CA, Dahlheimer J and Piwnica-Worms D (2001) Reversal of multidrug resistance with LY335979: functional analysis of P-glycoprotein-mediated transport activity and its modulation in vivo. *J Clin Pharmacol* **Suppl**:29S-38S.

Urquhart BL, Ware JA, Tirona RG, Ho RH, Leake BF, Schwarz UI, Zaher H, Palandra J, Gregor JC, Dresser GK and Kim RB (2008) Breast cancer resistance protein (ABCG2) and drug disposition: intestinal expression, polymorphisms and sulfasalazine as an in vivo probe. *Pharmacogenet Genomics* **18**:439-448.

Vavricka SR, Van Montfoort J, Ha HR, Meier PJ and Fattinger K (2002) Interactions of rifamycin SV and rifampicin with organic anion uptake systems of human liver. *Hepatology* **36**:164-172.

Wolf KK, Brouwer KR, Pollack GM and Brouwer KL (2008) Effect of albumin on the biliary clearance of compounds in sandwich-cultured rat hepatocytes. *Drug Metab Dispos* **36**:2086-2092.

Wolff NA, Thies K, Kuhnke N, Reid G, Friedrich B, Lang F and Burckhardt G (2003) Protein kinase C activation downregulates human organic anion transporter 1-mediated transport through carrier internalization. *J Am Soc Nephrol* **14**:1959-1968.

Wong M, Balleine RL, Blair EY, McLachlan AJ, Ackland SP, Garg MB, Evans S, Farlow D, Collins M, Rivory LP, Hoskins JM, Mann GJ, Clarke CL and Gurney H (2006) Predictors of vinorelbine pharmacokinetics and pharmacodynamics in patients with cancer. *J Clin Oncol* **24**:2448-2455.

Wong M, Evans S, Rivory LP, Hoskins JM, Mann GJ, Farlow D, Clarke CL, Balleine RL and Gurney H (2005) Hepatic technetium Tc 99m-labeled sestamibi elimination rate and ABCB1 (MDR1) genotype as indicators of ABCB1 (P-glycoprotein) activity in patients with cancer. *Clin Pharmacol Ther* **77**:33-42.

Yue W, Abe K and Brouwer KL (2009) Knocking Down Breast Cancer Resistance Protein (Bcrp) by Adenoviral Vector-Mediated RNA Interference (RNAi) in Sandwich-Cultured Rat Hepatocytes: A Novel Tool

To Assess the Contribution of Bcrp to Drug Biliary Excretion. *Mol Pharm* **6**:134-143.

Zamek-Gliszczynski MJ, Hoffmaster KA, Humphreys JE, Tian X, Nezasa K and Brouwer KL (2006) Differential involvement of Mrp2 (Abcc2) and Bcrp (Abcg2) in biliary excretion of 4-methylumbelliferyl glucuronide and sulfate in the rat. *J Pharmacol Exp Ther* **319**:459-467.

Zhang W, Yu BN, He YJ, Fan L, Li Q, Liu ZQ, Wang A, Liu YL, Tan ZR, Fen J, Huang YF and Zhou HH (2006) Role of BCRP 421C>A polymorphism on rosuvastatin pharmacokinetics in healthy Chinese males. *Clin Chim Acta* **373**:99-103.

Legend to Figures

Figure 4.1 Initial uptake rate of (A) MEB (5 μCi/mL), (B) MIBI (5 μCi/mL), (C) ^{3}H-E217G (1 μM), and (D) ^{14}C-TEA (20 μM) in suspended WT rat hepatocytes in the absence and presence of transport protein inhibitors (mean percentage ± SEM; n=3 livers per group, in duplicate or triplicate; Glcy Acid =glycyrrhizic acid); *, $p<0.05$ versus control.

Figure 4.2 Initial uptake rate of (A) MEB (5 μCi/mL), (B) ^{3}H-E217G (1 μM), and (C) ^{14}C-TEA (20 μM) in suspended human hepatocytes in the absence and presence of transport protein inhibitors (mean percentage ± SEM; n=2-3 livers per group, in duplicate or triplicate; Glcy Acid =glycyrrhizic acid); *, $p<0.05$ versus control.

Figure 4.3 MEB (A) basolateral (dark grey bars) and canalicular (white bars) efflux over 20 min (5 μCi/mL, 20-min preload) and (B) hepatocellular content (cross hatched bars) in cell lysate at the end of the 20-min efflux experiments in day 4 rat (WT and TR^{-}) and day 7 human (hatched) sandwich-cultured hepatocytes. Data were obtained after a 20-min efflux phase in incubation medium containing standard (basolateral) or Ca^{+}-free (basolateral + canalicular) HBSS (Mean ± SEM or Range; n=4 WT rat livers, n=3 TR^{-} rat livers and n=2 human livers in triplicate).

Figure 4.4 MIBI (A) basolateral (dark grey bars) and canalicular (white bars) efflux over 20 min (5 μCi/mL, 20-min preload) and (B) hepatocellular content (cross hatched bars) in cell lysate at the end of the 20-min efflux experiments in day 4 rat (WT and TR^{-}) and day 7 human (hatched) sandwich-cultured hepatocytes. Data were obtained after a 20-min efflux phase in incubation medium containing standard (basolateral) or Ca^{+}-free (basoleral + canalicular) HBSS (Mean ± SEM or Range; n=4 WT rat livers, n=3 TR^{-} rat livers and n=2 human livers in triplicate).

Figure 4.5 MIBI (A) accumulation in cells+bile (black bars) and cells (white bars), biliary excretion index (BEI) and *in vitro* $CL_{biliary}$ determined after a 10-min incubation with 0.5 μCi/mL MIBI in day 4 WT sandwich-cultured rat hepatocytes non-infected or infected with adenoviral vectors expressing short hairpin RNA targeting rat Bcrp (siBcrp) or a non-target control (siNT) (representative data; mean ± SD; n=3 livers). Bcrp (B) expression in day 4 non-infected (None) or sandwich-cultured rat hepatocytes infected with adenoviral vectors siNT and

siBcrp. Representative results are shown with β-actin as the loading control. Nitrofurantoin (C) accumulation in cells+bile (black bars) and cells (white bars), BEI and *in vitro* $CL_{biliary}$ determined after a 10-min incubation with 5 μM nitrofurantoin in day 4 WT sandwich-cultured rat hepatocytes non-infected or infected with siBcrp or siNT (representative data; mean ± SD).

Figure 4.1
(A)

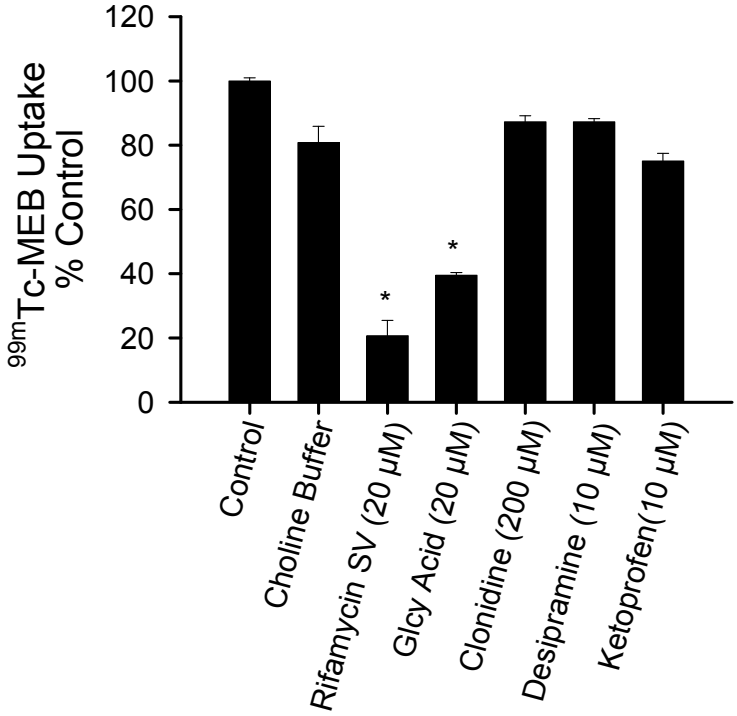
99mTc-MEB Uptake
% Control
120
100
80
60
40
20
0
*
*
Control
Choline Buffer
Rifamycin SV (20 µM)
Glcy Acid (20 µM)
Clonidine (200 µM)
Desipramine (10 µM)
Ketoprofen(10 µM)

(B)

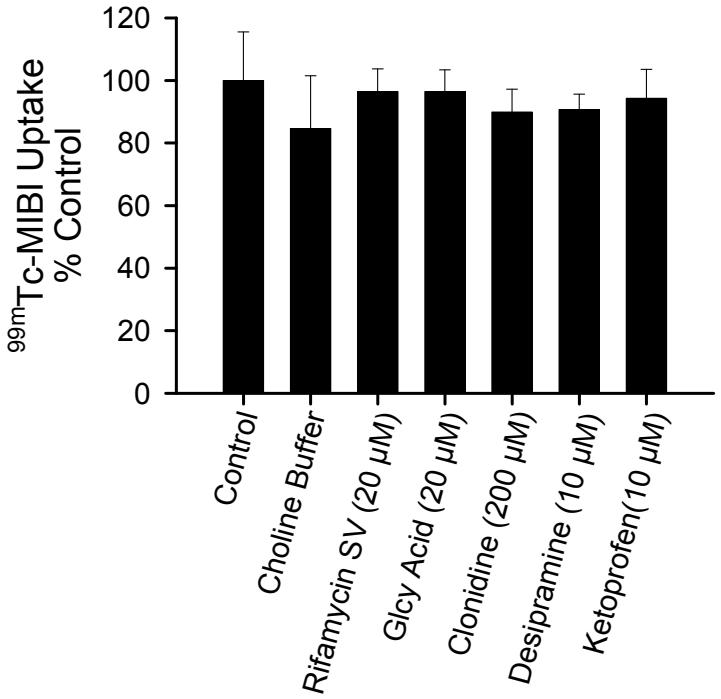
99mTc-MIBI Uptake
% Control
120
100
80
60
40
20
0
Control
Choline Buffer
Rifamycin SV (20 µM)
Glcy Acid (20 µM)
Clonidine (200 µM)
Desipramine (10 µM)
Ketoprofen(10 µM)

(C)

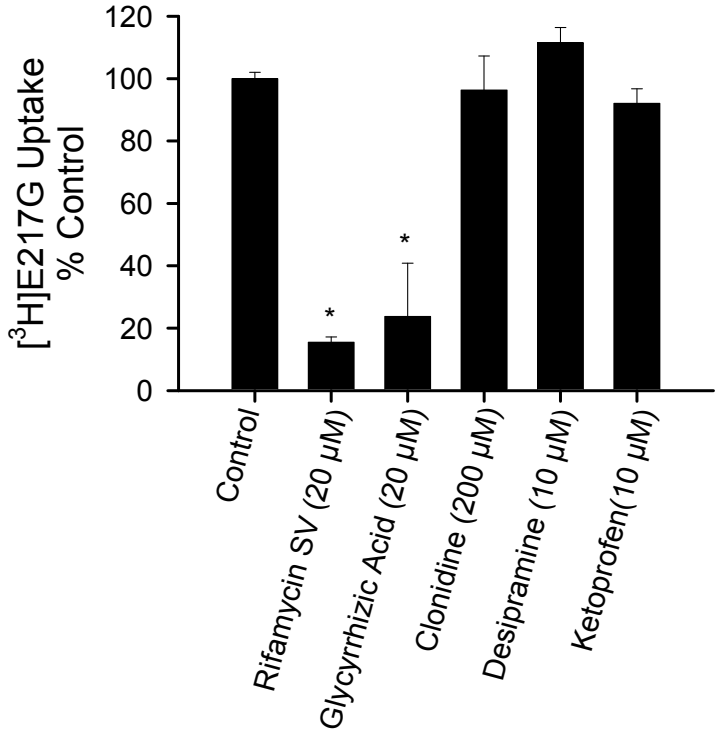
[3H]E217G Uptake
% Control
120
100
80
60
40
20
0
*
*
Control
Rifamycin SV (20 μM)
Glycyrrhizic Acid (20 μM)
Clonidine (200 μM)
Desipramine (10 μM)
Ketoprofen(10 μM)

(D)

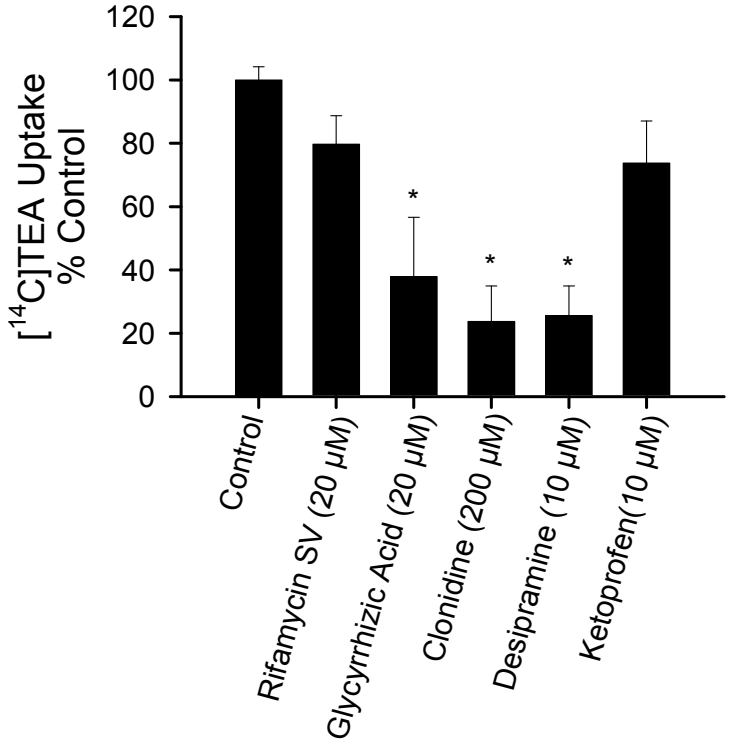
[14C]TEA Uptake
% Control
120
100
80
60
40
20
0
*
*
*
Control
Rifamycin SV (20 μM)
Glycyrrhizic Acid (20 μM)
Clonidine (200 μM)
Desipramine (10 μM)
Ketoprofen(10 μM)

Figure 4.2
(A)

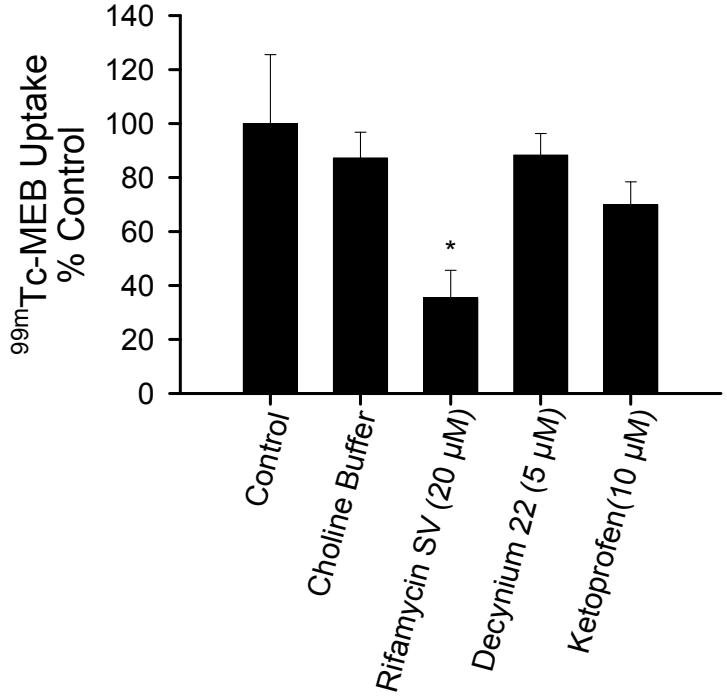
^{99m}Tc-MEB Uptake
% Control
140
120
100
80
60
40
20
0
*
Control
Choline Buffer
Rifamycin SV (20 µM)
Decynium 22 (5 µM)
Ketoprofen(10 µM)

(B)

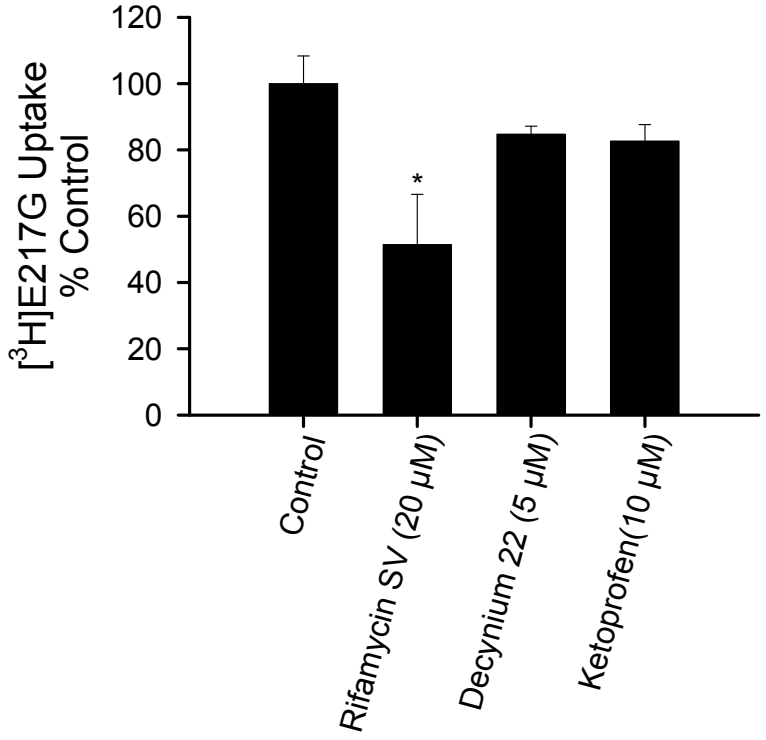
[^{3}H]E217G Uptake
% Control
120
100
80
60
40
20
0
*
Control
Rifamycin SV (20 µM)
Decynium 22 (5 µM)
Ketoprofen(10 µM)

(C)

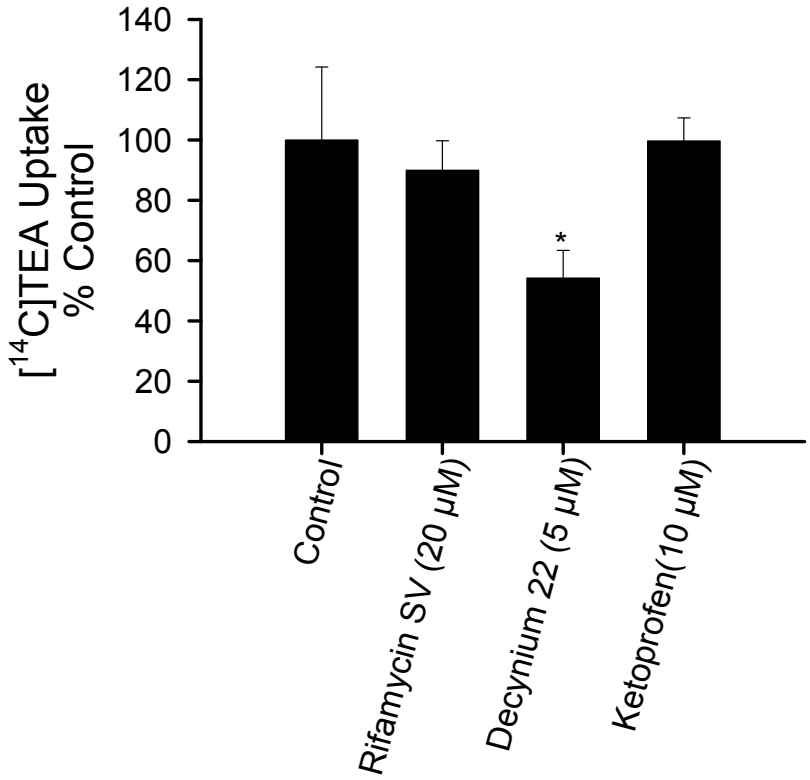
[14C]TEA Uptake
% Control
140
120
100
80
60
40
20
0
*
Control
Rifamycin SV (20 μM)
Decynium 22 (5 μM)
Ketoprofen(10 μM)

Figure 4.3

(A)

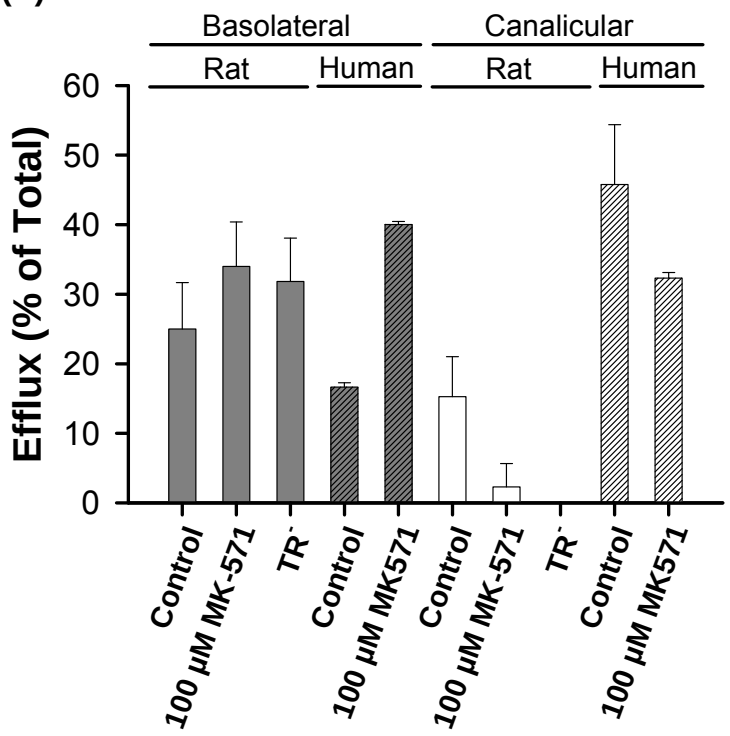
Basolateral
Canalicular
Rat
Human
Rat
Human
Efflux (% of Total)
60
50
40
30
20
10
0
Control
100 µM MK-571
TR-
Control
100 µM MK571
Control
100 µM MK-571
TR-
Control
100 µM MK571

(B)

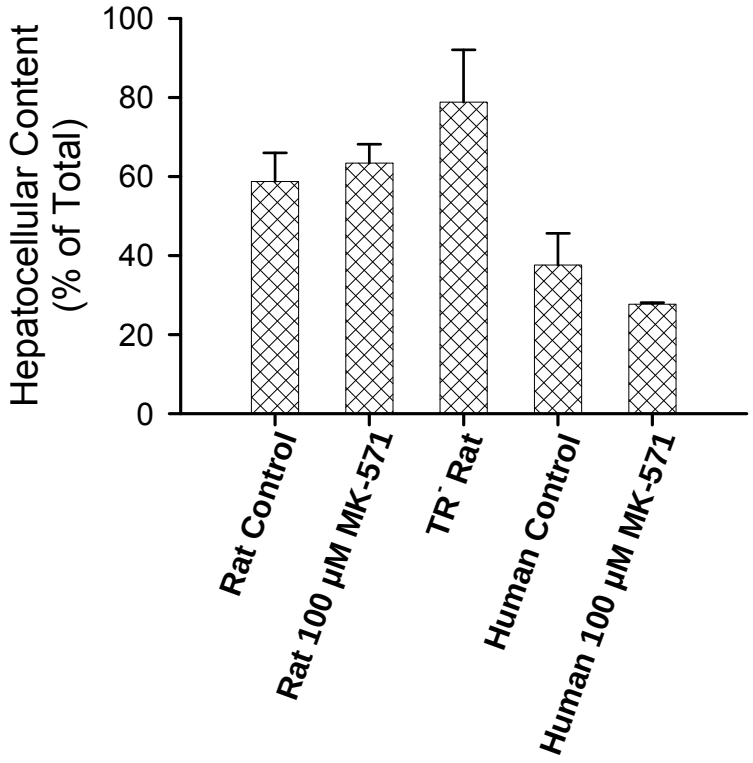
Hepatocellular Content
(% of Total)
100
80
60
40
20
0
Rat Control
Rat 100 µM MK-571
TR- Rat
Human Control
Human 100 µM MK-571

Figure 4.4

(A)

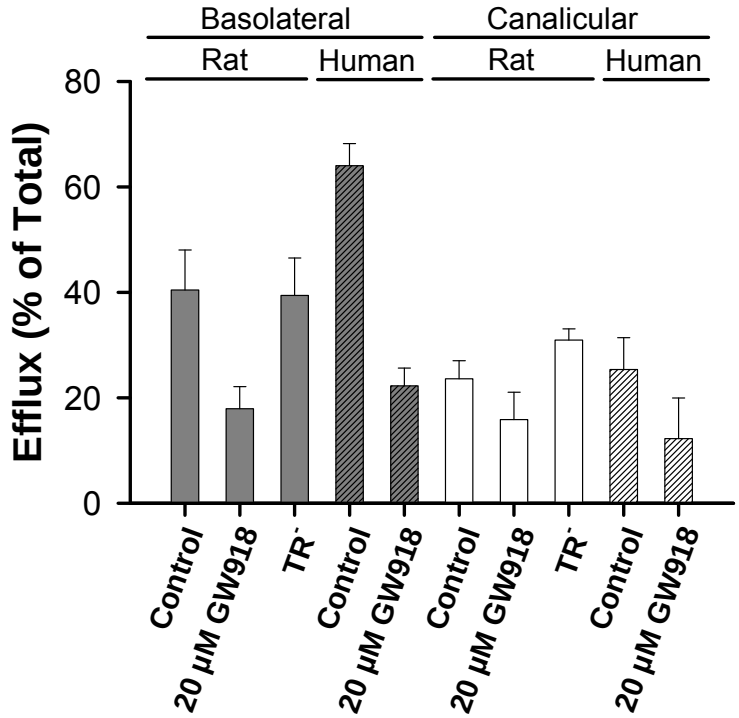
Basolateral
Canalicular
Rat
Human
Rat
Human
Efflux (% of Total)
80
60
40
20
0
Control
20 µM GW918
TR⁻
Control
20 µM GW918
Control
20 µM GW918
TR⁻
Control
20 µM GW918

(B)

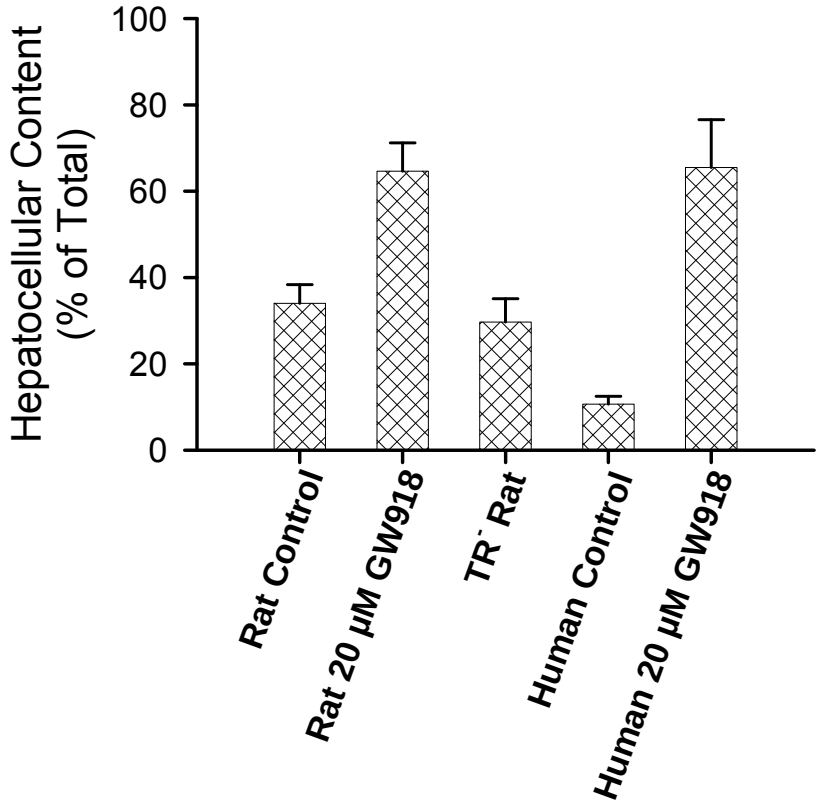
Hepatocellular Content
(% of Total)
100
80
60
40
20
0
Rat Control
Rat 20 µM GW918
TR⁻ Rat
Human Control
Human 20 µM GW918

Figure 4.5

(A)

BEI (%)	**18**	**36**	**0**	**27**	**0**
***in vitro* $Cl_{biliary}$**	**4.07**	**8.08**	**0.346**	**9.73**	**0**

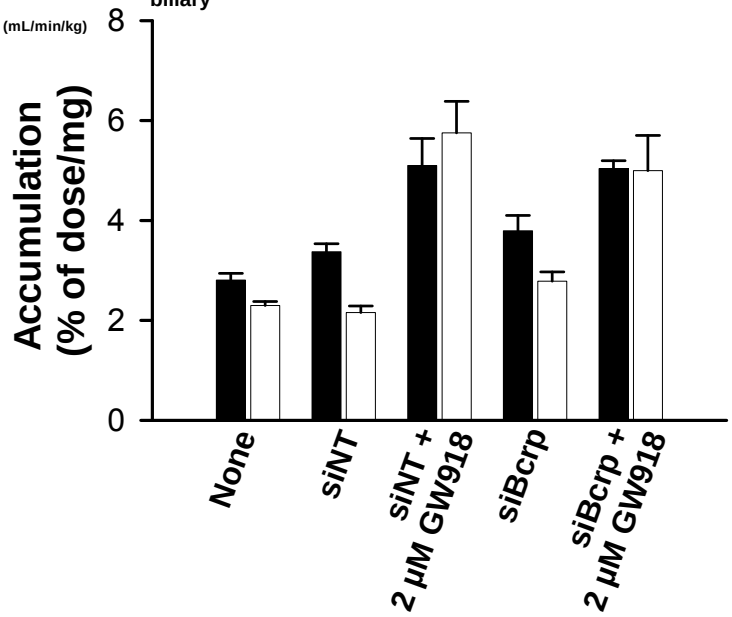

(B)

(C)

BEI (%)	**61**	**68**	**11**
***in vitro* $Cl_{biliary}$**	**3.7**	**3.4**	**0.7**

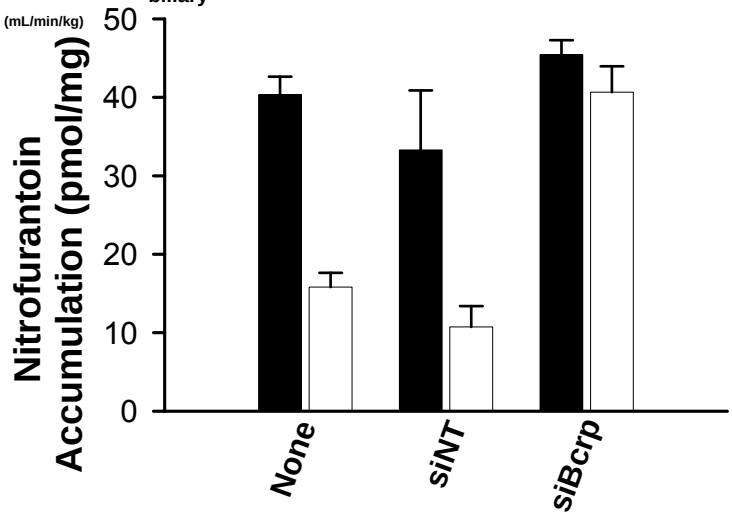

CHAPTER 5

Hepatobiliary Disposition of Sorafenib in Human Hepatocytes

This chapter will be submitted to Drug Metabolism and Disposition and is presented in the style of that journal.

Abstract

Sorafenib is an orally active tyrosine kinase inhibitor used in the treatment of renal and hepatocellular carcinoma. Emerging data suggest that transport proteins play an important role in sorafenib disposition in humans. This study was designed to identify the transport proteins responsible for the hepatic uptake of sorafenib, and to determine the extent of biliary excretion of sorafenib in human hepatocytes. Initial uptake was assessed in freshly isolated, suspended human hepatocytes in the presence of inhibitors and modulators. [^{14}C]Sorafenib (1 μM) uptake at 4°C was ~40 to 50% of the uptake at 37°C, suggesting a high degree of passive diffusion. Hepatocyte uptake of [^{14}C]sorafenib did not exhibit sodium dependence, and was not influenced by the organic anion transport (OAT) inhibitor ketoprofen. However, initial [^{14}C]sorafenib hepatocyte uptake was reduced to 54 and 70% of control values in the presence of the organic anion transporting polypeptide (OATP) inhibitor rifamycin SV, and the organic cation transporter (OCT) inhibitor decynium 22, respectively. Transport of [^{14}C]sorafenib also was studied in OCT1 stably transfected Chinese hamster ovary (CHO) cells. [^{14}C]sorafenib uptake in OCT1 transfected CHO cells was temperature dependent, similar to mock cells in the linear range up to 5 min, and increased ~2-fold compared to mock cells at $\geq$5 min. The OCT inhibitor, decynium 22, decreased [^{14}C]sorafenib uptake in OCT1 transfected CHO cells by 30% at all time points. Sandwich-cultured human hepatocytes were utilized to determine the extent of biliary excretion of sorafenib. The biliary excretion index (BEI) and the *in vitro* biliary clearance of sorafenib (1 μM) were low (1% and 1.0

ml/min/kg, respectively). These results suggest that sorafenib uptake in human hepatocytes occurs via passive diffusion and active transport mediated by OCT1 and OATPs.

Introduction

Sorafenib, an orally active multikinase inhibitor, blocks tumor cell proliferation by targeting Raf/MEK/ERK, and exerts an antiangiogenic effect by targeting vascular endothelial growth factor receptor-1/-2/-3 (VEGFR-1/-2/-3), and platelet derived growth factor receptor beta (PDGFR-β) tyrosine kinases (Wilhelm et al., 2004; Carlomagno et al., 2006). Sorafenib is approved for the treatment of renal and hepatocellular carcinomas, and has demonstrated activity toward other malignancies (Ratain et al., 2006; Llovet et al., 2008; Miller et al., 2009).

Following oral administration of [^{14}C]sorafenib to healthy volunteers, approximately 77% of a 100 mg oral dose was excreted in feces (51% as parent), and 19% of the dose was excreted in urine as glucuronidated metabolites (Lathia et al., 2006). Sorafenib is subject to two parallel pathways in man yielding the N-oxide mediated by cytochrome P450 3A4 (CYP3A4) and sorafenib glucuronide catalyzed by uridine disphosphate-glucuronsyl-transferase (UGT1A9) as primary metabolites (Lathia et al., 2006)(Radtke et al, 2005).; Approximately 17% of circulating radioactivity in plasma was in the form of sorafenib N-oxide (Lathia et al., 2006). Peak plasma concentrations of sorafenib occur within 2 to 3 hours (Strumberg et al., 2005) after a single, oral dose; secondary peaks in the plasma concentration-time profile have been attributed to enterohepatic recirculation of sorafenib following cleavage of the glucuronide conjugate or reduction of the N-oxide in the gut (Lathia et al., 2006). High interpatient variability in the C_{max} and AUC in human plasma of sorafenib and the

primary metabolite, sorafenib N-oxide, have been reported following multiple oral doses of sorafenib (Strumberg et al., 2007; Miller et al., 2009).

Sorafenib administration to patients with hepatic dysfunction who exhibited increased serum levels of total bilirubin, AST and albumin resulted in dose-limiting elevations in total bilirubin concentrations (Miller et al., 2009). Possible explanations for the sorafenib-mediated increases in serum bilirubin include UGT1A1 inhibition of bilirubin glucuronidation as has been demonstrated *in vitro* (Kalyanaraman et al., 2006), or possibly due to inhibition of the transport proteins responsible for the hepatobiliary disposition of bilirubin or its conjugates. Understanding the mechanisms of hepatic uptake and the extent of biliary excretion of sorafenib is particularly important in patients with unresectable hepatocellular carcinoma, where the target site of sorafenib is the liver.

Transport proteins play an important role in the clearance of drugs from hepatic sinusoidal blood, and the excretion of parent drug and/or metabolite(s) across the apical membrane into the bile canaliculus. The basolateral proteins that mediate uptake of endogenous and exogenous compounds into hepatocytes include members of the solute carrier (SLC) superfamily: Na^+-taurocholate co-transporting polypeptide (NTCP), organic anion transporters (OATs), organic cation transporters (OCTs), and organic anion transporting polypeptides (OATPs). NTCP is expressed exclusively in the liver, is sodium-dependent, and predominately accounts for uptake of bile acids (Ho et al., 2004). Recently, other drugs like rosuvastatin have been identified as NTCP substrates (Ho et al., 2006). The OATPs are characterized by having broad and overlapping substrate

specificity, and display an affinity for organic anions as well as some bulky cations and neutral steroids (Mikkaichi et al., 2004). In contrast to NTCP, the OATPs operate in a sodium-independent manner, and have been shown to function as bidirectional carriers (Li et al., 2000; Briz et al., 2006; Mahagita et al., 2007). There are three human isoforms, OATP1B1, 1B3 and 2B1, that play a substantial role in hepatic uptake of many endogenous and exogenous compounds including bilirubin (Konig et al., 2000; Cui et al., 2001), fexofenadine (Cvetkovic et al., 1999) and many statins (Shitara and Sugiyama, 2006). OCTs are electrogenic uniporters that primarily mediate transport of small cations, although transport of anions and uncharged compounds has been reported (Koepsell et al., 2003). The OATs constitute a family of proteins that mediate transport of negatively charged endogenous and exogenous compounds in exchange for dicarboxylate ions. OATs are predominantly expressed in the kidney, although OAT2 has higher expression on the sinusoidal membrane of hepatocytes compared to the basolateral membrane of proximal kidney tubules (Sun et al., 2001).

The objective of the present study was to identify the transport proteins responsible for the hepatic uptake of sorafenib, and to determine the extent of biliary excretion of sorafenib in human hepatocytes. Initial uptake was assessed in freshly isolated human hepatocytes and in OCT1 transfected CHO cells. Sandwich-cultured human hepatocytes were utilized to determine the extent of biliary excretion of sorafenib.

Material and Methods

Materials. Dulbecco's modified Eagle's medium (DMEM), F-12 Nutrient Mixture, MEM non-essential amino acids solution (100x), L-glutamine, penicillin G-streptomycin solution (100x), geneticin, and penicillin G-streptomycin-amphotericin B solution (100x) were purchased from Invitrogen (Carlsbad, CA). Rifamycin SV, ketoprofen, dexamethasone, tetraethylammonium (TEA), 1,1-dimethyl-biguanide hydrochloride (metformin), fetal bovine serum (FBS), Triton X-100, HEPES, D-glucose, dexamethasone, trypsin-EDTA solution (1x), and Hanks' balanced salt solution (HBSS) modified with (H-1387) or without (H-4891) calcium chloride were obtained from Sigma-Aldrich (St. Louis, MO). Sorafenib (purity 99.7%), [^{14}C]sorafenib (3.09 MBq/mg, radiochemical purity 99.2%), the internal standard [$^{2}H_3$, ^{15}N] sorafenib tosylate, and decynium 22 were provided by Bayer HealthCare AG (Wuppertal, Germany). [^{14}C]TEA (55 mCi/mmol) was purchased from American Radiolabeled Chemicals (St. Louis, MO). [^{14}C]biguanide (metformin, 110 mi/mmol) was purchased from Moraveck Biochemcials (Brea, CA). ITS+™ (insulin/transferrin/selenium) culture supplement was purchased from BD Biosciences Discovery Labware (Bedford, MA). Bicinchoninic acid (BCA) protein assay reagents and BSA for the protein assay standard were purchased from Pierce Chemical Co. (Rockford, IL). Ultima Gold™ XR scintillation cocktail, was purchased from Perkin Elmer Life Sciences (Boston, MA). All other chemicals and reagents were of analytical grade and available from commercial sources.

Suspended Hepatocyte Isolation and Uptake Studies.

CellzDirect, Life Technologies (RTP, NC) kindly provided freshly isolated human hepatocytes in suspension. Hepatocyte donors were a 60 yr old female Caucasian and a 63 yr old male Caucasian with no recent history of smoking or alcohol use. Hepatocyte viability, as determined by trypan blue exclusion, was 89 and 90%. Cells were suspended in cold modified Hank's buffer with 10 mM Tris/5 mM glucose (pH = 7.4) or Na^+-free choline buffer (10mM Tris, 5 mM glucose, 5.4 mM KCl, 1.8mM $CaCl_2$, 0.9 mM $MgSO_4$, 10 mM HEPES and 137 mM choline; pH = 7.4) and stored on ice prior to conducting uptake studies (Leslie et al., 2007). Isolated hepatocytes were suspended in the same buffer (1 x 10^6 cells/ml), placed on ice, and used immediately in experiments. Hepatocyte suspensions (1 ml; n = 2 livers, in triplicate) were preincubated in 16 x 100 mm glass test tubes at 37˚C for 3 min; 0.1% DMSO or chemical inhibitor was added 1 min before ^{14}C-sorafenib (0.09 μM; 3.86 nCi; 0.9% Methanol). The following concentrations of inhibitors were selected based upon reported affinities for the given active transport processes: 20 μM rifamycin SV (OATP1B1, 1B3 and 2B1 inhibitor), 5 μM decynium 22 (OCT inhibitor) and 10 μM ketoprofen (OAT2 inhibitor). Aliquots (100 μL) of the suspension were removed at timed intervals (up to 2.5 min), placed in 0.4-ml polyethylene tubes and centrifuged immediately through a top layer of silicone oil:mineral oil (82:18, v/v; 100 μL) into a bottom layer of 3M KOH (50 μL). ^{14}C-Sorafenib in the cell pellet and supernatant were analyzed by liquid scintillation counting. Adherent fluid volume was estimated with [^{14}C]inulin as previously described (Baur et al., 1975). Protein

concentrations for individual hepatocyte suspensions were determined with the BCA protein assay reagent kit (Pierce) as instructed by the manufacturer. BSA, as supplied by the manufacturer, was used as a standard (0.2 – 1 mg/mL).

Transport Studies in hOCT1-Expressing CHO cells.

Transfected CHO cells with empty vector (mock cells) and clone number 18 of hOCT1 were kindly provided by Dr. Dhiren Thakker (Ming et al., 2009). Transport studies were carried out five days post-seeding, as previously described (Ming et al., 2009). Briefly, stably transfected CHO cells were grown as monolayers in 24-well plates. Medium was changed every other day. Cells were preincubated for 30 min at 37°C in transport buffer (HBSS with calcium chloride, 25 mM D-glucose and 10 mM HEPES, pH 7.4). Experiments were initiated by replacement of the transport buffer with 0.4 mL of radiolabeled dose solutions in transport buffer. After incubation, dose solutions were aspirated and cells were washed four times with 4°C transport buffer. Cells were lysed with 500 μL of 0.1 N NaOH/0.1% sodium dodecyl sulfate (SDS) for 4 h on an orbital shaker, and samples were analyzed by liquid scintillation counting. Data were normalized to protein concentration in each well, determined in duplicate aliquots using BCA protein assay reagent kit (Pierce), as detailed above.

Sandwich-Cultured Human Hepatocyte Studies.

A B-CLEAR®-Human Kit was purchased from Qualyst, Inc. (RTP, NC). Human hepatocytes isolated from a 44 yr old Caucasian female were seeded ~1.75 x 10^6

cells/well on 6-well BioCoat™ plates in DMEM without phenol red supplemented with 2 mM L-glutamine, 1% (v/v) MEM non-essential amino acids, 100 units penicillin G sodium, 100 µg streptomycin sulfate, 1 µM dexamethasone, 5% (v/v) FBS, and 10 µM insulin (day 0 of culture), and allowed to attach for 2-6 h in a humidified incubator (95% O_2, 5% CO_2) at 37°C. After cell attachment, culture plates were swirled gently and the culture medium was replaced with the same medium. Cells were overlaid 16-24 h (day 1 of culture) after seeding with ice-cold Matrigel™ basement membrane matrix (0.25 mg/mL) in 2 mL/well cold serum-free DMEM containing 2 mM L-glutamine, 1% (v/v) MEM non-essential amino acids, 100 units penicillin G sodium, 100 µg streptomycin sulfate, 0.1 µM dexamethasone, and 1% (v/v) ITS+™. The culture medium was changed every 24 h until experiments were performed on day 7 of culture.

Accumulation Studies.

The method to determine substrate accumulation in sandwich-cultured hepatocytes has been described previously (Leslie et al., 2007; Wolf et al., 2008). Cells were incubated for 10 min at 37°C with 1.5 mL of sorafenib solution (1 and 10 µM). Medium samples were collected immediately, and hepatocytes were rinsed vigorously three times with 2 mL ice-cold standard buffer following the incubation. Substrate uptake was corrected for nonspecific binding by subtracting uptake on blank six-well Biocoat™ plates overlaid with Matrigel™. Data were normalized to protein concentration in each well, determined in duplicate with the BCA protein assay reagent kit (Pierce), as instructed by the

manufacturer. Due to incompatability of the protein assay with organic solvent, the average protein concentration for standard HBSS or Ca^{2+}-free HBSS incubations in the same liver preparation was used to normalize sorafenib content. Sorafenib-treated hepatocytes were stored immediately at -80ºC until analysis. The cells were lysed with 1mL of mobile phase containing internal standard, scraped off the plates and centrifuged at 10,000 g for 5 min before analysis by LC/MS/MS.

Sample Analysis.

Sorafenib and sorafenib N-oxide concentrations were determined by a LC-MS/MS assay using a LTQ Orbitrap XL(Thermo Scientific, Bremen, Germany) coupled to an Agilent 1200 system (Waldbronn, Germany). Sorafenib and its metabolites were eluted from a Synergi Hydro RP 2.5 µm (20 x 2 mm i.d., Phenomenex, Torrance, CA, USA) using a mobile phase gradient at a flow rate of 0.3 mL/min (A: 0.05% formic acid in water, B: 0.05% formic acid in acetonitrile); 0 min 30% B, 5 min 60% B, 5.3 min 30% B. The column effluent was monitored using a LTQ Orbitrap XL (Thermo Scientific, Bremen, Germany) by quantification of the exact mass of sorafenib, internal standard, sorafenib N-oxide and sorafenib glucuronide.

Data Analysis.

For accumulation studies in sandwich-cultured hepatocytes, the biliary excretion index (BEI, %) was calculated using B-CLEAR® technology [Qualyst, Inc., Raleigh, NC; (Liu et al., 1999)]:

$$BEI = \frac{Accumulation_{Cells+Bile} - Accumulation_{Cells}}{Accumulation_{Cells+Bile}} \times 100$$

where substrate accumulation in the cells+bile compartments was determined in hepatocytes preincubated in standard buffer; cellular accumulation of substrate was determined in hepatocytes preincubated with Ca^{2+}-free HBSS.

$$\textit{In Vitro}\ Cl_{biliary} = \frac{Accumulation_{Cells+Bile} - Accumulation_{Cells}}{AUC_{0-T}} \qquad (2)$$

where $AUC_{0\text{-}T}$ was calculated using the log trapezoidal method. *In vitro* $Cl_{biliary}$ values were scaled per kilogram body weight using 0.948 mg protein/1.75 x 10^6 cells (the typical value obtained in all preparations), 107 x 10^6 hepatocytes/g of human liver tissue (Wilson et al., 2003), and 25.7 g of liver tissue per kg of body weight (Davies and Morris, 1993).

Results.

Uptake of Sorafenib in Suspended Human Hepatocytes.

Initial uptake of [^{14}C]sorafenib into suspended human hepatocytes was linear up to ~ 2 min (Fig. 5.2.A). Uptake at 4°C was ~ 40 to 50% of the uptake at 37°C (Fig. 5.2.A - C). Sorafenib uptake at 1.5 min (Fig. 5.2.C) did not exhibit sodium dependence ([^{14}C]sorafenib uptake was within 4% of control values when sodium was replaced with choline in the uptake buffer), and was not influenced by ketoprofen (uptake was within 13% of control uptake). Initial [^{14}C]sorafenib uptake was reduced to 54 and 70% of control values in the presence of the OATP inhibitor rifamycin SV and the OCT inhibitor decynium 22, respectively (Fig. 5.2.C).

Transport of Sorafenib in hOCT1 Transfected CHO cells.

As expected, uptake of 10 μM [^{14}C]metformin (data not shown) and 5 μM [^{14}C]TEA in hOCT1 transfected CHO cells was increased ~7-fold compared to mock cells, confirming OCT1 function in these cells (Fig. 5.3.A). The uptake of 10 μM [^{14}C]TEA was completely abated in the presence of 10 μM decynium 22 (Fig. 5.3.A).

[^{14}C]sorafenib uptake was extensive and linear up to ~5 min in mock CHO cells incubated at 37°C. Uptake in mock CHO cells at 4°C was ~32 – 57% of the uptake at 37°C up to 30 min (data not shown). Interestingly, uptake of [^{14}C]sorafenib in hOCT1 transfected CHO cells was similar to mock cells in the

linear range, and increased ~2-fold compared to mock cells at 5 min and beyond. The OCT inhibitor, decynium 22, decreased [^{14}C]sorafenib uptake in OCT1 transfected CHO cells by 30% at all time points (Fig. 5.3.B).

Hepatobiliary Dispostion of Sorafenib in Human Sandwich-Cultured Hepatocytes.

The hepatobiliary disposition of [^{3}H]taurocholate and sorafenib was measured in human sandwich-cultured hepatocytes. Following a 10-min incubation with (1μM) ^{3}H-taurocholate, cellular accumulation of the model bile acid taurocholate (41.5 pmol/mg protein) and the BEI (64.8%) and *in vitro* biliary clearance (59.9 mL/min/kg) were consistent with previous data generated in this model system [data not shown; (Ghibellini et al., 2007; Swift et al., 2009)]. The percentage of the sorafenib dose that was recovered in day 7 sandwich-cultured human hepatocyte lysate after a 10-min incubation with either 2 or 10 μM sorafenib was greater than 94% (Table 5.1). The cellular accumulation of sorafenib and sorafenib N-oxide, the major metabolite in humans, was dose-proportionate (Table 5.1; Fig. 5.4). The cellular accumulation of sorafenib was approximately two orders of magnitude greater than the primary metabolite sorafenib N-oxide after a 10-min incubation at both the 2 and 10 μM doses (Fig. 5.4). Sorafenib BEI (6%) and *in vitro* biliary clearance (1 ml/min/kg) were relatively low compared to taurocholate (Fig. 5.4.A). Sorafenib glucuronide cellular accumulation was two-fold greater after a 10-min incubation with 2 μM sorafenib compared to the 10 μM dose (Fig. 5.4.C). Sorafenib N-oxide and

sorafenib glucuronide BEI were negligible following a 10-min incubation with 2 μM sorafenib, but increased to 22 and 20%, respectively, when sandwich-cultured human hepatocytes were incubated with 10 μM sorafenib for 10 min (Fig. 5.4.B and C). Sorafenib N-oxide concentrations were below the detection limit (<1 ng/mL) in medium following a 10-min incubation with either the 2 or 10 μM sorafenib, whereas the medium peak area ratio of sorafenib glucuronide was higher at 10-min following incubation with 10 compared to 2 μM sorafenib (Fig. 5.4.C).

Discussion.

Hepatic transport proteins are recognized increasingly as important determinants of the pharmacokinetics of many drugs, as well as key sites of drug-drug interactions (Soars et al., 2009). Genetic polymorphisms of uptake transport proteins have also been implicated in interindividual differences in the pharmacokinetics and pharmacodynamics of clinically relevant drugs such as the statins (Ieiri et al., 2009). In the present study, the transport proteins involved in the hepatic uptake of sorafenib were investigated, and the hepatobiliary disposition of sorafenib was assessed.

Sorafenib is a very lipophilic compound (log D_7 5.16; predicted properties SciFinder Scholar version 2007). The initial uptake of sorafenib in human hepatocytes was examined at 37°C vs. 4°C to assess the contribution of passive diffusion to overall uptake. Approximately 50 and 40% of [^{14}C]sorafenib initial uptake at 0.5 and 1 min, respectively, was due to passive diffusion (Fig. 5.2.A - C). There was also a high degree of passive diffusion in CHO cells (Fig. 5.3.B) that partially masked the contribution of OCT1 to the uptake of sorafenib. Furthermore, >94% of the sorafenib dose partitioned into human sandwich-cultured hepatocytes after a 10-min incubation with either 2 or 10 μM sorafenib (Table 5.1).

The active uptake of [^{14}C]sorafenib (1 μM) was investigated with transport protein modulators. Rifamycin SV (20 μM) was selected as an inhibitor of all the relevant human isoforms of OATP expressed in the liver: OATP1A2, OATP1B1,

OATP1B3 and OATP2B1 (Vavricka et al., 2002). Decynium 22 (5 μM) was used as an OCT inhibitor (Zhang et al., 1997; Hayer-Zillgen et al., 2002), and OAT2 function was inhibited with ketoprofen (10 μM) (Morita et al., 2001; Ohtsuki et al., 2002). To assess sodium-dependent transport by Ntcp, choline-based buffer was substituted for sodium-based buffer in suspended hepatocytes. The sensitivity of the transport proteins and specificity to the inhibitors rifamycin SV and decynium 22 were confirmed in the presence and absence of the model probe substrates [^{3}H]estradiol-17-β-D-glucuronide (OATP substrate) and [^{14}C]TEA (OCT substrate), as published previously (Chapter 4, Fig. 4.2). Sorafenib uptake at 1.5 min was sensitive to rifamycin SV and decynium 22, suggesting that the OATPs and OCTs are involved in the hepatic uptake of this tyrosine kinase inhbitor (Fig. 5.2.C). The involvement of OCT1 in sorafenib uptake was investigated further using a hOCT1-expressing CHO cell line. Imatinib, another tyrosine kinase inhibitor is an OCT1 substrate in the human T-lymphoblastoid cell line CCRF-CEM (Thomas et al., 2004). Some substrate overlap exists between OCTs and OATPs, which have affinity for some type II (bulky) cations such as N-methylquinine (van Montfoort et al., 1999).

Interestingly, the uptake of sorafenib over time was greater in OCT1 transfected CHO cells compared to mock transfected only after 5 min (Fig. 5.3.B). The high degree of passive diffusion masked the involvement of OCT1-mediated uptake in these CHO cells at early time points. Solubility limitations of sorafenib, coupled with high passive diffusion, make it challenging to accurately

characterize the K_m and V_{max} for sorafenib uptake in transfected CHO cells and suspended human hepatocytes. The OCT1-dependent uptake of sorafenib (determined as the difference in sorafenib uptake in OCT1-CHO cells compared to mock-CHO cells) was sensitive to 10 μM decynium 22, a potent inhibitor of organic cation transporters (Hayer-Zillgen et al., 2002), as demonstrated by complete inhibition of the positive control, TEA (Fig. 5.3.A). These data confirmed that sorafenib is an OCT1substrate.

To investigate the hepatobiliary disposition of sorafenib, studies were performed in human sandwich-cultured hepatocytes. Sorafenib exhibited a low BEI and *in vitro* $Cl_{biliary}$ which is not surprising due to the extent of CYP3A4- and UGT1A9-mediated metabolism seen *in vivo* (Lathia et al., 2006). Sorafenib plasma concentration-time profiles have been reported to increase less than proportional to increasing dose (Clark et al., 2005; Strumberg et al., 2005; Strumberg et al., 2007). The dosing solutions (2 and 10 μM) used in these studies which resulted in linear hepatocellular accumulation (Fig. 5.4) were in the range of the reported C_{max} in plasma (5 to 21 μM) after multiple oral doses of sorafenib (100 to 600 mg twice daily) (Strumberg et al., 2005). Furthermore, there was good agreement in the uptake rate in human sandwich-cultured hepatocytes (85 and 94 pmol/mg/min) compared to that in suspended hepatocytes (73 and 97 pmol/mg/min), suggesting linear pharmacokinetics in this *in vitro* system after a single dose.

Biotransformation of sorafenib to the N-oxide is mediated primarly by CYP3A4 (Lathia et al., 2006). The low formation of sorafenib N-oxide in day 7 human sandwich-cultured hepatocytes may be due to lower cytochrome P450 enzyme activity after isolation and culture (Hoen et al., 2000; Boess et al., 2003). Dexamethasone is a prototypical CYP inducer that is added to cell culture medium. In the present studies dexamethasone concentrations in the culture medium were only 0.1 μM, which is much lower than the 10 μM or higher concentrations utilized in human and rat sandwich-cultured hepatocyte studies to induce CYP3A4 and Cyp3A1/2 protein expression (Hoen et al., 2000; McCune et al., 2000; Lindley et al., 2002), and increased activity of CYP3A4 and Cyp3A1/2 as measured by testosterone 6β-hydroxylation formation (LeCluyse et al., 1996; McCune et al., 2000; Lindley et al., 2002). Sorafenib N-oxide is the primary circulating metabolite in human plasma (Lathia et al., 2006), however concentrations in medium, a surrogate for blood, were below the limit of quantitation, probably due to the short incubation time (10 min). In contrast, medium concentrations of sorafenib glucuronide were more extensive and thus basolateral efflux may represent the primary route of hepatic clearance.. Incubation with 10 μM sorafenib for 10 min resulted in 2-fold greater excretion into medium compared to the 2 μM treatment, in which cellular accumulation of sorafenib glucuronide was 2-fold greater (Fig. 5.4.C).

In conclusion sorafenib uptake in suspended human hepatocytes, CHO cells and sandwich-cultured human hepatocytes was extensive. Uptake into

human hepatocytes and CHO cells was temperature dependent and decreased only ~50% at 4°C, suggesting a high degree of passive diffusion. The active portion of hepatic uptake was sensitive to rifamycin SV and decynium 22, suggesting OATP- and OCT-mediated uptake in human hepatocytes. OCT1-mediated uptake of sorafenib was confirmed in OCT1 overexpressing CHO cells. Biliary excretion of sorafenib in human sandwich-cultured hepatocytes is low.

Acknowledgment.

This work was supported, in part, by Bayer HealthCare AG and the National Institutes of Health grant R01 GM41935. Dr. Dhiren Thakker provided the stably transfected hOCT1-expressing CHO cells. Special thanks to William R. Proctor for assistance in establishing the overexpression system and insightful comments. Drs. Mark J. Gnoth, Dieter Lang, and Martin Radtke of Bayer HealthCare AG provided labeled and unlabeled sorafenib, financial support in obtaining human hepatocytes, bioanalytical analysis and helpful suggestions in study design and data interpretation. Brandon Swift was supported by an Eli Lilly and Company predoctoral fellowship.

References

Baur H, Kasperek S and Pfaff E (1975) Criteria of viability of isolated liver cells. *Hoppe Seylers Z Physiol Chem* **356:**827-838.

Boess F, Kamber M, Romer S, Gasser R, Muller D, Albertini S and Suter L (2003) Gene expression in two hepatic cell lines, cultured primary hepatocytes, and liver slices compared to the in vivo liver gene expression in rats: possible implications for toxicogenomics use of in vitro systems. *Toxicol Sci* **73:**386-402.

Briz O, Romero MR, Martinez-Becerra P, Macias RI, Perez MJ, Jimenez F, San Martin FG and Marin JJ (2006) OATP8/1B3-mediated cotransport of bile acids and glutathione: an export pathway for organic anions from hepatocytes? *J Biol Chem* **281:**30326-30335.

Carlomagno F, Anaganti S, Guida T, Salvatore G, Troncone G, Wilhelm SM and Santoro M (2006) BAY 43-9006 inhibition of oncogenic RET mutants. *J Natl Cancer Inst* **98:**326-334.

Clark JW, Eder JP, Ryan D, Lathia C and Lenz HJ (2005) Safety and pharmacokinetics of the dual action Raf kinase and vascular endothelial growth factor receptor inhibitor, BAY 43-9006, in patients with advanced, refractory solid tumors. *Clin Cancer Res* **11:**5472-5480.

Cui Y, Konig J, Leier I, Buchholz U and Keppler D (2001) Hepatic uptake of bilirubin and its conjugates by the human organic anion transporter SLC21A6. *J Biol Chem* **276:**9626-9630.

Cvetkovic M, Leake B, Fromm MF, Wilkinson GR and Kim RB (1999) OATP and P-glycoprotein transporters mediate the cellular uptake and excretion of fexofenadine. *Drug Metab Dispos* **27:**866-871.

Davies B and Morris T (1993) Physiological parameters in laboratory animals and humans. *Pharm Res* **10:**1093-1095.

Ghibellini G, Vasist LS, Leslie EM, Heizer WD, Kowalsky RJ, Calvo BF and Brouwer KL (2007) In vitro-in vivo correlation of hepatobiliary drug clearance in humans. *Clin Pharmacol Ther* **81:**406-413.

Hayer-Zillgen M, Bruss M and Bonisch H (2002) Expression and pharmacological profile of the human organic cation transporters hOCT1, hOCT2 and hOCT3. *Br J Pharmacol* **136:**829-836.

Ho RH, Leake BF, Roberts RL, Lee W and Kim RB (2004) Ethnicity-dependent polymorphism in Na+-taurocholate cotransporting polypeptide (SLC10A1)

reveals a domain critical for bile acid substrate recognition. *J Biol Chem* **279:**7213-7222.

Ho RH, Tirona RG, Leake BF, Glaeser H, Lee W, Lemke CJ, Wang Y and Kim RB (2006) Drug and bile acid transporters in rosuvastatin hepatic uptake: function, expression, and pharmacogenetics. *Gastroenterology* **130:**1793-1806.

Hoen PA, Commandeur JN, Vermeulen NP, Van Berkel TJ and Bijsterbosch MK (2000) Selective induction of cytochrome P450 3A1 by dexamethasone in cultured rat hepatocytes: analysis with a novel reverse transcriptase-polymerase chain reaction assay section sign. *Biochem Pharmacol* **60:**1509-1518.

Ieiri I, Higuchi S and Sugiyama Y (2009) Genetic polymorphisms of uptake (OATP1B1, 1B3) and efflux (MRP2, BCRP) transporters: implications for inter-individual differences in the pharmacokinetics and pharmacodynamics of statins and other clinically relevant drugs. *Expert Opin Drug Metab Toxicol* **5:**703-729.

Ieiri I, Suzuki H, Kimura M, Takane H, Nishizato Y, Irie S, Urae A, Kawabata K, Higuchi S, Otsubo K and Sugiyama Y (2004) Influence of common variants in the pharmacokinetic genes (OATP-C, UGT1A1, and MRP2) on serum bilirubin levels in healthy subjects. *Hepatol Res* **30:**91-95.

Kalyanaraman N, Li C, Surapaneni SS and Kumar GN (2006) Tyrosine Kinase Inhibitors are Potent and Selective Inhibitors of UGT1A1: Tools for UGT Phenotyping, in: *International Society for the Study of Xenobiotics*, pp 1-258 Drug Metabolism Reviews Puerto Rico, USA.

Koepsell H, Schmitt BM and Gorboulev V (2003) Organic cation transporters. *Rev Physiol Biochem Pharmacol* **150:**36-90.

Konig J, Cui Y, Nies AT and Keppler D (2000) A novel human organic anion transporting polypeptide localized to the basolateral hepatocyte membrane. *Am J Physiol Gastrointest Liver Physiol* **278:**G156-164.

Lathia C, Lettieri J, Cihon F, Gallentine M, Radtke M and Sundaresan P (2006) Lack of effect of ketoconazole-mediated CYP3A inhibition on sorafenib clinical pharmacokinetics. *Cancer Chemother Pharmacol* **57:**685-692.

LeCluyse EL, Bullock PL, Parkinson A and Hochman JH (1996) Cultured rat hepatocytes. *Pharm Biotechnol* **8:**121-159.

Leslie EM, Watkins PB, Kim RB and Brouwer KL (2007) Differential inhibition of rat and human Na+-dependent taurocholate cotransporting polypeptide

(NTCP/SLC10A1)by bosentan: a mechanism for species differences in hepatotoxicity. *J Pharmacol Exp Ther* **321:**1170-1178.

Li L, Meier PJ and Ballatori N (2000) Oatp2 mediates bidirectional organic solute transport: a role for intracellular glutathione. *Mol Pharmacol* **58:**335-340.

Lindley C, Hamilton G, McCune JS, Faucette S, Shord SS, Hawke RL, Wang H, Gilbert D, Jolley S, Yan B and LeCluyse EL (2002) The effect of cyclophosphamide with and without dexamethasone on cytochrome P450 3A4 and 2B6 in human hepatocytes. *Drug Metab Dispos* **30:**814-822.

Liu X, LeCluyse EL, Brouwer KR, Gan LS, Lemasters JJ, Stieger B, Meier PJ and Brouwer KL (1999) Biliary excretion in primary rat hepatocytes cultured in a collagen-sandwich configuration. *Am J Physiol* **277:**G12-21.

Llovet JM, Ricci S, Mazzaferro V, Hilgard P, Gane E, Blanc JF, de Oliveira AC, Santoro A, Raoul JL, Forner A, Schwartz M, Porta C, Zeuzem S, Bolondi L, Greten TF, Galle PR, Seitz JF, Borbath I, Haussinger D, Giannaris T, Shan M, Moscovici M, Voliotis D and Bruix J (2008) Sorafenib in advanced hepatocellular carcinoma. *N Engl J Med* **359:**378-390.

Mahagita C, Grassl SM, Piyachaturawat P and Ballatori N (2007) Human organic anion transporter 1B1 and 1B3 function as bidirectional carriers and do not mediate GSH-bile acid cotransport. *Am J Physiol Gastrointest Liver Physiol* **293:**G271-278.

McCune JS, Hawke RL, LeCluyse EL, Gillenwater HH, Hamilton G, Ritchie J and Lindley C (2000) In vivo and in vitro induction of human cytochrome P4503A4 by dexamethasone. *Clin Pharmacol Ther* **68:**356-366.

Meier PJ, Eckhardt U, Schroeder A, Hagenbuch B and Stieger B (1997) Substrate specificity of sinusoidal bile acid and organic anion uptake systems in rat and human liver. *Hepatology* **26:**1667-1677.

Mikkaichi T, Suzuki T, Tanemoto M, Ito S and Abe T (2004) The organic anion transporter (OATP) family. *Drug Metab Pharmacokinet* **19:**171-179.

Miller AA, Murry DJ, Owzar K, Hollis DR, Kennedy EB, Abou-Alfa G, Desai A, Hwang J, Villalona-Calero MA, Dees EC, Lewis LD, Fakih MG, Edelman MJ, Millard F, Frank RC, Hohl RJ and Ratain MJ (2009) Phase I and pharmacokinetic study of sorafenib in patients with hepatic or renal dysfunction: CALGB 60301. *J Clin Oncol* **27:**1800-1805.

Ming X, Ju W, Wu H, Tidwell RR, Hall JE and Thakker DR (2009) Transport of dicationic drugs pentamidine and furamidine by human organic cation transporters. *Drug Metab Dispos* **37:**424-430.

Morita N, Kusuhara H, Sekine T, Endou H and Sugiyama Y (2001) Functional characterization of rat organic anion transporter 2 in LLC-PK1 cells. *J Pharmacol Exp Ther* **298:**1179-1184.

Ohtsuki S, Asaba H, Takanaga H, Deguchi T, Hosoya K, Otagiri M and Terasaki T (2002) Role of blood-brain barrier organic anion transporter 3 (OAT3) in the efflux of indoxyl sulfate, a uremic toxin: its involvement in neurotransmitter metabolite clearance from the brain. *J Neurochem* **83:**57-66.

Ratain MJ, Eisen T, Stadler WM, Flaherty KT, Kaye SB, Rosner GL, Gore M, Desai AA, Patnaik A, Xiong HQ, Rowinsky E, Abbruzzese JL, Xia C, Simantov R, Schwartz B and O'Dwyer PJ (2006) Phase II placebo-controlled randomized discontinuation trial of sorafenib in patients with metastatic renal cell carcinoma. *J Clin Oncol* **24:**2505-2512.

Shitara Y and Sugiyama Y (2006) Pharmacokinetic and pharmacodynamic alterations of 3-hydroxy-3-methylglutaryl coenzyme A (HMG-CoA) reductase inhibitors: drug-drug interactions and interindividual differences in transporter and metabolic enzyme functions. *Pharmacol Ther* **112:**71-105.

Soars MG, Webborn PJ and Riley RJ (2009) Impact of Hepatic Uptake Transporters on Pharmacokinetics and Drug-Drug Interactions: Use of Assays and Models for Decision Making in the Pharmaceutical Industry. *Mol Pharm*.

Strumberg D, Clark JW, Awada A, Moore MJ, Richly H, Hendlisz A, Hirte HW, Eder JP, Lenz HJ and Schwartz B (2007) Safety, pharmacokinetics, and preliminary antitumor activity of sorafenib: a review of four phase I trials in patients with advanced refractory solid tumors. *Oncologist* **12:**426-437.

Strumberg D, Richly H, Hilger RA, Schleucher N, Korfee S, Tewes M, Faghih M, Brendel E, Voliotis D, Haase CG, Schwartz B, Awada A, Voigtmann R, Scheulen ME and Seeber S (2005) Phase I clinical and pharmacokinetic study of the Novel Raf kinase and vascular endothelial growth factor receptor inhibitor BAY 43-9006 in patients with advanced refractory solid tumors. *J Clin Oncol* **23:**965-972.

Sun W, Wu RR, van Poelje PD and Erion MD (2001) Isolation of a family of organic anion transporters from human liver and kidney. *Biochem Biophys Res Commun* **283:**417-422.

Swift B, Tian X and Brouwer KL (2009) Integration of preclinical and clinical data with pharmacokinetic modeling and simulation to evaluate fexofenadine as a probe for hepatobiliary transport function. *Pharm Res* **26:**1942-1951.

Thomas J, Wang L, Clark RE and Pirmohamed M (2004) Active transport of imatinib into and out of cells: implications for drug resistance. *Blood* **104:**3739-3745.

van Montfoort JE, Hagenbuch B, Fattinger KE, Muller M, Groothuis GM, Meijer DK and Meier PJ (1999) Polyspecific organic anion transporting polypeptides mediate hepatic uptake of amphipathic type II organic cations. *J Pharmacol Exp Ther* **291:**147-152.

Vavricka SR, Van Montfoort J, Ha HR, Meier PJ and Fattinger K (2002) Interactions of rifamycin SV and rifampicin with organic anion uptake systems of human liver. *Hepatology* **36:**164-172.

Wilhelm SM, Carter C, Tang L, Wilkie D, McNabola A, Rong H, Chen C, Zhang X, Vincent P, McHugh M, Cao Y, Shujath J, Gawlak S, Eveleigh D, Rowley B, Liu L, Adnane L, Lynch M, Auclair D, Taylor I, Gedrich R, Voznesensky A, Riedl B, Post LE, Bollag G and Trail PA (2004) BAY 43-9006 exhibits broad spectrum oral antitumor activity and targets the RAF/MEK/ERK pathway and receptor tyrosine kinases involved in tumor progression and angiogenesis. *Cancer Res* **64:**7099-7109.

Wilson ZE, Rostami-Hodjegan A, Burn JL, Tooley A, Boyle J, Ellis SW and Tucker GT (2003) Inter-individual variability in levels of human microsomal protein and hepatocellularity per gram of liver. *Br J Clin Pharmacol* **56:**433-440.

Wolf KK, Brouwer KR, Pollack GM and Brouwer KL (2008) Effect of albumin on the biliary clearance of compounds in sandwich-cultured rat hepatocytes. *Drug Metab Dispos* **36:**2086-2092.

Zhang L, Dresser MJ, Gray AT, Yost SC, Terashita S and Giacomini KM (1997) Cloning and functional expression of a human liver organic cation transporter. *Mol Pharmacol* **51:**913-921.

Zhao M, Rudek MA, He P, Hafner FT, Radtke M, Wright JJ, Smith BD, Messersmith WA, Hidalgo M and Baker SD (2007) A rapid and sensitive method for determination of sorafenib in human plasma using a liquid chromatography/tandem mass spectrometry assay. *J Chromatogr B Analyt Technol Biomed Life Sci* **846:**1-7.

Legend to Figures

Figure 5.1 Chemical structure of sorafenib.

Figure 5.2 Uptake of (A and B) [^{14}C]sorafenib (0.9 μM) in suspended human hepatocytes over 2.5 min. Hepatocytes were incubated at 37°C (●) or 4°C (○) (mean ± SEM from a representative liver; n=2 livers in triplicate). Initial uptake of (C) [^{14}C]sorafenib (0.9 μM) at 1.5 min in suspended human hepatocytes incubated at 37°C unless otherwise specified in the absence and presence of transport protein modulators (n=2 livers; Mean Percentage ± Range).

Figure 5.3 Uptake of the positive control (A) [^{14}C]TEA (5 μM) in the absence and presence of 10 μM decynium 22 (hatched bar) was assessed in CHO-hOCT1 (white bars) and mock cells (black bars). Uptake of (B) [^{14}C]sorafenib (1 μM) in CHO-hOCT1 cells. CHO-hOCT1 cells were incubated in the absence (▲) and presence of 10 μM decynium 22 (Δ), and mock cells in the absence (●) and presence of 10 μM decynium 22 (○) for the designated times over 30 min. Data represent mean ± SD of experiments in triplicate.

Figure 5.4 Hepatobiliary disposition of (A) sorafenib, (B) sorafenib N-oxide and (C) sorafenib glucuronide in sandwich-cultured human hepatocytes. Accumulation in cells+bile (black bars) and cells (white bars) and the biliary excretion index (BEI) were determined after a 10-min incubation with 2 and 10 μM sorafenib in day 7 sandwich-cultured human hepatocytes; *in vitro* $CL_{biliary}$ also was calculated for sorafenib. Data represent mean ± SD (n=1) in triplicate.

Table 5.1 Mass balance of sorafenib in incubation medium and hepatocyte cell lysates after a 10-min incubation in day 7 sandwich-cultured human hepatocytes (Mean ± SD in triplicate).

Treatment	Medium (nM)	% of Total Dose in Medium	Cell Lysate (nM)	% of Total Dose in Cell Lysate	Total Dose (nM)
Sorafenib 2 μM	41.8 ± 3.7	1.9	2191 ± 43	98.1	2233
Sorafenib 10 μM	588 ± 143	5.6	9974 ± 690	94.4	10562

Figure 5.1

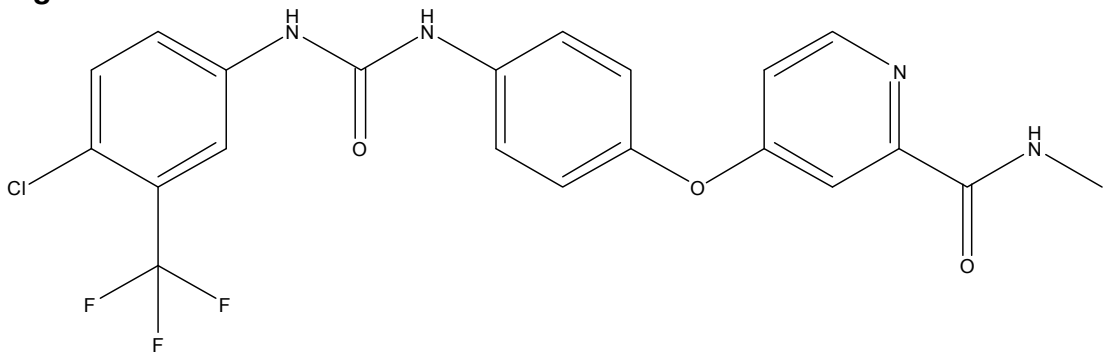

Figure 5.2
(A)

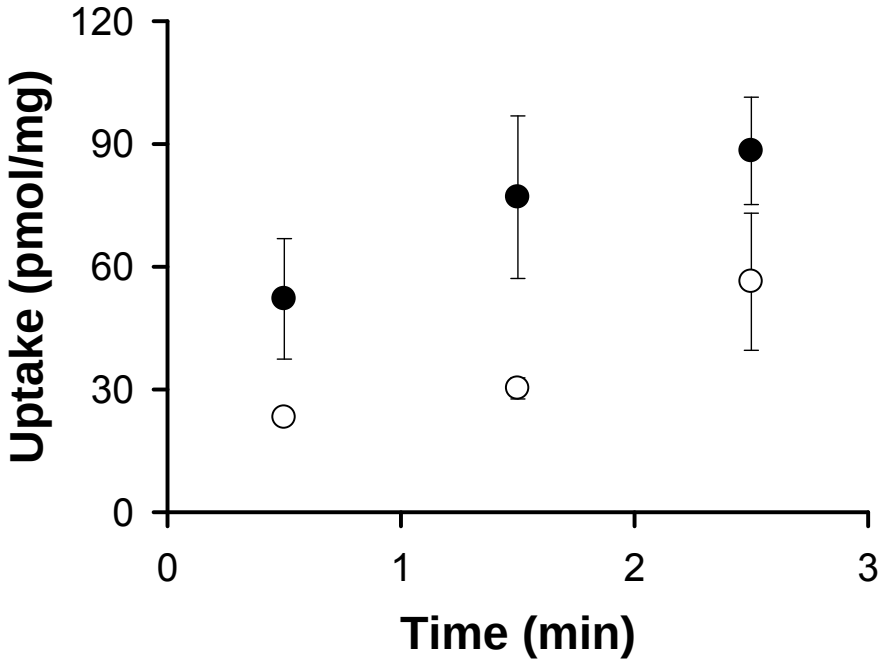
120
90
60
30
0
Uptake (pmol/mg)
0
1
2
3
Time (min)

(B)

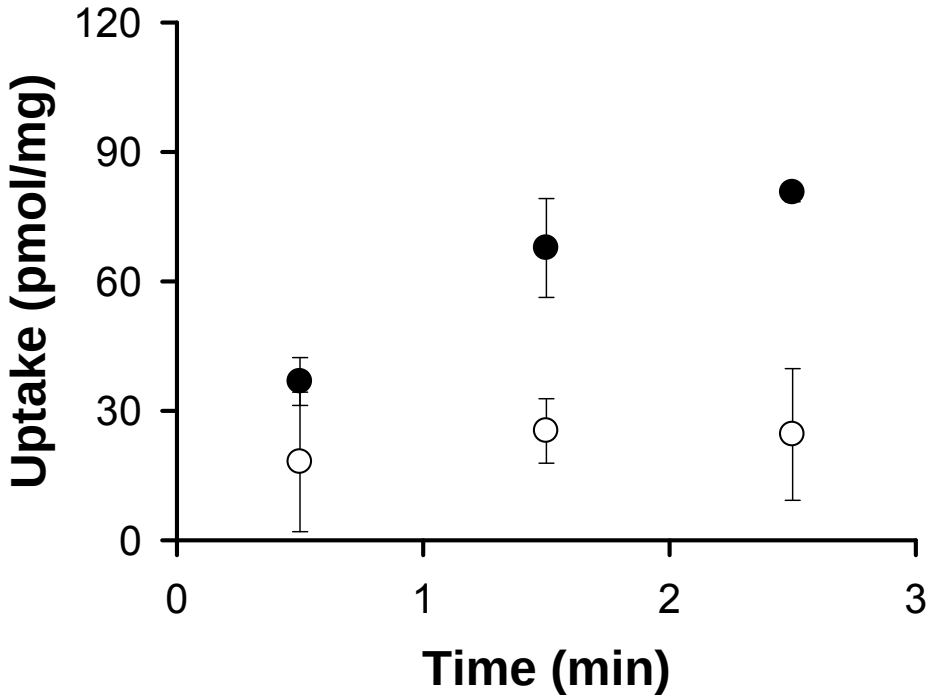
120
90
60
30
0
Uptake (pmol/mg)
0
1
2
3
Time (min)

(C)

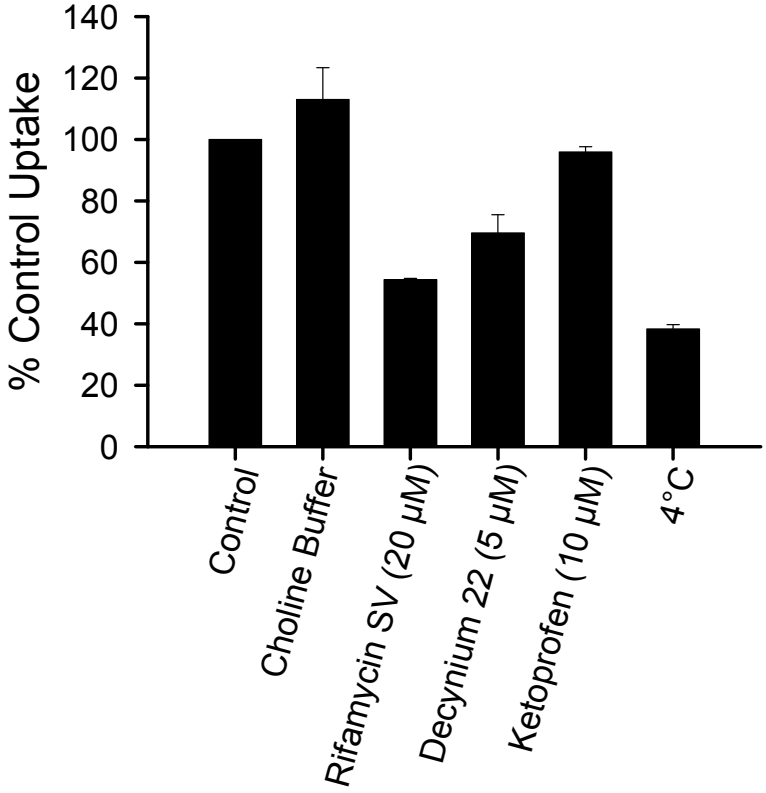
% Control Uptake
140
120
100
80
60
40
20
0
Control
Choline Buffer
Rifamycin SV (20 µM)
Decynium 22 (5 µM)
Ketoprofen (10 µM)
4°C

Figure 5.3
(A)

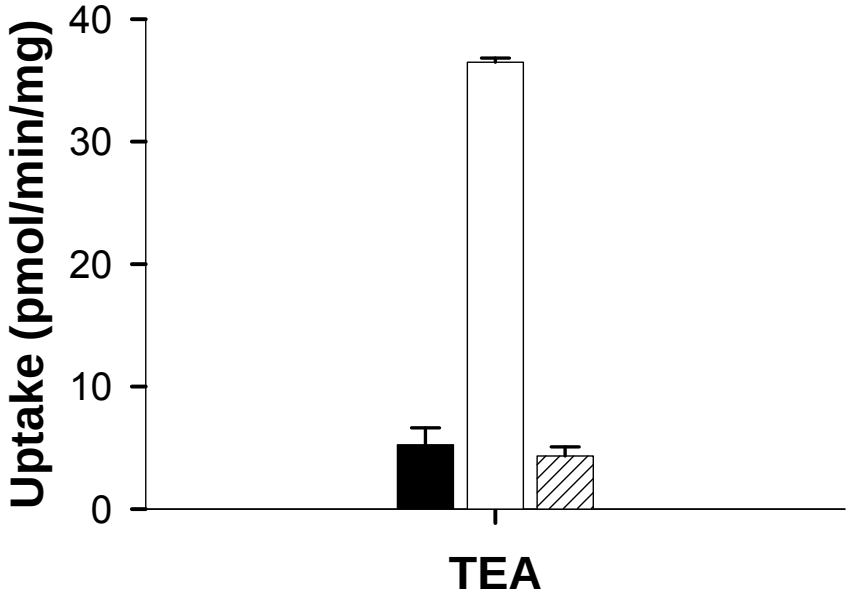
Uptake (pmol/min/mg)
40
30
20
10
0
TEA

(B)

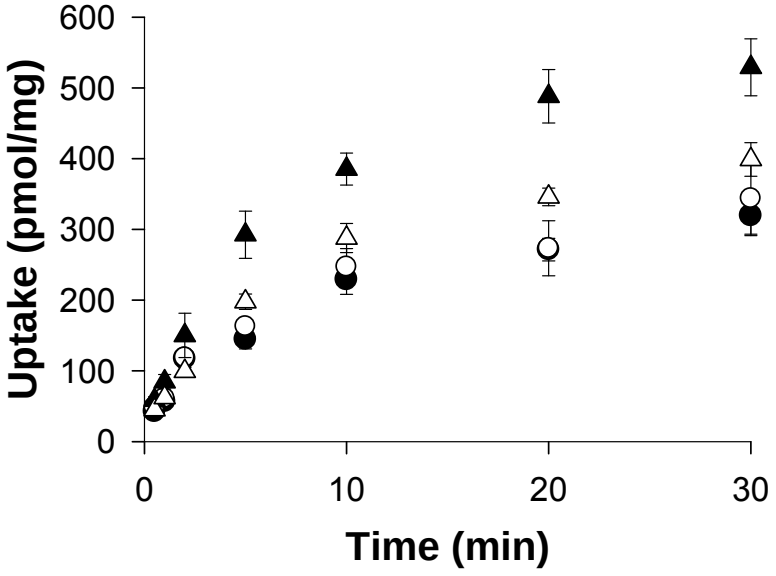
Uptake (pmol/mg)
600
500
400
300
200
100
0
0
10
20
30
Time (min)

Figure 5.4

(A)

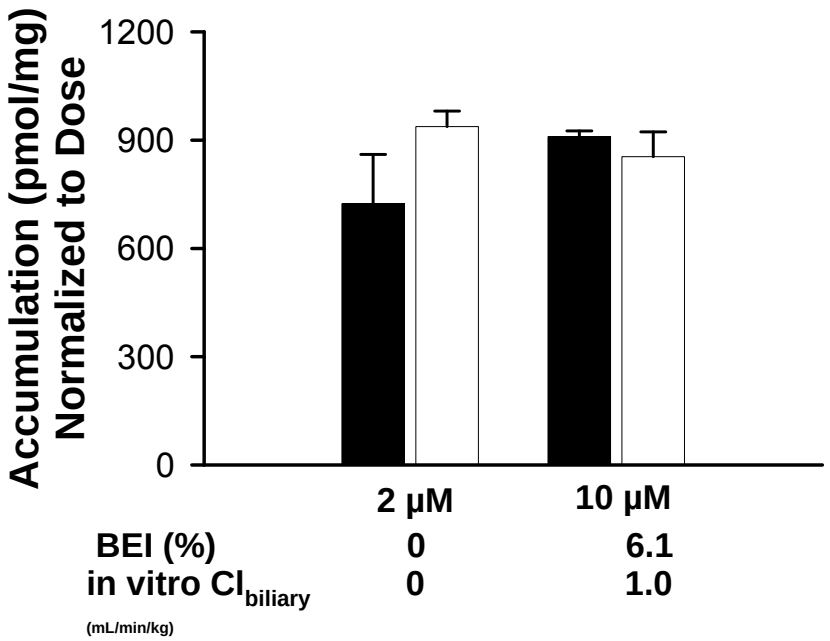
Accumulation (pmol/mg)
Normalized to Dose
1200
900
600
300
0
2 µM
10 µM
BEI (%)
0
6.1
in vitro Cl biliary
0
1.0
(mL/min/kg)

(B)

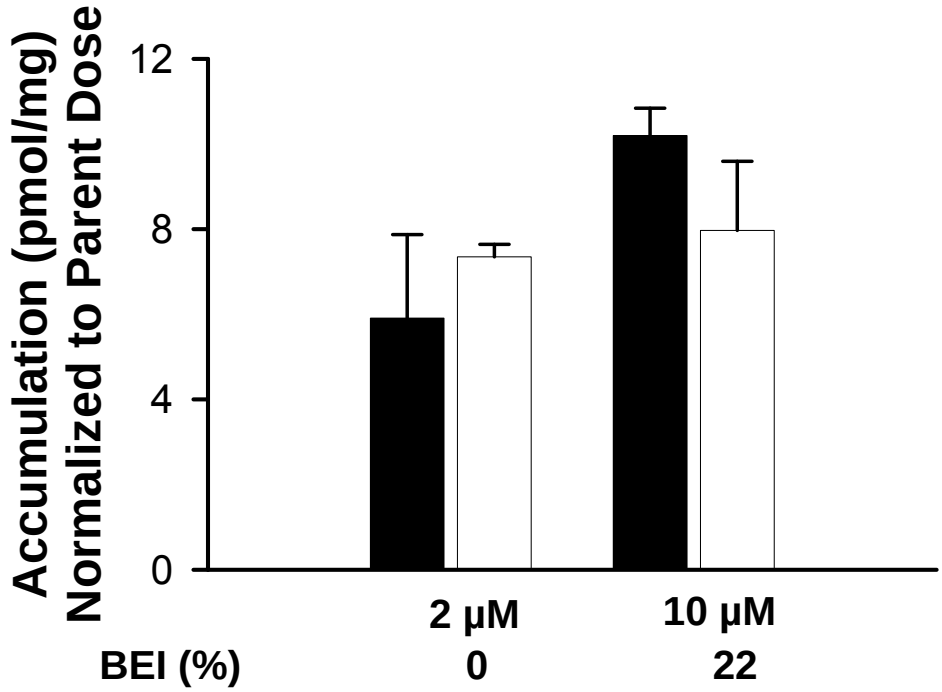
Accumulation (pmol/mg)
Normalized to Parent Dose
12
8
4
0
2 µM
10 µM
BEI (%)
0
22

(C)

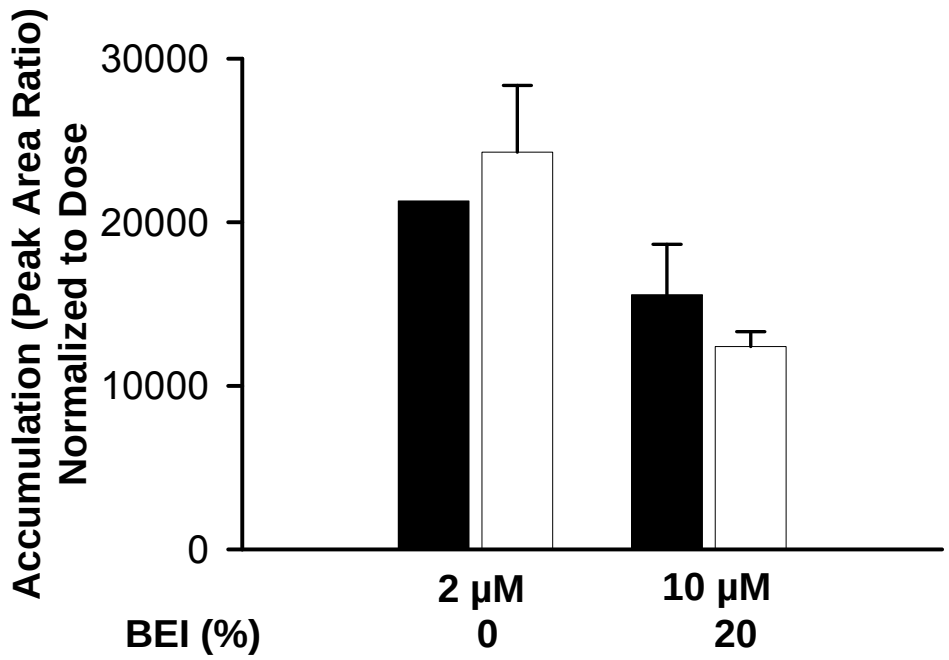
Accumulation (Peak Area Ratio)
Normalized to Dose
30000
20000
10000
0
2 µM
10 µM
BEI (%)
0
20

CHAPTER 6

Pharmacokinetics and Hepatic Exposure of ^{99m}Technetium-Sestamibi and ^{99m}Technetium-Mebrofenin In A Patient with Hepatocellular Carcinoma and Child's Pugh B Cirrhosis versus Healthy Human Volunteers: An Exploratory Analysis

Abstract

Hepatocellular carcinoma and cirrhosis of the liver result in adaptive changes in transport protein expression and function, potentially altering the disposition of many drugs. In the present study two phenotypic probes, ^{99m}Technetium-sestamibi (^{99m}Tc-MIBI) and ^{99m}Technetium-mebrofenin (^{99m}Tc-MEB), were used to predict the locus and extent of modulation in hepatic transport due to cirrhosis and hepatocellular carcinoma. Pharmacokinetic models were constructed to describe the distribution and elimination of ^{99m}Tc-MIBI and ^{99m}Tc-MEB in a patient with hepatocellular carcinoma and in healthy individuals. Rate constants representing hepatic uptake and renal excretion of ^{99m}Tc-MIBI were reduced ~58% and ~80%, respectively, while rate constants representing basolateral and biliary efflux were increased 5.4 and 4.0-fold, respectively, in a patient with hepatocellular carcinoma and Child's Pugh B cirrhosis compared to healthy subjects. The area under the hepatic mass-time profile was decreased 76% in the patient. The parameter for ^{99m}Tc-MEB intrinsic hepatic uptake clearance exceeded liver blood flow by 2.6-fold and at least ~4-fold in the patient and in healthy subjects,, respectively, suggesting hepatic blood flow is the rate-limiting step in ^{99m}Tc-MEB disposition. Intrinsic biliary clearance was reduced 3.6-fold in the patient compared to healthy volunteers, while the area under the hepatic mass-time profile was similar. Alterations in key rate constants representing hepatic uptake and efflux mechanisms secondary to disease may prove useful in predicting changes in drug disposition, and potentially drug action, for therapeutic

compounds that are handled by mechanisms similar to those governing hepatic exposure of ^{99m}Tc-MEB and ^{99m}Tc-MIBI.

Introduction

Cirrhosis is an advanced stage of liver fibrosis that is accompanied by distortion of the hepatic vasculature (1), which leads to shunting of the arterial and portal blood supply, and compromised sinusoidal blood flow. Ultimately, the perfusion changes that occur secondary to cirrhosis impair the access of blood-borne solutes to hepatocytes, the cells responsible for most liver functions (1). Cirrhosis, therefore, leads to impaired liver function and increased intrahepatic resistance (portal hypertension), potentially progressing to the development of hepatocellular carcinoma.

Hepatic uptake and biliary excretion of many drugs are mediated by transport proteins localized on the basolateral and apical membranes of hepatocytes (2-4). It is well recognized that adaptive changes in transport protein expression, aimed at protecting the hepatocyte from the intracellular accumulation of toxic compounds such as bile acids, are induced in patients with liver disease (5-7). For example, patients with primary biliary cirrhosis evidenced down-regulation of basolateral uptake proteins, while expression of canalicular and basolateral efflux proteins was maintained or even up-regulated (8-10). These modifications in clearance mechanisms (uptake from blood into liver, representing a form of systemic clearance; removal from the liver across either the basolateral or canalicular membrane, representing two routes of organ clearance) contribute to altered drug disposition, and ultimately drug action, in subjects with cirrhosis and hepatocellular carcinoma. Therefore, the ability to assess the functional consequences of disease-related modulation of hepatic

uptake or biliary excretion may facilitate the optimization of administration regimens for drugs with a narrow therapeutic window.

In vivo probes have been used to assess the function of drug-metabolizing enzymes and transport proteins in human subjects (11-14). Furthermore, the use of radiolabeled probes such as analogs of ^{99m}Technetium-sestamibi (^{99m}Tc-MIBI) and ^{99m}Technetium-mebrofenin [^{99m}Tc-MEB, (12, 14, 15)] coupled with imaging technology provides a noninvasive method to quantify tissue exposure *in vivo.* The concentration-time profile of the substrate in a relevant target tissue allows a more sophisticated elucidation of the functional consequences of changes in vectorial transport than is possible through examination of the systemic concentration-time profile alone (15-18).

^{99m}Tc-MIBI, a monovalent cation complex, is taken up into liver by passive diffusion [(19); Chapter 4]. The primary pathway for ^{99m}Tc-MIBI clearance in humans is into bile; 33% of an intravenously-injected dose appears in the feces, with 27% in urine, by 48 hr post-dose (Cardiolite® package insert). Biliary excretion of ^{99m}Tc-MIBI is mediated by multidrug resistance protein 1 [MDR1, P-glycoprotein, P-gp; (15-17, 20); Chapter 4]. ^{99m}Tc-MEB, an iminodiacetic acid derivative, is taken up extensively (98% of the dose) by the liver; the hepatic excretion half-life is short (16 min) and ~1.5% of the dose is recovered in urine after 24 hr in humans (21). The high hepatic extraction of ^{99m}Tc-MEB is governed by organic anion-transporting polypeptides 1B1- and 1B3- (OATP1B1,

OATP1B3) that mediate hepatic uptake, followed by rapid canalicular excretion into bile by multidrug resistance protein 2 [MRP2; (22); Chapter 4].

The present study was conducted to test the hypothesis that adaptive changes in transport protein expression secondary to hepatic disease result in functional changes and altered disposition of ^{99m}Tc-MIBI and ^{99m}Tc-MEB. Therefore, these probes can serve as tools to predict the locus and extent of modulation in hepatic transport due to cirrhosis and hepatocellular carcinoma. To address this hypothesis, pharmacokinetic models were constructed to describe the distribution and elimination of ^{99m}Tc-MIBI and ^{99m}Tc-MEB. These models in a patient with Child's Pugh B cirrhosis and hepatocellular carcinoma were supported by quantitative hepatic scintigraphy, blood concentrations, and cumulative mass excreted in urine for both probes. In healthy subjects, analogous models were supported by hepatic scintigraphy (^{99m}Tc-MEB only), blood concentrations, and cumulative mass excreted in bile and urine. Parameter values, especially those associated with the processes of hepatic uptake and efflux, were generated by fitting each pharmacokinetic model to the relevant data, and were compared between the patient and the healthy subjects. Hepatic exposure generated from quantitative hepatic scintigraphy of ^{99m}Tc-MIBI and ^{99m}Tc-MEB also was compared to assess the potential influence of the disease state on this important metric.

Materials and Methods

Clinical Protocol, Subject History and Demographics

Patient demographics and history are noted for three separate clinical studies. All procedures were approved by the Committee on the Protection of the Rights of Human Subjects (institutional review board), Clinical Research Advisory Committee, and Oncology Protocol Review Committee (where applicable) at the University of North Carolina.

Patient with hepatocellular carcinoma and Child's Pugh B cirrhosis

A 71 year-old female with end-stage liver disease of unknown etiology, multifocal (2 masses found by MRI), inoperable hepatocellular carcinoma confirmed after biopsy and Child's Pugh B cirrhosis participated in this study. This patient's history of present disease was positive for encephalopathy, portal hypertension, ascites, grade IV esophageal varices and type I gastric varices (over 1 yr ago), anemia, and osteomyelitis. Concomitant medications included lactulose, lisinopril, propranolol, spironolactone, furosemide, prilosec, calcium, fosamax, iron, vitamin K 5, and actigall. This patient's basic metabolic panel, liver function tests and CBC were all within normal limits except: urea nitrogen 34 mg/dL, creatinine 1.03 mg/dL, phosphorus 4.6, mg/dL, albumin 3.1 g/dL, AST 45 U/L, ALT 60 U/L, alkaline phosphatase 132 U/L, RBC 3.66 $x10^{12}$/L, platelets 92 x 10^9/L, and absolute lymphocytes 1.0 x 10^9/L. The patient was positive for hepatitis A total antibody and B surface antibody, and negative for hepatitis B surface antigen, hepatitis B core total and hepatitis C antibody.

Healthy Volunteers

^{99m}Tc-MIBI

The study design and disposition of ^{99m}Tc-MIBI in seven nonsmoking male volunteers (21-41 years of age) within 20% of their ideal body weight who received a 2.5 mCi dose of ^{99m}Tc-MIBI has been reported in detail previously (23). Unfortunately, quantitative hepatic scintigraphy data were not obtained in this patient population. However, bile samples were collected through the use of a custom-made oroenteric tube positioned in the duodenum for determination of the hepatic clearance of ^{99m}Tc-MIBI. This protocol was not feasible in the patient with hepatocellular carcinoma and cirrhosis.

^{99m}Tc-MEB

A study of ^{99m}Tc-MEB disposition in healthy volunteers (21 and 29 year old Caucasian male and a 21 year old Caucasian female) was conducted, as described previously (24), with modifications to the hepatic nuclear imaging as detailed below. All subjects were in good health as documented by medical history, physical examination, electrocardiogram, and routine laboratory tests. All subjects were asked to abstain from any medication for 2 weeks before the study, and to abstain from caffeine and alcohol during the study. A custom-made oroenteric catheter passed through the mouth and positioned in the duodenum was utilized to collect bile samples from the healthy volunteers, but was too invasive for the elderly patient with hepatocellular carcinoma.

Hepatic Nuclear Imaging

The patient fasted overnight and received a 5-mCi IV bolus dose of ^{99m}Tc-MEB (Choletec® Bracco Diagnostics, Princeton, NJ) followed 48 hr later by a 5-mCi IV bolus dose of ^{99m}Tc-MIBI (Cardiolite® Bristol-Myers Squibb, New York, NY). Both probe compounds were purchased from Cardinal Health (Research Triangle Park, NC).

Before injection of labeled compound, a transmission acquisition was performed using a ^{57}Cobalt-flood source (Isotope Products Laboratories, Burbank, CA) positioned posterior, and gamma rays were detected in the cobalt window (122 KeV ± 20%) for 10 min on the anterior detector in the absence and presence of the subject to correct for attenuation of the photons in the subject. The patient was positioned under a scintillation camera (E.Cam Dual Head 180º fixed angle SPECT and whole body system, Siemens) in the supine position and received an IV bolus of ^{99m}Tc-MEB or ^{99m}Tc-MIBI via an indwelling catheter placed in a forearm vein. The patient remained still while ^{99m}Tc was monitored (140 KeV ± 20%) for 180 min, as established in previous studies (23, 24). Continuous scan acquisition of the anterior and posterior abdomen on a dual-headed gamma camera occurred every minute for 3 hr for a total of 180 data points. Blood samples (~2 mL) were collected at 2.5, 5, 7.5, 10, 20, 40, 60, 80, 100, 120, 140, 165 and 180 min post-dose from the contralateral arm through an indwelling catheter. Urine was collected *in toto* at ~180 min. Blood and urine

samples were analyzed with a sodium iodide well counter, and corrected for decay (^{99m}Tc $t_{1/2}$=6.01 hr).

The geometric mean of the anterior and posterior gamma images was multiplied by a patient-specific attenuation correction factor. This correction factor was obtained by dividing the transmission acquisition of the ^{57}Cobalt-flood source without the patient (I_o) by the transmission acquisition of the ^{57}Cobalt-flood source with the patient (I), as described previously (25, 26). Time-activity curves were generated for each organ or tissue of interest, which included the heart, liver (excluding gall bladder), spleen, and kidney using Syngo MI applications version 6.5.9.19 (Siemens, New York, NY). The generated time-activity curves were converted to ^{99m}Tc concentrations based on standards and pilot experiments with an anthropomorphic torso phantom™ (Data Spectrum Corporation, Hillsborough, NC). Deconvolution analysis was performed as described previously (12, 27-29) with Matlab version 7.6.0.324 (R2008a; The MathWorks Inc., Natick, MA) to subtract the vascular component from the hepatic time-activity curve. This enabled separation of the "true" ^{99m}Tc concentration-time profile in liver tissue from the sum of the activity in tissue and blood resident in the organ.

Three healthy human volunteers fasted overnight and received a 2.5-mCi IV bolus dose of ^{99m}Tc-MEB. In these subjects, biliary secretions were collected utilizing a novel oroenteric catheter positioned in the duodenum, as described previously (24). Imaging and data analysis were performed as

described above. The study with ^{99m}Tc-MIBI in healthy human volunteers did not include quantitative hepatic scintigraphy, and therefore substrate mass in the liver was not available for modeling (23).

Determination of Protein Binding

Human liver tissue was obtained from the University of North Carolina Hospital by qualified medical personnel from surgical resection. Written informed consent was obtained from the subject prior to surgery. The tissue was flash frozen and stored at -80°C. To determine protein binding in liver, thawed tissue was homogenenized in two volumes (v/w) of 0.1 M phosphate buffer (pH 7.4). The liver homogenate was incubated with three concentrations of ^{99m}Tc-MEB (2, 20, and 225 μCi/mL which is 155 pM, 15.5 nM, and 1.55 nM, respectively) in triplicate for 30 min in a shaking 37°C water bath. Liver homogenate samples (1 mL) were placed in Centrifree® micropartition devices and centrifuged at 1380 x g at room temperature for 5 min to pass < 10% of the original volume through the filter. Preliminary experiments were conducted in the absence of protein to assess non-specific binding to the device. Samples of liver homogenate (total concentration in the presence of protein) and ultrafiltrate (unbound concentration) were collected post-centrifugation, analyzed with a sodium iodide well counter, and corrected for decay. The unbound fraction determined from the diluted liver tissue homogenate (fu_2) was calculated as the ratio of unbound concentration to total concentration, and was corrected to yield an estimate of the true unbound

fraction in undiluted tissue (fu) acccording to a previously published approach (30):

$$fu = \frac{1/D}{((1/fu_2) - 1) + 1/D}$$

where D represents the dilution factor (tissue-to-buffer ratio; w/v) .

Pharmacokinetic Modeling

During the first few minutes post-dose, concentrations obtained from the arm contralateral to the injection site increased with time. These data points, obtained prior to substrate equilibration throughout the venous blood pool, were not used to support development of compartmental models. Such models are based on an assumption of well-stirred distributional units, which clearly was not the case at early time points in this study (31). Differential equations describing the disposition of ^{99m}Tc-MIBI and ^{99m}TC-MEB in each of the compartments, as well as excretory sites (urine, bile) were fit simultaneously to blood, hepatic, urine and bile profiles using nonlinear least-squares regression (WinNonlin v. 5.2.1 Pharsight Corporation, Mountain View, CA). All processes were assumed to be approximately linear under the present experimental conditions [only trace amounts (2.5 mCi = ~194 nmol of ^{99m}TC-MEB and ^{99m}Tc-MIBI) were administered] and therefore, were modeled with first-order rate constants. Goodness of fit assessment was based on Akaike's Information Criterion, the residual sum of squares, coefficients of variation on the parameter estimates, the condition number, and visual inspection of the residual plots. Due to differences

in the number of data points supporting each pharmacokinetic function, each data point was assigned a weight of $\frac{1}{y} \times (1-n)$, where n is the fraction of the total number of data points that support a particular sample matrix. The final parameter estimates were selected after fitting the model to the data using different sets of initial values combined with a broad range of lower and upper bounds to avoid convergence at a local minimum.

^{99m}Tc-MIBI Pharmacokinetic Modeling

Six different compartmental models were developed (including multiple peripheral compartments in addition to the liver compartment, with elimination from the peripheral, central, and/or liver compartments) to describe the concentration- and mass-time profiles. The optimal model that best described the data is shown schematically in Figure 6.1. In the patient, the blood concentration at 80 min resulted in a second peak during the elimination phase and was given a weight of zero to aid the model fit to the entire profile. This model included a compartment depicting the systemic circulation described by the blood concentration-time profile after an intravenous bolus dose (X_{iv}). A first-order rate constant, K_{uptake}, governed MIBI uptake from the central compartment into a peripheral compartment, representing the liver. $K_{basolateral}$ represented a first-order rate constant for hepatic basolateral efflux; K_{bile} and K_{urine} represented biliary and urinary excretion rate constants, respectively. A second peripheral compartment with a first-order distributional rate constant (K_{13}) governing MIBI

uptake from the central compartment into a peripheral compartment represented MIBI distribution into the heart and spleen, which is extensive based on the distributional properties reported previously (32); K_{31} governs efflux back into the central compartment. The following differential equations described MIBI disposition in healthy human and diseased subjects (initial conditions were denoted with a superscript zero):

$$\frac{dC_C}{dt} = -K_{uptake} \times C_c + K_{basolateral} \times X_{liver} \times \frac{1}{V_c} - K_{13} \times C_c + K_{31} \times X_{peripheral} \times \frac{1}{V_c} - K_{urine} \times C_c$$

$$C_C^0 = \frac{X_{iv}}{V_c}$$

$$\frac{dX_{liver}}{dt} = K_{uptake} \times C_c \times V_c - K_{basolateral} \times X_{liver} - K_{bile} \times X_{liver} \qquad X_{liver}^0 = 0$$

$$\frac{dX_{peripheral}}{dt} = K_{13} \times C_c \times V_c - K_{31} \times X_{peripheral}$$

$$X_{peripheral}^0 = 0$$

$$\frac{dX_{bile}}{dt} = K_{bile} \times X_{liver} \qquad X_{bile}^0 = 0$$

$$\frac{dX_{urine}}{dt} = K_{urine} \times C_c \times V_c \qquad X_{urine}^0 = 0$$

^{99m}Tc-MEB Pharmacokinetic Modeling

A semi-physiologic pharmacokinetic model was developed to describe the distribution and elimination of ^{99m}Tc-MEB. The trans-hepatic extraction of this

drug is high; consequently, the hepatic clearance of ^{99m}Tc-MEB is expected to be dependent on hepatic blood flow, which is altered in patients with Child's Pugh B cirrhosis. Three different models were developed using the concentration- and mass-time profiles in healthy and diseased subjects. Four physiologic parameters were fixed based on literature values and scaled to body weight for each subject. Liver volume was fixed at 24.1 mL/kg for all subjects; liver blood flow was fixed at 20.7 mL/min/kg (33) for healthy subjects, and at 9.86 mL/min/kg for the patient with Child's Pugh B cirrhosis, as previously reported based on magnetic resonance imaging (34). The unbound fraction of ^{99m}Tc-MEB in plasma ($f_{u,p}$) was determined by ultrafiltration as described below. The 40- and 60-min blood samples were chosen so that the ultrafiltrate would exceed the minimum sensitivity of the detector and to allow for protein binding equilibration. The blood samples were centrifuged at 600 x g for 10 min at room temperature. The plasma was placed in Centrifree® micropartition devices and centrifuged in a fixed angle rotor at 1380 x g at room temperature for 5 min to pass < 10% of the original volume through the filter. Samples of plasma (total concentration in the presence of protein) and ultrafiltrate (unbound concentration) were collected post-centrifugation and analyzed with a sodium iodide well counter. The unbound concentration in blood ($f_{u,B}$) was determined by the product of $f_{u,p}$ and total concentration in the plasma divided by the total concentration in the blood. The unbound fraction of ^{99m}Tc-MEB in liver ($f_{u,H}$) was determined as detailed above and fixed at 0.078 (see Results section).

A stepwise modeling approach was used to analyze the disposition of ^{99m}Tc-MEB. In the first step of the analysis, the blood concentration-time profile for each subject was fit individually with an integrated biexponential function. The final estimates for the macro-rate constants (alpha and beta) and the concentration intercepts (A and B) were fixed, and the resulting subject-specific biexponential equation was used to represent ^{99m}Tc-MEB concentrations in blood. In the second modeling step, differential equations describing the disposition of ^{99m}Tc-MEB in each of the distributional and excretory compartments were fit simultaneously to urine, liver, and bile (healthy volunteers only) concentration or mass versus time data with nonlinear least-squares regression.

The optimal model that best described the disposition of ^{99m}Tc-MEB is shown schematically in Figure 6.2. This model consisted of a central compartment describing the blood concentration-time profile after an intravenous bolus dose (X_{iv}), where V_c represents the apparent volume of distribution; a hepatic sinusoidal compartment where Q_H represents hepatic blood flow, with $Cl'_{i,uptake}$ and $Cl'_{i,basolateral}$ representing uptake into and basolateral efflux from the liver compartment; and V_H represents the liver volume. Urinary (Cl_{renal}) and biliary ($Cl'_{i,biliary}$) elimination were described as unidirectional flux from the central compartment and liver compartment, respectively. The amount of ^{99m} Tc-MEB in the liver, bile, and urine compartments was expressed as X_{liver}, X_{bile}, and X_{urine}, respectively. In the three healthy volunteers, no mass in urine was detected, the elimination of ^{99m}Tc-MEB was more rapid, and the error associated with Cl_{renal}

and $Cl'_{i,basolateral}$ estimates was very high. Therefore, Cl_{renal} and $Cl'_{i,basolateral}$ were not required to describe the disposition of ^{99m} Tc-MEB in healthy volunteers only. The following differential equations described ^{99m} Tc-MEB disposition in healthy and diseased subjects (initial conditions were denoted with a superscript zero):

$$\frac{dC_C}{dt} = Q_H \times C_{sinusoid} - Q_H \times C_C - Cl_{renal} \times C_c$$

$$C_C^0 = \frac{X_{iv}}{V_c}$$

$$\frac{dX_{sinusoid}}{dt} = Q_H \times C_C - Q_H \times C_{sinsusoid} - Cl'_{i,uptake} \times f_{u,B} \times C_{sinsusoid} + Cl'_{i,basolateral} \times f_{u,H} \times \frac{X_{liver}}{V_H}$$

$$X_{sinusoid}^0 = 0$$

$$\frac{dX_{liver}}{dt} = Cl'_{i,uptake} \times f_{u,B} \times C_{sinsusoid} - Cl'_{i,basolateral} \times f_{u,H} \times \frac{X_{liver}}{V_H} - Cl'_{i,biliary} \times f_{u,H} \times \frac{X_{liver}}{V_H}$$

$$X_{liver}^0 = 0$$

$$\frac{dX_{bile}}{dt} = Cl'_{i,biliary} \times f_{u,H} \times \frac{X_{liver}}{V_H}$$

$$X_{bile}^0 = 0$$

$$\frac{dX_{urine}}{dt} = Cl_{renal} \times C_c$$

$$X_{urine}^0 = 0$$

Where $f_{u,B}$ and $f_{u,H}$ equal the unbound fraction of ^{99m}Tc-MEB in blood and the liver, respectively.

In addition, the AUC of the hepatic mass-time profile was calculated by standard noncompartmental analysis using the trapezoidal rule for the time imaged ($AUC_{0\rightarrow 180}$) and extrapolation to infinity for $AUC_{0\rightarrow\infty}$.

Results

^{99m}Tc-MIBI Disposition

The model depicted in Figure 6.1 was suitable for describing ^{99m} Tc-MIBI disposition in all subjects. The fit of this model to the data obtained from the patient, together with that for a representative healthy subject, is shown in Figure 6.3. The estimates and associated coefficients of variation for relevant pharmacokinetic parameters derived from the patient data are compared to those for healthy subjects, utilizing data obtained from a previously-published study (23), in Table 6.1. The apparent volume of the central compartment (V_c) was 4.52 L in the patient and a mean of 8.10 L in healthy subjects, respectively, suggesting that distribution within this compartment was restricted primarily to the blood pool [~5.2 L of blood for a 70 kg person; (33)].

The rate constants representing hepatic uptake (K_{uptake}) and renal excretion (K_{renal}) of ^{99m}Tc-MIBI were reduced ~58% and ~80%, respectively, in the patient compared to healthy subjects. Basolateral ($K_{basolateral}$) and biliary ($K_{biliary}$) efflux rate constants were increased 5.4 and 4.0-fold, respectively, in the patient as compared to healthy subjects; ^{99m}Tc-MIBI partitioning into the non-liver peripheral compartment also was increased in the patient.

The hepatic mass-time profiles in healthy individuals were simulated using the final parameter estimates listed in Table 6.1. $AUC_{0\rightarrow180}$ of the hepatic mass-time profile was decreased 76% in the patient (26.3 normalized μCi*min) compared to the average $AUC_{0\rightarrow180}$ of the simulated hepatic exposure in healthy individuals (110 ± 13 normalized μCi*min; Figure 6.4).

^{99m}Tc-MEB Disposition

The model scheme depicted in Figure 6.2 best described the ^{99m}Tc-MEB blood concentration-time profile, hepatic mass-time profile and the cumulative mass in urine and bile. Information regarding biliary excretion, obtained with a novel oroenteric tube protocol in healthy volunteers, was not available in the patient. The estimates and associated coefficients of variation for the relevant pharmacokinetic parameters are reported in Table 6.2.

In healthy subjects the predominant process that determined ^{99m}Tc-MEB fate was excretion into bile; the data from healthy subjects indicated that $Cl'_{i,basolateral}$ and Cl_{renal} did not have an impact on the disposition of ^{99m}Tc-MEB. In the patient, the modeling suggested that ^{99m}Tc-MEB was excreted from the liver back into sinusoidal blood for eventual reuptake by the liver or excretion into urine. ^{99m}Tc-MEB intrinsic hepatic uptake clearance ($Cl_{i,uptake}$) exceeded liver blood flow by ~2.6-fold and at least ~4-fold in diseased and healthy subjects, respectively (Table 6.2) suggesting that hepatic blood flow is the rate-limiting step in ^{99m}Tc-MEB hepatic clearance. There was a marginal difference in the volume of distribution (V_c) between the patient and healthy subjects. The shape of the hepatic mass-time profile obtained via scintigraphy was notably different between the patient and the healthy subjects (Figure 6.6). However, the $AUC_{0\rightarrow180}$ and $AUC_{0\rightarrow\infty}$ were comparable between healthy volunteers (28.1 ± 10.2 and 29.2 ± 9.9 normalized μCi*min, respectively) and the patient (28.1 and 29.4 normalized μCi*min, respectively). Intrinsic biliary clearance ($Cl'_{i,biliary}$) was

reduced 3.6-fold in the patient compared to the average $Cl'_{i,biliary}$ in healthy volunteers despite the similar hepatic exposure.

Discussion.

The purpose of the present study was to evaluate the utility of ^{99m}Tc-MIBI and ^{99m}Tc-MEB as phenotypic probes, and in particular to assess their sensitivity to changes in hepatic function due to hepatocellular carcinoma and cirrhosis. The potential use of quantitative hepatic scintigraphy, coupled with blood concentration monitoring, to support a robust pharmacokinetic model describing the disposition of the two probes was of particular interest. Perturbations in discrete mechanisms of hepatobiliary drug disposition, secondary to disease, drug interactions, or other reasons, logically would be easiest to evaluate with liver tissue concentration-time data of the compound of interest. Of course, this is not achievable with standard approaches. The technique evaluated in this study represents an attractive option, assuming that relevant labeled probe compounds are available.

Due to the fact that only one patient was available for this study, the present results are intended only to represent “proof-of-concept” of the principle (i.e., that scintigraphy coupled with comprehensive sampling and sophisticated mathematical modeling has the potential to provide insight into subtle changes in drug disposition in the liver secondary to disease). The underlying concept is that hepatic scintigraphy provides a more accurate indication of hepatic handling of these two probes than blood sampling alone. The blood concentration-time

profile, while an important indicator of the time course and extent of systemic exposure, is not always predictive, or even necessarily reflective, of substrate exposure in relevant organs or tissue spaces (18, 35, 36). The present data demonstrate that scintigraphy has the potential to fill that information void, assuming that appropriate-labeled probe substrates are available.

The compartmental model depicted in Figure 6.1 adequately described ^{99m}Tc-MIBI blood concentrations, hepatic mass of ^{99m}Tc-MIBI in the patient, cumulative excretion of ^{99m}Tc-MIBI in the bile of healthy subjects, and cumulative excretion of ^{99m}Tc-MIBI in the urine (Figure 6.3). The parameters associated with the pharmacokinetic model were estimated with reasonably low variability (Table 6.1). The parameter representing hepatic uptake (k_{uptake}) was reduced, and the basolateral efflux parameter ($k_{basolateral}$) was increased, in the patient compared to healthy human volunteers, consistent with the known decreased liver function, decreased total hepatic blood flow, altered liver perfusion, and up-regulated basolateral efflux proteins in this disease state (1, 8, 9, 37). ^{99m}Tc-MIBI biliary excretion is mediated by P-gp (15-17) and the rate constant governing biliary excretion ($K_{biliary}$) was increased ~4-fold in the patient (Table 6.1), consistent with previous observations that P-gp mRNA and protein are upregulated in patients with primary biliary cirrhosis (9, 37). The urinary excretion rate constant (K_{renal}) was reduced 80% in the patient compared to the healthy volunteers. This could be explained by a decrease in the glomerular filtration rate (GFR) as a result of age and disease state. Based on laboratory values, the estimated GFR in this patient was ~52.8 mL/min/1.73m^2 a 50% decrease compared to the average

value obtained in healthy volunteers (101 ± 17 mL/min/1.73m^2) with a mean age of 41 ± 11 yrs using the modification of diet in renal disease (MDRD) study method, and would be decreased further if comparing to the GFR for the younger healthy volunteer population used in this study (age distribution 21-41 yrs) (38, 39).

Based on pharmacokinetic modeling the, net decrease in hepatic exposure of ^{99m}Tc-MIBI, secondary to disease state, was attributed to a decrease in the rate constant for hepatic uptake and an increase in the rate constants representing hepatic efflux across the basolateral and canalicular membranes. Unfortunately, hepatic scintigraphy data were not obtained for ^{99m}Tc-MIBI in healthy subjects in the previous study (22). To address this deficiency, the time course of substrate mass in liver was simulated in each healthy subject utilizing the parameter estimates (Table 6.1) obtained from modeling the available data in these subjects (Figure 6.1). ^{99m}Tc-MIBI hepatic exposure for the time domain over which imaging was performed was ~76% lower in the patient compared to the mean simulated hepatic exposure of ^{99m}Tc-MIBI in healthy individuals (Figure 6.4). The terminal phase of the ^{99m}Tc-MIBI hepatic mass-time profile was not captured completely in this study. Therefore, future studies would need to incorporate a longer imaging time.

^{99m}Tc-MEB has a high trans-hepatic extraction (21, 22); such compounds would be expected to evidence a hepatic clearance that is limited by hepatic blood flow (40). Given this situation, a semi-physiologic pharmacokinetic model

incorporating hepatic blood flow was developed to predict changes in biliary clearance secondary to alterations in liver perfusion. Initially, fitting *in toto* the model depicted in Figure 6.2 to the data resulted in a poor fit of the blood concentration-time profile. The inability of this model to describe the blood concentration data adequately may have been due to the disparity in the amount of blood concentration data (n=13) relative to the amount of hepatic mass data (n=178). Differential weighting of these two functions did not rectify the problem. Therefore, a stepwise nonlinear least-squares regression approach was taken to analyze these data, with a simple biexponential function, representing a two compartment model, fit to the blood concentration-time data in each subject as the first step. The macro-constants recovered from this step of the analysis (A, α, B, and β) were used to define the blood concentration-time profile, while the parameters associated with the semi-physiologic model (governing hepatic uptake) were determined in the second step of the analysis. Using this approach, the model depicted in Figure 6.2 described the data form the patient as well as the healthy subjects (Figure 6.5).

The robustness of the semi-physiologic model was supported further by the agreement between the estimates for hepatic intrinsic uptake clearance the major route of elimination of ^{99m}Tc-MEB, and total systemic clearance (Cl_{total}) using model independent methods calculated as the administered dose divided by the blood $AUC_{0\rightarrow\infty}$ determined by the trapezoidal rule. Using the well-stirred model to calculate hepatic clearance (Cl_H), which is equal to the product of the hepatic blood flow and intrinsic clearance divided by the sum of the hepatic blood

flow and intrinsic clearance (40) Cl_H is ~1.23 and ~0.120 L/min in healthy subjects and the patient, respectively. This is in excellent agreement with the value obtained for Cl_{total} (1.38 and 0.148 L/min in healthy subjects and the patient, respectively) and is very similar to the hepatic blood flow, which was fixed for the model based on literature reported values (1.45 L/min and 0.492 L/min in healthy subjects and the patient, respectively) demonstrating that ^{99m}Tc-MEB has a high hepatic clearance (Table 6.2).

In healthy subjects, hepatic blood flow was the rate-limiting step in ^{99m}Tc-MEB hepatic clearance; the estimates for $Cl'_{i,uptake}$ were ~4-fold or greater than liver blood flow (Table 6.2). The model structure in healthy individuals did not require a process for either basolateral efflux of ^{99m}Tc-MEB back into sinusoidal blood or renal clearance, ^{99m}Tc-MEB was not detected in urine upon completion of imaging. These results differ from those reported by Ghibellini et al. (2008) in which a rate constant associated with basolateral efflux was incorporated into a compartmental model. This difference in model structure may be due to recovery of ^{99m}Tc-MEB in the urine in the former study. Because hepatic uptake of ^{99m}Tc-MEB is so efficient, it is likely that measurable renal excretion of the probe would occur only if it can escape the liver and re-enter the systemic circulation, a process that would proceed with kinetics defined by a rate constant representing basolateral efflux.

In order to fit the ^{99m}Tc-MEB data obtained from the patient, the model required inclusion of both basolateral efflux and renal clearance. This difference

between the patient and healthy subjects is understandable. If the disease state resulted in impaired hepatic uptake of ^{99m}Tc-MEB, more of the probe compound would be available for renal excretion; if the disease state resulted in impaired biliary excretion of ^{99m}Tc-MEB, more of the probe compound would be available for basolateral efflux (and also subsequently for renal excretion). The presence of basolateral efflux would prolong the residence time of ^{99m}Tc-MEB in blood, which also would explain the longer terminal half-life of the compound in the patient as compared to healthy subjects.

^{99m}Tc-MEB is a known substrate of MRP3 (22), which is located on the basolateral membrane of hepatocytes and is up-regulated in subjects with primary biliary cirrhosis (8, 9). Furthermore, MRP2 is primarily responsible for ^{99m}Tc-MEB biliary excretion (22, 41). MRP3 acts as a compensatory mechanism when MRP2 is impaired, decreasing hepatocellular accumulation of potentially toxic drugs (42, 43). The parameter estimates for ^{99m}Tc-MEB hepatobiliary disposition obtained in the present study [higher basolateral clearance (0.214 L/min) than intrinsic biliary clearance (0.0997 L/min) and a 3.6-fold decreased biliary clearance] in the patient compared to healthy subjects (Table 6.2) are consistent with a disease-dependent decrease in MRP2 and compensatory increase in MRP3. Therefore, the recovery of ^{99m}Tc-MEB in urine in the presence of liver disease may be the result of increased basolateral efflux and a redirection of MEB from excretion into bile.

Surprisingly, the dose-normalized hepatic exposure $AUC_{0\rightarrow180}$ and $AUC_{0\rightarrow\infty}$ to ^{99m}Tc-MEB was similar in the patient with hepatocellular carcinoma and cirrhosis compared to healthy individuals (Figure 6.6). Both the intrinsic uptake clearance and biliary clearance decreased ~5-fold in the patient compared to healthy subjects (Table 6.2). However, a basolateral clearance process also was present in the diseased subject, which would be expected to decrease the hepatic exposure of ^{99m}Tc-MEB in the patient more significantly compared to healthy individuals. The presence of a compensatory basolateral efflux process was only evident in the hepatic mass-time profile in which the maximum mass in the patient was ~3-fold lower compared to the average profile in healthy subjects. However, prolonged exposure at a higher hepatic mass for more than two-thirds of the profile was noted (Higher mass starting at ~50 min in the patient compared to healthy volunteers, Figure 6.6).

In conclusion, the results of the present study suggest that ^{99m}Tc-MIBI and ^{99m}Tc-MEB may be very useful phenotypic probes that are sensitive to changes in hepatic function associated with liver disease. The hepatic exposure to ^{99m}Tc-MIBI was decreased in the patient with hepatocellular carcinoma and cirrhosis compared to healthy volunteers, whereas the hepatic exposure of ^{99m}Tc-MEB was similar but the hepatic exposure profile was notably different with a lower maximum but more prolonged exposure. Alterations in key rate constants representing hepatic uptake and efflux mechanisms secondary to disease may prove useful in predicting changes in drug disposition, and potentially drug

action, for therapeutic compounds that are handled by mechanisms similar to those governing hepatic exposure to ^{99m}Tc-MIBI and ^{99m}Tc-MEB.

Acknowledgment.

This work was supported, in part, by Bayer HealthCare AG and the National Institutes of Health grant R01 GM41935 and by grant UL1RR025747 from the Clinical and Translational Science Award program from the Division of Research Resources. The expertise of Dr. Marijana Ivanovic in establishing the attenuation correction and hepatic scintigraphy methods, Dr. Bert O'Neil in the execution of the hepatocellular carcinoma with Child's Pugh B clinical study, Dr. Gary Pollack in pharmacokinetic modeling and insightful comments in the preparation of this manuscript, and Nathan Pfeifer for his assistance in conducting the clinical studies. Brandon Swift was supported by an Eli Lilly and Company predoctoral fellowship.

References

1. D. Schuppanand N. H. Afdhal. Liver cirrhosis. *Lancet* **371**: 838-51 (2008).

2. P. Chandraand K. L. Brouwer. The complexities of hepatic drug transport: current knowledge and emerging concepts. *Pharm Res* **21**: 719-35 (2004).

3. A. Ayrtonand P. Morgan. Role of transport proteins in drug discovery and development: a pharmaceutical perspective. *Xenobiotica* **38**: 676-708 (2008).

4. C. Funk. The role of hepatic transporters in drug elimination. *Expert Opin Drug Metab Toxicol* **4**: 363-79 (2008).

5. J. Leeand J. L. Boyer. Molecular alterations in hepatocyte transport mechanisms in acquired cholestatic liver disorders. *Semin Liver Dis* **20**: 373-84 (2000).

6. M. Trauner, P. J. Meier, and J. L. Boyer. Molecular pathogenesis of cholestasis. *N Engl J Med* **339**: 1217-27 (1998).

7. G. Zollnerand M. Trauner. Mechanisms of cholestasis. *Clin Liver Dis* **12**: 1-26, vii (2008).

8. H. Kojima, A. T. Nies, J. Konig, W. Hagmann, H. Spring, M. Uemura, H. Fukui, and D. Keppler. Changes in the expression and localization of hepatocellular transporters and radixin in primary biliary cirrhosis. *J Hepatol* **39**: 693-702 (2003).

9. G. Zollner, P. Fickert, D. Silbert, A. Fuchsbichler, H. U. Marschall, K. Zatloukal, H. Denk, and M. Trauner. Adaptive changes in hepatobiliary transporter expression in primary biliary cirrhosis. *J Hepatol* **38**: 717-27 (2003).

10. G. Zollner, M. Wagner, P. Fickert, D. Silbert, J. Gumhold, K. Zatloukal, H. Denk, and M. Trauner. Expression of bile acid synthesis and detoxification enzymes and the alternative bile acid efflux pump MRP4 in patients with primary biliary cirrhosis. *Liver Int* **27**: 920-9 (2007).

11. R. H. Mathijssen, F. A. de Jong, R. H. van Schaik, E. R. Lepper, L. E. Friberg, T. Rietveld, P. de Bruijn, W. J. Graveland, W. D. Figg, J. Verweij, and A. Sparreboom. Prediction of irinotecan pharmacokinetics by use of cytochrome P450 3A4 phenotyping probes. *J Natl Cancer Inst* **96**: 1585-92 (2004).

12. M. Michael, M. Thompson, R. J. Hicks, P. L. Mitchell, A. Ellis, A. D. Milner, J. Di Iulio, A. M. Scott, V. Gurtler, J. M. Hoskins, S. J. Clarke, N. C. Tebbut, K. Foo, M. Jefford, and J. R. Zalcberg. Relationship of hepatic functional imaging to irinotecan pharmacokinetics and genetic parameters of drug elimination. *J Clin Oncol* **24**: 4228-35 (2006).

13. L. P. Rivoryand P. B. Watkins. Erythromycin breath test. *Clin Pharmacol Ther* **70**: 395-9 (2001).

14. M. Wong, R. L. Balleine, E. Y. Blair, A. J. McLachlan, S. P. Ackland, M. B. Garg, S. Evans, D. Farlow, M. Collins, L. P. Rivory, J. M. Hoskins, G. J. Mann, C. L. Clarke, and H. Gurney. Predictors of vinorelbine pharmacokinetics and pharmacodynamics in patients with cancer. *J Clin Oncol* **24**: 2448-55 (2006).

15. M. Wong, S. Evans, L. P. Rivory, J. M. Hoskins, G. J. Mann, D. Farlow, C. L. Clarke, R. L. Balleine, and H. Gurney. Hepatic technetium Tc 99m-labeled sestamibi elimination rate and ABCB1 (MDR1) genotype as indicators of ABCB1 (P-glycoprotein) activity in patients with cancer. *Clin Pharmacol Ther* **77**: 33-42 (2005).

16. C. C. Chen, B. Meadows, J. Regis, G. Kalafsky, T. Fojo, J. A. Carrasquillo, and S. E. Bates. Detection of in vivo P-glycoprotein inhibition by PSC 833 using Tc-99m sestamibi. *Clin Cancer Res* **3**: 545-52 (1997).

17. G. D. Luker, P. M. Fracasso, J. Dobkin, and D. Piwnica-Worms. Modulation of the multidrug resistance P-glycoprotein: detection with technetium-99m-sestamibi in vivo. *J Nucl Med* **38**: 369-72 (1997).

18. L. Sasongko, J. M. Link, M. Muzi, D. A. Mankoff, X. Yang, A. C. Collier, S. C. Shoner, and J. D. Unadkat. Imaging P-glycoprotein transport activity at the human blood-brain barrier with positron emission tomography. *Clin Pharmacol Ther* **77**: 503-14 (2005).

19. M. L. Chiu, J. F. Kronauge, and D. Piwnica-Worms. Effect of mitochondrial and plasma membrane potentials on accumulation of hexakis (2-methoxyisobutylisonitrile) technetium(I) in cultured mouse fibroblasts. *J Nucl Med* **31**: 1646-53 (1990).

20. C. A. Slapak, J. Dahlheimer, and D. Piwnica-Worms. Reversal of multidrug resistance with LY335979: functional analysis of P-glycoprotein-mediated transport activity and its modulation in vivo. *J Clin Pharmacol* **Suppl**: 29S-38S (2001).

21. G. T. Krishnamurthyand F. E. Turner. Pharmacokinetics and clinical application of technetium 99m-labeled hepatobiliary agents. *Semin Nucl Med* **20**: 130-49 (1990).

22. G. Ghibellini, E. M. Leslie, G. M. Pollack, and K. L. Brouwer. Use of tc-99m mebrofenin as a clinical probe to assess altered hepatobiliary transport: integration of in vitro, pharmacokinetic modeling, and simulation studies. *Pharm Res* **25**: 1851-60 (2008).

23. G. Ghibellini, L. S. Vasist, E. M. Leslie, W. D. Heizer, R. J. Kowalsky, B. F. Calvo, and K. L. Brouwer. In vitro-in vivo correlation of hepatobiliary drug clearance in humans. *Clin Pharmacol Ther* **81**: 406-13 (2007).

24. G. Ghibellini, B. M. Johnson, R. J. Kowalsky, W. D. Heizer, and K. L. Brouwer. A novel method for the determination of biliary clearance in humans. *Aaps J* **6**: e33 (2004).

25. G. Delpon, L. Ferrer, A. Lisbona, and M. Bardies. Impact of scatter and attenuation corrections for iodine-131 two-dimensional quantitative imaging in patients. *Cancer Biother Radiopharm* **18**: 191-9 (2003).

26. C. Miller, L. Filipow, S. Jackson, and T. Riauka. Planar imaging quantification using 3D attenuation correction data and Monte Carlo simulated buildup factors. *Phys Med Biol* **41**: 1401-23 (1996).

27. J. E. Juniand R. Reichle. Measurement of hepatocellular function with deconvolutional analysis: application in the differential diagnosis of acute jaundice. *Radiology* **177**: 171-5 (1990).

28. J. E. Juni, J. H. Thrall, J. W. Froelich, R. C. Wiggins, D. A. Campbell, Jr., and M. Tuscan. The appended curve technique for deconvolutional analysis--method and validation. *Eur J Nucl Med* **14**: 403-7 (1988).

29. J. M. Lima, J. J. Lima, J. Isidoro, and P. Lapa. [A new method for quantification of hepatobiliary scintigraphy using 99mTc-mebrofenin. A comparative study]. *Rev Esp Med Nucl* **22**: 244-9 (2003).

30. J. C. Kalvassand T. S. Maurer. Influence of nonspecific brain and plasma binding on CNS exposure: implications for rational drug discovery. *Biopharm Drug Dispos* **23**: 327-38 (2002).

31. M. Weiss. Modelling of initial distribution of drugs following intravenous bolus injection. *Eur J Clin Pharmacol* **24**: 121-6 (1983).

32. F. J. Wackers, D. S. Berman, J. Maddahi, D. D. Watson, G. A. Beller, H. W. Strauss, C. A. Boucher, M. Picard, B. L. Holman, R. Fridrich, and et al. Technetium-99m hexakis 2-methoxyisobutyl isonitrile: human biodistribution, dosimetry, safety, and preliminary comparison to thallium-201 for myocardial perfusion imaging. *J Nucl Med* **30**: 301-11 (1989).

33. B. Daviesand T. Morris. Physiological parameters in laboratory animals and humans. *Pharm Res* **10**: 1093-5 (1993).

34. L. Annet, R. Materne, E. Danse, J. Jamart, Y. Horsmans, and B. E. Van Beers. Hepatic flow parameters measured with MR imaging and Doppler US: correlations with degree of cirrhosis and portal hypertension. *Radiology* **229**: 409-14 (2003).

35. B. Swift, X. Tian, and K. L. Brouwer. Integration of preclinical and clinical data with pharmacokinetic modeling and simulation to evaluate fexofenadine as a probe for hepatobiliary transport function. *Pharm Res* **26**: 1942-51 (2009).

36. T. Watanabe, H. Kusuhara, K. Maeda, Y. Shitara, and Y. Sugiyama. Physiologically based pharmacokinetic modeling to predict transporter-mediated clearance and distribution of pravastatin in humans. *J Pharmacol Exp Ther* **328**: 652-62 (2009).

37. S. N. Barnes, L. M. Aleksunes, L. Augustine, G. L. Scheffer, M. J. Goedken, A. B. Jakowski, I. M. Pruimboom-Brees, N. J. Cherrington, and J. E. Manautou. Induction of hepatobiliary efflux transporters in acetaminophen-induced acute liver failure cases. *Drug Metab Dispos* **35**: 1963-9 (2007).

38. A. S. Levey, J. P. Bosch, J. B. Lewis, T. Greene, N. Rogers, and D. Roth. A more accurate method to estimate glomerular filtration rate from serum creatinine: a new prediction equation. Modification of Diet in Renal Disease Study Group. *Ann Intern Med* **130**: 461-70 (1999).

39. A. D. Rule, T. S. Larson, E. J. Bergstralh, J. M. Slezak, S. J. Jacobsen, and F. G. Cosio. Using serum creatinine to estimate glomerular filtration rate: accuracy in good health and in chronic kidney disease. *Ann Intern Med* **141**: 929-37 (2004).

40. K. S. Pangand M. Rowland. Hepatic clearance of drugs. I. Theoretical considerations of a "well-stirred" model and a "parallel tube" model. Influence of hepatic blood flow, plasma and blood cell binding, and the hepatocellular enzymatic activity on hepatic drug clearance. *J Pharmacokinet Biopharm* **5**: 625-53 (1977).

41. T. Pinos, J. M. Constansa, A. Palacin, and C. Figueras. A new diagnostic approach to the Dubin-Johnson syndrome. *Am J Gastroenterol* **85**: 91-3 (1990).

42. T. Hirohashi, H. Suzuki, K. Ito, K. Ogawa, K. Kume, T. Shimizu, and Y. Sugiyama. Hepatic expression of multidrug resistance-associated protein-

like proteins maintained in eisai hyperbilirubinemic rats. *Mol Pharmacol* **53**: 1068-75 (1998).

43. J. Konig, D. Rost, Y. Cui, and D. Keppler. Characterization of the human multidrug resistance protein isoform MRP3 localized to the basolateral hepatocyte membrane. *Hepatology* **29**: 1156-63 (1999).

Legend to Figures

Figure 6.1 Model scheme for ^{99m}Tc-MIBI disposition in a patient with hepatocellular carcinoma and Child's Pugh B cirrhosis and healthy subjects. C_C represents the concentration of ^{99m}Tc-MIBI in the central compartment (systemic circulation) with an apparent volume V_C; K_{uptake} represents the first–order rate constant for hepatic uptake; $K_{basolateral}$ represents the first-order rate constant for hepatic basolateral efflux; X_{liver} represents the amount of ^{99m}Tc-MIBI in the liver; K_{bile} represents the first–order rate constant for biliary excretion; K_{urine} represents the first–order rate constant for urinary excretion; K_{13} represents the first–order rate constant for uptake into the peripheral compartment; K_{31} represents the first-order rate constant for egress from the peripheral compartment to the central compartment; $X_{peripheral}$ represents the amount of ^{99m}Tc-MIBI in the peripheral compartment.

Figure 6.2 Semi-physiologic model scheme for ^{99m}Tc-MEB disposition in a patient with hepatocellular carcinoma and Child's Pugh B cirrhosis and in healthy subjects. C_C represents the concentration of ^{99m}Tc-MEB in the central compartment (systemic circulation) with apparent volume V_C; Q_H represents hepatic blood flow through the sinusoids of the liver; exchange of ^{99m}Tc-MEB between liver sinusoidal space and hepatocytes is characterized by $Cl'_{i,uptake}$ and $Cl'_{l,basolateral}$; X_{liver} represents the amount of ^{99m}Tc-MEB in the liver with volume V_H; $Cl'_{l,biliary}$ represents biliary excretion; Cl_{renal} represents urinary excretion.

Figure 6.3 Representative ^{99m}Tc-MIBI disposition in a patient with hepatocellular carcinoma and Child's Pugh B cirrhosis (A) and a representative healthy subject (23) (B). Symbols represent observed data; lines represent the best fit of the pharmacokinetic model (scheme depicted in Fig. 6.1) to the data. Blood concentrations (●; solid line) are plotted on a log scale, while substrate mass in the liver (x; dashed line) and cumulative mass in urine (◊; dashed line) and bile (□; dashed line) are plotted on a linear scale.

Figure 6.4 Dose-normalized hepatic mass-time profile of ^{99m}Tc-MIBI in a patient with hepatocellular carcinoma and Child's Pugh B cirrhosis (x; n=1), and simulated hepatic mass-time profile, using final parameter estimates listed in Table 6.1, in healthy human volunteers (line; Mean ± SD, n=7).

Figure 6.5 Representative ^{99m}Tc-MEB disposition in a patient with hepatocellular carcinoma and Child's Pugh B cirrhosis (A) and a representative healthy subject (B). Symbols represent observed data; lines represent the best fit of the semi-

physiologic pharmacokinetic model (scheme depicted in Fig. 6.2) to the data. Blood concentrations (●; solid line) are plotted on a log scale while substrate mass in the liver (x; dashed line), and cumulative mass in urine (◊; dashed line) and bile (□; dashed line) are plotted on a linear scale.

Figure 6.6 Dose normalized hepatic mass-time profile of ^{99m}Tc-MEB in a patient with hepatocellular carcinoma and Child's Pugh B cirrhosis (x; n=1) and healthy human volunteers (○; Mean ± SD, n=3)

Tables

Table 6.1 Parameter estimates and associated variability (coefficient of variation) for ^{99m}Tc-MIBI disposition in the patient with hepatocellular carcinoma and Child's Pugh B cirrhosis and in healthy subjects. Modeling was based on the compartmental model scheme depicted in Fig. 6.1. Parameter estimates for healthy humans were generated from previously published data (23).

		Healthy Volunteers[b]								
	Patient[a]	**Subject 1**	**Subject 2**	**Subject 3**	**Subject 4**	**Subject 5**	**Subject 6**	**Subject 7**	**Mean**	**SD**
Dose (μCi)	3860	2503	3384	3166	3182	3037	3563	3100	3134	331
V_C (L)	4.52 (30.5)	5.34 (5.8)	16.0 (4.3)	10.5 (9.7)	5.99 (5.7)	5.58 (9.9)	4.51 (20.4)	8.78 (5.0)	8.10	4.09
K_{uptake} (min^{-1})	0.135 (8.24)	0.394 (9.7)	0.182 (35.8)	0.248 (21.8)	0.485 (8.0)	0.291 (20.1)	0.430 (25.4)	0.193 (32.4)	0.318	0.119
$K_{basolateral}$ (min^{-1})	0.0221 (23.4)	0.00563 (13.7)	0.00412 (62.5)	0.00387 (34.7)	0.00666 (11.5)	0.00232 (45.8)	0.00378 (32.9)	0.00214 (96.5)	0.00407	0.00163
$K_{biliary}$ (min^{-1})	0.00817 (29.7)	0.00204 (2.5)	0.00222 (20.7)	0.00194 (10.4)	0.00215 (1.5)	0.00158 (10.0)	0.00156 (10.5)	0.00254 (18.9)	0.00200	0.0003
K_{renal} (min^{-1})	0.00975 (27.8)	0.0747 (6.1)	0.0107 (4.9)	0.00327 (8.2)	0.0603 (6.1)	0.0656 (7.6)	0.0623 (15.4)	0.0491 (5.7)	0.0466	0.0281
K_{13} (min^{-1})	0.429 (10.7)	0.272 (12.1)	0.223 (26.5)	0.134 (32.5)	0.133 (18.5)	0.210 (22.6)	0.298 (25.5)	0.258 (22.4)	0.218	0.065
K_{31} (min^{-1})	0.0178 (31.0)	0.0952 (19.3)	0.0347 (31.8)	0.0362 (42.1)	0.149 (34.2)	0.029 (26.5)	0.0345 (26.2)	0.0321 (29.0)	0.0587	0.0461

a) Model fit to blood, cumulative mass in urine and hepatic scintigraphy data.
b) Model fit to blood and cumulative mass in urine and bile data.

Table 6.2 Summary of ^{99m}Tc-MEB dose, recovery, gallbladder ejection fraction and pharmacokinetic parameters and associated variability (coefficient of variation) in a patient with hepatocellular carcinoma and Child's Pugh B cirrhosis and healthy humans. Modeling was conducted according to the pharmacokinetic model scheme depicted in Fig. 6.2.

		Healthy Volunteers[b] (n=3)				
	Patient[a]	Subject 1	Subject 2	Subject 3	Mean	SD
Dose (μCi)	4818	2272	2407	2719	2466	229
Weight (kg)	49.9	69.2	58.3	81.9	69.8	11.8
Urinary Recovery (% of Dose)[a]	0.33	0	0	0	0	0
Biliary Recovery corrected for EF (% of dose)[c]	N/A	63.8	23.4	49.1	45.4	20
Ejection Fraction (EF)	N/A	0.96	0.68	0.54	0.727	0
Fixed Parameters						
Liver Blood Flow (L/min)	0.492	1.43	1.21	1.70	1.45	0.25
Liver Volume (L)	1.20	1.42	1.20	1.68	1.68	0.28
Unbound Fraction in Blood ($F_{u,B}$)	0.123	0.0825[d]	0.0825[d]	0.0825		
Unbound Fraction in Liver ($F_{u,H}$)[e]	0.078	0.078	0.078	0.078		
Alpha[f]	0.00711	0.00508	0.00601	0.00878	0.00662	0.00192
A[f]	240	5.97	3.33	4.53	4.61	1.32
Beta[f]	0.0998	0.18	0.141	0.196	0.172	0.028
B[f]	642	377	95.5	325	266	150
Parameter estimates (CV%)						
Cl_{renal} (L/min)	0.00604 (28.9)					
$Cl'_{i,uptake}$ (L/min)	1.29 (4.6)	5.49 (7.94)	15.7 (26.4)	8.29 (15.78)	9.83	5.28
$Cl'_{basolateral}$ (L/min)	0.214 (13.1)					
$Cl'_{i,biliary}$ (L/min)	0.0997 (4.9)	0.364 (1.63)	0.271 (2.45)	0.439 (2.63)	0.358	0.084
V_c (L)	2.70 (3.1)	1.44 (1.66)	3.52 (2.49)	1.71 (2.72)	2.22	1.13

(a) Model fit to blood, cumulative mass in urine and hepatic scintigraphy data.
(b) Model fit to blood, cumulative mass in urine and bile and hepatic scintigraphy data.
(c) Urinary and biliary (healthy only) recovery of ^{99m}Tc-MEB was measured after IV administration to one patient with hepatocellular carcinoma and Child's Pugh B cirrhosis and three healthy human volunteers. The biliary recovery was corrected for the degree of gallbladder contraction in response to pharmacological stimulation, thereby correcting the amount of ^{99m}Tc-MEB recovered in bile for the residual amount remaining in the gallbladder.
(d) Blood ($f_{u,B}$) unbound fraction was not determined and fixed based on subject #3 data.
(e) Liver ($f_{u,H}$) unbound fraction was estimated *in vitro* by ultrafiltration as described in the methods section.
(f) The macroconstants (A, α, B, β) were obtained by fitting the blood concentration-time curve using nonlinear regression analysis with the algebraic function: concentration = $Ae^{-\alpha t}+Be^{-\beta t}$.

Figure 6.1

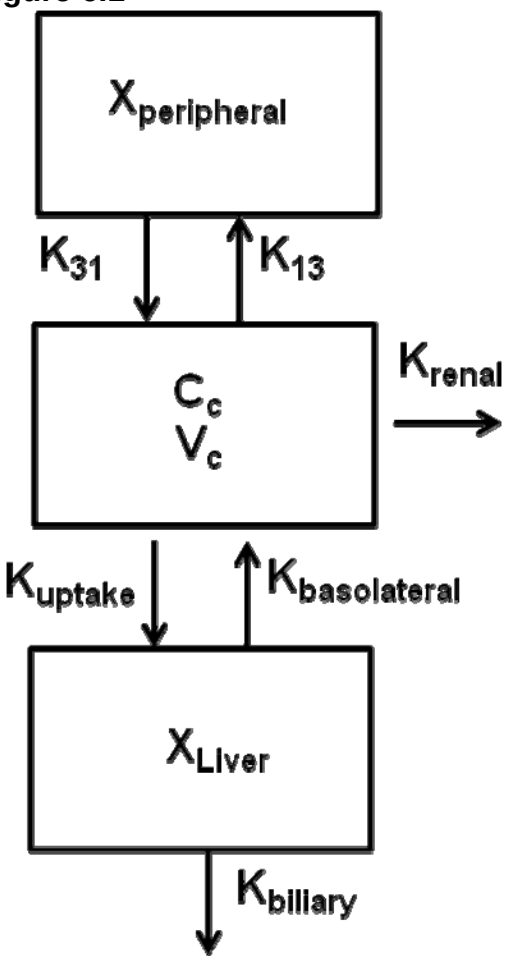
$X_{peripheral}$
K_{31}
K_{13}
C_c
V_c
K_{renal}
K_{uptake}
$K_{basolateral}$
X_{Liver}
$K_{biliary}$

Figure 6.2

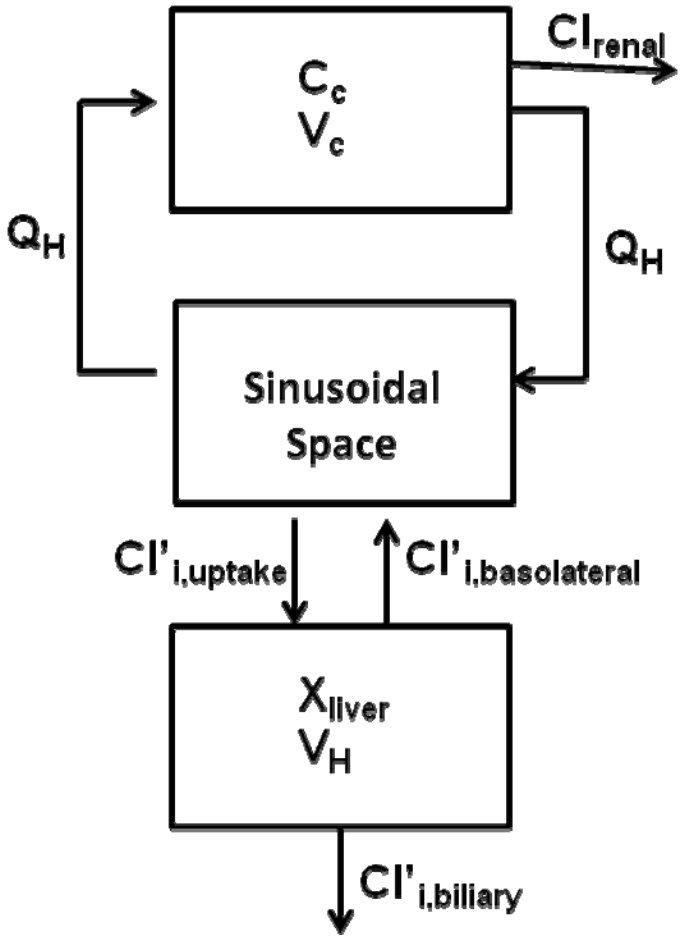
Cl_{renal}
C_c
V_c
Q_H
Q_H
Sinusoidal Space
$Cl'_{i,uptake}$
$Cl'_{i,basolateral}$
X_{liver}
V_H
$Cl'_{i,biliary}$

Figure 6.3

(A)

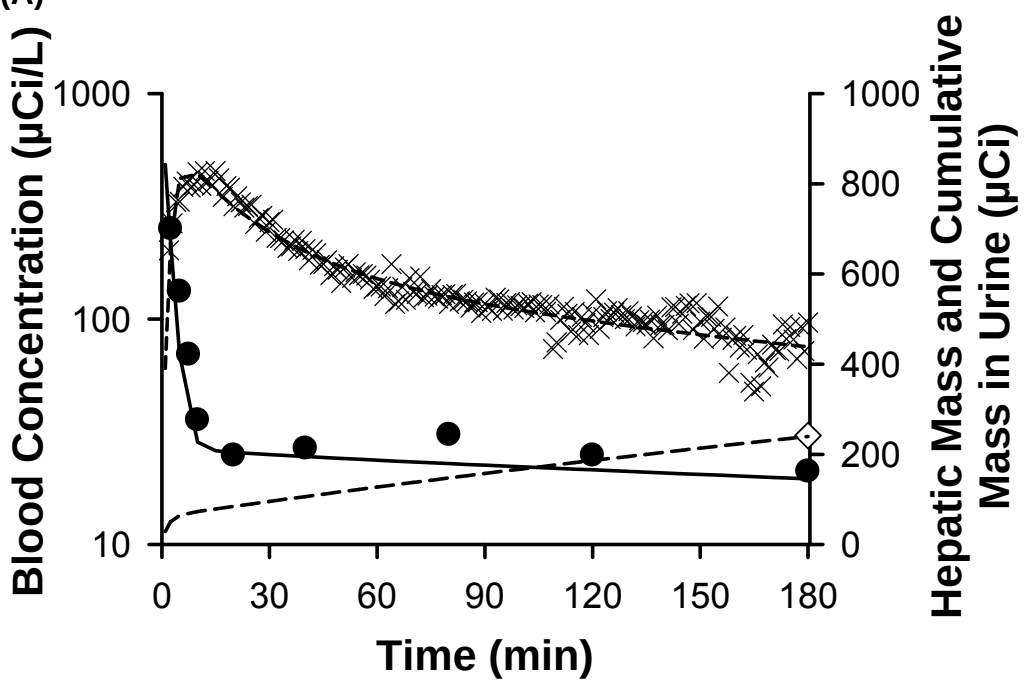
Blood Concentration (µCi/L)
1000
100
10
0
30
60
90
120
150
180
Time (min)
1000
800
600
400
200
0
Hepatic Mass and Cumulative Mass in Urine (µCi)

(B)

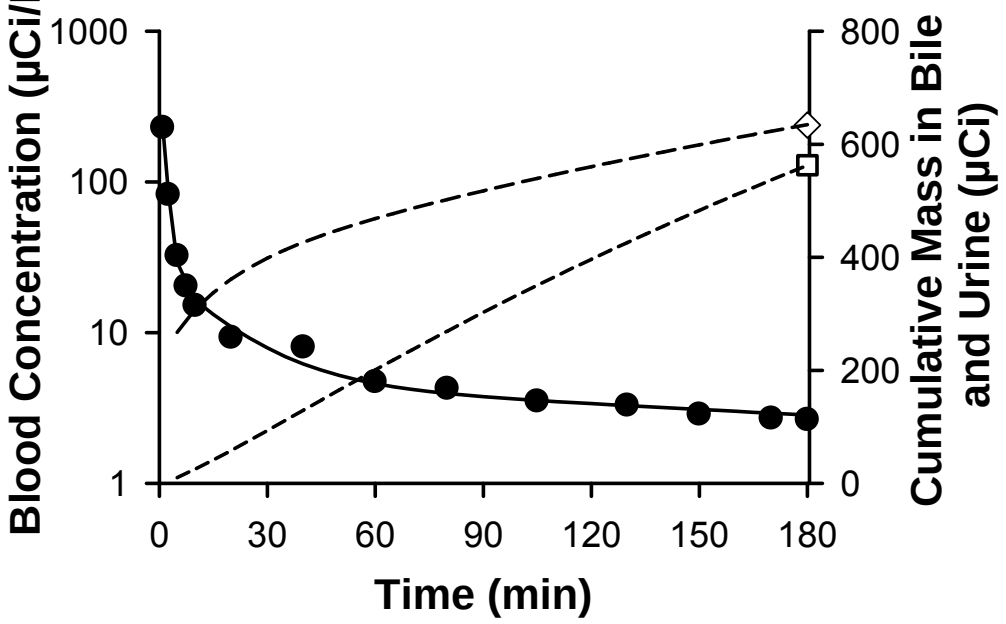
Blood Concentration (µCi/L)
1000
100
10
1
0
30
60
90
120
150
180
Time (min)
800
600
400
200
0
Cumulative Mass in Bile and Urine (µCi)

Figure 6.4

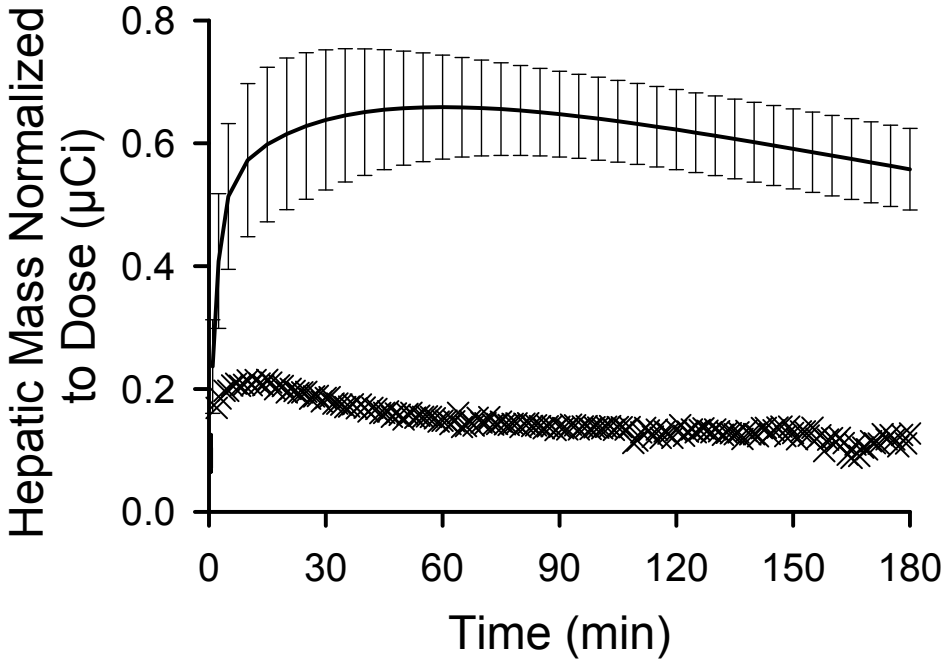
Hepatic Mass Normalized to Dose (µCi)
0.8
0.6
0.4
0.2
0.0
0
30
60
90
120
150
180
Time (min)

Figure 6.5

(A)

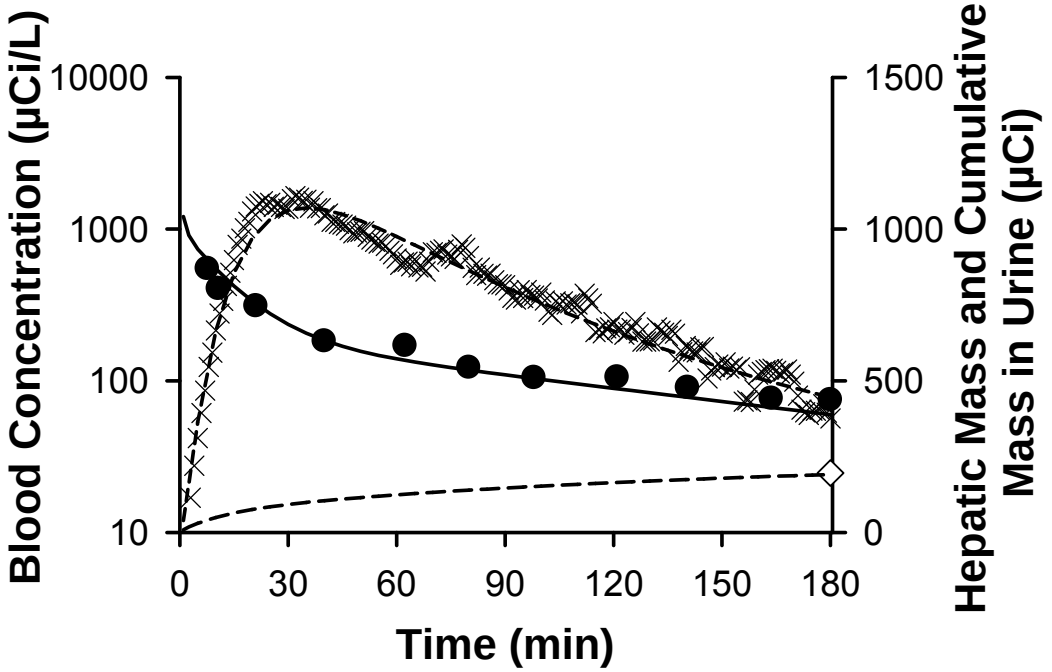
Blood Concentration (µCi/L)
10000
1000
100
10
0
30
60
90
120
150
180
Time (min)
1500
1000
500
0
Hepatic Mass and Cumulative Mass in Urine (µCi)

(B)

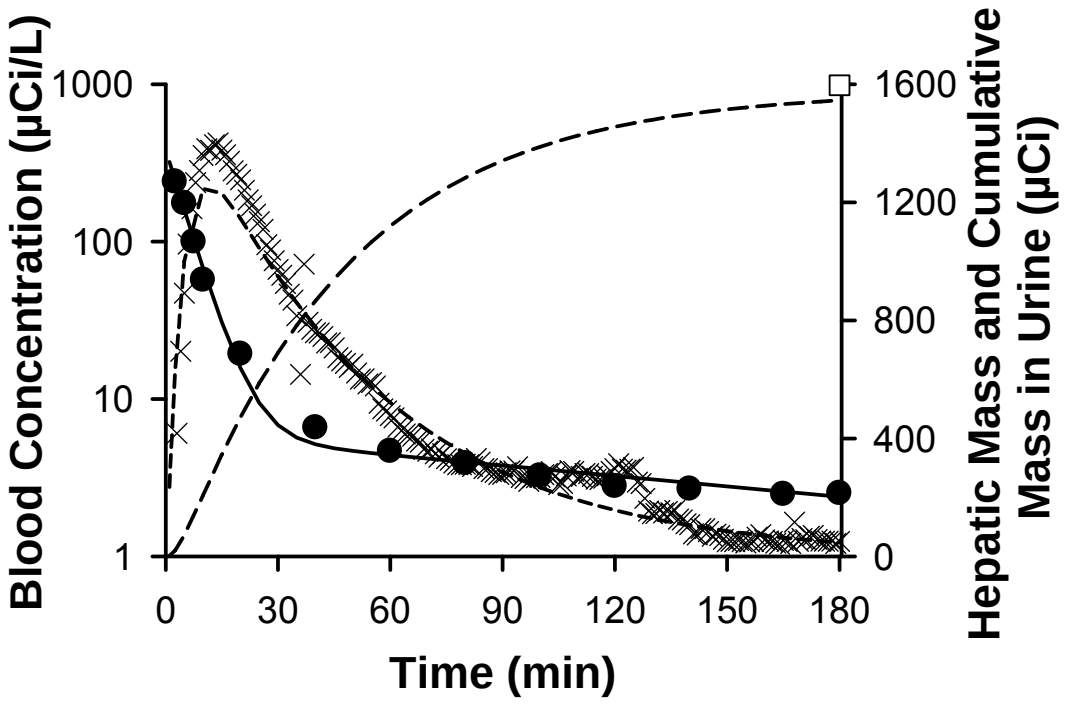
Blood Concentration (µCi/L)
1000
100
10
1
0
30
60
90
120
150
180
Time (min)
1600
1200
800
400
0
Hepatic Mass and Cumulative Mass in Urine (µCi)

Figure 6.6

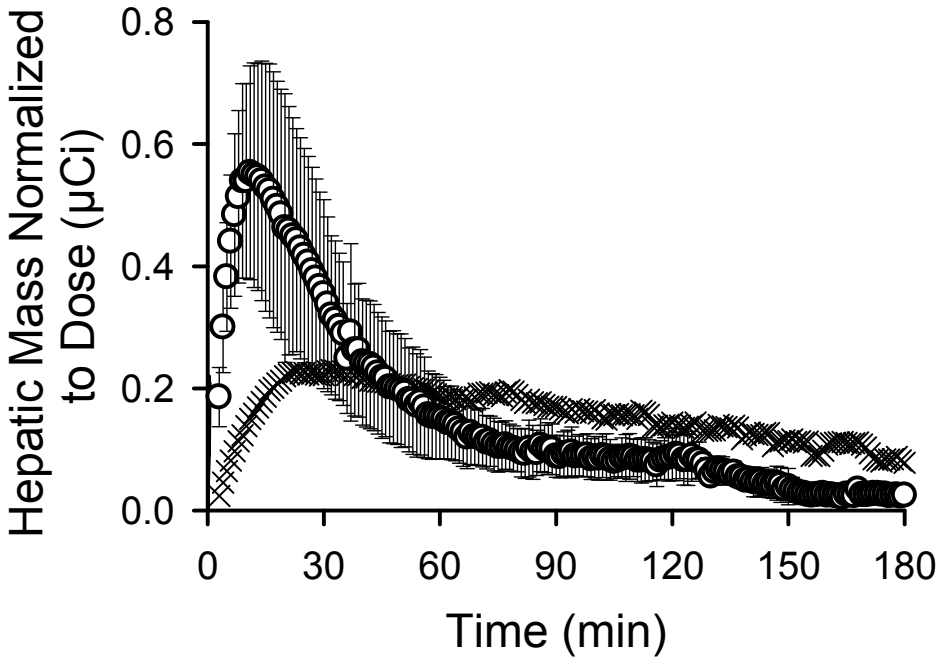
Hepatic Mass Normalized to Dose (µCi)
0.8
0.6
0.4
0.2
0.0
0
30
60
90
120
150
180
Time (min)

CHAPTER 7

Conclusions and Future Directions

The objective of this research project was to identify and characterize substrates as probes for specific hepatic transport proteins for the purpose of elucidating the role of these transport proteins in hepatobiliary disposition of drugs in humans. Identification of specific probe substrates for basolateral and canalicular transport proteins is necessary to elucidate mechanisms of hepatobiliary drug transport, phenotype for interindividual differences in transport protein function, and identify potential drug-drug interactions at the hepatic transport level. Three probe substrates were selected for investigation: fexofenadine, ^{99m}Technetium mebrofenin (^{99m}Tc-MEB), and ^{99m}Technetium sestamibi (^{99m}Tc-MIBI). An important advantage of ^{99m}Tc-MEB and ^{99m}Tc-MIBI is that the gamma emitting properties of the ^{99m}Tc label allow non-invasive scintigraphic imaging for the quantitative assessment of hepatic exposure, which may be significantly different than systemic exposure based on readily obtained blood concentrations.

Integration of Preclinical and Clinical Data with Pharmacokinetic Modeling and Simulation to Evaluate Fexofenadine as a Probe for Hepatobiliary Transport Function (Chapter 2)

Fexofenadine has been labeled as a P-gp specific probe substrate (1), although current literature suggests that other proteins are involved in the hepatic disposition of this compound (2, 3). Therefore, studies were designed to examine the suitablity of fexofenadine as a probe substrate for altered

hepatobiliary transport in humans. A pharmacokinetic model was developed to describe the disposition of fexofenadine in healthy human subjects, and simulations were conducted to examine the effect of inhibition or induction of hepatic transport processes on fexofenadine disposition. To assess the influence of alterations in hepatic uptake or excretion on fexofenadine systemic and hepatic exposure, a simulation approach was utilized, and the rate constants representing the active transport processes governing hepatic uptake and efflux were modulated in a systematic manner. Based on these simulations, systemic fexofenadine concentrations were most sensitive to changes in fexofenadine hepatic uptake. Increased or decreased hepatocyte concentrations, as a result of impaired or induced biliary or hepatic basolateral efflux, associated with drug-drug interactions or genetic mutations, had minimal impact on fexofenadine systemic exposure.

Studies were performed in human sandwich-cultured hepatocytes (SCH) using the inhibitor GF120918 [P-gp and BCRP inhibitor] in order to investigate the changes in systemic and hepatic exposure after inhibition of fexofenadine biliary excretion, and to examine the involvement of P-gp in the biliary excretion of fexofenadine in humans. The possible involvement of BCRP was ruled out based on previously published data demonstrating that BCRP does not transport fexofenadine generated in MDCKII cells transfected with human BCRP (2). Results suggested that a GF120918-sensitive protein(s) (presumably P-gp) played a minor role in fexofenadine biliary excretion in human hepatocytes. Quite possibly, other canalicular transport proteins fully compensate when

GF120918-sensitive protein(s) is/are inhibited. These data imply that fexofenadine would not be a suitable probe substrate in humans to assess altered biliary excretion associated with a specific canalicular transport process.

Due to the limited availability of human hepatocytes, the lack of specific MRP2 inhibitors that would not affect OATP-mediated fexofenadine uptake, and the multiplicity of efflux transport proteins involved in fexofenadine hepatobiliary disposition in humans (3, 4), further investigations were conducted in rat perfused livers to avoid the use of a chemical inhibitor and take advantage of the naturally occurring Mrp2-deficient (TR^-) rats. Previous studies demonstrated that the biliary excretion and intrinsic biliary clearance of fexofenadine were not significantly different in wild-type and TR^- rats (3, 5). Therefore, TR^- rats were employed to rule out any compensatory role of Mrp2 in the biliary excretion of fexofenadine. TR^- rat livers were perfused *in situ* in a single-pass manner in the presence and absence of the Bsep inhibitor bosentan (6), and GF120918 to examine the impact of modulation of uptake and efflux proteins on fexofendadine hepatobiliary disposition. Furthermore, the taurocholate infusion in perfused livers was withheld to perturb trafficking of ATP-binding cassette (ABC) transport proteins to the canalicular membrane (7, 8) in order to assess the contribution of impaired biliary excretion to fexofenadine disposition. Fexofenadine intrinsic biliary clearance was only significantly decreased in the presence of GF120918. Studies in perfused livers from TR^- rats demonstrated that fexofenadine biliary excretion is mediated primarily by a GF120918-sensitive (presumably P-gp) mechanism.

Impact of Basolateral Mrp3 and Mrp4 on the Hepatobiliary Disposition of Fexofenadine in Perfused Mouse Livers (Chapter 3)

Mrp2 is the primary efflux pump responsible for the biliary excretion of fexofenadine in mice (3). Infusion of fexofenadine to *Abcc2(-/-)* mouse livers resulted in an ~85% decrease in biliary excretion, but interestingly, concentrations of fexofenadine in outflow perfusate were significantly higher, and total and unbound concentrations in the liver were reduced compared to wild-type (WT) livers, emphasizing the importance of basolateral efflux. Because many Mrp2 substrates also undergo basolateral export into the blood by Mrp3, the roles of Mrp2, Mrp3, and Mrp4 in the hepatobiliary disposition of fexofenadine were examined in perfused livers from relevant transporter-gene knockout mice. The study design involved an infusion to steady state to preload the liver followed by a washout phase to determine the degree of basolateral and canalicular efflux. Decreased fexofenadine perfusate concentrations were observed at the initiation of the washout phase of perfusion in *Abcc3(-/-)* mice. In order to quantify the impact of Mrp3 and Mrp4 on the basolateral efflux of fexofenadine from the liver, recovery of fexofenadine in perfusate during the washout phase was expressed as the percentage of liver drug content at the end of the infusion. The fraction of fexofenadine excreted into outflow perfusate was significantly decreased ~50% in livers from *Abcc3(-/-)* mice. In contrast, hepatic basolateral excretion of fexofenadine in livers from *Abcc4(-/-)* mice was unchanged. The

fraction of fexofenadine excreted into perfusate was significantly increased ~60% in *Abcc2(-/-)* relative to WT mouse livers. Interestingly, hepatic basolateral excretion of fexofenadine in livers from *Abcc2(-/-)/Abcc3(-/-)* mice was not decreased, and was even ~10% higher than in WT control livers.

Fexofenadine recovery in bile was significantly decreased in *Abcc2(-/-)* and *Abcc2(-/-)/Abcc3(-/-)* mice and unchanged in *Abcc3(-/-)* and *Abcc4(-/-)* mouse livers relative to WT controls. Total recovery of fexofenadine in bile during the washout phase (normalized to drug liver content at the end of the infusion) was significantly lower in *Abcc2(-/-)* and *Abcc2(-/-)/Abcc3(-/-)* relative to WT mice, ~61% and ~53%, respectively. In summary, fexofenadine, in the hepatocyte undergoes bidirectional excretion via Mrp2, Mrp3, and residual unknown transport mechanisms. Mrp4 did not appear to contribute to hepatic basolateral excretion of fexofenadine in the intact mouse liver. This further supports fexofenadine as a substrate of multiple transport proteins in the liver, making it a poor candidate probe substrate for specific hepatic transport proteins such as P-gp.

Evaluation of ^{99m}Tc-MEB and ^{99m}Tc-MIBI as Specific Probes for Hepatic Transport Protein Function in Rats and Humans (Chapter 4)

^{99m}Tc-MIBI and analogs of ^{99m}Tc-MEB have been used as probe substrates to assess interindividual variation in hepatic drug handling and function (9-11). ^{99m}Tc-MIBI has been used to phenotype P-gp function with the

P-gp inhibitors PSC833 and LY335979 resulting in prolonged hepatic exposure (12-14). Alterations in ^{99m}Tc-MIBI pharmacokinetics were assessed in a cohort of cancer patients with common single nucleotide polymorphisms (SNPs) in *ABCB1* exons 12 (C1236T) and 26 (C3435T) resulting in a significantly decreased elimination rate constant (11). However, the mechanisms of hepatic transport have not been fully investigated, including potential compensatory proteins involved in hepatobiliary disposition.

Uptake in human and rat hepatocytes was assessed with the use of specific inhibitors for each subfamily of hepatic transport proteins [i.e. OATPs/Oatps, organic anion transporters (OATs/Oats) and organic cation transporters (OCTs/Octs)] validated with the use of probes (i.e. estradiol-17-β-D-glucuronide, para-aminohippuric acid and tetraethylammonium) to confirm their specificity. To assess sodium-dependent transport by the sodium taurocholate co-transporting polypeptide (Ntcp), choline-based buffer was substituted for sodium-based buffer in suspended hepatocytes. ^{99m}Tc-MIBI initial uptake was within 10% of control, and not influenced by inhibitors or the absence of sodium suggesting that an active transport process is not involved in ^{99m}Tc-MIBI hepatic uptake at these low concentrations. This is consistent with previous reports that uptake is a function of free diffusion based on electrical potentials across the plasma and mitochondrial membranes, with localization in the mitochondria by electrostatic forces (15, 16). Similar findings were expected in human hepatocytes and therefore, experiments were not continued in human hepatocytes to conserve this limited resource. As expected, ^{99m}Tc-MEB initial

uptake was sodium-independent, and was only affected by the OATP/Oatp inhibitors rifamycin SV and glycyrrhizic acid. These data support the hypothesis that ^{99m}Tc-MEB uptake is predominantly mediated by OATPs/Oatps in human and rat and is in agreement with data demonstrating ^{99m}Tc-MEB is a substrate of OATP1B1 and OATP1B3 (17).

Further studies were undertaken to examine the efflux processes involved in ^{99m}Tc-MEB hepatic disposition. ^{99m}Tc-MEB canalicular efflux was completely abated in TR$^-$ rat sandwich-cultured hepatocytes and decreased in WT rat and human sandwich-cultured hepatocytes 665% and only 30% in the presence of the Mrp2 inhibitor MK571. ^{99m}Tc-MEB basolateral efflux was increased in TR$^-$ sandwich-cultured rat hepatocytes compared to WT, and in the presence of MK571, while intracellular accumulation of ^{99m}Tc-MEB was unchanged. These important findings suggest that this probe can be redirected from biliary excretion to basolateral efflux. This increase in basolateral efflux also could be due, in part, to inhibition of ^{99m}Tc-MEB hepatic re-uptake, because MK571 has been shown to inhibit OATP1B3 with a reported K_i of 0.6 μM (18).

Further studies were conducted to investigate the efflux processes involved in ^{99m}Tc-MIBI hepatic disposition. The absence of Mrp2 based on efflux studies in TR$^-$ rat SCH did not alter basolateral or canalicular efflux, suggesting that either Mrp2 is not involved, or other proteins (e.g. P-gp) are able to fully compensate. ^{99m}Tc-MIBI basolateral efflux was GW918 sensitive, suggesting an active transport process. Recently, GW918 was demonstrated to inhibit MRP4 in

inside-out membrane vesicles prepared from transiently transfected HEK293 cells (19). ^{99m}Tc-MIBI canalicular efflux also was GW918 sensitive, consistent with a role for P-gp and/or Bcrp in biliary excretion of this probe. Hepatocellular accumulation of ^{99m}Tc-MIBI increased in the presence GW918 due to the decreased basolateral and canalicular efflux of ^{99m}Tc-MIBI.

In order to investigate further the transport processes involved in ^{99m}Tc-MIBI biliary excretion, accumulation studies were conducted in rat SCH. The involvement of Bcrp in the biliary excretion of ^{99m}Tc-MIBI was assessed with the use of RNAi knockdown of Bcrp, which did not affect ^{99m}Tc-MIBI cellular accumulation or biliary excretion. ^{99m}Tc-MIBI biliary excretion was completely inhibited by 2 μM GF120918, used previously to inhibit P-gp in rat SCH (20). Cellular accumulation also increased in the presence of GF120918, suggesting that Pgp is the primary protein responsible for the biliary excretion of ^{99m}Tc-MIBI in rat SCH.

In summary, the hepatic uptake of ^{99m}Tc-MIBI appears to occur by passive diffusion; ^{99m}Tc-MIBI biliary excretion is mediated by P-gp. ^{99m}Tc-MEB hepatic uptake is predominantly Oatp/OATP-mediated with biliary excretion by MRP2/Mrp2. Remarkable species differences exist between rat and human in the total efflux and route of efflux for ^{99m}Tc-MEB. Preloading SCH and measurement of efflux over 20 min in SCH is a useful approach to investigate the route of hepatic excretion (basolateral vs. canalicular), species differences in basolateral and canalicular efflux, and compensatory changes in canalicular and

basolateral efflux due to impaired transport function associated with drug interactions, disease state alterations or genetic variation.

Hepatobiliary Disposition of Sorafenib in Human Hepatocytes (Chapter 5)

The objective of this aim was to validate the use of ^{99m}Tc-MEB and/or ^{99m}Tc-MIBI as probe substrates to predict the hepatic clearance of the anticancer agent, sorafenib, by confirming similar mechanisms of hepatic transport. Sorafenib, a recently developed oral multikinase inhibitor, relies heavily on the liver for elimination in humans. The liver is also the target site for individuals with unresectable hepatocellular carcinoma (HCC). Furthermore, sorafenib administration in patients with hepatic dysfunction, defined by increased serum concentrations of total bilirubin, aspartate transaminase and albumin, resulted in dose-limiting elevations in total bilirubin concentrations (21). Possible explanations for the sorafenib-mediated increases in serum bilirubin include inhibition of the transport proteins responsible for the hepatobiliary disposition of bilirubin or its conjugates, or UGT1A1 inhibition of bilirubin glucuronidation, as demonstrated *in vitro* (22). Therefore, elucidating the mechanisms of hepatic uptake and the extent of biliary excretion of sorafenib in humans is of utmost importance.

Sorafenib uptake in suspended human hepatocytes, CHO cells and sandwich-cultured human hepatocytes was extensive. Uptake into human hepatocytes and CHO cells was temperature dependent and decreased ~50% at

4°C, suggesting a high degree of passive diffusion. The hepatic uptake in freshly isolated suspended human hepatocytes was sensitive to rifamycin SV and decynium 22, suggesting OATP- and OCT-mediated uptake. OCT1-mediated uptake of sorafenib was confirmed in OCT1 overexpressing CHO cells. Biliary excretion of sorafenib in human SCH was low.

Thus, of the model probes selected, both undergo similar routes of hepatic uptake as sorafenib. ^{99m}Tc-MIBI would be predictive of the predominant process of uptake which occurs by passive diffusion. Sorafenib's rifamycin SV-sensitive uptake mechanism (presumably OATP-mediated) is the predominant uptake route for ^{99m}Tc-MEB. The biliary excretion of sorafenib is low, suggesting this is not an important elimination pathway. However, sorafenib is a substrate and inhibitor of P-gp (Mark Gnoth, personal communication), which also primarily excretes ^{99m}Tc-MIBI. Secondly, sorafenib undergoes phase II glucuronidation catalyzed by uridine disphosphate-glucuronsyl-transferase (UGT1A9) (23). It is well understood that glucuronide conjugates are substrates of MRP2 and MRP3 (24-26), which are responsible for biliary excretion and basolateral efflux into sinusoidal blood, respectively. These are the predominant transport proteins governing the hepatobiliary disposition of the probe substrate ^{99m}Tc-MEB. Therefore, it appears both probes are necessary to phenotype function of the transport proteins responsible for sorafenib hepatic disposition.

Pharmacokinetics and Hepatic Exposure of ^{99m}Tc-MEB and ^{99m}Tc-MIBI Compared Between a Patient with Hepatocellular Carcinoma and Child's Pugh B Cirrhosis versus Healthy Volunteers: An Exploratory Analysis (Chapter 6)

Many patients with HCC and cirrhosis have impaired hepatic function, which results in highly variable clearance of drugs. In fact, the apparent oral clearance of sorafenib has been reported to be highly variable [median 5.32 (range, 0.17 – 26.4) L/hr], and does not appear to be related to age, body weight, sex or hepatic dysfunction (oral clearance was not different among mild, moderate, severe and very severe hepatic dysfunction cohorts). Among the four hepatic dysfunction cohorts, only the cohort with mild liver dysfunction was able to tolerate the recommended dose of 400 mg BID; other cohorts experienced dose-limiting toxicities resulting in decreased maximal tolerated doses (27). The variability in sorafenib pharmacokinetics could be attributed, in part, to differences in hepatic transport protein levels and function. It is well recognized that patients with liver disease develop adaptive changes in transport protein expression, which protect the hepatocyte from the intracellular accumulation of toxic compounds such as bile acids (28-30). For example, patients with primary biliary cirrhosis exhibit down-regulation of basolateral uptake transport proteins often coupled with up-regulation of canalicular and basolateral efflux proteins (31-33). These changes in protein levels result in functional changes which can be assessed *in vivo* with the use of probes that have been shown to be sensitive to specific clearance mechanisms, such as metabolizing enzymes or transport

proteins (9, 10, 34, 35). Furthermore, because systemic concentrations may not represent intracellular concentrations, the use of radiolabeled probes provides a noninvasive method to quantify tissue exposure *in vivo* in order to elucidate functional changes in vectorial transport (11-13, 36).

Thus, the long-term objective of these studies was to compare sorafenib pharmacokinetics with the pharmacokinetics and hepatic exposure of the non-invasive imaging agents, ^{99m}Tc-MEB and ^{99m}Tc-MIBI, in patients with locally advanced or metastatic HCC and Child's B cirrhosis. However, due to slow patient accrual, an interim analysis was not possible in a reasonable timeframe. Therefore, the studies detailed in this dissertation were designed to test the hypothesis that adaptive changes in transport protein expression due to cirrhosis and HCC result in functional changes that impact the disposition of substrates, and that the two probes, ^{99m}Tc-MEB and ^{99m}Tc-MIBI, can serve as tools to predict the locus and extent of modulation in hepatic transport. Pharmacokinetic models were developed to describe the distribution and elimination of ^{99m}Tc-MEB and ^{99m}Tc-MIBI utilizing quantitative hepatic scintigraphy, blood concentrations, and cumulative mass in bile (only in healthy volunteers) and urine from patients with Child's Pugh B cirrhosis and HCC, and from healthy human volunteers. Parameters generated from the pharmacokinetic models representing the hepatic uptake and efflux mechanisms, and hepatic exposure generated form quantitative hepatic scintigraphy, were compared between healthy and diseased subjects.

Overall, the rate constants representing the disposition of ^{99m}Tc-MIBI in the liver were modulated to decrease hepatic exposure. ^{99m}Tc-MIBI hepatic exposure over the 180-min imaging time was decreased ~76% in the patient with HCC and Child's Pugh B cirrhosis compared to the mean simulated hepatic exposure in healthy individuals. The parameter representing hepatic uptake was reduced and the basolateral efflux parameter was increased in the subject with HCC and cirrhosis compared to healthy subjects, consistent with the known decreased hepatic uptake, decreased hepatic blood flow, altered liver perfusion and up-regulated basolateral efflux proteins in this disease state (31, 32, 37, 38). As shown in Chapter 4, ^{99m}Tc-MIBI biliary excretion is mediated by P-gp (11-13); the rate constant governing biliary excretion was increased ~4-fold in the patient with HCC and cirrhosis, consistent with previous reports of increased mRNA and protein in patients with primary biliary cirrhosis (32, 37).

^{99m}Tc-MEB has a high hepatic extraction; therefore, a semi-physiologic pharmacokinetic model incorporating hepatic blood flow was used to describe the data. In In healthy subjects, hepatic blood flow was the rate-limiting step; the estimates for $Cl_{i,uptake}$ were ~4-fold or greater than liver blood flow. The model structure that best described the data in healthy subjects did not require a process for basolateral efflux of ^{99m}Tc-MEB from the hepatocyte into sinusoidal blood, nor a process for renal clearance of ^{99m}Tc-MEB because no radiolabeled compound was detected in urine during the study period. However, in the patient with HCC and cirrhosis, the model that best described the data included basolateral efflux and renal clearance processes; parameter estimates for

basolateral clearance (0.214 L/min) were greater than biliary clearance (0.0997 L/min). The biliary clearance in the HCC with Child's Pugh B cirrhosis patient compared to healthy subjects was decreased 3.6-fold. Furthermore, ^{99m}Tc-MEB recovery in urine was increased in the patient with HCC and cirrhosis due to increased basolateral efflux, resulting in redirection of ^{99m}Tc-MEB from biliary to urinary excretion. Surprisingly, the dose normalized hepatic exposure of MEB was similar between the subject with HCC and cirrhosis compared to healthy individuals. This appears to be due to the decrease in uptake clearance and increase in basolateral efflux clearance in the diseased subject compared to healthy subjects, and further supports MRP3 as a compensatory mechanism that enables excretion of MRP2 substrates into the systemic circulation, thus avoiding excessive accumulation of organic anions in the hepatocyte (24, 39, 40).

These results suggest that ^{99m}Tc-MEB and ^{99m}Tc-MIBI are potentially useful phenotypic probes that are sensitive to changes in hepatic function associated with liver disease. The hepatic exposure to ^{99m}Tc-MIBI was decreased in the patient with HCC and cirrhosis compared to healthy volunteers, whereas the hepatic exposure of ^{99m}Tc-MEB was similar. Alterations in key rate constants representing hepatic uptake and efflux mechanisms secondary to disease may prove useful in predicting changes in drug disposition, and potentially drug action, for therapeutic compounds that are handled by mechanisms similar to those governing hepatic exposure of ^{99m}Tc-MEB and ^{99m}Tc-MIBI.

Significance

Of the three probes investigated in this dissertation, ^{99m}Tc-MEB and ^{99m}Tc-MIBI are most promising due to their specificity for particular transport proteins, as elucidated *in vitro* utilizing whole hepatocyte experiments with all the relevant hepatic transport proteins expressed. ^{99m}Tc-MEB is an organic anion that is taken up by the OATPs and subsequently excreted by MRP2; ^{99m}Tc-MIBI, an organic cation, passively diffuses into hepatocytes and is excreted by P-gp. Both probes are ideal due to the gamma emitting properties of the ^{99m}Tc label, which allows for quantification of hepatic concentrations to assess functional changes in both uptake and efflux. The *in vitro* studies in this dissertation validate both probes to assess hepatic uptake by OATP and biliary secretion by MRP2 and P-gp. However, more work is necessary to elucidate the proteins that are involved in the hepatic sinusoidal (basolateral) efflux of these probes into the bloodstream. For example, it remains unclear whether ^{99m}Tc-MEB is a specific substrate for MRP3, and what GF120918-sensitive protein is responsible for the basolateral efflux of ^{99m}Tc-MIBI. These are important issues in disease states where transport proteins involved in hepatic uptake are down-regulated, and hepatic efflux proteins on both the basolateral and apical membranes are up-regulated. This became apparent in the clinical study when comparing ^{99m}Tc-MEB and ^{99m}Tc-MIBI pharmacokinetics and hepatic exposure between a subject with hepatocellular carcinoma and cirrhosis vs. healthy volunteers. Both probes exhibited a decreased hepatic uptake and increased hepatic efflux *in vivo* based on the model parameters representing these transport processes. Most

importantly, data obtained from hepatic scintigraphy demonstrated that the hepatic exposure of ^{99m}Tc-MEB was similar between the diseased subject and healthy volunteers, but the hepatic exposure of ^{99m}Tc-MIBI was decreased in the diseased subject compared to healthy individuals. Interestingly, blood concentrations of ^{99m}Tc-MIBI in the diseased subject were higher than healthy volunteers, but that did not translate to higher liver exposure; this finding emphasizes the importance of measuring tissue concentrations. Therefore, use of these probes to assess hepatic exposure of drugs that undergo similar mechanisms of hepatic clearance would be advantageous, especially when the liver is the target site (*e.g.* statins or anti-cancer drugs for hepatocellular carncinoma).

The importance of obtaining liver concentrations initially was highlighted by the work with fexofenadine in Chapter 2 through the use of compartmental modeling and simulation. The simulation exercises demonstrated that a potential drug-drug interaction on the apical membrane of the hepatocyte would result in modulation of the liver concentrations without a subsequent change in the systemic compartment. For this reason, fexofenadine would not be an optimal probe for phenotyping the function of a canalicular protein because blood concentrations do not reflect hepatobiliary disposition of this probe, and it is not practical to directly obtain liver concentrations in humans. Furthermore, *in vitro* work in this dissertation demonstrated that fexofenadine is not a specific substrate for P-gp in human hepatocytes, thereby invalidating its use as a specific P-gp probe. Based on studies utilizing transfected systems,

fexofenadine is a substrate *in vitro* for multiple transport proteins; loss of function of one protein due to chemical inhibition or genetic knockout in preclinical models results in full compensation by other hepatic transport proteins.

In summary, transport protein probe substrates that can be imaged quantitatively to determine tissue concentrations have distinct advantages. Such imaging agents can be used to assess alterations in the disposition of compounds due to modulation of uptake and efflux proteins in polarized cells and compartments that are not readily accessible for sampling in humans. Of the two probes identified, ^{99m}Tc-MEB is limited to phenotyping hepatic transport proteins, but ^{99m}Tc-MIBI could be used to assess transport function at other barriers, including the kidney. More work is necessary to identify probes for phentoyping all of the clinically relevant drug transport proteins at barrier epithelium.

Future Directions

This research has prompted a number of proposed future studies regarding species differences in the basolateral and canalicular efflux of fexofenadine, ^{99m}Tc-MEB and ^{99m}Tc-MIBI, the challenge in assessing tissue exposure based on systemic concentration measurements, and the utility of quantitative hepatic scintigraphy coupled with blood concentrations to construct a robust pharmacokinetic model to assess changes in systemic or tissue concentrations and clearance pathways.

Species Differences in Drug Transport

Rodent models are used to investigate the impact of transport proteins on the pharmacokinetics of clinically important drugs. For example, Mrp2-mediated biliary excretion of drugs and metabolites is most extensively investigated in the naturally occurring Mrp2-deficient (TR^-) rat and Mrp2 knockout mouse (26, 41, 42). These tools facilitate our understanding of the involvement of Mrp2 in the processes of drug absorption, distribution, and elimination. Furthermore, these models offer the possibility of exploring how modulators (i.e., inhibitors or inducers) of the transport protein can modify the pharmacokinetics of a drug. However, data obtained in preclinical species may not necessarily correlate to findings in humans. For instance, harmol sulfate biliary excretion was reduced significantly (~10-100-fold) in isolated perfused Bcrp-knockout mouse livers, but was unaffected in Mrp2- and Mdr1a/1b-knockout mouse livers (43). However, in isolated perfused rat livers, GF120918 (P-gp and Bcrp inhibitor) had no effect on harmol sulfate biliary excretion, but the cumulative mass in bile after a 90-min infusion was decreased ~2.7-fold in TR^- rats deficient in Mrp2 (44). These findings demonstrated fundamental species differences in the hepatobiliary disposition of harmol sulfate, which is predominantly a substrate of Bcrp in mouse and Mrp2 in rat. Zimmermann et al. demonstrated that human MRP2 and mouse Mrp2 have similar substrate specificities including vinblastine, docetaxel, saquinavir and etoposide, but have marked differences regarding transport efficiencies and in the modulation of transport by other compounds (45). Their investigations demonstrated that sulfinpyrazone stimulated transport of saquinavir and estradiol-17-β-D-glucuronide by human MRP2, but strongly

inhibited saquinavir transport by mouse Mrp2 (45). These differences could be explained by the 78% amino acid identity between mouse Mrp2 and human MRP2 (46). Many amino acid substitutions occur throughout the protein and, as shown by Ito et al., a single amino acid change in the last transmembrane segment of the protein altered MRP2 substrate specificity resulting in loss of the ability to transport methotrexate (47).

Work by Tian et al., demonstrated that in isolated perfused mouse livers the fexofenadine biliary excretion rate decreased 85%, and intrinsic biliary clearance decreased 50%, in Mrp2-knockout mice compared to wild-type control mice (3). In contrast to mice, fexofenadine biliary excretion rate and intrinsic biliary clearance were unchanged in Mrp2-deficient TR^- rats compared to wild-type control rats. These apparently contradictory findings suggest that other transport proteins can completely compensate for the loss of Mrp2 function in the rat (3). In this dissertation, coadministration of fexofenadine and GF120918 (specific P-gp and Bcrp inhibitor) resulted in a 75% decrease in fexofenadine biliary excretion rate and a ~3.6-fold decrease in intrinsic biliary clearance [Chapter 2, (48)]. Fexofenadine is not a substrate of human or mouse BCRP/Bcrp based on previously published data generated in MDCKII cells transfected with human BCRP, or in Bcrp-knockout mice (2, 5). Therefore, the predominant pathway for fexofenadine excretion into rat bile is likely P-gp. Furthermore, fexofenadine biliary excretion index and *in vitro* biliary clearance were unchanged in the presence of the P-gp inhibitor GF120918 utilizing human SCH. These data suggest that GF120918-senstive protein(s) (presumably P-gp)

play a minor role in fexofenadine biliary excretion in human hepatocytes. Thus, the key question is, which species is more predictive of human fexofenadine biliary excretion, and why is Mrp2 predominantly involved in biliary excretion of this substrate in the mouse, wereas P-gp is primarily involved in biliary excretion of fexofenadine in the rat, but not in human hepatocytes? Species differences in the affinity of the protein for fexofenadine, or differences in the amount of functional protein residing on the membrane, could help answer this question. Interestingly, the amount of MRP2/Mrp2 protein in the membrane fraction from liver samples was 10-fold higher in rats than in humans, as quantified by LC-MS/MS (49). Based on this information, Mrp2 should be more involved in fexofenadine biliary excretion in rats, than in mice or humans. The greater influence of P-gp in rats may be due to a higher expression level or affinity for rat P-gp compared to mouse and human or perhaps just a lower affinity for Mrp2 in rats. To help help explain this species difference in biliary excretion experiments using transfected systems that express Mrp2 and P-gp for each species individually to determine differences in K_m and V_{max} for fexofenadine.

Remarkable species differences existed in the fraction of canalicular vs. basolateral efflux of ^{99m}Tc-MEB in rats (38.0% and 62.0%, respectively) and humans (73.3% and 26.7%, respectively), suggesting that biliary excretion would be the preferential route of hepatic elimination of this probe in humans. This cannot be attributed to differences in the absolute amount of Mrp2/MRP2 protein primarily responsible for biliary excretion of ^{99m}Tc-MEB (Chapter 4). Based on work by Li et al., total Mrp2/MRP2 protein was not significantly different in day 4

rat and day 7 human SCH (~4 fmol/μg protein) utilizing a quantitative LC-MS/MS analysis (50). However, these apparent species differences could be explained by affinity differences, or different amounts of functional Mrp2/MRP2 protein residing on the canalicular membrane. The high degree of ^{99m}Tc-MEB biliary excretion is consistent with *in vivo* data from healthy human subjects indicating that ~84% of a 2.3 μCi dose of intravenously administered ^{99m}Tc-MEB was recovered in bile (17). In contrast, the fraction of canalicular vs. basolateral efflux of ^{99m}Tc-MIBI in rats (36.8% and 63.2%, respectively) and humans (28.3% and 71.7%, respectively), basolateral excretion of ^{99m}Tc-MIBI appears to be the preferential route of hepatic elimination of this probe in both rats and humans. This finding is consistent with biliary recovery of ~22% of a 3.1 μCi dose of intraveneously administered ^{99m}Tc-MIBI in healthy human subjects (17). Further work assessing basolateral and biliary efflux of ^{99m}Tc-MEB and ^{99m}Tc-MIBI *in vivo* in rats is necessary to establish this efflux method in sandwich-cultured hepatocytes for examining the preferential route of hepatic efflux (canalicular vs. basolateral) and elucidating species differences in hepatic efflux. To further establish this methodology perhaps another compound to assess would be the degree of canalicular vs. basolateral efflux of acetaminophen glucuronide in rats vs. humans. In the recirculating rat isolated perfused liver a 66 μmol bolus dose of acetaminophen resulted in a 2-fold greater recovery of acetaminophen glucuronide in bile (16 ± 4% of dose) compared to perfusate (8 ± 2% of dose) (51). In contrast, after a 1 g dose of paracetamol in humans the bile (1.2 mg) to urine (433.9 mg) recovery ratio of paracetamol glucuronide was 0.31% (52, 53).

The methods for determining species differences in drug transport are improving. Transfected systems expressing each species-specific isoform of a given transport protein in the same cell line are becoming available, and some comparisons have been published. This allows for investigation of differences in affinity or K_m. Furthermore, as mentioned above, methods to quantify absolute levels of transport proteins are being developed and published using LC-MS/MS methodology allowing for differences in V_{max} to be assessed. However, this is for total protein in the cell. Utilizing methods to isolate the membrane fraction (54) would be more useful for determining the amount of functional protein. Lastly, species differences in basolateral and canalicular efflux in hepatocytes can be assessed in isolated perfused livers. However, in order to assess differences in humans, novel approaches are needed. Sandwich-cultured hepatocytes may be one system that can be used to address this issue.

This does call into question the usefulness of preclinical species to predict the human transport proteins involved in disposition and underlines the issue with extrapolating clearance across species to predict human clearance. There are many available tools to study *in vitro* uptake and efflux of drugs with human materials. However, the extrapolation to *in vivo* is limited due to the lack of corresponding *in vivo* kinetic parameters for determining the scaling factors to extrapolate the in *vitro* parameters to *in vivo*. The use of radiolabeled probes will facilitate the *in vitro*-*in vivo* extrapolation by quantifying tissue concentrations, which are useful for obtaining tissue partition coefficients and to calculate clearance.

Organ Exposure is Not Always Represented by Systemic Concentrations

Drug-drug interactions may result in pharmacokinetic changes that alter drug efficacy and/or toxicity, especially for drugs that have a narrow therapeutic window. Most of the work on drug-drug interactions is focused on changes in absorption, bioavailability or systemic concentrations of a drug. However, it is increasingly being recognized that drug-drug interactions can affect the distribution of the victim drug into a particular compartment or tissue without significantly affecting the systemic concentration-time profile of that drug (48, 55). For example, drug-drug interactions can result in CNS effects of drugs that normally are not targeted to the brain (56).

The lack of significant changes in systemic exposure, despite increased concentrations in a particular compartment (e.g. brain, liver) may be explained by a relatively small amount of drug distributing into that particular compartment compared to the total amount of drug in the body. Alternatively, the clearance of the drug from the body may be mediated by a different mechanism (e.g. transport protein or metabolizing enzyme) than the pathway affected by the drug-drug interaction in the organ where the drug distributes. However, it is difficult to assess changes in the exposure of a drug in a particular compartment *in vivo*. The use of noninvasive imaging methods to measure tissue exposure is one approach that may address this dilemma. For example, Sasongko et al. utilized the P-gp substrate ^{11}C-verapamil to measure brain concentrations by positron

emission tomography in the presence and absence of the P-gp inhibitor cyclosporine. Data demonstrated an 88% increase in the AUC_{brain}/AUC_{blood} ratio of ^{11}C-radioactivity in the presence of cyclosporine, while the blood-to-plasma AUC ratio for ^{11}C-radioacitivity during the 45-min imaging time did not differ significantly in the presence and absence of cyclosporine (36). Furthermore, the increase in brain exposure was not confounded by changes in plasma protein binding, ^{11}C-verapamil metabolism or cerebral blood flow for this rapidly diffusing drug.

In this dissertation, pharmacokinetic modeling and simulation studies were employed to examine the impact of hepatic transport modulation on the systemic and hepatic exposure of fexofenadine in humans. Simulations revealed that systemic fexofenadine concentrations were most sensitive to changes in the fexofenadine hepatic uptake rate constant, rather than the basolateral efflux rate constant, or the biliary excretion rate constant [Chapter 2, (48)]. In contrast, results indicated that hepatic fexofenadine exposure in humans was sensitive to alterations in either the hepatic uptake rate constant or the biliary excretion rate constant. Most importantly, the marked increase in fexofenadine hepatic exposure due to modulation in biliary excretion was not reflected by changes in the systemic concentration-time profile [Chapter 2, (48)]. This demonstrates the importance of assessing hepatic exposure; systemic concentrations of a substrate like fexofenadine may not accurately reflect hepatic exposure. A similar finding has been shown using a physiologically based pharmacokinetic model of pravastatin in humans. Simulations showed that changes in the hepatic

uptake of pravastatin altered plasma concentrations markedly, but had a minimal effect on liver concentrations; in contrast, changes in canalicular efflux of pravastatin altered liver concentrations of pravastatin markedly, but had minor effects on the plasma concentration (55). These findings are supported by an increase in plasma C_{max} and AUC in patients with SNPs that decrease OATP1B1 function compared to the reference allele (57-59) and decreased inhibitory effect on cholesterol synthesis presumably due to decreased concentrations in the hepatocytes (60-62). What is more difficult to determine are changes in hepatic concentrations as a result of inhibition of biliary excretion. Pravastatin is a substrate of BCRP, MRP2 and BSEP (63-67). Ho et al. investigated the effects of polymorphisms in the efflux proteins MRP2 (*ABCC2*), BSEP (*ABCB11*) and BCRP (*ABCG2*), following a single 40 mg oral dose of pravastatin in healthy European-Americans and African-Americans (68). The *ABCC2*, *ABCB11* or *ABCG2* genotypes were not associated with differences in pravastatin pharmacokinetics and support the findings from the simulations. However what was not assessed were the changes in liver exposure. This could be ascertained by indirectly assessing increases in hepatic concentrations of pravastatin by measuring decreases in cholesterol synthesis in patients with reduced BCRP, MRP2 and BSEP function through a combination of chemical inhibition and naturally occurring genetic deficiencies in these three proteins.

Pharmacokinetic modeling is a powerful tool to simulate concentrations in non-accessible sampling sites such as the brain and liver. Physiologically-based pharmacokinetic (PBPK) modeling has been utilized extensively to assess tissue

exposure. However, this is considered more of an *in silico* approach, and is difficult to show experimentally in humans. In the clinical setting, brain concentrations of drugs can be determined by the use of microdialysis, but under very special circumstances such as brain surgery. Moreover, biopsies of a particular tissue can be performed, but data analysis will be limited when only a single data point is available. Furthermore, obtaining this data is typically in a specific patient population that wouldn't reflect healthy individuals making it difficult to translate the results. A more reasonable and noninvasive method is to assess tissue exposure through the use of radiolabeled (gamma emitters or positron emitters) probes. Imaging studies also allow continuous assessment of tissue concentrations of probes over multiple time points. A radiolabeled probe is useful for assessing the effect of inhibitors or inducers due to drug-drug interactions particularly when the effect does not result in changes in systemic concentrations. For example, inhibition of MRP2 in the liver may result in increased liver concentrations that are not represented in the blood compartment. Therefore, this interaction could be elucidated with the use of quantitative scintigraphy when using a radiolabeled probe.

Pharmacokinetic Modeling of Clinical Data Coupled with Quantitative Imaging

The advantages of quantitative imaging have been discussed above, including a noninvasive method for capturing concentration data in a clinical

setting, the access to compartments (e.g. liver or brain) that are difficult to measure directly, and the continuous sampling of data over multiple time points. In addition, the ability to obtain tissue concentrations with a radiolabeled probe are not limited to a specific setting, as is the case with other methods (i.e. biopsy or microdialysis), in which the typical patient population undergoing this intervention would not be reflective of healthy individuals. Combining the quantitative imaging data that can be obtained in any patient population with the readily accessible blood, urine and/or fecal concentrations allows for the construction of a robust pharmacokinetic model to describe the disposition of a radiolabeled probe.

Applying quantitative imaging data is advantageous in building a PBPK model. These types of models are difficult to build to predict the disposition and elimination of a drug in humans due to the quality of the data sets. Often data from preclinical species must be scaled up to assist model development. With the use of tissue concentrations obtained from imaging, a more robust PBPK model can be developed. An important parameter necessary for building a PBPK model and for describing the steady-state concentration of a drug in a tissue compared with blood is the partition coefficient for that tissue. This parameter can be estimated with the use of imaging when the tissue concentration-time profile reaches equilibrium distribution with the blood concentration-time profile.

Further application of a complex pharmacokinetic model incorporating quantitative imaging can be used to assess interindividual differences in discrete

drug handling pathways (e.g. metabolizing enzymes and transport proteins). ^{99m}Tc-MIBI and an analog of ^{99m}Tc-MEB have been applied as probe substrates to phenotype hepatic transport protein function. In an attempt to individualize dosing and reduce toxicity the time activity curves of ^{99m}Tc-MIBI and an analog of ^{99m}Tc-MEB were correlated with the pharmacokinetics of two anticancer drugs, vinorelbine and irinotecan (9, 10). However, these studies did not quantify the scintigraphy data or attempt to model the data to further define interindividual differences in hepatic drug transport responsible for clearance of the two anticancer drugs. Examining the relationship between hepatic functional imaging of ^{99m}Tc-MEB and ^{99m}Tc-MIBI and the pharmacokinetics of drugs used in the treatment of patients with inoperable HCC and Child's B cirrhosis may assist in the development of individualized dosage regimens. This approach may be particularly valuable for drugs that exhibit a narrow range between therapeutic and toxic concentrations and a wide inter-subject variability in clearance and may be useful in optimizing efficacy. This approach is being utilized in an ongoing clinical study to individualize sorafenib dosing and decrease toxicity in patients with hepatocellular carcinoma and Child's Pugh B cirrhosis. Both ^{99m}Tc-MEB and ^{99m}Tc-MIBI are being used to assess individual variability in hepatic uptake and biliary excretion, and parameters generated from the functional hepatic nuclear imaging will be correlated with sorafenib pharmacokinetics and toxicity.

In conclusion, pharmacokinetic modeling of clinical data coupled with quantitative imaging is a powerful tool to describe the distribution and elimination of radiolabeled probes to elucidate changes in clearance pathways (e.g.

metabolizing enzymes and transport proteins) due to drug-drug interactions, genetic polymorphism or disease state modifications. Furthermore, application of this tool to assess and explain interindividual differences in drug clearance mechanisms may help reduce toxicity while optimizing efficacy. Alterations in critical rate constants representing key clearance mechanisms may be useful in predicting changes in drug disposition, and potential drug action, for therapeutic compounds that are handled by mechanisms similar to the radiolabeled probes.

References

1. G. T. Tucker, J. B. Houston, and S. M. Huang. Optimizing drug development: strategies to assess drug metabolism/transporter interaction potential-toward a consensus. *Clin Pharmacol Ther* **70**: 103-14 (2001).

2. S. Matsushima, K. Maeda, H. Hayashi, Y. Debori, A. H. Schinkel, J. D. Schuetz, H. Kusuhara, and Y. Sugiyama. Involvement of multiple efflux transporters in hepatic disposition of fexofenadine. *Mol Pharmacol* **73**: 1474-83 (2008).

3. X. Tian, M. J. Zamek-Gliszczynski, J. Li, A. S. Bridges, K. Nezasa, N. J. Patel, T. J. Raub, and K. L. Brouwer. Multidrug resistance-associated protein 2 is primarily responsible for the biliary excretion of fexofenadine in mice. *Drug Metab Dispos* **36**: 61-4 (2008).

4. S. Matsushima, K. Maeda, H. Hayashi, Y. Debori, A. H. Schinkel, J. D. Schuetz, H. Kusuhara, and Y. Sugiyama. Involvement of multiple efflux transporters in hepatic disposition of fexofenadine. *Mol Pharmacol* (2008).

5. H. Tahara, H. Kusuhara, E. Fuse, and Y. Sugiyama. P-glycoprotein plays a major role in the efflux of fexofenadine in the small intestine and blood-brain barrier, but only a limited role in its biliary excretion. *Drug Metab Dispos* **33**: 963-8 (2005).

6. K. Fattinger, C. Funk, M. Pantze, C. Weber, J. Reichen, B. Stieger, and P. J. Meier. The endothelin antagonist bosentan inhibits the canalicular bile salt export pump: a potential mechanism for hepatic adverse reactions. *Clin Pharmacol Ther* **69**: 223-31 (2001).

7. Z. C. Gatmaitan, A. T. Nies, and I. M. Arias. Regulation and translocation of ATP-dependent apical membrane proteins in rat liver. *Am J Physiol* **272**: G1041-9 (1997).

8. H. Kipp, N. Pichetshote, and I. M. Arias. Transporters on demand: intrahepatic pools of canalicular ATP binding cassette transporters in rat liver. *J Biol Chem* **276**: 7218-24 (2001).

9. M. Michael, M. Thompson, R. J. Hicks, P. L. Mitchell, A. Ellis, A. D. Milner, J. Di Iulio, A. M. Scott, V. Gurtler, J. M. Hoskins, S. J. Clarke, N. C. Tebbut, K. Foo, M. Jefford, and J. R. Zalcberg. Relationship of hepatic functional imaging to irinotecan pharmacokinetics and genetic parameters of drug elimination. *J Clin Oncol* **24**: 4228-35 (2006).

10. M. Wong, R. L. Balleine, E. Y. Blair, A. J. McLachlan, S. P. Ackland, M. B. Garg, S. Evans, D. Farlow, M. Collins, L. P. Rivory, J. M. Hoskins, G. J. Mann, C. L. Clarke, and H. Gurney. Predictors of vinorelbine

pharmacokinetics and pharmacodynamics in patients with cancer. *J Clin Oncol* **24**: 2448-55 (2006).

11. M. Wong, S. Evans, L. P. Rivory, J. M. Hoskins, G. J. Mann, D. Farlow, C. L. Clarke, R. L. Balleine, and H. Gurney. Hepatic technetium Tc 99m-labeled sestamibi elimination rate and ABCB1 (MDR1) genotype as indicators of ABCB1 (P-glycoprotein) activity in patients with cancer. *Clin Pharmacol Ther* **77**: 33-42 (2005).

12. G. D. Luker, P. M. Fracasso, J. Dobkin, and D. Piwnica-Worms. Modulation of the multidrug resistance P-glycoprotein: detection with technetium-99m-sestamibi in vivo. *J Nucl Med* **38**: 369-72 (1997).

13. C. C. Chen, B. Meadows, J. Regis, G. Kalafsky, T. Fojo, J. A. Carrasquillo, and S. E. Bates. Detection of in vivo P-glycoprotein inhibition by PSC 833 using Tc-99m sestamibi. *Clin Cancer Res* **3**: 545-52 (1997).

14. C. A. Slapak, J. Dahlheimer, and D. Piwnica-Worms. Reversal of multidrug resistance with LY335979: functional analysis of P-glycoprotein-mediated transport activity and its modulation in vivo. *J Clin Pharmacol* **Suppl**: 29S-38S (2001).

15. M. L. Chiu, J. F. Kronauge, and D. Piwnica-Worms. Effect of mitochondrial and plasma membrane potentials on accumulation of hexakis (2-methoxyisobutylisonitrile) technetium(I) in cultured mouse fibroblasts. *J Nucl Med* **31**: 1646-53 (1990).

16. L. I. Delmon-Moingeon, D. Piwnica-Worms, A. D. Van den Abbeele, B. L. Holman, A. Davison, and A. G. Jones. Uptake of the cation hexakis(2-methoxyisobutylisonitrile)-technetium-99m by human carcinoma cell lines in vitro. *Cancer Res* **50**: 2198-202 (1990).

17. G. Ghibellini, E. M. Leslie, G. M. Pollack, and K. L. Brouwer. Use of tc-99m mebrofenin as a clinical probe to assess altered hepatobiliary transport: integration of in vitro, pharmacokinetic modeling, and simulation studies. *Pharm Res* **25**: 1851-60 (2008).

18. K. Letschert, M. Komatsu, J. Hummel-Eisenbeiss, and D. Keppler. Vectorial transport of the peptide CCK-8 by double-transfected MDCKII cells stably expressing the organic anion transporter OATP1B3 (OATP8) and the export pump ABCC2. *J Pharmacol Exp Ther* **313**: 549-56 (2005).

19. J. K. Lee. Role of Hepatic Transport Proteins in Drug Disposition and Drug-Induced Liver Injury, *School of Pharmacy*, Vol. Ph.D., University of North Carolina at Chapel Hill, Chapel Hill, 2009, pp. 257.

20. P. P. Annaert, R. Z. Turncliff, C. L. Booth, D. R. Thakker, and K. L. Brouwer. P-glycoprotein-mediated in vitro biliary excretion in sandwich-cultured rat hepatocytes. *Drug Metab Dispos* **29**: 1277-83 (2001).

21. A. A. Miller, D. J. Murry, K. Owzar, D. R. Hollis, E. B. Kennedy, G. Abou-Alfa, A. Desai, J. Hwang, M. A. Villalona-Calero, E. C. Dees, L. D. Lewis, M. G. Fakih, M. J. Edelman, F. Millard, R. C. Frank, R. J. Hohl, and M. J. Ratain. Phase I and pharmacokinetic study of sorafenib in patients with hepatic or renal dysfunction: CALGB 60301. *J Clin Oncol* **27**: 1800-5 (2009).

22. N. Kalyanaraman, C. Li, S. S. Surapaneni, and G. N. Kumar. Tyrosine Kinase Inhibitors are Potent and Selective Inhibitors of UGT1A1: Tools for UGT Phenotyping, *International Society for the Study of Xenobiotics*, Vol. 38, Drug Metabolism Reviews Puerto Rico, USA, 2006, pp. 1-258

23. C. Lathia, J. Lettieri, F. Cihon, M. Gallentine, M. Radtke, and P. Sundaresan. Lack of effect of ketoconazole-mediated CYP3A inhibition on sorafenib clinical pharmacokinetics. *Cancer Chemother Pharmacol* **57**: 685-92 (2006).

24. T. Hirohashi, H. Suzuki, X. Y. Chu, I. Tamai, A. Tsuji, and Y. Sugiyama. Function and expression of multidrug resistance-associated protein family in human colon adenocarcinoma cells (Caco-2). *J Pharmacol Exp Ther* **292**: 265-70 (2000).

25. H. Xiong, K. C. Turner, E. S. Ward, P. L. Jansen, and K. L. Brouwer. Altered hepatobiliary disposition of acetaminophen glucuronide in isolated perfused livers from multidrug resistance-associated protein 2-deficient TR(-) rats. *J Pharmacol Exp Ther* **295**: 512-8 (2000).

26. M. J. Zamek-Gliszczynski, K. A. Hoffmaster, K. Nezasa, M. N. Tallman, and K. L. Brouwer. Integration of hepatic drug transporters and phase II metabolizing enzymes: mechanisms of hepatic excretion of sulfate, glucuronide, and glutathione metabolites. *Eur J Pharm Sci* **27**: 447-86 (2006).

27. M. D. Miller AA, Owzar K, Hollis DR, Abou-Alfa GK, Desai A, Hwang J, Villalona-Calero M, Dees EC, Lewis LD, Ratain MJ. Pharmacokinetic (PK) and phase I study of sorafenib (S) for solid tumors and hematologic malignancies in patients with hepatic or renal dysfunction (HD or RD): CALGB 60301. 2007 ASCO Annual Meeting Proceedings Part I. *Journal of Clinical Oncology* **25**: (2007).

28. J. H. Shon, Y. R. Yoon, W. S. Hong, P. M. Nguyen, S. S. Lee, Y. G. Choi, I. J. Cha, and J. G. Shin. Effect of itraconazole on the pharmacokinetics

and pharmacodynamics of fexofenadine in relation to the MDR1 genetic polymorphism. *Clin Pharmacol Ther* **78**: 191-201 (2005).

29. M. Trauner, P. J. Meier, and J. L. Boyer. Molecular pathogenesis of cholestasis. *N Engl J Med* **339**: 1217-27 (1998).

30. G. Zollnerand M. Trauner. Mechanisms of cholestasis. *Clin Liver Dis* **12**: 1-26, vii (2008).

31. H. Kojima, A. T. Nies, J. Konig, W. Hagmann, H. Spring, M. Uemura, H. Fukui, and D. Keppler. Changes in the expression and localization of hepatocellular transporters and radixin in primary biliary cirrhosis. *J Hepatol* **39**: 693-702 (2003).

32. G. Zollner, P. Fickert, D. Silbert, A. Fuchsbichler, H. U. Marschall, K. Zatloukal, H. Denk, and M. Trauner. Adaptive changes in hepatobiliary transporter expression in primary biliary cirrhosis. *J Hepatol* **38**: 717-27 (2003).

33. G. Zollner, M. Wagner, P. Fickert, D. Silbert, J. Gumhold, K. Zatloukal, H. Denk, and M. Trauner. Expression of bile acid synthesis and detoxification enzymes and the alternative bile acid efflux pump MRP4 in patients with primary biliary cirrhosis. *Liver Int* **27**: 920-9 (2007).

34. R. H. Mathijssen, F. A. de Jong, R. H. van Schaik, E. R. Lepper, L. E. Friberg, T. Rietveld, P. de Bruijn, W. J. Graveland, W. D. Figg, J. Verweij, and A. Sparreboom. Prediction of irinotecan pharmacokinetics by use of cytochrome P450 3A4 phenotyping probes. *J Natl Cancer Inst* **96**: 1585-92 (2004).

35. L. P. Rivoryand P. B. Watkins. Erythromycin breath test. *Clin Pharmacol Ther* **70**: 395-9 (2001).

36. L. Sasongko, J. M. Link, M. Muzi, D. A. Mankoff, X. Yang, A. C. Collier, S. C. Shoner, and J. D. Unadkat. Imaging P-glycoprotein transport activity at the human blood-brain barrier with positron emission tomography. *Clin Pharmacol Ther* **77**: 503-14 (2005).

37. S. N. Barnes, L. M. Aleksunes, L. Augustine, G. L. Scheffer, M. J. Goedken, A. B. Jakowski, I. M. Pruimboom-Brees, N. J. Cherrington, and J. E. Manautou. Induction of hepatobiliary efflux transporters in acetaminophen-induced acute liver failure cases. *Drug Metab Dispos* **35**: 1963-9 (2007).

38. D. Schuppanand N. H. Afdhal. Liver cirrhosis. *Lancet* **371**: 838-51 (2008).

39. J. Konig, D. Rost, Y. Cui, and D. Keppler. Characterization of the human multidrug resistance protein isoform MRP3 localized to the basolateral hepatocyte membrane. *Hepatology* **29**: 1156-63 (1999).

40. M. Kuroda, Y. Kobayashi, Y. Tanaka, T. Itani, R. Mifuji, J. Araki, M. Kaito, and Y. Adachi. Increased hepatic and renal expressions of multidrug resistance-associated protein 3 in Eisai hyperbilirubinuria rats. *J Gastroenterol Hepatol* **19**: 146-53 (2004).

41. J. S. Lagas, M. L. Vlaming, O. van Tellingen, E. Wagenaar, R. S. Jansen, H. Rosing, J. H. Beijnen, and A. H. Schinkel. Multidrug resistance protein 2 is an important determinant of paclitaxel pharmacokinetics. *Clin Cancer Res* **12**: 6125-32 (2006).

42. M. L. Vlaming, K. Mohrmann, E. Wagenaar, D. R. de Waart, R. P. Elferink, J. S. Lagas, O. van Tellingen, L. D. Vainchtein, H. Rosing, J. H. Beijnen, J. H. Schellens, and A. H. Schinkel. Carcinogen and anticancer drug transport by Mrp2 in vivo: studies using Mrp2 (Abcc2) knockout mice. *J Pharmacol Exp Ther* **318**: 319-27 (2006).

43. M. J. Zamek-Gliszczynski, K. Nezasa, X. Tian, J. C. Kalvass, N. J. Patel, T. J. Raub, and K. L. Brouwer. The important role of Bcrp (Abcg2) in the biliary excretion of sulfate and glucuronide metabolites of acetaminophen, 4-methylumbelliferone, and harmol in mice. *Mol Pharmacol* **70**: 2127-33 (2006).

44. M. J. Zamek-Gliszczynski, K. A. Hoffmaster, K. Nezasa, and K. L. Brouwer. Apparent differences in mechanisms of harmol sulfate biliary excretion in mice and rats. *Drug Metab Dispos* **36**: 2156-8 (2008).

45. C. Zimmermann, K. van de Wetering, E. van de Steeg, E. Wagenaar, C. Vens, and A. H. Schinkel. Species-dependent transport and modulation properties of human and mouse multidrug resistance protein 2 (MRP2/Mrp2, ABCC2/Abcc2). *Drug Metab Dispos* **36**: 631-40 (2008).

46. A. T. Niesand D. Keppler. The apical conjugate efflux pump ABCC2 (MRP2). *Pflugers Arch* **453**: 643-59 (2007).

47. K. Ito, C. J. Oleschuk, C. Westlake, M. Z. Vasa, R. G. Deeley, and S. P. Cole. Mutation of Trp1254 in the multispecific organic anion transporter, multidrug resistance protein 2 (MRP2) (ABCC2), alters substrate specificity and results in loss of methotrexate transport activity. *J Biol Chem* **276**: 38108-14 (2001).

48. B. Swift, X. Tian, and K. L. Brouwer. Integration of preclinical and clinical data with pharmacokinetic modeling and simulation to evaluate

fexofenadine as a probe for hepatobiliary transport function. *Pharm Res* **26**: 1942-51 (2009).

49. N. Li, Y. Zhang, F. Hua, and Y. Lai. Absolute difference of hepatobiliary transporter multidrug resistance-associated protein (MRP2/Mrp2) in liver tissues and isolated hepatocytes from rat, dog, monkey, and human. *Drug Metab Dispos* **37**: 66-73 (2009).

50. N. Li, Y. A. Bi, D. B. Duignan, and Y. Lai. Quantitative expression profile of hepatobiliary transporters in sandwich cultured rat and human hepatocytes. *Mol Pharm* **6**: 1180-9 (2009).

51. M. J. Zamek-Gliszczynski, K. A. Hoffmaster, X. Tian, R. Zhao, J. W. Polli, J. E. Humphreys, L. O. Webster, A. S. Bridges, J. C. Kalvass, and K. L. Brouwer. Multiple mechanisms are involved in the biliary excretion of acetaminophen sulfate in the rat: role of Mrp2 and Bcrp1. *Drug Metab Dispos* **33**: 1158-65 (2005).

52. K. S. Jayasinghe, C. J. Roberts, and A. E. Read. Is biliary excretion of paracetamol significant in man? *Br J Clin Pharmacol* **22**: 363-6 (1986).

53. C. P. Siegers, W. Loeser, J. Gieselmann, and D. Oltmanns. Biliary and renal excretion of paracetamol in man. *Pharmacology* **29**: 301-3 (1984).

54. K. Kobayashi, Y. Sogame, H. Hara, and K. Hayashi. Mechanism of glutathione S-conjugate transport in canalicular and basolateral rat liver plasma membranes. *J Biol Chem* **265**: 7737-41 (1990).

55. T. Watanabe, H. Kusuhara, K. Maeda, Y. Shitara, and Y. Sugiyama. Physiologically based pharmacokinetic modeling to predict transporter-mediated clearance and distribution of pravastatin in humans. *J Pharmacol Exp Ther* **328**: 652-62 (2009).

56. C. J. Endres, P. Hsiao, F. S. Chung, and J. D. Unadkat. The role of transporters in drug interactions. *Eur J Pharm Sci* **27**: 501-17 (2006).

57. J. Mwinyi, A. Johne, S. Bauer, I. Roots, and T. Gerloff. Evidence for inverse effects of OATP-C (SLC21A6) 5 and 1b haplotypes on pravastatin kinetics. *Clin Pharmacol Ther* **75**: 415-21 (2004).

58. M. Niemi, E. Schaeffeler, T. Lang, M. F. Fromm, M. Neuvonen, C. Kyrklund, J. T. Backman, R. Kerb, M. Schwab, P. J. Neuvonen, M. Eichelbaum, and K. T. Kivisto. High plasma pravastatin concentrations are associated with single nucleotide polymorphisms and haplotypes of organic anion transporting polypeptide-C (OATP-C, SLCO1B1). *Pharmacogenetics* **14**: 429-40 (2004).

59. Y. Nishizato, I. Ieiri, H. Suzuki, M. Kimura, K. Kawabata, T. Hirota, H. Takane, S. Irie, H. Kusuhara, Y. Urasaki, A. Urae, S. Higuchi, K. Otsubo, and Y. Sugiyama. Polymorphisms of OATP-C (SLC21A6) and OAT3 (SLC22A8) genes: consequences for pravastatin pharmacokinetics. *Clin Pharmacol Ther* **73**: 554-65 (2003).

60. M. Niemi, P. J. Neuvonen, U. Hofmann, J. T. Backman, M. Schwab, D. Lutjohann, K. von Bergmann, M. Eichelbaum, and K. T. Kivisto. Acute effects of pravastatin on cholesterol synthesis are associated with SLCO1B1 (encoding OATP1B1) haplotype *17. *Pharmacogenet Genomics* **15**: 303-9 (2005).

61. R. Tachibana-Iimori, Y. Tabara, H. Kusuhara, K. Kohara, R. Kawamoto, J. Nakura, K. Tokunaga, I. Kondo, Y. Sugiyama, and T. Miki. Effect of genetic polymorphism of OATP-C (SLCO1B1) on lipid-lowering response to HMG-CoA reductase inhibitors. *Drug Metab Pharmacokinet* **19**: 375-80 (2004).

62. H. Takane, M. Miyata, N. Burioka, C. Shigemasa, E. Shimizu, K. Otsubo, and I. Ieiri. Pharmacogenetic determinants of variability in lipid-lowering response to pravastatin therapy. *J Hum Genet* **51**: 822-6 (2006).

63. M. Hirano, K. Maeda, H. Hayashi, H. Kusuhara, and Y. Sugiyama. Bile salt export pump (BSEP/ABCB11) can transport a nonbile acid substrate, pravastatin. *J Pharmacol Exp Ther* **314**: 876-82 (2005).

64. S. Matsushima, K. Maeda, C. Kondo, M. Hirano, M. Sasaki, H. Suzuki, and Y. Sugiyama. Identification of the hepatic efflux transporters of organic anions using double-transfected Madin-Darby canine kidney II cells expressing human organic anion-transporting polypeptide 1B1 (OATP1B1)/multidrug resistance-associated protein 2, OATP1B1/multidrug resistance 1, and OATP1B1/breast cancer resistance protein. *J Pharmacol Exp Ther* **314**: 1059-67 (2005).

65. M. Hasegawa, H. Kusuhara, D. Sugiyama, K. Ito, S. Ueda, H. Endou, and Y. Sugiyama. Functional involvement of rat organic anion transporter 3 (rOat3; Slc22a8) in the renal uptake of organic anions. *J Pharmacol Exp Ther* **300**: 746-53 (2002).

66. B. Hsiang, Y. Zhu, Z. Wang, Y. Wu, V. Sasseville, W. P. Yang, and T. G. Kirchgessner. A novel human hepatic organic anion transporting polypeptide (OATP2). Identification of a liver-specific human organic anion transporting polypeptide and identification of rat and human hydroxymethylglutaryl-CoA reductase inhibitor transporters. *J Biol Chem* **274**: 37161-8 (1999).

67. D. Kobayashi, T. Nozawa, K. Imai, J. Nezu, A. Tsuji, and I. Tamai. Involvement of human organic anion transporting polypeptide OATP-B (SLC21A9) in pH-dependent transport across intestinal apical membrane. *J Pharmacol Exp Ther* **306**: 703-8 (2003).

68. R. H. Ho, L. Choi, W. Lee, G. Mayo, U. I. Schwarz, R. G. Tirona, D. G. Bailey, C. Michael Stein, and R. B. Kim. Effect of drug transporter genotypes on pravastatin disposition in European- and African-American participants. *Pharmacogenet Genomics* **17**: 647-56 (2007).

APPENDIX A

Influence of Seeding Density and Extracellular Matrix on Bile Acid Transport and Mrp4 Expression in Sandwich-Cultured Mouse Hepatocytes

This chapter has been accepted for publication in Molecular Pharmaceutics and is presented in the style of that journal.

Abstract

This study was undertaken to examine the influence of seeding density, extracellular matrix and days in culture on bile acid transport proteins and hepatobiliary disposition of the model bile acid taurocholate. Mouse hepatocytes were cultured in a sandwich configuration on six-well Biocoat™ plates with an overlay of Matigel™ (BC/MG) or gelled-collagen (BC/GC) for 3 or 4 days at seeding densities of 1.0, 1.25 or 1.5 x 10^6 cells/well. The lower seeding densities of 1.0 and 1.25 x 10^6 cells/well resulted in good hepatocyte morphology and bile canalicular network formation, as visualized by 5- (and 6)-carboxy-2',7'dichlorofluorescein accumulation. In general, taurocholate cellular accumulation tended to increase as a function of seeding density in BC/GC; cellular accumulation was significantly increased in hepatocytes cultured in BC/MG compared to BC/GC at the same seeding density on both days 3 and 4 of culture. *In vitro* intrinsic biliary clearance of taurocholate was increased significantly in hepatocytes seeded at 1.0 x 10^6 cells/well compared to 1.5 x 10^6 cells/well on day 4 of culture. Levels of bile acid transport proteins on days 3 and 4 were not markedly influenced by seeding density or extracellular matrix except for multidrug resistance protein 4 (Mrp4), which was inversely related to seeding density. Mrp4 levels decreased ~2- to 3-fold between seeding densities of 1.0 x 10^6 and 1.25 x 10^6 cells/well regardless of extracellular matrix; an additional ~3- to 5-fold decrease in Mrp4 protein was noted in BC/GC between seeding densities of 1.25 x 10^6 and 1.5 x 10^6 cells/well. Results suggest that seeding density, extracellular matrix and days in culture profoundly influence Mrp4

expression in sandwich-cultured mouse hepatocytes. Primary mouse hepatocytes seeded in a BC/MG configuration at densities of 1.25 x 10^6 cells/well and 1.0 x 10^6, and cultured for 3 days, yielded optimal transport based on the probes studied. This work demonstrates the applicability of the sandwich-cultured model to mouse hepatocytes.

Introduction

Primary hepatocytes are a widely accepted *in vitro* tool to evaluate hepatic drug uptake, metabolism and cytochrome P450 induction. Maintaining hepatocytes between two layers of gelled collagen (sandwich-culture configuration) facilitates the development of intact canalicular networks, reestablishment of polarized excretory function and maintenance of hepatic transport protein expression and function [1-5]. Dunn et al. first demonstrated that the sandwich configuration enhanced the morphology and viability of hepatocytes, and helped maintain normal secretion of many liver-specific proteins and organic compounds [6-8]. Subsequent studies have demonstrated that the sandwich configuration facilitates the formation of gap junctions and functional bile canalicular networks during culture [2, 3]. Several studies also have shown that sandwich-cultured hepatocytes are capable of performing a wide variety of cellular functions normally attributed to hepatocytes *in vivo* including albumin secretion, bile acid synthesis and excretion, and P450 enzyme induction, especially when compared to hepatocytes cultured under conventional conditions [2, 3, 8-11].

Sandwich-cultured hepatocytes have been used to investigate hepatic accumulation and excretion of a wide variety of substrates [12-14]. In fact, the *in vitro* intrinsic biliary clearance generated from the sandwich-cultured hepatocyte model has been shown to correlate with *in vivo* biliary clearance data in rats [15, 16] and humans [17, 18]. Thus, the sandwich-cultured hepatocyte model is very

promising for characterizing biliary excretion and the hepatic disposition of drug candidates. With all relevant hepatic transport proteins and xenobiotic metabolizing enzymes expressed, substrate uptake, metabolism, and parent/metabolite efflux can be assessed. Recent work has demonstrated that sandwich-cultured primary mouse hepatocytes maintain metabolic competence longer than rat hepatocytes based on gene expression profiles and cytochrome P450 activity [19]. Furthermore, the application of this method to hepatocytes from gene-disrupted mice in which specific transport proteins have been knocked out may provide new insight into the many roles of hepatic transport proteins. Numerous investigators have examined the influence of culture conditions on hepatic transport protein expression and function in sandwich-cultured rat and human hepatocytes [9, 20-23]. However, culture conditions have not been optimized for transport protein expression and function in sandwich-cultured mouse hepatoctyes. As interest grows in utilizing the phenotypic diversity of various mouse strains (*e.g.,* the Collaborative Cross [24]) to predict drug-induced hepatotoxicity, higher throughput screening systems, such as sandwich-cultured mouse hepatocytes, may prove to be particularly useful.

Hepatic transport proteins play an important role in the vectorial transport of bile acids from sinusoidal blood into the bile canaliculi. Sodium taurocholate cotransporting polypeptide (Ntcp) is expressed exclusively in the liver and mediates sodium-dependent uptake of bile acids [25, 26]. The organic anion-transporting polypeptides (Oatps), also localized on the basolateral membrane, translocate bile acids in a sodium-independent manner [26]. The multidrug

resistance proteins 3 and 4 (Mrp3 and Mrp4) are involved in the basolateral excretion of bile acids from the hepatocyte across the sinusoidal membrane into blood [27-29]. In addition, data generated in mice deficient in the organic solute transporter (Ost)-α subunit have suggested that Ostα-Ostβ, a heteromeric organic solute and steroid transporter, also is involved in the basolateral efflux of bile acids [30]. The apical (canalicular) transport proteins involved in biliary excretion of bile acids include the bile salt export pump (Bsep) [31], the multidrug resistance protein 2 (Mrp2) [32, 33] and more recently, multidrug resistance P-glycoprotein (Mdr1a/1b) [34]. Interestingly, triple knockout mice deficient in Mdr1a/1b and Bsep exhibited a significantly more severe phenotype than *bsep*$^{-/-}$ and wild-type mice, including impaired bile formation, jaundice, flaccid gallbladder and hepatic inflammation [34].

The purpose of the present studies was to examine the influence of seeding density, extracellular matrix and days in culture on hepatic bile acid transport protein expression and taurocholate hepatobiliary disposition. The criteria used for the selection of optimal conditions were hepatocyte morphology, transport protein expression, substrate accumulation, as well as the biliary excretion index (BEI) and biliary clearance (*in vitro* $Cl_{biliary}$) of taurocholate.

Experimental Details

Materials. Dulbecco's modified Eagle's medium (DMEM), MEM non-essential amino acids solution (100x), L-glutamine, insulin, penicillin G-streptomycin solution, and 5- (and 6)-carboxy-2',7'dichlorofluorescein (CDF) diacetate (CDFDA) were purchased from Invitrogen (Carlsbad, CA). Collagenase (type 4), fetal bovine serum (FBS), sodium taurocholate, Triton X-100, dexamethasone, and Hanks' balanced salt solution (HBSS) modified with (H-1387) or without (H-4891) calcium chloride were obtained from Sigma-Aldrich (St. Louis, MO). BioCoat™ collagen I plates, Matrigel™ basement membrane matrix, rat tail collagen (type I), and ITS+™ (insulin/transferrin/selenium) culture supplement were purchased from BD Biosciences Discovery Labware (Bedford, MA). [^{3}H]Taurocholate (5 Ci/mmol, >97% purity) was obtained from PerkinElmer Life and Analytical Sciences (Boston, MA). Bio-Safe II™ liquid scintillation cocktail was obtained from Research Products International (Mt. Prospect, IL). Bicinchoninic acid (BCA) protein assay reagents and BSA for the protein assay standard were purchased from Pierce Chemical Co. (Rockford, IL). All other chemicals and reagents were of analytical grade and available from commercial sources.

Isolation and *In Vitro* Culture of Primary Mouse Hepatocytes

Male C57BL/6 mice (27.7-30.3 g) were purchased from Charles River Laboratories, Inc. (Raleigh, NC). Mice had free access to water and food prior to surgery. All animal procedures complied with the guidelines of the Institutional

Animal Care and Use Committee (University of North Carolina, Chapel Hill, NC). Hepatocytes were isolated by a two-step collagenase perfusion, as described previously [35], with modifications. The inferior vena cava was cannulated and buffers were perfused retrograde to blood flow. Cell viability, determined by trypan blue exclusion, was 89–93%. In pilot studies, hepatocytes were seeded on six-well plates with gelled collagen solution, as described previously [21], or six-well Biocoat™ plates. In subsequent studies, hepatocytes were seeded at 1.0, 1.25 or 1.5 x 10^6 cells/well in 6-well BioCoat™ plates in DMEM without phenol red supplemented with 2 mM L-glutamine, 1% (v/v) MEM non-essential amino acids, 100 units penicillin G sodium, 100 µg streptomycin sulfate, 1 µM dexamethasone, 5% (v/v) FBS, and 10 µM insulin (day 0 of culture), and allowed to attach for 2-6 h in a humidified incubator (95% O_2, 5% CO_2) at 37°C. After cell attachment, culture plates were swirled gently and the culture medium was replaced with the same medium. Cells were overlaid 16-24 h (day 1 of culture) after seeding with ice-cold Matrigel™ basement membrane matrix (BC/MG) or gelled collagen (BC/GC). Matrigel was overlaid at a concentration of 0.25 mg/mL in 2 mL/well cold serum-free DMEM containing 2 mM L-glutamine, 1% (v/v) MEM non-essential amino acids, 100 units penicillin G sodium, 100 µg streptomycin sulfate, 0.1 µM dexamethasone, and 1% (v/v) ITS+™. Gelled collagen solution (~1.5 mg/mL) was prepared by adding 4 mL of rat tail type I collagen, 4 mL sterile deionized water, and 1 mL of 10X DMEM, and the pH was adjusted to 7.4 with 2N NaOH. Hepatocyte cultures were aspirated and the monolayer was overlaid with 0.1 mL/well of ice-cold neutralized type I gelled

collagen and placed at 37°C in a humidified incubator for ~1 hour to allow the matrix to gel, followed by the addition of 1.5 mL/well of warm DMEM with the same supplements as the cells overlaid with matrigel. The culture medium was changed every 24 h until experiments were performed on day 3-4 of culture.

Accumulation Experiments

The method to determine substrate accumulation in sandwich-cultured hepatocytes has been described previously [16]. Briefly, hepatocytes were rinsed twice with 2 mL warm HBSS containing Ca^{2+} (standard buffer) or Ca^{2+}-free HBSS, and incubated with 2 mL of the same buffer for 10 min at 37°C to maintain tight junction integrity and bile canalicular networks (cells+bile), or disrupt tight junctions and open bile canalicular networks (cells), respectively. The buffer was removed, and the cells were incubated for 10 min at 37°C with 1.5 mL of [^{3}H]taurocholate (1 μM) or CDFDA (2 μM) in standard buffer. Hepatocytes were rinsed vigorously three times with 2 mL ice-cold standard buffer following the incubation. CDFDA-treated hepatocytes were viewed immediately and digital images captured with a Zeiss Axiovert 200TV inverted phase contrast microscope. Taurocholate-treated hepatocytes were lysed with 1 mL 0.5% (v/v) Triton X-100 in phosphate-buffered saline by placing plates on an orbital shaker for a minimum of 20 min at room temperature. Taurocholate uptake was corrected for nonspecific binding by subtracting uptake on blank six-well Biocoat™ plates overlaid with Matrigel™ or gelled collagen. Data were normalized to protein concentration in each well, determined in duplicate aliquots

using BCA protein assay reagent kit (Pierce) as instructed by the manufacturer. BSA, as supplied by the manufacturer, was used as a standard (0.2–2 mg/mL). The [^{3}H]taurocholate samples were analyzed by liquid scintillation spectroscopy in a Packard Tri-Carb scintillation counter (PerkinElmer Life and Analytical Sciences).

Cytotoxicity Assay.

The activity of lactate dehydrogenase (LDH), a stable cytosolic enzyme that is released upon cell lysis, was measured in the medium of sandwich-cultured hepatocytes using a cytotoxicity kit according to the manufacturer's instructions (Roche, Indianapolis, IN). The degree of LDH release was expressed as a percentage of the maximum cellular LDH release, measured by adding 0.5% Triton X-100 to sandwich-cultured mouse hepatocytes at each seeding density.

Immunoblots.

Cells were washed once with HBSS, and resuspended in lysis buffer consisting of 1% SDS, 1 mM EDTA and Complete protease inhibitor cocktail tablets (Roche Diagnostics, Mannheim, Germany). Protein concentrations were determined by the BCA assay. Whole-cell lysates (30-40 µg) were resolved on NuPAGE 4 to 20% Bis-Tris gel (Invitrogen Corp, Carlsbad, CA) and the proteins were transferred to polyvinylidene difluoride (PVDF) membranes. After blocking in 5% milk-Tris-buffered saline with Tween 20 (TBST) for 30 min, blots were incubated overnight at 4°C with the following antibodies: Mrp2 (*Abcc2*; M2III-6), Mrp3

(*Abcc3*; M3II-21), Mrp4 (*Abcc4*; M4I-10), Mdr1a/1b (*Abcb1*; C-219), Breast cancer resistance protein [Bcrp (*Abcg2*); BXP-53], which were supplied by Alexis Biochemicals, San Diego, CA; Bsep (*Abcb11*; K44) and Ntcp (*Slc10a1*; K4), which were a kind gift from Drs. Bruno Stieger and Peter Meier; and β-actin (C4, Chemicon, San Francisco, CA). After incubation with HRP-conjugated secondary antibody, signals were detected by chemiluminescent substrate Supersignal West Dura (Pierce, Rockford, IL) with a Bio-Rad VersaDoc imaging system; densitometry analysis was performed using Quantity One v4.1 software (Bio-Rad Laboratories, Hercules, CA).

Data Analysis

For accumulation studies, the biliary excretion index (BEI, %) and *in vitro* intrinsic biliary clearance ($CL_{biliary}$, mL/min/kg) were calculated using B-CLEAR® technology (Qualyst, Inc., Raleigh, NC;[16]):

$$BEI = \frac{Accumulation_{Cells+Bile} - Accumulation_{Cells}}{Accumulation_{Cells+Bile}} \times 100 \quad (1)$$

where substrate accumulation in the cells+bile compartments was determined in hepatocytes preincubated in standard buffer; cellular accumulation of substrate was determined in hepatocytes preincubated with Ca^{2+}-free HBSS.

$$\textit{In Vitro}\ Cl_{biliary} = \frac{Accumulation_{Cells+Bile} - Accumulation_{Cells}}{AUC_{0-T}} \quad (2)$$

where $AUC_{0\text{-}T}$ represents the product of the incubation time (T) and the initial taurocholate concentration in the medium. *In vitro* $Cl_{biliary}$ values were scaled per kilogram body weight using 0.63, 0.72 and 0.78 mg protein per 1.0, 1.25, and 1.5 x 10^6 cells, respectively (the average value obtained in all preparations), 135 x 10^6 hepatocytes/g of mouse liver tissue [36], and 87.5 g of liver tissue per kg of body weight (1.75 g/ 0.02 kg mouse) [37].

Statistical analysis of the [^{3}H]taurocholate cellular accumulation and *in vitro* intrinsic biliary clearance data was performed using a three-way analysis of variance for the factors of day in culture, seeding density and extracellular matrix, with Bonferroni's post hoc test (SAS version 9.1, Cary, NC).

Results

Sandwich-Cultured Mouse Hepatocyte Viability and Bile Canalicular Network Formation

Initial experiments plating mouse hepatocytes on gelled collagen plates resulted in decreased attachment and adherence after overlay compared to Biocoat™ plates. Therefore, subsequent experiments utilized Biocoat™ plates only, on which hepatocytes flattened to form confluent monolayers. Hepatocyte morphology was evaluated by light microscopy, and canalicular network formation was determined by CDF imaging. Mouse hepatocytes cultured in sandwich-configuration and maintained in DMEM for up to 4 days were cuboidal in shape and formed extensive canalicular networks (Fig. A.1.1 and A.1.2). The intensity of CDF accumulation in the bile canaliculi appeared to be more extensive in mouse hepatocytes cultured in the BC/GC configuration compared to the BC/MG configuration based on visual inspection; the BC/MG matrix appeared to have greater intracellular accumulation of CDF compared to BC/GC. Based on the light microscopy images, the higher seeding density of 1.5×10^6 cells/well resulted in greater accumulation of dead cells and debris compared to the lower seeding densities (Fig. A.1.1 and A.1.2). Based on LDH leakage, cell death primarily occurred in the first 24 hr before overlay; medium LDH levels during the first 24 hr after plating reached ~25% of Triton X-100 control. Cumulative LDH leakage after overlay through day 4 in culture was negligible (<

12% of Triton X-100 control), regardless of seeding density or extracellular matrix (data not shown).

Transport Protein Expression

Representative immunoblots of Ntcp, Mrp4, Mrp3, Mrp2, Bsep, Bcrp, and Mdr1a/1b in sandwich-cultured mouse hepatocytes seeded at different densities on BC/MG and BC/GC are shown in Figure A.1.3. Relevant bile acid transport proteins were expressed in sandwich-cultured mouse hepatocytes by day 3; culture configuration and seeding density had modest effects on Mrp3, Mrp2, Bcrp, Ntcp Mdr1a/1b or Bsep protein. Interestingly, Mrp4 protein increased (~2-fold or greater) as seeding density decreased, regardless of extracellular matrix on both day 3 and 4 (Fig. A.1.3 and A.1.4).

Hepatobiliary Disposition of the Model Bile Acid Taurocholate

The influence of seeding density, overlay matrix composition and days in culture on the accumulation and biliary excretion of [^{3}H]taurocholate was assessed in sandwich-cultured mouse hepatocytes. Cellular accumulation of [^{3}H]taurocholate was significantly lower on day 4 compared to day 3 (Fig. A.1.5). [^{3}H]Taurocholate cellular accumulation tended to increase as a function of seeding density for BC/GC; [^{3}H]taurocholate cellular accumulation was significantly greater in mouse hepatocytes cultured in the BC/MG configuration compared to the BC/GC configuration at each seeding density on both days 3

and 4 of culture (Fig. A.1.5). *In vitro* intrinsic biliary clearance of taurocholate significantly increased comparing 1.0 x 10^6 cells/well to 1.5 x 10^6 cells/well, taurocholate BEI values were not significantly different across seeding density (Table A.1.1).

Discussion

Sandwich-cultured primary hepatocytes have been used extensively to study hepatic uptake, metabolism and efflux. To date, limited data have been published utilizing sandwich-cultured mouse hepatocytes to study hepatic transport mechanisms and biliary excretion. Previous reports have demonstrated the influence of culture conditions including the type of culture media, media supplements, extracellular matrix and confluency on cell morphology, bile canalicular network formation, substrate accumulation and BEI in both rat and cryopreserved human hepatoctyes [20-22]. In the present study, the influence of seeding density, extracellular matrix and days in culture on protein levels of bile acid transporters, and the hepatobiliary disposition of taurocholate in sandwich-cultured mouse hepatocytes were assessed.

Both extracellular matrix overlay and seeding density had profound effects on the health, morphology, and bile canalicular network formation of sandwich-cultured mouse hepatocytes. The cell morphology of mouse hepatocytes cultured on Biocoat™ plates was similar to prior observations with rat hepatocytes; cells spread out to form a confluent monolayer resulting in a flattened appearance on this rigid collagen when compared to hepatocytes cultured on gelled collagen [2, 22]. Mouse hepatocytes overlaid with Matrigel™ (BC/MG) exhibited a similar attachment efficiency and cell morphology compared to those overlaid with gelled collagen (BC/GC). However, Matrigel™ provides a more uniform, reproducible overlay. CDFDA, which is hydrolyzed to fluorescent

CDF inside hepatocytes, is a good Mrp2 probe substrate [38] that has been used extensively to visualize the bile canaliculi [2, 20, 21]. CDF was excreted into bile canaliculi in all culture conditions. However, more CDF accumulation in bile canalicular networks was observed by fluorescense microscopy in BC/GC compared to BC/MG at lower seeding densities, which may be attributed to more extensive formation of bile canalicular networks (Fig. A.1.1 and A.1.2). Although levels of Mrp2 protein were similar across extracellular matrix and days in culture (Fig. A.1.3), differences in the amount of functional Mrp2 protein on the apical membrane also may contribute to the increased accumulation of CDF in bile canalicular networks observed at the lower seeding densities. Furthermore, CDF intracellular accumulation was greater in mouse hepatocytes cultured on BC/MG compared to BC/GC based on visual inspection of the fluorescent images (Fig. A.1.1 and A.1.2); similar findings were noted for taurocholate cellular accumulation (Fig. A.1.5).

Mouse hepatocytes seeded at 1.5 x 10^6 cells/well resulted in greater accumulation of dead cells and decreased network formation, as visualized by CDF. Cell death occurred primarily during the first day of culture, shortly after hepatocytes were seeded, based on LDH measurements. Most of the unattached and dead cells were washed away when the medium was changed at 24 hr, prior to overlay, but some cell debris presumably was stuck to the collagen, as visualized in Fig. A.1.1 and A.1.2. The cell death observed in this study may be attributed primarily to collagenase digestion used during hepatocyte isolation, which has been shown by many investigators to influence

cell viability [39-42], and cannot be explained by complete consumption of nutrients or growth factors in the cell medium. Greater cell death at higher seeding densities was similar to findings observed in mouse hepatocytes cultured at an overconfluent stage, which resulted in cell death by apoptosis [43]. The observation that mouse hepatocytes perform better at a lower seeding density compared to other species (rat and human hepatocytes typically are seeded at ~1.75 x 10^6 cells/well on 6-well plates [44, 45]) may be attributed to the increased oxygen demand *in vivo* in mice (liver blood flow in mice is ~90 ml/min/kg compared to ~55.2 and ~20.7 ml/min/kg in rats and humans, respectively [37].

Overlay matrix composition (BC/MG or BC/GC) and days in culture (day 3 or 4) appeared to have little effect on protein levels of Bsep, Bcrp, Ntcp, Mrp3, Mrp2 and Mdr1a/1b in sandwich-cultured mouse hepatocytes. Surprisingly, protein levels of Ntcp were well-maintained compared to sandwich-cultured rat hepatocytes, where significant down-regulation of Ntcp protein [3] (~80% decrease [46]) and a ~75-80% decrease in mRNA [47] have been reported over days in culture.

Another profound observation noted in the present studies was that Mrp4 protein levels were higher at lower seeding densities (Fig. A.1.3 and A.1.4). Mrp4 is localized on the basolateral membrane of hepatocytes and has been shown to efflux bile acids in a glutathione-dependent manner [28]. Mrp4 plays an important role in detoxifying the liver; bile-duct ligated *Mrp4*$^{-/-}$ mice exhibited increased liver toxicity based on histological analysis, with a 4-fold decrease in

serum bile acid concentrations and increased serum liver enzymes, compared to bile duct-ligated wild-type mice [48]. Although, levels of the basolateral efflux transport protein Mrp3 were increased modestly in common bile duct-ligated mice compared to sham-operated controls [49], in bile duct-ligated mice lacking Mrp3, serum and liver bile acid concentrations were similar compared to sham-operated wild-type controls [50, 51]. Furthermore, Mrp4 protein was increased more than 2-fold in bile duct-ligated wild-type mice while Mrp3 protein was unchanged compared to sham-operated wild-type controls [48]. As an adaptive response to cholestasis, Mrp3 and Mrp4 are upregulated to efflux bile acids across the basolateral membrane, thereby reducing intracellular accumulation of bile acids in hepatocytes and subsequent toxicity due to the detergent effects on the cell membrane and resulting mitochondrial dysfunction [52, 53]. When mouse hepatocytes were seeded at 1 x 10^6 cells/well, less bile canalicular networks formed compared to those seeded at 1.25 x 10^6 cells/well (Fig. A.1.1 and A.1.2), potentially leading to increased hepatocellular accumulation of endogenous bile acids and upregulation of Mrp4 as a compensatory mechanism; no change in Mrp3 protein was observed in sandwich-cultured mouse hepatocytes across extracellular matrix and days in culture (Fig. A.1.3).

Taurocholate accumulation in mouse hepatocytes cultured on both BC/MG and BC/GC supported the observation that Mrp4 protein decreased as a function of increased seeding density (Fig. A.1.4 and A.1.5). Clearly, on day 4 of culture, cellular accumulation (white bars) of [^{3}H]taurocholate increased from 93.6 to 121 pmol/mg protein in BC/MG, and from 49.2 to 83.0 pmol/mg protein in

BC/GC in mouse hepatocytes seeded at 1.0 x 10^6 and 1.5 x 10^6 cells/well, respectively (Fig. A.1.5). This could not be attributed to differences in the primary bile acid transport proteins because total protein levels of Ntcp, Mdr1a/1b and Bsep were similar across seeding density and collagen matrix (Fig. A.1.4). However, Mrp4 was decreased ~3-fold when mouse hepatocytes were seeded at a density of 1.0 x 10^6 cells/well compared to 1.25 x 10^6 cells/well on BC/MG, and decreased ~8-fold when mouse hepatocytes were seeded at a density of 1.0 x 10^6 cells/well compared to 1.5 x 10^6 cells/well on BC/GC (Fig. A.1.4). Perhaps the increased Mrp4 expression at lower seeding densities resulted in redirection of some taurocholate excretion across the basolateral rather than the canalicular membrane, thus reducing the cellular accumulation of taurocholate compared to the higher seeding density in which Mrp4 expression was ~3- to 8-fold lower and cellular accumulation was higher (Table A.1.1, Fig. A.1.4). Furthermore, the cellular accumulation of [^{3}H]taurocholate in BC/MG was higher than BC/GC for all seeding densities, whereas Mrp4 protein was lower in BC/MG compared to BC/GC for all seeding densities.

The hepatocyte accumulation of [^{3}H]taurocholate in sandwich-cultured mouse hepatocytes was increased when compared to sandwich-cultured rat and human hepatocytes. The cellular accumulation of taurocholate on day 3 following a 10-min incubation with 1 μM [^{3}H]taurocholate in sandwich-cultured mouse hepatocytes seeded at 1.5 x 10^6 cells/well was 187 ± 16 and 116 ± 3 pmol/mg protein on BC/MG and BC/GC, respectively (Fig. A.1.5). This was much greater than the reported cellular accumulation of taurocholate on day 4

following a 10-min incubation with 1 μM [^{3}H]taurocholate in sandwich-cultured rat hepatocytes on BC/MG and BC/GC (<10[44, 54] and ~50[16] pmol/mg protein, respectively), or day 7 sandwich-cultured human hepatocytes (67.0 ± 25.0[18] and 65.8 ± 11.3[55] pmol/mg protein, both cultured on BC/MG). The *in vitro* intrinsic biliary clearance also was greater in mouse sandwich-cultured hepatocytes relative to rat and human sandwich-cultured hepatocytes. On day 3, the *in vitro* $Cl_{biliary}$ in mouse sandwich-cultured hepatocytes seeded at 1.5 x 10^6 cells/well on BC/MG and BC/GC, was 73.7 ± 24.6 and 96 ± 21.1 mL/min/kg, respectively, compared to 34.9 ± 12.0[44] and ~55[16] mL/min/kg, respectively, in day 4 rat sandwich-cultured hepatocytes, and 15.8 ± 4.5[18] and 15.2 ± 5.0[55] mL/min/kg (both cultured on BC/MG only) in day 7 human sandwich-cultured hepatocytes. The differences in taurocholate accumulation and *in vitro* intrinsic biliary clearance are controlled by the transport proteins responsible for uptake, biliary excretion and basolateral efflux of bile acids. The observed differences are not due to the affinity of these hepatic transport proteins for taurocholate in mouse compared to rat and human hepatocytes because the K_m values for NTCP/Ntcp, OATPs/Oatps and BSEP/Bsep are similar between species [48, 56-60]. K_m values have been reported for human MRP4 (25.8 μM) [27]. Therefore, the reason for greater taurocholate accumulation and *in vitro* intrinsic biliary clearance in sandwich-cultured mouse hepatocytes relative to sandwich-cultured rat and human hepatocytes may be attributed, in part, to maintenance of Ntcp and decreased Mrp4 (Fig. A.1.4) protein when seeded at 1.5 x 10^6 cells/well.

Alternatively, species-dependent differences in the taurocholate K_m for Mrp4 may exist.

Conclusion

In summary, extracellular matrix, seeding density and days in culture impact Mrp4 protein expression, bile canalicular network formation and taurocholate hepatobiliary disposition in sandwich-cultured primary mouse hepatocytes. Mouse hepatocytes seeded at densities of 1.25 x 10^6 cells/well, or below, resulted in improved attachment, more extensive bile canalicular network formation and overall healthier hepatocytes. Total protein levels of Mrp3, Mrp2, Ntcp, Bcrp, Mdr1a/1b and Bsep were similar across seeding density and collagen matrix. Taurocholate accumulation was greater in BC/MG compared to BC/GC, and tended to increase as a function of seeding density for BC/GC. *In vitro* intrinsic biliary clearance was significantly increased comparing 1.0 x 10^6 cells/well to 1.5 x 10^6 cells/well while taurocholate BEI trended to increase without reaching significance. Hepatocellular accumulation and *in vitro* intrinsic biliary clearance of taurocholate were greater on day 3 compared to day 4. CDF biliary excretion also was more extensive on day 3 compared to day 4 suggesting more extensive formation of bile canalicular networks. Primary mouse hepatocytes seeded in a BC/MG configuration at densities of 1.25 x 10^6 and 1.0 x 10^6 cells/well, and cultured for 3 days, yielded optimal transport based on the probes utilized in this study. This higher-throughput *in vitro* system could maximize the use of gene-disrupted mice from various strains to study hepatic

function and to investigate the influence of gene disruption on hepatobiliary drug/metabolite disposition and hepatotoxicity.

Abbreviations Used

Sodium taurocholate cotransporting polypeptide, Ntcp; multidrug resistance protein 4, Mrp4 multidrug resistance protein 3, Mrp3; organic solute transporter, Ost; bile salt export pump, Bsep; multidrug resistance protein 2, Mrp2; breast cancer resistance protein, Bcrp; multidrug resistance P-glycoprotein, Mdr1a/1b; Biliary excretion index, BEI; biliary clearance, *in vitro* $Cl_{biliary}$; Dulbecco's modified Eagle's medium, DMEM; 5- (and 6)-carboxy-2',7'dichlorofluorescein diacetate, CDFDA; fetal bovine serum, FBS; Hanks' balanced salt solution, HBSS; Bicinchoninic acid, BCA, Matrigel^{TM} basement membrane matrix, MG; gelled rat tail collagen type I, GC; polyvinylidene difluoride, PVDF; Tris-buffered saline with Tween 20, TBST.

Acknowledgements

The authors would like to thank Yiwei Rong, for her technical expertise in the isolation of mouse hepatocytes. We sincerely thank Drs. Bruno Stieger and Peter Meier for providing Ntcp and Bsep antibodies. This research was supported by a grant from the National Institutes of Health (R01 GM41935).

References

1. Hoffmaster, K. A.; Turncliff, R. Z.; LeCluyse, E. L.; Kim, R. B.; Meier, P. J.; Brouwer, K. L. R. P-glycoprotein expression, localization, and function in sandwich-cultured primary rat and human hepatocytes: relevance to the hepatobiliary disposition of a model opioid peptide. *Pharm Res* **2004,** 21, (7), 1294-302.

2. LeCluyse, E. L.; Audus, K. L.; Hochman, J. H. Formation of extensive canalicular networks by rat hepatocytes cultured in collagen-sandwich configuration. *Am J Physiol* **1994,** 266, (6 Pt 1), C1764-74.

3. Liu, X.; Brouwer, K. L.; Gan, L. S.; Brouwer, K. R.; Stieger, B.; Meier, P. J.; Audus, K. L.; LeCluyse, E. L. Partial maintenance of taurocholate uptake by adult rat hepatocytes cultured in a collagen sandwich configuration. *Pharm Res* **1998,** 15, (10), 1533-9.

4. Turncliff, R. Z.; Meier, P. J.; Brouwer, K. L. Effect of dexamethasone treatment on the expression and function of transport proteins in sandwich-cultured rat hepatocytes. *Drug Metab Dispos* **2004,** 32, (8), 834-9.

5. Zhang, P.; Tian, X.; Chandra, P.; Brouwer, K. L. R. Role of glycosylation in trafficking of Mrp2 in sandwich-cultured rat hepatocytes. *Mol Pharmacol* **2005,** 67, (4), 1334-41.

6. Dunn, J. C.; Tompkins, R. G.; Yarmush, M. L. Hepatocytes in collagen sandwich: evidence for transcriptional and translational regulation. *J Cell Biol* **1992,** 116, (4), 1043-53.

7. Dunn, J. C.; Yarmush, M. L.; Koebe, H. G.; Tompkins, R. G. Hepatocyte function and extracellular matrix geometry: long-term culture in a sandwich configuration. *Faseb J* **1989,** 3, (2), 174-7.

8. Dunn, J. C.; Tompkins, R. G.; Yarmush, M. L. Long-term in vitro function of adult hepatocytes in a collagen sandwich configuration. *Biotechnol Prog* **1991,** 7, (3), 237-45.

9. Turncliff, R. Z.; Meier, P. J.; Brouwer, K. L. R. Effect of dexamethasone treatment on the expression and function of transport proteins in sandwich-cultured rat hepatocytes. *Drug Metab Dispos* **2004,** 32, (8), 834-9.

10. Faucette, S. R.; Zhang, T. C.; Moore, R.; Sueyoshi, T.; Omiecinski, C. J.; LeCluyse, E. L.; Negishi, M.; Wang, H. Relative activation of human pregnane X receptor versus constitutive androstane receptor defines

distinct classes of CYP2B6 and CYP3A4 inducers. *J Pharmacol Exp Ther* **2007,** 320, (1), 72-80.

11. Sahi, J.; Shord, S. S.; Lindley, C.; Ferguson, S.; LeCluyse, E. L. Regulation of cytochrome P450 2C9 expression in primary cultures of human hepatocytes. *J Biochem Mol Toxicol* **2009,** 23, (1), 43-58.

12. Annaert, P. P.; Brouwer, K. L. Assessment of drug interactions in hepatobiliary transport using rhodamine 123 in sandwich-cultured rat hepatocytes. *Drug Metab Dispos* **2005,** 33, (3), 388-94.

13. Govindarajan, R.; Endres, C. J.; Whittington, D.; LeCluyse, E.; Pastor-Anglada, M.; Tse, C. M.; Unadkat, J. D. Expression and hepatobiliary transport characteristics of the concentrative and equilibrative nucleoside transporters in sandwich-cultured human hepatocytes. *Am J Physiol Gastrointest Liver Physiol* **2008,** 295, (3), G570-80.

14. Hoffmaster, K. A.; Zamek-Gliszczynski, M. J.; Pollack, G. M.; Brouwer, K. L. Multiple transport systems mediate the hepatic uptake and biliary excretion of the metabolically stable opioid peptide [D-penicillamine2,5]enkephalin. *Drug Metab Dispos* **2005,** 33, (2), 287-93.

15. Abe, K.; Bridges, A. S.; Yue, W.; Brouwer, K. L. In vitro biliary clearance of angiotensin II receptor blockers and 3-hydroxy-3-methylglutaryl-coenzyme A reductase inhibitors in sandwich-cultured rat hepatocytes: comparison with in vivo biliary clearance. *J Pharmacol Exp Ther* **2008,** 326, (3), 983-90.

16. Liu, X.; Chism, J. P.; LeCluyse, E. L.; Brouwer, K. R.; Brouwer, K. L. Correlation of biliary excretion in sandwich-cultured rat hepatocytes and in vivo in rats. *Drug Metab Dispos* **1999,** 27, (6), 637-44.

17. Abe, K.; Bridges, A. S.; Brouwer, K. L. Use of sandwich-cultured human hepatocytes to predict biliary clearance of angiotensin II receptor blockers and HMG-CoA reductase inhibitors. *Drug Metab Dispos* **2009,** 37, (3), 447-52.

18. Ghibellini, G.; Vasist, L. S.; Leslie, E. M.; Heizer, W. D.; Kowalsky, R. J.; Calvo, B. F.; Brouwer, K. L. In vitro-in vivo correlation of hepatobiliary drug clearance in humans. *Clin Pharmacol Ther* **2007,** 81, (3), 406-13.

19. Mathijs, K.; Kienhuis, A. S.; Brauers, K. J.; Jennen, D. G.; Lahoz, A.; Kleinjans, J. C.; van Delft, J. H. Assessing the metabolic competence of sandwich-cultured mouse primary hepatocytes. *Drug Metab Dispos* **2009,** 37, (6), 1305-11.

20. Bi, Y. A.; Kazolias, D.; Duignan, D. B. Use of cryopreserved human hepatocytes in sandwich culture to measure hepatobiliary transport. *Drug Metab Dispos* **2006,** 34, (9), 1658-65.

21. Chandra, P.; Lecluyse, E. L.; Brouwer, K. L. Optimization of culture conditions for determining hepatobiliary disposition of taurocholate in sandwich-cultured rat hepatocytes. *In Vitro Cell Dev Biol Anim* **2001,** 37, (6), 380-5.

22. Turncliff, R. Z.; Tian, X.; Brouwer, K. L. R. Effect of culture conditions on the expression and function of Bsep, Mrp2, and Mdr1a/b in sandwich-cultured rat hepatocytes. *Biochem Pharmacol* **2006,** 71, (10), 1520-9.

23. Rose, K. A.; Kostrubsky, V.; Sahi, J. Hepatobiliary disposition in primary cultures of dog and monkey hepatocytes. *Mol Pharm* **2006,** 3, (3), 266-74.

24. Threadgill, D. W.; Hunter, K. W.; Williams, R. W. Genetic dissection of complex and quantitative traits: from fantasy to reality via a community effort. *Mamm Genome* **2002,** 13, (4), 175-8.

25. Mita, S.; Suzuki, H.; Akita, H.; Hayashi, H.; Onuki, R.; Hofmann, A. F.; Sugiyama, Y. Vectorial transport of unconjugated and conjugated bile salts by monolayers of LLC-PK1 cells doubly transfected with human NTCP and BSEP or with rat Ntcp and Bsep. *Am J Physiol Gastrointest Liver Physiol* **2006,** 290, (3), G550-6.

26. Pauli-Magnus, C.; Meier, P. J. Hepatobiliary transporters and drug-induced cholestasis. *Hepatology* **2006,** 44, (4), 778-87.

27. Rius, M.; Hummel-Eisenbeiss, J.; Hofmann, A. F.; Keppler, D. Substrate specificity of human ABCC4 (MRP4)-mediated cotransport of bile acids and reduced glutathione. *Am J Physiol Gastrointest Liver Physiol* **2006,** 290, (4), G640-9.

28. Rius, M.; Nies, A. T.; Hummel-Eisenbeiss, J.; Jedlitschky, G.; Keppler, D. Cotransport of reduced glutathione with bile salts by MRP4 (ABCC4) localized to the basolateral hepatocyte membrane. *Hepatology* **2003,** 38, (2), 374-84.

29. Zelcer, N.; Saeki, T.; Bot, I.; Kuil, A.; Borst, P. Transport of bile acids in multidrug-resistance-protein 3-overexpressing cells co-transfected with the ileal Na+-dependent bile-acid transporter. *Biochem J* **2003,** 369, (Pt 1), 23-30.

30. Ballatori, N.; Fang, F.; Christian, W. V.; Li, N.; Hammond, C. L. Ostalpha-Ostbeta is required for bile acid and conjugated steroid disposition in the

intestine, kidney, and liver. *Am J Physiol Gastrointest Liver Physiol* **2008,** 295, (1), G179-G186.

31. Gerloff, T.; Stieger, B.; Hagenbuch, B.; Madon, J.; Landmann, L.; Roth, J.; Hofmann, A. F.; Meier, P. J. The sister of P-glycoprotein represents the canalicular bile salt export pump of mammalian liver. *J Biol Chem* **1998,** 273, (16), 10046-50.

32. Gerk, P. M.; Li, W.; Megaraj, V.; Vore, M. Human multidrug resistance protein 2 transports the therapeutic bile salt tauroursodeoxycholate. *J Pharmacol Exp Ther* **2007,** 320, (2), 893-9.

33. Jedlitschky, G.; Hoffmann, U.; Kroemer, H. K. Structure and function of the MRP2 (ABCC2) protein and its role in drug disposition. *Expert Opin Drug Metab Toxicol* **2006,** 2, (3), 351-66.

34. Wang, R.; Chen, H. L.; Liu, L.; Sheps, J. A.; Phillips, M. J.; Ling, V. Compensatory role of P-glycoproteins in knockout mice lacking the bile salt export pump. *Hepatology* **2009**.

35. LeCluyse, E. L.; Bullock, P. L.; Parkinson, A.; Hochman, J. H. Cultured rat hepatocytes. *Pharm Biotechnol* **1996,** 8, 121-59.

36. Sohlenius-Sternbeck, A. K. Determination of the hepatocellularity number for human, dog, rabbit, rat and mouse livers from protein concentration measurements. *Toxicol In Vitro* **2006,** 20, (8), 1582-6.

37. Davies, B.; Morris, T. Physiological parameters in laboratory animals and humans. *Pharm Res* **1993,** 10, (7), 1093-5.

38. Kitamura, T.; Jansen, P.; Hardenbrook, C.; Kamimoto, Y.; Gatmaitan, Z.; Arias, I. M. Defective ATP-dependent bile canalicular transport of organic anions in mutant (TR-) rats with conjugated hyperbilirubinemia. *Proc Natl Acad Sci U S A* **1990,** 87, (9), 3557-61.

39. Klaunig, J. E.; Goldblatt, P. J.; Hinton, D. E.; Lipsky, M. M.; Chacko, J.; Trump, B. F. Mouse liver cell culture. I. Hepatocyte isolation. *In Vitro* **1981,** 17, (10), 913-25.

40. Klaunig, J. E.; Goldblatt, P. J.; Hinton, D. E.; Lipsky, M. M.; Trump, B. F. Mouse liver cell culture. II. Primary culture. *In Vitro* **1981,** 17, (10), 926-34.

41. Seglen, P. O. Preparation of rat liver cells. 3. Enzymatic requirements for tissue dispersion. *Exp Cell Res* **1973,** 82, (2), 391-8.

42. Williams, G. M.; Bermudez, E.; San, R. H.; Goldblatt, P. J.; Laspia, M. F. Rat hepatocyte primary cultures. IV. Maintenance in defined medium and

the role of production of plasminogen activator and other proteases. *In Vitro* **1978,** 14, (10), 824-37.

43. Shinzawa, K.; Watanabe, Y.; Akaike, T. Primary cultured murine hepatocytes but not hepatoma cells regulate the cell number through density-dependent cell death. *Cell Death Differ* **1995,** 2, (2), 133-40.

44. Wolf, K. K.; Brouwer, K. R.; Pollack, G. M.; Brouwer, K. L. Effect of albumin on the biliary clearance of compounds in sandwich-cultured rat hepatocytes. *Drug Metab Dispos* **2008,** 36, (10), 2086-92.

45. Yue, W.; Abe, K.; Brouwer, K. L. Knocking down breast cancer resistance protein (Bcrp) by adenoviral vector-mediated RNA interference (RNAi) in sandwich-cultured rat hepatocytes: a novel tool to assess the contribution of Bcrp to drug biliary excretion. *Mol Pharm* **2009,** 6, (1), 134-43.

46. Swift, B.; Pfeifer, N. D.; Brouwer, K. L. R. Sandwich-Cultured Hepatocytes: An In Vitro Model to Evaluate Hepatobiliary Transporter-Based Drug Interactions and Hepatotoxicity. *Drug Metabolism Reviews* **In press**.

47. Luttringer, O.; Theil, F. P.; Lave, T.; Wernli-Kuratli, K.; Guentert, T. W.; de Saizieu, A. Influence of isolation procedure, extracellular matrix and dexamethasone on the regulation of membrane transporters gene expression in rat hepatocytes. *Biochem Pharmacol* **2002,** 64, (11), 1637-50.

48. Mennone, A.; Soroka, C. J.; Cai, S. Y.; Harry, K.; Adachi, M.; Hagey, L.; Schuetz, J. D.; Boyer, J. L. Mrp4-/- mice have an impaired cytoprotective response in obstructive cholestasis. *Hepatology* **2006,** 43, (5), 1013-21.

49. Soroka, C. J.; Mennone, A.; Hagey, L. R.; Ballatori, N.; Boyer, J. L. Mouse organic solute transporter alpha deficiency enhances renal excretion of bile acids and attenuates cholestasis. *Hepatology* **2009**.

50. Zelcer, N.; van de Wetering, K.; de Waart, R.; Scheffer, G. L.; Marschall, H. U.; Wielinga, P. R.; Kuil, A.; Kunne, C.; Smith, A.; van der Valk, M.; Wijnholds, J.; Elferink, R. O.; Borst, P. Mice lacking Mrp3 (Abcc3) have normal bile salt transport, but altered hepatic transport of endogenous glucuronides. *J Hepatol* **2006,** 44, (4), 768-75.

51. Belinsky, M. G.; Dawson, P. A.; Shchaveleva, I.; Bain, L. J.; Wang, R.; Ling, V.; Chen, Z. S.; Grinberg, A.; Westphal, H.; Klein-Szanto, A.; Lerro, A.; Kruh, G. D. Analysis of the in vivo functions of Mrp3. *Mol Pharmacol* **2005,** 68, (1), 160-8.

52. Delzenne, N. M.; Calderon, P. B.; Taper, H. S.; Roberfroid, M. B. Comparative hepatotoxicity of cholic acid, deoxycholic acid and lithocholic

acid in the rat: in vivo and in vitro studies. *Toxicol Lett* **1992,** 61, (2-3), 291-304.

53. Gores, G. J.; Miyoshi, H.; Botla, R.; Aguilar, H. I.; Bronk, S. F. Induction of the mitochondrial permeability transition as a mechanism of liver injury during cholestasis: a potential role for mitochondrial proteases. *Biochim Biophys Acta* **1998,** 1366, (1-2), 167-75.

54. McRae, M. P.; Lowe, C. M.; Tian, X.; Bourdet, D. L.; Ho, R. H.; Leake, B. F.; Kim, R. B.; Brouwer, K. L. R.; Kashuba, A. D. Ritonavir, saquinavir, and efavirenz, but not nevirapine, inhibit bile acid transport in human and rat hepatocytes. *J Pharmacol Exp Ther* **2006,** 318, (3), 1068-75.

55. Swift, B.; Tian, X.; Brouwer, K. L. Integration of Preclinical and Clinical Data with Pharmacokinetic Modeling and Simulation to Evaluate Fexofenadine as a Probe for Hepatobiliary Transport Function. *Pharm Res* **2009**.

56. Byrne, J. A.; Strautnieks, S. S.; Mieli-Vergani, G.; Higgins, C. F.; Linton, K. J.; Thompson, R. J. The human bile salt export pump: characterization of substrate specificity and identification of inhibitors. *Gastroenterology* **2002,** 123, (5), 1649-58.

57. Funk, C.; Pantze, M.; Jehle, L.; Ponelle, C.; Scheuermann, G.; Lazendic, M.; Gasser, R. Troglitazone-induced intrahepatic cholestasis by an interference with the hepatobiliary export of bile acids in male and female rats. Correlation with the gender difference in troglitazone sulfate formation and the inhibition of the canalicular bile salt export pump (Bsep) by troglitazone and troglitazone sulfate. *Toxicology* **2001,** 167, (1), 83-98.

58. Saeki, T.; Takahashi, N.; Kanamoto, R.; Iwami, K. Characterization of cloned mouse Na+/taurocholate cotransporting polypeptide by transient expression in COS-7 cells. *Biosci Biotechnol Biochem* **2002,** 66, (5), 1116-8.

59. Hata, S.; Wang, P.; Eftychiou, N.; Ananthanarayanan, M.; Batta, A.; Salen, G.; Pang, K. S.; Wolkoff, A. W. Substrate specificities of rat oatp1 and ntcp: implications for hepatic organic anion uptake. *Am J Physiol Gastrointest Liver Physiol* **2003,** 285, (5), G829-39.

60. Hagenbuch, B.; Meier, P. J. Molecular cloning, chromosomal localization, and functional characterization of a human liver Na+/bile acid cotransporter. *J Clin Invest* **1994,** 93, (3), 1326-31.

Legends

Figure A.1.1. Effect of seeding density and extracellular matrix on cell morphology and bile canalicular network formation in day 3 sandwich-cultured mouse hepatocytes. Representative (n =3) CDF fluorescence (A – F) and light microscopy (G – L) images of mouse hepatocytes cultured in a Biocoat^{TM}/Matrigel^{TM} (BC/MG; A-C & G-I) or Biocoat^{TM}/gelled-collagen (BC/GC; D-F & J-L) sandwich configuration in six-well plates (maintained with DMEM for 3 days); seeding densities (1.0, 1.25 or 1.5 x 10^6 cells/well) are noted at the top of each column. Sandwich-cultured mouse hepatocytes were incubated with 2 μM CDFDA for 10 min.

Figure A.1.2. Effect of seeding density and extracellular matrix on cell morphology and bile canalicular network formation in day 4 sandwich-cultured mouse hepatocytes. Representative (n = 3) CDF fluorescence (A – F) and light microscopy (G – L) images of mouse hepatocytes cultured in a Biocoat^{TM}/Matrigel^{TM} (BC/MG; A-C & G-I) or Biocoat^{TM}/gelled-collagen (BC/GC; D-F & J-L) sandwich configuration in six-well plates (maintained with DMEM for 4 days); seeding densities (1.0, 1.25 or 1.5 x 10^6 cells/well) are noted at the top of each column. Sandwich-cultured mouse hepatocytes were incubated with 2 μM CDFDA for 10 min.

Figure A.1.3. Influence of seeding density, extracellular matrix and day in culture on transport protein levels in sandwich-cultured mouse hepatocytes. Representative immunoblots of Bcrp, Ntcp, Mrp4, Mrp3, Mrp2, Bsep, and Mdr1a/1b in mouse hepatocytes cultured in Biocoat^{TM}/Matrigel^{TM} (BC/MG) or Biocoat^{TM}/gelled-collagen (BC/GC) sandwich configuration in six-well plates and maintained with DMEM for 3 or 4 days (n = 2). B-actin was used as a loading control.

Figure A.1.4. Relative expression of Mrp4 protein compared with β-actin in sandwich-cultured mouse hepatocytes cultured in Biocoat^{TM}/Matrigel^{TM} (BC/MG) or Biocoat^{TM}/gelled-collagen (BC/GC) sandwich configuration in six-well plates

and maintained with DMEM for 3-4 days. Densitometry was performed with Quantity One software (version 4.1; Bio-Rad, Hercules, CA).

Figure A.1.5. Accumulation in cells+bile (black bars) and cells (white bars) after a 10-min incubation with 1 μM [^{3}H]taurocholate in mouse hepatocytes cultured in Biocoat^{TM}/Matrigel^{TM} (BC/MG) or Biocoat^{TM}/gelled-collagen (BC/GC) sandwich configuration in six-well plates and maintained with DMEM for 3 or 4 days (Mean ± S.E.M.; n=3). Cellular accumulation (white bars) of [^{3}H]taurocholate was significantly increased on day 3 compared to day 4, and significantly greater when cultured in BC/MG configuration compared to the BC/GC configuration on both days 3 and 4 of culture. * $p < 0.05$

Tables

Table A.1.1. Mean biliary excretion index (BEI) and *in vitro* biliary clearance (*in vitro* $Cl_{biliary}$) of [^{3}H]taurocholate after a 10-min incubation with 1 µM [^{3}H]taurocholate in sandwich-cultured mouse hepatocytes. (Mean ± SEM; n = 3 per group). Primary mouse hepatocytes were seeded at designated densities and cultured in Biocoat™/Matrigel™ (BC/MG) or Biocoat™/gelled-collagen (BC/GC) sandwich configuration in six-well plates and maintained with DMEM for 3 or 4 days. *In vitro* intrinsic biliary clearance of [^{3}H]taurocholate was significantly increased as a function of seeding density within culture day. (†, * 1.0 x 10^6 is different than 1.25 x 10^6 and 1.5 x 10^6 , ** p < 0.05)

Day in Culture		BC/MG			BC/GC		
		1.0 x 10^6 cells/well	1.25 x 10^6 cells/well	1.5 x 10^6 cells/well	1.0 x 10^6 cells/well	1.25 x 10^6 cells/well	1.5 x 10^6 cells/well
3	**BEI (%)**	26.3 ± 10.8	27.6 ± 5.5	29.6 ± 8.2	35.4 ± 3.9	49.9 ± 6.3	46.9 ± 6.4
	***In Vitro* $Cl_{biliary}$ (mL/min/kg)**	48.7 ± 20.5	60.4 ± 15.8	73.7 ± 24.6	33.6 ± 7.6 †	84.0 ± 15.6†	96.0 ± 21.1†
4	**BEI (%)**	36.2 ± 9.0	32.5 ± 10.3	34.2 ± 5.0	32.4 ± 7.7	39.9 ± 3.5	43.5 ± 6.4
	***In Vitro* $Cl_{biliary}$ (mL/min/kg)**	38.3 ± 5.0**	45.4 ± 10.6	57.8 ± 14.7**	18.0 ± 6.4*	40.4 ± 5.7*	60.3 ± 19.3*

Figure A.1.1.

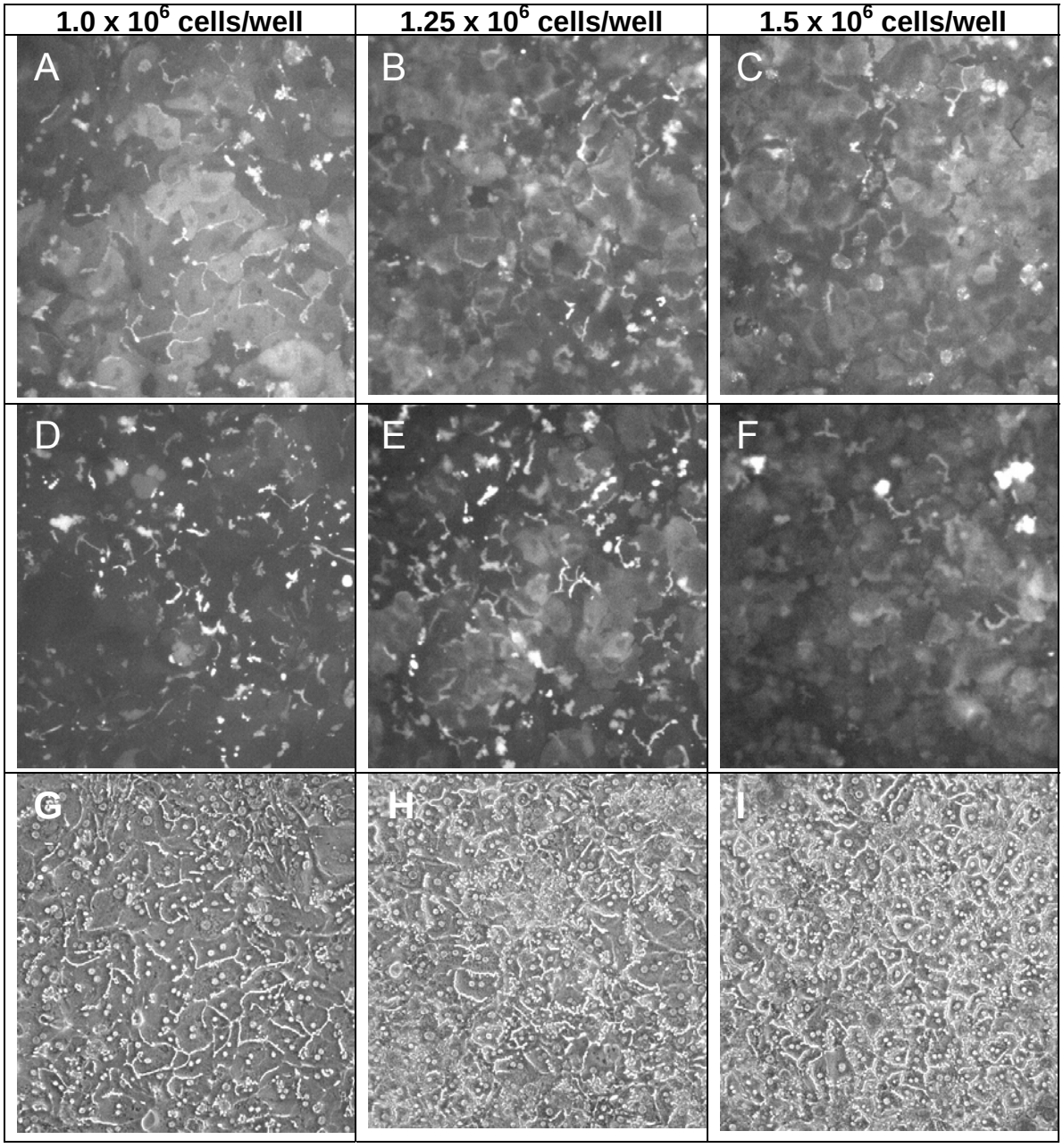
1.0 x 10^6 cells/well
1.25 x 10^6 cells/well
1.5 x 10^6 cells/well
A
B
C
D
E
F
G
H
I

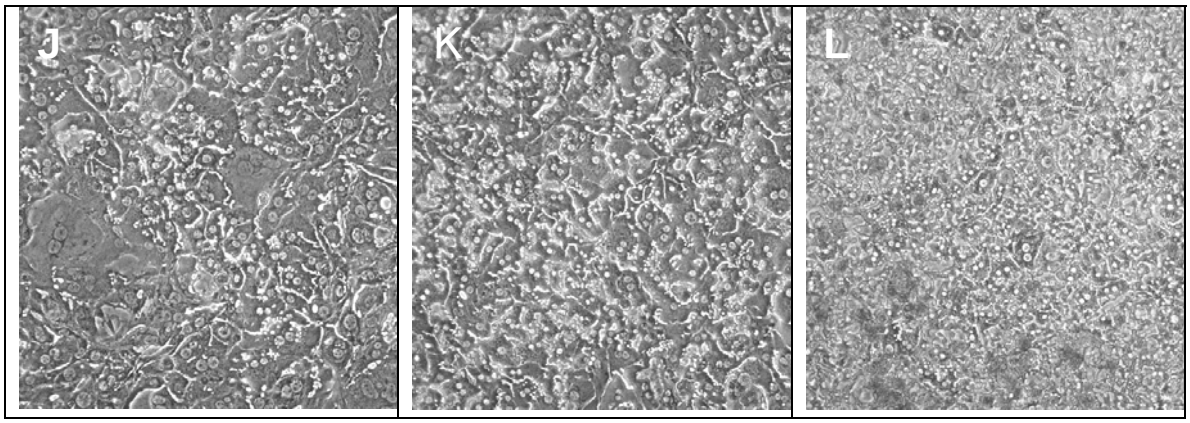
J
K
L

Figure A.1.2.

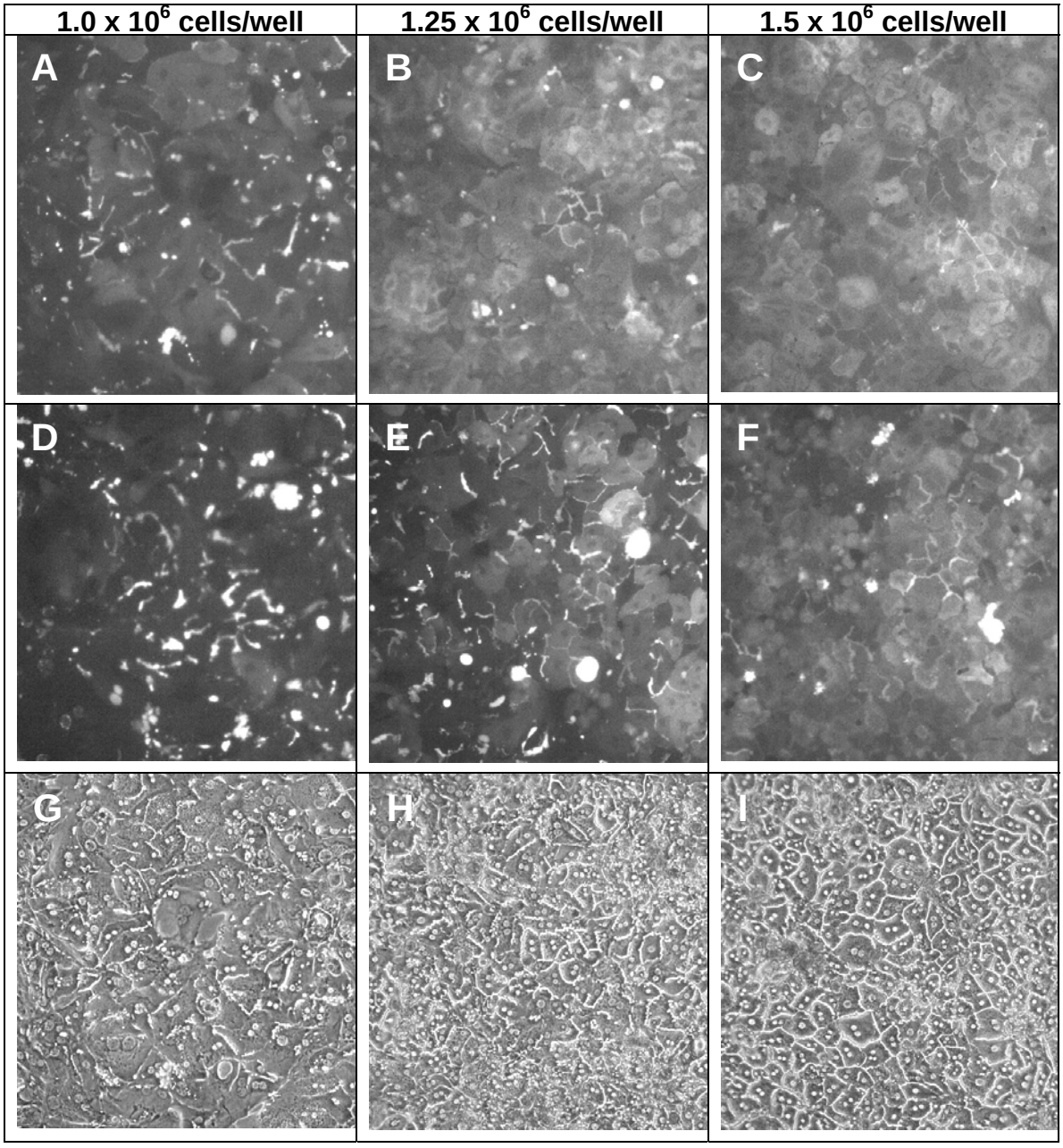
1.0 x 10^6 cells/well
1.25 x 10^6 cells/well
1.5 x 10^6 cells/well
A
B
C
D
E
F
G
H
I

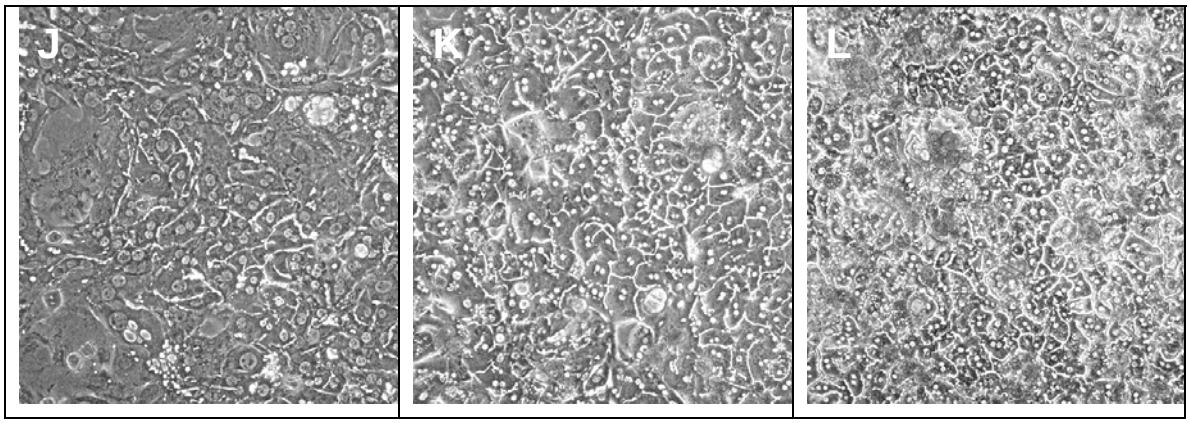
J
K
L

Figure A.1.3.

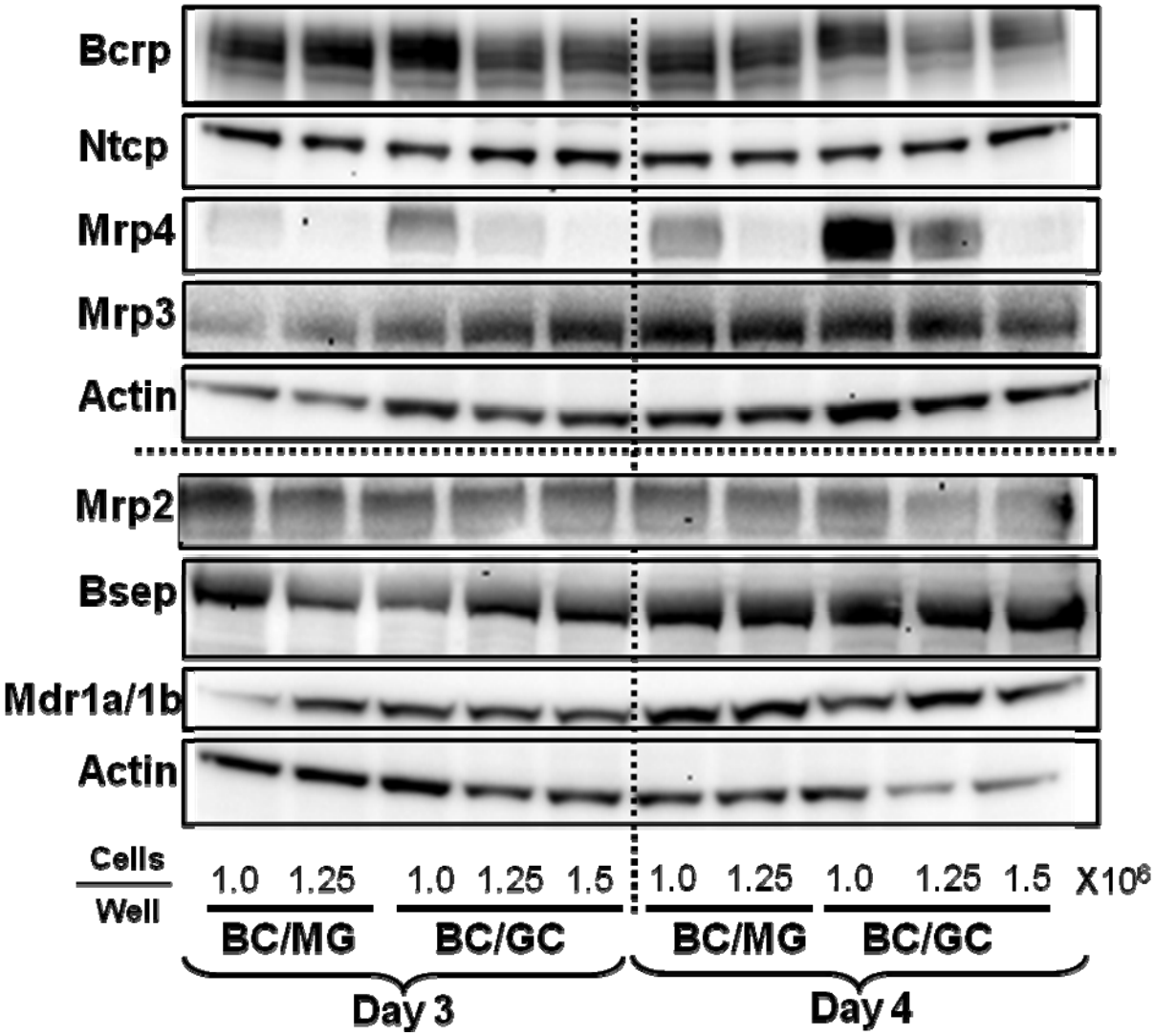
Bcrp
Ntcp
Mrp4
Mrp3
Actin
Mrp2
Bsep
Mdr1a/1b
Actin
Cells
Well
1.0 1.25 1.0 1.25 1.5 1.0 1.25 1.0 1.25 1.5 X10^6
BC/MG
BC/GC
BC/MG
BC/GC
Day 3
Day 4

Figure A.1.4.

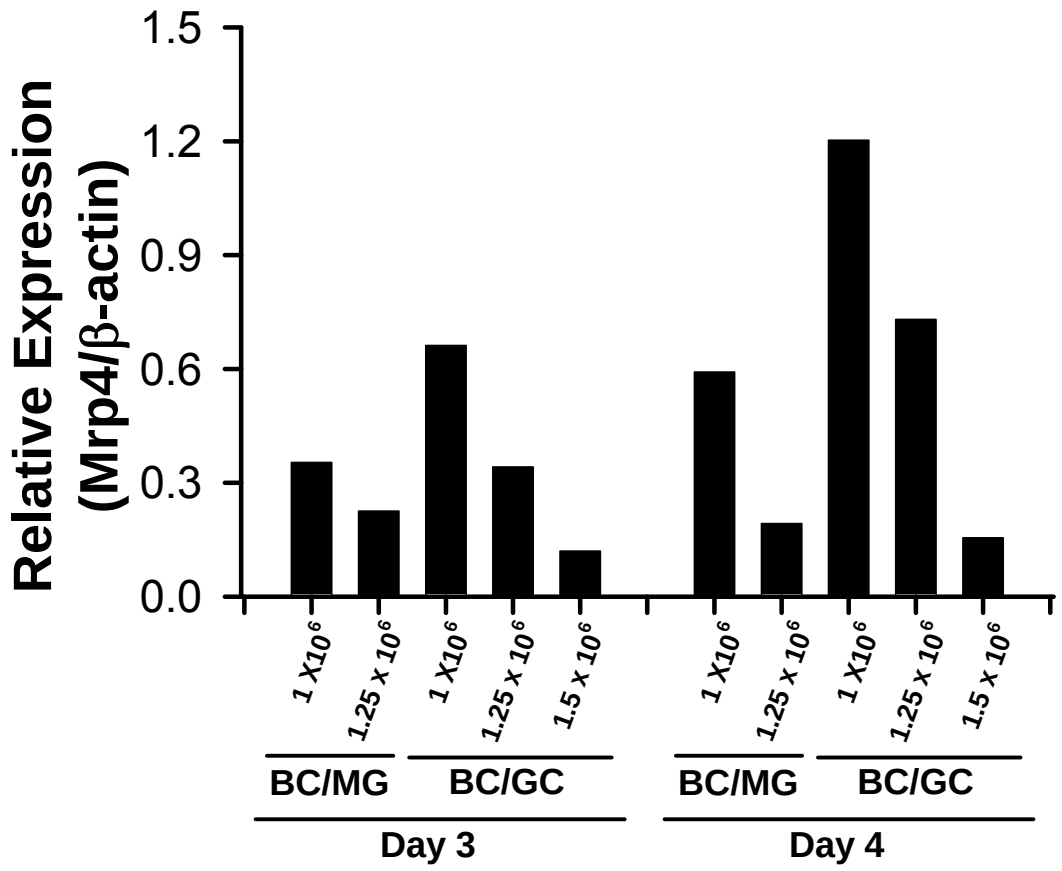
Relative Expression
(Mrp4/β-actin)
1.5
1.2
0.9
0.6
0.3
0.0
1 X10^6
1.25 x 10^6
1 X10^6
1.25 x 10^6
1.5 x 10^6
1 X10^6
1.25 x 10^6
1 X10^6
1.25 x 10^6
1.5 x 10^6
BC/MG
BC/GC
BC/MG
BC/GC
Day 3
Day 4

Figure A.1.5.

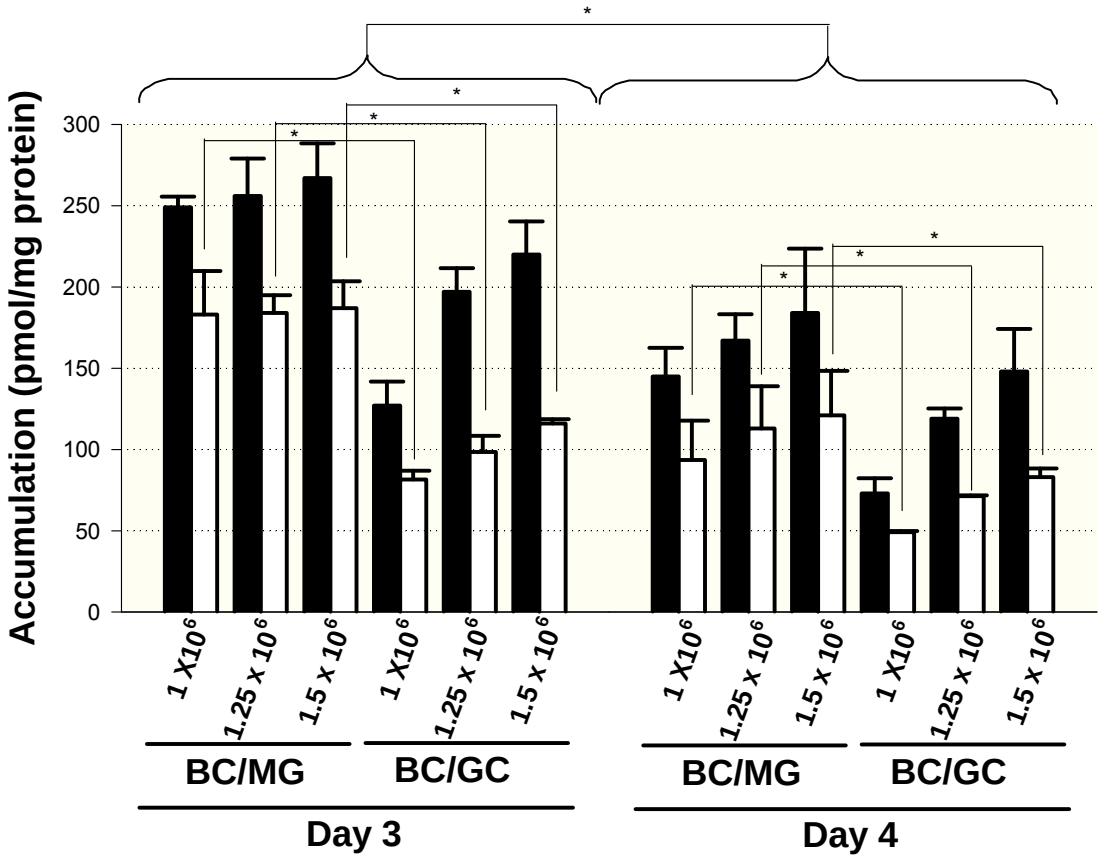
Accumulation (pmol/mg protein)
300
250
200
150
100
50
0
1 X10^6
1.25 x 10^6
1.5 x 10^6
1 X10^6
1.25 x 10^6
1.5 x 10^6
1 X10^6
1.25 x 10^6
1.5 x 10^6
1 X10^6
1.25 x 10^6
1.5 x 10^6
BC/MG
BC/GC
BC/MG
BC/GC
Day 3
Day 4

Raw Data

Bile Flow

8-16-07 Fex only					
Mid Time (min)	Tube Weight	Total Weight	Bile Vol (µl)	Bile Flow Rate (µl/min)	Normalized to Liver WT
5	0.4193	0.4569	37.600	3.760	0.3579
15	0.4247	0.4642	39.500	3.950	0.3760
25	0.4191	0.4773	58.200	5.820	0.5541
35	0.4247	0.484	59.300	5.930	0.5645
45	0.4272	0.4826	55.400	5.540	0.5274
55	0.4188	0.4709	52.100	5.210	0.4960
Liver Weight(g)	10.5044				
10-16-07 Fex only					
Mid Time (min)	Tube Weight	Total Weight	Bile Vol (µl)	Bile Flow Rate (µl/min)	Normalized to Liver WT
5	0.4247	0.4867	62.000	6.200	0.6046
15	0.4225	0.4811	58.600	5.860	0.5715
25	0.4192	0.4837	64.500	6.450	0.6290
35	0.4216	0.4806	59.000	5.900	0.5754
45	0.4189	0.4732	54.300	5.430	0.5295
55	0.4189	0.4821	63.200	6.320	0.6163
Liver Weight(g)	10.2546				
10-22-07 Fex only					
Mid Time (min)	Tube Weight	Total Weight	Bile Vol (µl)	Bile Flow Rate (µl/min)	Normalized to Liver WT
5	0.4183	0.4726	54.300	5.430	0.4199
15	0.4168	0.4753	58.500	5.850	0.4524
25	0.4185	0.4747	56.200	5.620	0.4346
35	0.4213	0.4785	57.200	5.720	0.4423
45	0.4275	0.4873	59.800	5.980	0.4624
55	0.4194	0.4919	72.500	7.250	0.5606
Liver Weight(g)	12.932				

10-23-07 Fex only					
Mid Time (min)	Tube Weight	Total Weight	Bile Vol (µl)	Bile Flow Rate (µl/min)	Normalized to Liver WT
5	0.4214	0.4698	48.400	4.840	0.4839
15	0.4189	0.4688	49.900	4.990	0.4989
25	0.4218	0.472	50.200	5.020	0.5019
35	0.4169	0.4657	48.800	4.880	0.4879
45	0.4172	0.465	47.800	4.780	0.4779
55	0.4216	0.4751	53.500	5.350	0.5349
Liver Weight(g)	10.0027				
10-24-07 Fex only					
Mid Time (min)	Tube Weight	Total Weight	Bile Vol (µl)	Bile Flow Rate (µl/min)	Normalized to Liver WT
5	0.4189	0.4689	50.000	5.000	0.4390
15	0.4188	0.4747	55.900	5.590	0.4908
25	0.4253	0.4817	56.400	5.640	0.4952
35	0.4276	0.4875	59.900	5.990	0.5260
45	0.4213	0.4828	61.500	6.150	0.5400
55	0.4277	0.4906	62.900	6.290	0.5523
Liver Weight(g)	11.3885				
10-17-07 Fex no TC					
Mid Time (min)	Tube Weight	Total Weight	Bile Vol (µl)	Bile Flow Rate (µl/min)	Normalized to Liver WT
5	0.4188	0.463	44.200	4.420	0.3578
15	0.4173	0.4596	42.300	4.230	0.3424
25	0.4248	0.4651	40.300	4.030	0.3262
35	0.4188	0.4604	41.600	4.160	0.3367
45	0.4276	0.4684	40.800	4.080	0.3302
54	0.4189	0.4594	40.500	4.050	0.3278
Liver Weight(g)	12.3545				

10-29-07 Fex no TC					
Mid Time (min)	Tube Weight	Total Weight	Bile Vol (µl)	Bile Flow Rate (µl/min)	Normalized to Liver WT
5	0.4268	0.4735	46.700	4.670	0.4199
15	0.4214	0.4611	39.700	3.970	0.3570
25	0.4271	0.4641	37.000	3.700	0.3327
35	0.4214	0.4631	41.700	4.170	0.3749
45	0.4211	0.4562	35.100	3.510	0.3156
54	0.4249	0.4572	32.300	3.230	0.2904
Liver Weight(g)	11.1219				
11-1-07 Fex no TC					
Mid Time (min)	Tube Weight	Total Weight	Bile Vol (µl)	Bile Flow Rate (µl/min)	Normalized to Liver WT
5	0.423	0.4597	36.700	3.670	0.2850
15	0.4172	0.4544	37.200	3.720	0.2889
25	0.4178	0.4637	45.900	4.590	0.3565
35	0.4167	0.4501	33.400	3.340	0.2594
45	0.4276	0.4599	32.300	3.230	0.2508
54	0.4293	0.4603	31.000	3.100	0.2407
Liver Weight(g)	12.8765				
11-8-07 Fex no TC					
Mid Time (min)	Tube Weight	Total Weight	Bile Vol (µl)	Bile Flow Rate (µl/min)	Normalized to Liver WT
5	0.4188	0.4478	29.000	2.900	0.2340
15	0.4217	0.4488	27.100	2.710	0.2187
25	0.4194	0.4423	22.900	2.290	0.1848
35	0.4188	0.4391	20.300	2.030	0.1638
45	0.4224	0.4422	19.800	1.980	0.1598
54	0.4212	0.4409	19.700	1.970	0.1590
Liver Weight(g)	12.3932				

9-7-07 2µM GF120918					
Mid Time (min)	Tube Weight	Total Weight	Bile Vol (µl)	Bile Flow Rate (µl/min)	Normalized to Liver WT
5	0.4227	0.4723	49.600	4.960	0.4235
15	0.4223	0.4772	54.900	5.490	0.4688
25	0.4193	0.4745	55.200	5.520	0.4713
35	0.4248	0.478	53.200	5.320	0.4542
45	0.4194	0.4691	49.700	4.970	0.4244
55	0.4223	0.476	53.700	5.370	0.4585
Liver Weight(g)	11.7118				
11-1-07 2µM GF120918					
Mid Time (min)	Tube Weight	Total Weight	Bile Vol (µl)	Bile Flow Rate (µl/min)	Normalized to Liver WT
5	0.4277	0.4869	59.200	5.920	0.5527
15	0.4211	0.48	58.900	5.890	0.5499
25	0.4244	0.4858	61.400	6.140	0.5732
35	0.4247	0.4844	59.700	5.970	0.5574
45	0.4217	0.4804	58.700	5.870	0.5480
55	0.4215	0.4803	58.800	5.880	0.5490
Liver Weight(g)	10.7113				
11-26-07 2µM GF120918					
Mid Time (min)	Tube Weight	Total Weight	Bile Vol (µl)	Bile Flow Rate (µl/min)	Normalized to Liver WT
5	0.4191	0.4632	44.100	4.410	0.4115
15	0.422	0.4803	58.300	5.830	0.5441
25	0.4216	0.4797	58.100	5.810	0.5422
35	0.4174	0.4738	56.400	5.640	0.5263
45	0.4278	0.4843	56.500	5.650	0.5273
55	0.4218	0.4761	54.300	5.430	0.5067
Liver Weight(g)	10.7159				

10-16-07 5µM Bosentan					
Mid Time (min)	Tube Weight	Total Weight	Bile Vol (µl)	Bile Flow Rate (µl/min)	Normalized to Liver WT
5	0.4186	0.453	34.400	3.440	0.3082
15	0.4276	0.4715	43.900	4.390	0.3933
25	0.4223	0.4702	47.900	4.790	0.4292
35	0.4229	0.4781	55.200	5.520	0.4946
45	0.4193	0.4788	59.500	5.950	0.5331
55	0.427	0.4838	56.800	5.680	0.5089
Liver Weight(g)	11.1608				
10-26-07 5µM Bosentan					
Mid Time (min)	Tube Weight	Total Weight	Bile Vol (µl)	Bile Flow Rate (µl/min)	Normalized to Liver WT
5	0.429	0.4955	66.500	6.650	0.6783
15	0.4188	0.4866	67.800	6.780	0.6916
25	0.4218	0.4958	74.000	7.400	0.7548
35	0.4222	0.5002	78.000	7.800	0.7956
45	0.4246	0.4983	73.700	7.370	0.7518
55	0.423	0.4942	71.200	7.120	0.7263
Liver Weight(g)	9.8036				
10-29-07 5µM Bosentan					
Mid Time (min)	Tube Weight	Total Weight	Bile Vol (µl)	Bile Flow Rate (µl/min)	Normalized to Liver WT
5	0.4173	0.477	59.700	5.970	0.4750
15	0.4216	0.4863	64.700	6.470	0.5147
25	0.4247	0.491	66.300	6.630	0.5275
35	0.4216	0.4916	70.000	7.000	0.5569
45	0.4246	0.5019	77.300	7.730	0.6150
55	0.4248	0.5011	76.300	7.630	0.6070
Liver Weight(g)	12.5695				

10-31-07 5µM Bosentan					
Mid Time (min)	Tube Weight	Total Weight	Bile Vol (µl)	Bile Flow Rate (µl/min)	Normalized to Liver WT
5	0.4192	0.4957	76.500	7.650	0.6354
15	0.4225	0.4901	67.600	6.760	0.5615
25	0.4248	0.4984	73.600	7.360	0.6113
35	0.4183	0.4966	78.300	7.830	0.6503
45	0.4217	0.4996	77.900	7.790	0.6470
55	0.4167	0.4948	78.100	7.810	0.6487
Liver Weight(g)	12.04				

Perfusate Concentrations

	8-16-07 Fex only			**10-16-07 Fex only**		
Time	Calculated Conc	Amount		Calculated Conc	Amount	
min	ng/ml	ng	pmole/ml	ng/ml	ng	pmole/ml
10	65.6	20336	130.76	44.1	12480.3	87.90
20	68.5	20892.5	136.54	36.7	10459.5	73.15
30	72	22320	143.51	33	9405	65.78
40	64.9	19794.5	129.36	33.1	9268	65.98
50	66.1	20160.5	131.75	42.2	11605	84.11
60	71	21655	141.52	37.9	10422.5	75.54

	10-22-07 Fex only			**10-23-07 Fex only**			**10-24-07 Fex only**		
Time	Calculated Conc	Amount		Calculated Conc	Amount		Calculated Conc	Amount	
min	ng/ml	ng	pmole/ml	ng/ml	ng	pmole/ml	ng/ml	ng	pmole/ml
10	43	12341	85.71	47.8	13384	95.28	35.5	9762.5	70.76
20	44.9	12796.5	89.50	37.1	10573.5	73.95	38.8	10864	77.34
30	50.3	14335.5	100.26	48.2	13737	96.07	36.3	10164	72.35
40	52.1	14848.5	103.85	54.2	15447	108.03	151	42280	
50	44.1	12568.5	87.90	55.7	15596	111.02	41.9	11732	83.52
60	34.2	9747	68.17	48.3	13524	96.27	40.1	11228	79.93

	10-17-07 Fex no TC			10-29-07 Fex no TC		
Time	Calculated Conc	Amount		Calculated Conc	Amount	
min	ng/ml	ng	pmole/ml	ng/ml	ng	pmole/ml
10	66.9	18732	133.35	49.9	15469	99.46
20	64.3	18132.6	128.16	42.1	13051	83.91
30	62.6	17841	124.78	40.4	12524	80.53
40	62.3	17755.5	124.18	39.8	12935	79.33
50	64.1	17948	127.77	42.7	12596.5	85.11
60	66.7	19009.5	132.95	58.6	19045	116.80
	11-1-07 Fex no TC			**11-8-07 Fex no TC**		
Time	Calculated Conc	Amount		Calculated Conc	Amount	
min	ng/ml	ng	pmole/ml	ng/ml	ng	pmole/ml
10	52.2	16182	104.05	50.6	14421	100.86
20	96.8	30492	192.94	52.8	15312	105.24
30	48.7	15097	97.07	55	15675	109.63
40	56.2	17422	112.02	62.6	17841	124.78
50	60.7	19120.5	120.99	70.9	19852	141.32
60	62.9	19499	125.37	83.2	23296	165.84

	9-7-07 2µM GF120918			11-1-07 2µM GF120918			11-26-07 2µM GF120918		
Time	Calculated Conc	Amount		Calculated Conc	Amount		Calculated Conc	Amount	
min	ng/ml	ng	pmole/ml	ng/ml	ng	pmole/ml	ng/ml	ng	pmole/ml
10	41.3	11977	82.32	35.6	11036	70.96	38.1	11049	75.94
20	50.5	14645	100.66	47.8	14818	95.28	44.2	13039	88.10
30	55.1	15979	109.83	56.2	17422	112.02	49.5	14602.5	98.66
40	63.6	18444	126.77	59.6	18595.2	118.80	56.8	16756	113.22
50	111	31635	221.25	65.3	20243	130.16	70.1	20679.5	139.72
60	120	34800	239.19	67.2	20832	133.94	70.9	21270	141.32

	10-16-07 5µM Bosentan			10-26-07 5µM Bosentan		
Time	Calculated Conc	Amount		Calculated Conc	Amount	
min	ng/ml	ng	pmole/ml	ng/ml	ng	pmole/ml
10	69.8	17101	139.13	69.4	21514	138.33
20	98.3	26541	195.93	90.7	28117	180.79
30	105	28350	209.29	85.2	26412	169.82
40	109	29430	217.26	83.8	25978	167.03
50	85.4	23058	170.22	87	26970	173.41
60	94.5	25515	188.36	104	32240	207.30
	10-29-07 5µM Bosentan			**10-31-07 5µM Bosentan**		
Time	Calculated Conc	Amount		Calculated Conc	Amount	
min	ng/ml	ng	pmole/ml	ng/ml	ng	pmole/ml
10	67.8	21018	135.14	60.8	18848	121.19
20	80.7	25017	160.85	81.9	25389	163.24
30	88.3	27373	176.00	89	27590	177.40
40	105	32550	209.29	98.4	30996	196.13
50	102	31620	203.31	113	35030	225.23
60	103	31930	205.30	118	36580	235.20

Bilary Excretion Rate

		8-16-07 Fex only							
Time	Mid Time	Calculated Conc	Dilution Factor	Bile Vol	Amount	Amount	BER	BER	BER
min	min	ng/ml	ng/ml (*100)	µl	ng	nmole	pmol/min	pmol/min/g liver	pmol/hr/g liver
10	5	181	18100	37.600	680.56	1.36	135.651	12.914	774.8226685
20	15	1140	114000	39.500	4503	8.98	897.548	85.445	5126.699301
30	25	1670	167000	58.200	9719.4	19.37	1937.293	184.427	11065.60986
40	35	1840	184000	59.300	10911.2	21.75	2174.846	207.041	12422.4831
50	45	2180	218000	55.400	12077.2	24.07	2407.255	229.166	13749.98286
60	55	2080	208000	52.100	10836.8	21.60	2160.016	205.630	12337.77815
Liver WT	10.5044								
		10-16-07 Fex only							
Time	Mid Time	Calculated Conc	Dilution Factor	Bile Vol	Amount	Amount	BER	BER	BER
min	min	ng/ml	ng/ml (*100)	µl	ng	nmole	pmol/min	pmol/min/g liver	pmol/hr/g liver
10	5	236	23600	62.0	1463	2.92	291.648	28.441	1706.444301
20	15	1410	141000	58.6	8263	16.47	1646.920	160.603	9636.185539
30	25	1980	198000	64.5	12771	25.46	2545.545	248.234	14894.06791
40	35	2180	218000	59.0	12862	25.64	2563.683	250.003	15000.19587
50	45	2750	275000	54.3	14933	29.76	2976.380	290.248	17414.89853
60	55	2670	267000	63.2	16874	33.63	3363.444	327.994	19679.62255
Liver WT	10.2546								

		10-22-07 Fex only							
Time	Mid Time	Calculated Conc	Dilution Factor	Bile Vol	Amount	Amount	BER	BER	BER
min	min	ng/ml	ng/ml (*100)	µl	ng	nmole	pmol/min	pmol/min/g liver	pmol/hr/g liver
10	5	213	21300	54.300	1156.59	2.31	230.534	17.827	1069.598749
20	15	1020	102000	58.500	5967	11.89	1189.356	91.970	5518.200691
30	25	1550	155000	56.200	8711	17.36	1736.297	134.264	8055.814684
40	35	1800	180000	57.200	10296	20.52	2052.222	158.693	9521.601193
50	45	1790	179000	59.800	10704.2	21.34	2133.586	164.985	9899.099018
60	55	1730	173000	72.500	12542.5	25.00	2500.000	193.319	11599.13393
Liver WT	12.932								
		10-23-07 Fex only							
Time	Mid Time	Calculated Conc	Dilution Factor	Bile Vol	Amount	Amount	BER	BER	BER
min	min	ng/ml	ng/ml (*100)	µl	ng	nmole	pmol/min	pmol/min/g liver	pmol/hr/g liver
10	5	278	27800	48.4	1345.52	2.68	268.192	20.739	1244.318652
20	15	909	90900	49.9	4535.91	9.04	904.108	69.912	4194.748064
30	25	1550	155000	50.2	7781	15.51	1550.927	119.929	7195.763294
40	35	1930	193000	48.8	9418.4	18.77	1877.297	145.167	8710.008612
50	45	1830	183000	47.8	8747.4	17.44	1743.552	134.825	8089.476911
60	55	1820	182000	53.5	9737	19.41	1940.801	150.077	9004.645572
Liver WT	10.0027								

		10-24-07 Fex only							
Time	Mid Time	Calculated Conc	Dilution Factor	Bile Vol	Amount	Amount	BER	BER	BER
min	min	ng/ml	ng/ml (*100)	µl	ng	nmole	pmol/min	pmol/min/g liver	pmol/hr/g liver
10	5	258	25800	50.0	1290	2.57	257.126	19.883	1192.974508
20	15	1210	121000	55.9	6763.9	13.48	1348.196	104.253	6255.163006
30	25	1830	183000	56.4	10321.2	20.57	2057.245	159.082	9544.905811
40	35	1910	191000	59.9	11440.9	22.80	2280.427	176.340	10580.38919
50	45	2100	210000	61.5	12915	25.74	2574.248	199.060	11943.61688
60	55	2210	221000	62.9	13900.9	27.71	2770.759	214.256	12855.36383
Liver WT	11.3885								
		10-17-07 Fex no TC							
Time	Mid Time	Calculated Conc	Dilution Factor	Bile Vol	Amount	Amount	BER	BER	BER
min	min	ng/ml	ng/ml (*100)	µl	ng	nmole	pmol/min	pmol/min/g liver	pmol/hr/g liver
10	5	119	11900	44.2	525.98	1.05	104.840	8.107	486.419172
20	15	502	50200	42.3	2123.46	4.23	423.253	32.729	1963.747015
30	25	1050	105000	40.3	4231.5	8.43	843.432	65.221	3913.233823
40	35	1370	137000	41.6	5699.2	11.36	1135.978	87.842	5270.542882
50	45	1720	172000	40.8	7017.6	13.99	1398.764	108.163	6489.781326
60	55	1810	181000	40.5	7330.5	14.61	1461.132	112.986	6779.147003
Liver WT	12.3545								

		10-29-07 Fex no TC							
Time	Mid Time	Calculated Conc	Dilution Factor	Bile Vol	Amount	Amount	BER	BER	BER
min	min	ng/ml	ng/ml (*100)	µl	ng	nmole	pmol/min	pmol/min/g liver	pmol/hr/g liver
10	5	295	29500	46.700	1377.65	2.75	274.596	26.141	1568.464866
20	15	1300	130000	39.700	5161	10.29	1028.702	97.931	5875.83724
30	25	1970	197000	37.000	7289	14.53	1452.860	138.310	8298.581214
40	35	2050	205000	41.700	8548.5	17.04	1703.907	162.209	9732.531418
50	45	2410	241000	35.100	8459.1	16.86	1686.087	160.512	9630.748847
60	55	2760	276000	32.300	8914.8	17.77	1776.918	169.159	10149.56672
Liver WT	11.1219								
		11-1-07 Fex no TC							
Time	Mid Time	Calculated Conc	Dilution Factor	Bile Vol	Amount	Amount	BER	BER	BER
min	min	ng/ml	ng/ml (*100)	µl	ng	nmole	pmol/min	pmol/min/g liver	pmol/hr/g liver
10	5	190	19000	36.700	697.3	1.39	138.987	13.231	793.8812842
20	15	1300	130000	37.200	4836	9.64	963.923	91.764	5505.822301
30	25	1810	181000	45.900	8307.9	16.56	1655.950	157.643	9458.606512
40	35	2300	230000	33.400	7682	15.31	1531.194	145.767	8746.014664
50	45	2570	257000	32.300	8301.1	16.55	1654.594	157.514	9450.864661
60	55	2760	276000	31.000	8556	17.05	1705.402	162.351	9741.070225
Liver WT	12.8765								

		11-8-07 Fex no TC							
Time	Mid Time	Calculated Conc	Dilution Factor	Bile Vol	Amount	Amount	BER	BER	BER
min	min	ng/ml	ng/ml (*100)	µl	ng	nmole	pmol/min	pmol/min/g liver	pmol/hr/g liver
10	5	138	13800	29.000	400.2	0.80	79.769	7.594	455.6307041
20	15	1110	111000	27.100	3008.1	6.00	599.581	57.079	3424.74443
30	25	1970	197000	22.900	4511.3	8.99	899.203	85.602	5136.148914
40	35	2500	250000	20.300	5075	10.12	1011.561	96.299	5777.925595
50	45	2770	277000	19.800	5484.6	10.93	1093.203	104.071	6244.258269
60	55	2700	270000	19.700	5319	10.60	1060.195	100.929	6055.721426
Liver WT	12.3932								
		9-7-07 2µM GF120918							
Time	Mid Time	Calculated Conc	Dilution Factor	Bile Vol	Amount	Amount	BER	BER	BER
min	min	ng/ml	ng/ml (*100)	µl	ng	nmole	pmol/min	pmol/min/g liver	pmol/hr/g liver
10	5	84.3	8430	49.600	418.128	0.83	83.342	7.934	476.0418666
20	15	521	52100	54.900	2860.29	5.70	570.120	54.274	3256.461635
30	25	608	60800	55.200	3356.16	6.69	668.958	63.684	3821.013353
40	35	653	65300	53.200	3473.96	6.92	692.438	65.919	3955.129537
50	45	711	71100	49.700	3533.67	7.04	704.339	67.052	4023.10982
60	55	577	57700	53.700	3098.49	6.18	617.598	58.794	3527.654123
Liver WT	11.7118								

		11-1-07 2μM GF120918							
Time	Mid Time	Calculated Conc	Dilution Factor	Bile Vol	Amount	Amount	BER	BER	BER
min	min	ng/ml	ng/ml (*100)	μl	ng	nmole	pmol/min	pmol/min/g liver	pmol/hr/g liver
10	5	140	14000	59.200	828.8	1.65	165.198	15.727	943.5950213
20	15	591	59100	58.900	3480.99	6.94	693.839	66.052	3963.133245
30	25	741	74100	61.400	4549.74	9.07	906.865	86.332	5179.913142
40	35	699	69900	59.700	4173.03	8.32	831.778	79.184	4751.025979
50	45	598	59800	58.700	3510.26	7.00	699.673	66.608	3996.457359
60	55	552	55200	58.800	3245.76	6.47	646.952	61.589	3695.322124
Liver WT	10.7113								
		11-26-07 2μM GF120918							
Time	Mid Time	Calculated Conc	Dilution Factor	Bile Vol	Amount	Amount	BER	BER	BER
min	min	ng/ml	ng/ml (*100)	μl	ng	nmole	pmol/min	pmol/min/g liver	pmol/hr/g liver
10	5	157	15700	44.100	692.37	1.38	138.005	13.138	788.2684422
20	15	474	47400	58.300	2763.42	5.51	550.811	52.436	3146.174413
30	25	575	57500	58.100	3340.75	6.66	665.886	63.391	3803.468952
40	35	568	56800	56.400	3203.52	6.39	638.533	60.787	3647.231567
50	45	466	46600	56.500	2632.9	5.25	524.796	49.960	2997.576414
60	55	480	48000	54.300	2606.4	5.20	519.514	49.457	2967.405965
Liver WT	10.7159								

		10-16-07 5μM Bosentan							
Time	Mid Time	Calculated Conc	Dilution Factor	Bile Vol	Amount	Amount	BER	BER	BER
min	min	ng/ml	ng/ml (*100)	μl	ng	nmole	pmol/min	pmol/min/g liver	pmol/hr/g liver
10	5	59.7	5970	34.400	205.368	0.41	40.934	3.897	233.8130096
20	15	501	50100	43.900	2199.39	4.38	438.387	41.734	2504.022024
30	25	636	63600	47.900	3046.44	6.07	607.223	57.807	3468.394808
40	35	757	75700	55.200	4178.64	8.33	832.896	79.290	4757.413006
50	45	614	61400	59.500	3653.3	7.28	728.184	69.322	4159.309473
60	55	926	92600	56.800	5259.68	10.48	1048.372	99.803	5988.185161
Liver WT	11.1608								
		10-26-07 5μM Bosentan							
Time	Mid Time	Calculated Conc	Dilution Factor	Bile Vol	Amount	Amount	BER	BER	BER
min	min	ng/ml	ng/ml (*100)	μl	ng	nmole	pmol/min	pmol/min/g liver	pmol/hr/g liver
10	5	237	23700	66.500	1576.05	3.14	314.142	29.906	1794.344755
20	15	877	87700	67.800	5946.06	11.85	1185.182	112.827	6769.633943
30	25	959	95900	74.000	7096.6	14.15	1414.511	134.659	8079.53237
40	35	1170	117000	78.000	9126	18.19	1819.015	173.167	10390.0195
50	45	1250	125000	73.700	9212.5	18.36	1836.257	174.808	10488.5004
60	55	1200	120000	71.200	8544	17.03	1703.010	162.123	9727.408134
Liver WT	9.8036								

		10-29-07 5μM Bosentan							
Time	Mid Time	Calculated Conc	Dilution Factor	Bile Vol	Amount	Amount	BER	BER	BER
min	min	ng/ml	ng/ml (*100)	μl	ng	nmole	pmol/min	pmol/min/g liver	pmol/hr/g liver
10	5	185	18500	59.700	1104.45	2.20	220.142	20.957	1257.424615
20	15	853	85300	64.700	5518.91	11.00	1100.042	104.722	6283.320462
30	25	1160	116000	66.300	7690.8	15.33	1532.948	145.934	8756.03353
40	35	1050	105000	70.000	7350	14.65	1465.019	139.467	8368.030172
50	45	1180	118000	77.300	9121.4	18.18	1818.098	173.080	10384.78237
60	55	1090	109000	76.300	8316.7	16.58	1657.704	157.810	9468.625378
Liver WT	12.5695								
		10-31-07 5μM Bosentan							
Time	Mid Time	Calculated Conc	Dilution Factor	Bile Vol	Amount	Amount	BER	BER	BER
min	min	ng/ml	ng/ml (*100)	μl	ng	nmole	pmol/min	pmol/min/g liver	pmol/hr/g liver
10	5	240	24000	76.500	1836	3.66	365.956	34.838	2090.299782
20	15	868	86800	67.600	5867.68	11.70	1169.559	111.340	6680.397725
30	25	1100	110000	73.600	8096	16.14	1613.713	153.623	9217.356772
40	35	1240	124000	78.300	9709.2	19.35	1935.260	184.233	11053.99708
50	45	1040	104000	77.900	8101.6	16.15	1614.830	153.729	9223.732414
60	55	1000	100000	78.100	7810	15.57	1556.707	148.196	8891.743625
Liver WT	12.04								

Liver Concentrations

	Calculated Conc	Dilution Factor	Liver Weight	Total Mass	Conc	Mass		Concentration	
	ng/ml	*10	g	ng	nM = pmol/ml	Mean	SD	Mean	SD
Homogenate Fex only 8-16-07	412	4120	10.5044	129834.38	8212.08				
Homogenate Fex only 10-16-07	366	3660	10.2546	112595.51	7295.20				
Homogenate Fex only 10-22-07	394	3940	12.932	152856.24	7853.30				
Homogenate Fex only 10-23-07	346	3460	10.0027	103828.03	6896.55				
Homogenate Fex only 10-24-07	312	3120	11.3885	106596.36	6218.86	121142	20407	7295	786
Homogenate Fex no TC 10-17-07	258	2580	12.3545	95623.83	5142.52				
Homogenate Fex no TC 10-29-07	437	4370	11.1219	145808.11	8710.38				
Homogenate Fex no TC 11-1-07	394	3940	12.8765	152200.23	7853.30				
Homogenate Fex no TC 11-8-07	347	3470	12.3932	129013.21	6916.48	130661	25323	7156	1529
Homogenate Fex + 918 9-7-07	370	3700	11.7118	130000.98	7374.93				
Homogenate Fex + 918 11-1-07	441	4410	10.7113	141710.50	8790.11				
Homogenate Fex + 918 11-26-07	417	4170	10.7159	134055.91	8311.74	135256	5946	8159	720
Homogenate Fex + Bos 10-16-07	282	2820	11.1608	94420.37	5620.89				
Homogenate Fex + Bos 10-26-07	281	2810	9.8036	82644.35	5600.96				
Homogenate Fex + Bos 10-29-07	330	3300	12.5695	124438.05	6577.64				
Homogenate Fex + Bos 10-31-07	223	2230	12.04	80547.60	4444.89	95513	20227	5561	873

Chapter 3: Fexofenadine in Single Pass Perfused Mouse Livers Perfusate Concentrations

Time(min)	WT-2	WT-3	WT-4	WT-5	AVG (ng/mL)	SD	Amount (ng)	Cumulative Amount (ng)	Avg PS Rate (ng/min)
1	74.5	302	239	311	115.8125	54.8	579.0625	579.0625	579.0625
2	237	525	406	481	206.125	63.4	2061.25	2640.313	1030.625
4	356	699	428	534	252.125	74.5	2521.25	5161.563	1260.625
6	340	644	410	585	247.375	71.6	2473.75	7635.313	1236.875
10	460	691	457	651	282.375	61.9	5647.5	13282.81	1411.875
15	574	770	505	682	316.375	58.5	7909.375	21192.19	1581.875
20	571	824	545	689	328.625	63.8	8215.625	29407.81	1643.125
25	544	758	596	695	324.125	48.2	8103.125	37510.94	1620.625
30	656	745	676	705	347.75	19.3	8693.75	46204.69	1738.75
30.25	531	639	545	568	285.375	24.0	356.7188	46561.41	1426.875
30.75	494	719	504	599	289.5	52.3	723.75	47285.16	1447.5
32	412	465	378	516	221.375	30.3	1383.594	48668.75	1106.875
36	279	157	199	283	114.75	31.0	2295	50963.75	573.75
40	198	90.1	138	184	76.2625	24.4	1525.25	52489	381.3125
45	182	64.4	108	153	63.425	25.8	1585.625	54074.63	317.125
50	169	47	101	136	56.625	26.1	1415.625	55490.25	283.125
55	147	42.8	90.3	131	51.3875	23.3	1284.688	56774.94	256.9375
60	143	41.2	87.4	106	47.2	21.2	1180	57954.94	236
65	142	32.6	75	92.8	42.8	22.6	1070	59024.94	214
70	136	30.1	68.9	97.1	41.5125	22.4	1037.813	60062.75	207.5625
75	131	32.2	64.7	87.5	39.425	20.8	985.625	61048.38	197.125

Time(min)	Mrp3KO-1	Mrp3KO-2	Mrp3KO-4	AVG (ng/mL)	SD	Amount (ng)	Cumulative Amount (ng)	Avg PS Rate (ng/min)
1	243	153	246	107	26.42442	535	535	535
2	518	323	534	229.1667	58.73741	2291.667	2826.667	1145.833
4	807	510	651	328	74.28156	3280	6106.667	1640
6	828	665	744	372.8333	40.75639	3728.333	9835	1864.167
10	1000	630	752	397	94.27089	7940	17775	1985
15	1000	624	807	405.1667	94.01108	10129.17	27904.17	2025.833
20	957	680	671	384.6667	81.29319	9616.667	37520.83	1923.333
25	1030	656	772	409.6667	95.72008	10241.67	47762.5	2048.333
30	1020	709	815	424	79.0522	10600	58362.5	2120
30.25	837	490	571	316.3333	90.76664	395.4167	58757.92	1581.667
30.75	789	505	577	311.8333	73.8196	779.5833	59537.5	1559.167
32	531	401	415	224.5	35.67913	1403.125	60940.63	1122.5
36	187	177	177	90.16667	2.886751	1803.333	62743.96	450.8333
40	80.5	93.1	97.6	45.2	4.431986	904	63647.96	226
45	66.4	77.4	77.9	36.95	3.25	923.75	64571.71	184.75
50	52.7	65.7	70.8	31.53333	4.666458	788.3333	65360.04	157.6667
55	48	59.1	67.8	29.15	4.962106	728.75	66088.79	145.75
60	46.2	61	61.5	28.11667	4.346359	702.9167	66791.71	140.5833
65	35	54.2	73.2	27.06667	9.550044	676.6667	67468.38	135.3333
70	40.2	50.1	65.7	26	6.427869	650	68118.38	130
75	33.8	52.8	57.1	23.95	6.199395	598.75	68717.13	119.75

Time(min)	Mrp4KO-1	Mrp4KO-2	Mrp4KO-3	Mrp4KO-4	AVG (ng/mL)	SD	Amount (ng)	Cumulative Amount (ng)	Avg PS Rate (ng/min)
1	146	173	334	186	104.875	42.24606	524.375	524.375	524.375
2	342	449	584	341	214.5	57.54563	2145	2669.375	1072.5
4	490	519	758	435	275.25	71.32613	2752.5	5421.875	1376.25
6	513	690	840	480	315.375	83.60958	3153.75	8575.625	1576.875
10	518	585	934	488	315.625	102.9331	6312.5	14888.13	1578.125
15	563	564	1000	521	331	113.1113	8275	23163.13	1655
20	646	699	871	568	348	64.23784	8700	31863.13	1740
25	700	743	892	609	368	59.02683	9200	41063.13	1840
30	740	812	890	647	386.125	51.77898	9653.125	50716.25	1930.625
30.25	682	521	718	504	303.125	54.73325	378.9063	51095.16	1515.625
30.75	643	501	655	553	294	36.86462	735	51830.16	1470
32	620	617	485	474	274.5	40.19328	1715.625	53545.78	1372.5
36	408	199	199	298	138	49.80462	2760	56305.78	690
40	346	131	95.9	230	100.3625	56.13355	2007.25	58313.03	501.8125
45	309	83.1	61.6	224	84.7125	58.83441	2117.813	60430.84	423.5625
50	291	85	56.7	171	75.4625	52.63749	1886.563	62317.41	377.3125
55	251	103	49.6	188	73.95	44.64351	1848.75	64166.16	369.75
60	223	76	54.3	179	66.5375	40.47496	1663.438	65829.59	332.6875
65	198	64.6	35.3	156	56.7375	38.13676	1418.438	67248.03	283.6875
70	167	74.5	35	139	51.9375	30.03496	1298.438	68546.47	259.6875
75	150	64.6	35.1	138	48.4625	27.9454	1211.563	69758.03	242.3125

Time(min)	Mrp2/3KO-2	Mrp2/3KO-3	Mrp2/3KO-4	AVG (ng/mL)	SD	Amount (ng)	Cumulative Amount (ng)	Avg PS Rate (ng/min)
1	183	129	113	70.83333	18.33939	354.1667	354.1667	354.1667
2	449	300	325	179	39.89674	1790	2144.167	895
4	694	483	436	268.8333	68.7065	2688.333	4832.5	1344.167
6	836	553	548	322.8333	82.42623	3228.333	8060.833	1614.167
10	953	596	555	350.6667	109.4559	7013.333	15074.17	1753.333
15	957	548	509	335.6667	124.081	8391.667	23465.83	1678.333
20	1080	667	580	387.8333	133.563	9695.833	33161.67	1939.167
25	1090	578	539	367.8333	153.7403	9195.833	42357.5	1839.167
30	1080	647	648	395.8333	124.8522	9895.833	52253.33	1979.167
30.25	723	557	579	309.8333	45.08141	387.2917	52640.63	1549.167
30.75	819	536	528	313.8333	82.8739	784.5833	53425.21	1569.167
32	690	399	473	260.3333	75.62132	1627.083	55052.29	1301.667
36	398	214	273	147.5	46.97606	2950	58002.29	737.5
40	244	120	205	94.83333	31.70305	1896.667	59898.96	474.1667
45	175	97.2	229	83.53333	33.12859	2088.333	61987.29	417.6667
50	157	83	260	83.33333	44.44753	2083.333	64070.63	416.6667
55	137	92.1	290	86.51667	51.87703	2162.917	66233.54	432.5833
60	117	80.2	241	73.03333	42.12426	1825.833	68059.38	365.1667
65	95.7	83.1	215	65.63333	36.39417	1640.833	69700.21	328.1667
70	75.2	77.9	186	56.51667	31.6027	1412.917	71113.13	282.5833
75	73.1	84	183	56.68333	30.275	1417.083	72530.21	283.4167

Time(min)	Mrp2KO-1	Mrp2KO-2	Mrp2KO-3	AVG (ng/mL)	SD	Amount (ng)	Cumulative Amount (ng)	Avg PS Rate (ng/min)
1	289	288	191	128	28.15	640	640	640
2	517	529	452	249.6667	20.71	2496.667	3136.667	1248.333
4	845	689	554	348	72.81	3480	6616.667	1740
6	938	800	642	396.6667	74.06	3966.667	10583.33	1983.333
10	1000	919	716	439.1667	73.15	8783.333	19366.67	2195.833
15	1000	918	781	449.8333	55.32	11245.83	30612.5	2249.167
20	1140	950	820	485	80.47	12125	42737.5	2425
25	1210	996	886	515.3333	82.38	12883.33	55620.83	2576.667
30	1180	1070	976	537.6667	51.05	13441.67	69062.5	2688.333
30.25	926	854	786	427.6667	35.00	534.5833	69597.08	2138.333
30.75	903	766	781	408.3333	37.57	1020.833	70617.92	2041.667
32	761	589	555	317.5	55.22	1984.375	72602.29	1587.5
36	450	365	434	208.1667	22.59	4163.333	76765.63	1040.833
40	308	254	345	151.1667	22.88	3023.333	79788.96	755.8333
45	255	198	339	132	35.46	3300	83088.96	660
50	215	166	262	107.1667	24.00	2679.167	85768.13	535.8333
55	166	150	235	91.83333	22.59	2295.833	88063.96	459.1667
60	146	132	218	82.66667	23.07	2066.667	90130.63	413.3333
65	117	118	204	73.16667	24.97	1829.167	91959.79	365.8333
70	93.9	107	173	62.31667	21.20	1557.917	93517.71	311.5833
75	90.4	90.9	157	56.38333	19.15	1409.583	94927.29	281.9167

Biliary Excretion Rate

WT-2

Time (min)	MidTim(min)	Tube Weight	Total Weight	Bile Vol. (uL)	Bile Rate (uL/min)	Amount(ng)	Cumulative Amunt(ng)	Biliary Excretion Rate (ng/min)
7	**3.5**	3318	3426	10.8	1.542857	1.836	1.836	0.262285714
14	**10.5**	3282	3411	12.9	1.842857	291.54	293.376	41.64857143
21	**17.5**	3286	3404	11.8	1.685714	1178.82	1472.196	168.4028571
28	**24.5**	3339	3451	11.2	1.6	1881.6	3353.796	268.8
35	**31.5**	3358	3460	10.2	1.457143	1999.2	5352.996	285.6
42	**38.5**	3396	3490	9.4	1.342857	2180.8	7533.796	311.5428571
49	**45.5**	3298	3377	7.9	1.128571	1603.7	9137.496	229.1
56	**52.5**	3354	3442	8.8	1.257143	1346.4	10483.896	192.3428571
63	**59.5**	3313	3377	6.4	0.914286	736	11219.896	105.1428571
70	**66.5**	3318	3412	9.4	1.342857	826.26	12046.156	118.0371429
77	**73.5**	3365	3433	6.8	0.971429	409.36	12455.516	58.48
Liver Wt		1.4			1.371429	12455.516		
Body Wt		28.4						

WT-3								
Time (min)	**MidTime (min)**	**Tube Weight**	**Total Weight**	**Bile Vol.**	**Bile Rate (uL/min)**	**Amount(ng)**	**Cumulative Amunt(ng)**	**Biliary Excretion Rate (ng/min)**
7	**3.5**	3370	3464	9.4	1.342857	1.2972	1.2972	0.185314286
14	**10.5**	3358	3450	9.2	1.314286	135.24	136.5372	19.32
21	**17.5**	3359	3450	9.1	1.3	518.7	655.2372	74.1
28	**24.5**	3316	3412	9.6	1.371429	1056	1711.2372	150.8571429
35	**31.5**	3355	3446	9.1	1.3	1283.1	2994.3372	183.3
42	**38.5**	3344	3435	9.1	1.3	1610.7	4605.0372	230.1
49	**45.5**	3369	3457	8.8	1.257143	1654.4	6259.4372	236.3428571
56	**52.5**	3357	3456	9.9	1.414286	1514.7	7774.1372	216.3857143
63	**59.5**	3353	3444	9.1	1.3	1046.5	8820.6372	149.5
70	**66.5**	3361	3451	9	1.285714	972	9792.6372	138.8571429
77	**73.5**	3324	3406	8.2	1.171429	807.7	10600.3372	115.3857143
Liver Wt		1.18			1.305195	10600.3372		
Body Wt		28.9						

WT-4								
Time (min)	**Mid Time (min)**	**Tube Weight**	**Total Weight**	**Bile Vol.**	**Bile Rate (uL/min)**	**Amount(ng)**	**Cumulative Amunt(ng)**	**Biliary Excretion Rate (ng/min)**
7	**3.5**	3363	3482	11.9	1.7	5.831	5.831	0.833
14	**10.5**	3334	3481	14.7	2.1	396.9	402.731	56.7
21	**17.5**	3368	3491	12.3	1.757143	950.79	1353.521	135.8271429
28	**24.5**	3339	3470	13.1	1.871429	1755.4	3108.921	250.7714286
35	**31.5**	3317	3430	11.3	1.614286	1808	4916.921	258.2857143
42	**38.5**	3359	3455	9.6	1.371429	1881.6	6798.521	268.8
49	**45.5**	3359	3449	9	1.285714	1989	8787.521	284.1428571
56	**52.5**	3296	3402	10.6	1.514286	2162.4	10949.921	308.9142857
63	**59.5**	3338	3427	8.9	1.271429	1593.1	12543.021	227.5857143
70	**66.5**	3330	3421	9.1	1.3	1392.3	13935.321	198.9
77	**73.5**	3333	3449	11.6	1.657143	1589.2	15524.521	227.0285714
Liver Wt		1			1.585714	15524.521		
Body Wt		26.4						

WT-5								
Time (min)	**MidTime (min)**	**Tube Weight**	**Total Weight**	**Bile Vol.**	**Bile Rate (uL/min)**	**Amount(ng)**	**Cumulative Amunt(ng)**	**Biliary Excretion Rate (ng/min)**
7	**3.5**	3360	3503	14.3	2.042857	46.046	46.046	6.578
14	**10.5**	3326	3416	9	1.285714	399.6	445.646	57.08571429
21	**17.5**	3362	3466	10.4	1.485714	1175.2	1620.846	167.8857143
28	**24.5**	3395	3492	9.7	1.385714	1416.2	3037.046	202.3142857
35	**31.5**	3339	3470	13.1	1.871429	2397.3	5434.346	342.4714286
42	**38.5**	3362	3454	9.2	1.314286	2088.4	7522.746	298.3428571
49	**45.5**	3320	3415	9.5	1.357143	2289.5	9812.246	327.0714286
56	**52.5**	3289	3394	10.5	1.5	1911	11723.246	273
63	**59.5**	3360	3459	9.9	1.414286	1534.5	13257.746	219.2142857
70	**66.5**	3368	3449	8.1	1.157143	1093.5	14351.246	156.2142857
77	**73.5**	3354	3452	9.8	1.4	1048.6	15399.846	149.8
Liver Wt		0.92		**Mean**	1.474026	15399.846		
Body Wt		26.1						

Mrp3KO-1								
Time (min)	**MidTime (min)**	**Tube Weight**	**Total Weight**	**Bile Vol.**	**Bile Rate (uL/min)**	**Amount(ng)**	**Cumulative Amunt(ng)**	**Biliary Excretion Rate (ng/min)**
7	**3.5**	3330	3462	13.2	1.885714	3.8544	3.8544	0.550628571
14	**10.5**	3324	3432	10.8	1.542857	201.96	205.8144	28.85142857
21	**17.5**	3365	3471	10.6	1.514286	655.08	860.8944	93.58285714
28	**24.5**	3366	3476	11	1.571429	1287	2147.8944	183.8571429
35	**31.5**	3360	3463	10.3	1.471429	1565.6	3713.4944	223.6571429
42	**38.5**	3360	3456	9.6	1.371429	1785.6	5499.0944	255.0857143
49	**45.5**	3362	3458	9.6	1.371429	1660.8	7159.8944	237.2571429
56	**52.5**	3355	3449	9.4	1.342857	1579.2	8739.0944	225.6
63	**59.5**	3325	3414	8.9	1.271429	1263.8	10002.8944	180.5428571
70	**66.5**	3318	3400	8.2	1.171429	1016.8	11019.6944	145.2571429
77	**73.5**	3308	3411	10.3	1.471429	1112.4	12132.0944	158.9142857
Liver Wt		1.3		**Mean**	1.453247	12132.0944		
Body Wt		29.7						

Mrp3KO-2								
Time (min)	**MidTim(min)**	**Tube Weight**	**Total Weight**	**Bile Vol.**	**Bile Rate (uL/min)**	**Amount(ng)**	**Cumulative Amunt(ng)**	**BiliaryExcretion Rate(ng/min)**
7	**3.5**	3363	3525	16.2	2.314286	50.058	50.058	7.151142857
14	**10.5**	3367	3483	11.6	1.657143	658.88	708.938	94.12571429
21	**17.5**	3365	3491	12.6	1.8	1638	2346.938	234
28	**24.5**	3372	3494	12.2	1.742857	2379	4725.938	339.8571429
35	**31.5**	3318	3448	13	1.857143	3068	7793.938	438.2857143
42	**38.5**	3363	3491	12.8	1.828571	3392	11185.938	484.5714286
49	**45.5**	3365	3485	12	1.714286	2844	14029.938	406.2857143
56	**52.5**	3345	3481	13.6	1.942857	2679.2	16709.138	382.7428571
63	**59.5**	3398	3489	9.1	1.3	1528.8	18237.938	218.4
70	**66.5**	3334	3447	11.3	1.614286	1649.8	19887.738	235.6857143
77	**73.5**	3316	3440	12.4	1.771429	1711.2	21598.938	244.4571429
Liver Wt		1.23		**Mean**	1.776623	21598.938		
Body Wt		29.7						

Mrp3KO-4								
Time (min)	**MidTim(min)**	**Tube Weight**	**Total Weight**	**Bile Vol.**	**Bile Rate (uL/min)**	**Amount(ng)**	**Cumulative Amunt(ng)**	**Biliary Excretion Rate (ng/min)**
7	**3.5**	3311	3413	10.2	1.457143	0.3876	0.3876	0.055371429
14	**10.5**	3366	3498	13.2	1.885714	186.12	186.5076	26.58857143
21	**17.5**	3366	3469	10.3	1.471429	580.92	767.4276	82.98857143
28	**24.5**	3359	3434	7.5	1.071429	810	1577.4276	115.7142857
35	**31.5**	3357	3462	10.5	1.5	1680	3257.4276	240
42	**38.5**	3355	3466	11.1	1.585714	2331	5588.4276	333
49	**45.5**	3363	3463	10	1.428571	2110	7698.4276	301.4285714
56	**52.5**	3316	3436	12	1.714286	2244	9942.4276	320.5714286
63	**59.5**	3358	3468	11	1.571429	1760	11702.4276	251.4285714
70	**66.5**	3334	3437	10.3	1.471429	1359.6	13062.0276	194.2285714
77	**73.5**	3370	3469	9.9	1.414286	1128.6	14190.6276	161.2285714
Liver Wt		1.04		**Mean**	1.506494	14190.6276		
Body Wt		24.36						

Mrp4KO-1								
Time (min)	**MidTime (min)**	**Tube Weight**	**Total Weight**	**Bile Vol.**	**Bile Rate (uL/min)**	**Amount(ng)**	**Cumulative Amunt(ng)**	**Biliary Excretion Rate (ng/min)**
7	**3.5**	3285	3418	13.3	1.9	11.1055	11.1055	1.5865
14	**10.5**	3341	3456	11.5	1.642857	388.7	399.8055	55.52857143
21	**17.5**	3294	3407	11.3	1.614286	1152.6	1552.4055	164.6571429
28	**24.5**	3351	3460	10.9	1.557143	1678.6	3231.0055	239.8
35	**31.5**	3334	3434	10	1.428571	2000	5231.0055	285.7142857
42	**38.5**	3318	3410	9.2	1.314286	1987.2	7218.2055	283.8857143
49	**45.5**	3326	3410	8.4	1.2	1722	8940.2055	246
56	**52.5**	3322	3403	8.1	1.157143	1215	10155.2055	173.5714286
63	**59.5**	3332	3400	6.8	0.971429	856.8	11012.0055	122.4
70	**66.5**	3355	3421	6.6	0.942857	693	11705.0055	99
77	**73.5**	3333	3411	7.8	1.114286	720.72	12425.7255	102.96
Liver Wt		1.23		**Mean**	1.349351	12425.7255		
Body Wt		26.8						

Mrp4KO-2								
Time (min)	**MidTime (min)**	**Tube Weight**	**Total Weight**	**Bile Vol.**	**Bile Rate (uL/min)**	**Amount(ng)**	**Cumulative Amunt(ng)**	**Biliary Excretion Rate (ng/min)**
7	**3.5**	3339	3362	2.3	0.328571	0	0	0
14	**10.5**	3313	3402	8.9	1.271429	106.8	106.8	15.25714286
21	**17.5**	3322	3433	11.1	1.585714	1143.3	1250.1	163.3285714
28	**24.5**	3367	3481	11.4	1.628571	2052	3302.1	293.1428571
35	**31.5**	3334	3421	8.7	1.242857	1887.9	5190	269.7
42	**38.5**	3345	3443	9.8	1.4	2136.4	7326.4	305.2
49	**45.5**	3357	3447	9	1.285714	1989	9315.4	284.1428571
56	**52.5**	3296	3377	8.1	1.157143	1368.9	10684.3	195.5571429
63	**59.5**	3286	3496	21	3	1942.5	12626.8	277.5
70	**66.5**	3338	3489	15.1	2.157143	1091.73	13718.53	155.9614286
77	**73.5**	3343	3458	11.5	1.642857	953.35	14671.88	136.1928571
Liver Wt		1.23		**Mean**	1.518182	14671.88		
Body Wt		28.9						

Mrp4KO-3								
Time (min)	**MidTime (min)**	**Tube Weight**	**Total Weight**	**Bile Vol.**	**Bile Rate (uL/min)**	**Amount(ng)**	**Cumulative Amunt(ng)**	**Biliary Excretion Rate (ng/min)**
7	**3.5**	3294	3363	6.9	0.985714	0	0	0
14	**10.5**	3366	3450	8.4	1.2	57.12	57.12	8.16
21	**17.5**	3318	3390	7.2	1.028571	475.2	532.32	67.88571429
28	**24.5**	3364	3438	7.4	1.057143	1058.2	1590.52	151.1714286
35	**31.5**	3357	3431	7.4	1.057143	1413.4	3003.92	201.9142857
42	**38.5**	3330	3403	7.3	1.042857	1708.2	4712.12	244.0285714
49	**45.5**	3358	3450	9.2	1.314286	1794	6506.12	256.2857143
56	**52.5**	3344	3397	5.3	0.757143	757.9	7264.02	108.2714286
63	**59.5**	3377	3450	7.3	1.042857	963.6	8227.62	137.6571429
70	**66.5**	3315	3396	8.1	1.157143	874.8	9102.42	124.9714286
77	**73.5**	3364	3466	10.2	1.457143	984.3	10086.72	140.6142857
Liver Wt		1.06		**Mean**	1.1	10086.72		
Body Wt		25.3						

Mrp4KO-4								
Time (min)	**MidTime (min)**	**Tube Weight**	**Total Weight**	**Bile Vol.**	**Bile Rate (uL/min)**	**Amount(ng)**	**Cumulative Amunt(ng)**	**Biliary Excretion Rate (ng/min)**
7	**3.5**	3342	3473	13.1	1.871429	29.344	29.344	4.192
14	**10.5**	3365	3479	11.4	1.628571	599.64	628.984	85.66285714
21	**17.5**	3368	3489	12.1	1.728571	1645.6	2274.584	235.0857143
28	**24.5**	3333	3442	10.9	1.557143	2299.9	4574.484	328.5571429
35	**31.5**	3364	3457	9.3	1.328571	2427.3	7001.784	346.7571429
42	**38.5**	3366	3447	8.1	1.157143	2235.6	9237.384	319.3714286
49	**45.5**	3314	3400	8.6	1.228571	2098.4	11335.784	299.7714286
56	**52.5**	3310	3490	18	2.571429	3582	14917.784	511.7142857
63	**59.5**	3316	3459	14.3	2.042857	2288	17205.784	326.8571429
70	**66.5**	3357	3416	5.9	0.842857	767	17972.784	109.5714286
77	**73.5**	3360	3436	7.6	1.085714	904.4	18877.184	129.2
Liver Wt		0.82		**Mean**	1.549351	18877.184		
Body Wt		23.33						

Mrp2/3KO-2								
Time (min)	**MidTime (min)**	**Tube Weight**	**Total Weight**	**Bile Vol.**	**Bile Rate (uL/min)**	**Amount(ng)**	**Cumulative Amunt(ng)**	**Biliary Excretion Rate (ng/min)**
7	**3.5**	3362	3436	7.4	1.057143	0.69782	0.69782	0.099688571
14	**10.5**	3370	3440	7	1	30.94	31.63782	4.42
21	**17.5**	3364	3447	8.3	1.185714	251.49	283.12782	35.92714286
28	**24.5**	3354	3442	8.8	1.257143	497.2	780.32782	71.02857143
35	**31.5**	3322	3406	8.4	1.2	677.88	1458.20782	96.84
42	**38.5**	3359	3439	8	1.142857	744	2202.20782	106.2857143
49	**45.5**	3326	3400	7.4	1.057143	677.84	2880.04782	96.83428571
56	**52.5**	3333	3407	7.4	1.057143	502.46	3382.50782	71.78
63	**59.5**	3335	3440	10.5	1.5	569.1	3951.60782	81.3
70	**66.5**	3358	3428	7	1	313.6	4265.20782	44.8
77	**73.5**	3318	3404	8.6	1.228571	304.44	4569.64782	43.49142857
Liver Wt		1.47		**Mean**	1.153247	4569.64782		
Body Wt		25.7						

Mrp2/3KO-3								
Time (min)	**MidTime (min)**	**Tube Weight**	**Total Weight**	**Bile Vol.**	**Bile Rate (uL/min)**	**Amount(ng)**	**Cumulative Amunt(ng)**	**Biliary Excretion Rate (ng/min)**
7	**3.5**	3289	3489	20	2.857143	0.362	0.362	0.051714286
14	**10.5**	3339	3442	10.3	1.471429	41.921	42.283	5.988714286
21	**17.5**	3360	3416	5.6	0.8	127.68	169.963	18.24
28	**24.5**	3360	3490	13	1.857143	700.7	870.663	100.1
35	**31.5**	3321	3372	5.1	0.728571	302.94	1173.603	43.27714286
42	**38.5**	3367	3496	12.9	1.842857	1071.99	2245.593	153.1414286
49	**45.5**	3321	3452	13.1	1.871429	379.9	2625.493	54.27142857
56	**52.5**	3355	3511	15.6	2.228571	427.44	3052.933	61.06285714
63	**59.5**	3335	3450	11.5	1.642857	511.75	3564.683	73.10714286
70	**66.5**	3330	3520	19	2.714286	695.4	4260.083	99.34285714
77	**73.5**	3341	3568	22.7	3.242857	537.99	4798.073	76.85571429
Liver Wt		1.8		**Mean**	1.932468	4798.073		
Body Wt		28.8						

Mrp2/3KO-4								
Time (min)	**MidTime (min)**	**Tube Weight**	**Total Weight**	**Bile Vol.**	**Bile Rate (uL/min)**	**Amount(ng)**	**Cumulative Amunt(ng)**	**Biliary Excretion Rate (ng/min)**
7	**3.5**	3356	3484	12.8	1.828571	6.6816	6.6816	0.954514286
14	**10.5**	3298	3414	11.6	1.657143	226.2	232.8816	32.31428571
21	**17.5**	3343	3468	12.5	1.785714	751.25	984.1316	107.3214286
28	**24.5**	3332	3447	11.5	1.642857	1288	2272.1316	184
35	**31.5**	3349	3435	8.6	1.228571	1178.2	3450.3316	168.3142857
42	**38.5**	3360	3451	9.1	1.3	1419.6	4869.9316	202.8
49	**45.5**	3359	3440	8.1	1.157143	1312.2	6182.1316	187.4571429
56	**52.5**	3335	3404	6.9	0.985714	966	7148.1316	138
63	**59.5**	3363	3430	6.7	0.957143	783.9	7932.0316	111.9857143
70	**66.5**	3343	3416	7.3	1.042857	788.4	8720.4316	112.6285714
77	**73.5**	3361	3458	9.7	1.385714	979.7	9700.1316	139.9571429
Liver Wt		1.77		**Mean**	1.361039	9700.1316		
Body Wt		28.9						

Mrp2/3KO-5								
Time (min)	**MidTime (min)**	**Tube Weight**	**Total Weight**	**Bile Vol.**	**Bile Rate (uL/min)**	**Amount(ng)**	**Cumulative Amunt(ng)**	**Biliary Excretion Rate (ng/min)**
7	**3.5**	3363	3473	11	1.571429	1.76	1.76	0.251428571
14	**10.5**	3361	3466	10.5	1.5	67.725	69.485	9.675
21	**17.5**	3371	3461	9	1.285714	353.7	423.185	50.52857143
28	**24.5**	3316	3398	8.2	1.171429	664.2	1087.385	94.88571429
35	**31.5**	3361	3439	7.8	1.114286	803.4	1890.785	114.7714286
42	**38.5**	3325	3414	8.9	1.271429	1157	3047.785	165.2857143
49	**45.5**	3361	3455	9.4	1.342857	1240.8	4288.585	177.2571429
56	**52.5**	3315	3395	8	1.142857	1016	5304.585	145.1428571
63	**59.5**	3296	3363	6.7	0.957143	757.1	6061.685	108.1571429
70	**66.5**	3324	3392	6.8	0.971429	700.4	6762.085	100.0571429
77	**73.5**	3295	3401	10.6	1.514286	1019.72	7781.805	145.6742857
Liver Wt		1.62		**Mean**	1.258442	7781.805		
Body Wt		27.3						

Mrp2KO-1								
Time (min)	**MidTime (min)**	**Tube Weight**	**Total Weight**	**Bile Vol.**	**Bile Rate (uL/min)**	**Amount(ng)**	**Cumulative Amunt(ng)**	**Biliary Excretion Rate (ng/min)**
7	**3.5**	3318	3431	11.3	1.614286	0	0	0
14	**10.5**	3332	3427	9.5	1.357143	67.26	67.26	9.608571429
21	**17.5**	3366	3467	10.1	1.442857	307.04	374.3	43.86285714
28	**24.5**	3320	3426	10.6	1.514286	520.46	894.76	74.35142857
35	**31.5**	3292	3395	10.3	1.471429	622.12	1516.88	88.87428571
42	**38.5**	3295	3401	10.6	1.514286	695.36	2212.24	99.33714286
49	**45.5**	3317	3420	10.3	1.471429	622.12	2834.36	88.87428571
56	**52.5**	3363	3456	9.3	1.328571	398.04	3232.4	56.86285714
63	**59.5**	3356	3450	9.4	1.342857	326.18	3558.58	46.59714286
70	**66.5**	3297	3387	9	1.285714	256.5	3815.08	36.64285714
77	**73.5**	3370	3474	10.4	1.485714	221.52	4036.6	31.64571429
Liver Wt		1.68		**Mean**	1.438961	4036.6		
Body Wt		30.9						

Mrp2KO-2								
Time (min)	**MidTime (min)**	**Tube Weight**	**Total Weight**	**Bile Vol.**	**Bile Rate (uL/min)**	**Amount(ng)**	**Cumulative Amunt(ng)**	**Biliary Excretion Rate (ng/min)**
7	**3.5**	3362	3449	8.7	1.242857	0	0	0
14	**10.5**	3336	3433	9.7	1.385714	59.849	59.849	8.549857143
21	**17.5**	3338	3437	9.9	1.414286	393.03	452.879	56.14714286
28	**24.5**	3341	3448	10.7	1.528571	735.09	1187.969	105.0128571
35	**31.5**	3313	3419	10.6	1.514286	981.56	2169.529	140.2228571
42	**38.5**	3368	3445	7.7	1.1	831.6	3001.129	118.8
49	**45.5**	3331	3464	13.3	1.9	1327.34	4328.469	189.62
56	**52.5**	3339	3413	7.4	1.057143	613.46	4941.929	87.63714286
63	**59.5**	3358	3450	9.2	1.314286	681.72	5623.649	97.38857143
70	**66.5**	3353	3453	10	1.428571	617	6240.649	88.14285714
77	**73.5**	3349	3434	8.5	1.214286	438.6	6679.249	62.65714286
Liver Wt		1.55		**Mean**	1.372727	6679.249		
Body Wt		30						

Mrp2KO-3								
Time (min)	**MidTime (min)**	**Tube Weight**	**Total Weight**	**Bile Vol.**	**Bile Rate (uL/min)**	**Amount(ng)**	**Cumulative Amunt(ng)**	**Biliary Excretion Rate (ng/min)**
7	**3.5**	3344	3425	8.1	1.157143	0	0	0
14	**10.5**	3342	3449	10.7	1.528571	119.84	119.84	17.12
21	**17.5**	3359	3469	11	1.571429	528	647.84	75.42857143
28	**24.5**	3286	3390	10.4	1.485714	859.04	1506.88	122.72
35	**31.5**	3289	3382	9.3	1.328571	976.5	2483.38	139.5
42	**38.5**	3289	3381	9.2	1.314286	966	3449.38	138
49	**45.5**	3361	3439	7.8	1.114286	881.4	4330.78	125.9142857
56	**52.5**	3343	3427	8.4	1.2	661.92	4992.7	94.56
63	**59.5**	3336	3403	6.7	0.957143	510.54	5503.24	72.93428571
70	**66.5**	3338	3409	7.1	1.014286	438.07	5941.31	62.58142857
77	**73.5**	3314	3403	8.9	1.271429	429.87	6371.18	61.41
Liver Wt		1.47		**Mean**	1.267532	6371.18		
Body Wt		27.3						

Mass Balance at the end of the 75 perfusion

		Amount in	Amount in	Amount in				
	Total Dose (ng)	Perfusate (ng)	Bile (ng)	Liver (ng)	% in Perfusate	% in Bile	% in Liver	Total
WT	111750	58303	12456	5670	52.2	11.1	5.1	68.4
	100875	63256	10600	4035.6	62.7	10.5	4.0	77.2
	99750	52361	15525	5370	52.5	15.6	5.4	73.4
	117000	66151	15400	4968	56.5	13.2	4.2	73.9
Mrp3KO	121500	80038	12132	3350.1	65.9	10.0	2.8	78.6
	123375	56873	21599	6383.7	46.1	17.5	5.2	68.8
	125250	65804	14191	6364.8	52.5	11.3	5.1	68.9
Mrp4KO	139875	75098	12426	4723.2	53.7	8.9	3.4	65.9
	127875	61740	14672	6051.6	48.3	11.5	4.7	64.5
	116625	75115	10087	2385.0	64.4	8.6	2.0	75.1
	124500	62790	18877	3985.2	50.4	15.2	3.2	68.8
Mrp2/3KO	117000	91774	4570	4895.1	78.4	3.9	4.2	86.5
	124125	55786	4798	8964.0	44.9	3.9	7.2	56.0
	132375	67345	9700	10195.2	50.9	7.3	7.7	65.9
Mrp2KO	148500	102762	4037	2182.32	69.2	2.7	1.5	73.4
	123750	89398	6679	4082.7	72.2	5.4	3.3	80.9
	129750	88877	6371	5424.3	68.5	4.9	4.2	77.6

Chapter 4:

^{99m}Tc-MIBI uptake in suspended Rat Hepatocytes

	Time (min)	Mean	SD	Time (min)	Mean	SD	Mean	SD
	1	0.025	0.003	0.5	0.020	0.001	0.020	0.001
	2.5	0.045	0.002	1	0.034	0.006	0.030	0.001
Ctrl	5	0.078	0.013	2.5	0.060	0.003	0.061	0.003
	1	0.024	0.002	0.5	0.016	0.001	0.020	0.002
	2.5	0.044	0.004	1	0.037	0.015	0.035	0.002
Rifamycin SV	5	0.078	0.004	2.5	0.055	0.003	0.063	0.007
	1	0.024	0.001	0.5	0.017	0.002	0.019	0.000
	2.5	0.043	0.001	1	0.027	0.001	0.031	0.003
Glycyrrhizic Acid	5	0.072	0.002	2.5	0.056	0.003	0.063	0.001
	1	0.022	0.001	0.5	0.017	0.003	0.019	0.001
	2.5	0.039	0.001	1	0.026	0.004	0.029	0.002
Clonidine	5	0.065	0.004	2.5	0.054	0.006	0.059	0.006
	1	0.021	0.002	0.5	0.015	0.001	0.020	0.000
	2.5	0.041	0.003	1	0.025	0.001	0.030	0.001
Desipramine	5	0.064	0.002	2.5	0.053	0.002	0.058	0.002
	1	0.023	0.002	0.5	0.015	0.001	0.020	0.001
	2.5	0.045	0.003	1	0.028	0.003	0.034	0.001
Ketoprofen	5	0.067	0.005	2.5	0.050	0.001	0.062	0.006
	1	0.019	0.000	0.5	0.015	0.001	0.021	0.001
	2.5	0.035	0.001	1	0.023	0.001	0.037	0.004
Choline Buffer	5	0.056	0.001	2.5	0.045	0.003	0.063	0.002

^{99m}Tc-MEB uptake in suspended Rat Hepatocytes

	Time (min)	Mean	SD	Mean	SD	Mean	SD
	0.5	0.092	0.006	0.115	0.003	0.087	0.004
	1	0.117	0.007	0.156	0.001	0.116	0.005
Ctrl	1.5	0.123	0.008	0.175	0.001	0.145	0.006
	0.5	0.015	0.002	0.025	0.001	0.027	0.003
	1	0.018	0.002	0.024	0.005	0.031	0.004
Rifamycin SV	1.5	0.021	0.002	0.033	0.008	0.038	0.000
	0.5			0.034	0.003	0.033	0.003
	1			0.053	0.005	0.038	0.007
Glycyrrhizic Acid	1.5			0.068	0.001	0.058	0.001
	0.5	0.079	0.005	0.094	0.011	0.076	0.003
	1	0.095	0.006	0.131	0.019	0.110	0.008
Clonidine	1.5	0.104	0.004	0.151	0.023	0.130	0.006
	0.5	0.078	0.002	0.096	0.003	0.073	0.005
	1	0.102	0.004	0.134	0.002	0.112	0.016
Desipramine	1.5	0.107	0.002	0.152	0.006	0.126	0.008
	0.5	0.065	0.005	0.086	0.007	0.056	0.019
	1	0.084	0.004	0.114	0.010	0.082	0.021
Ketoprofen	1.5	0.093	0.001	0.132	0.012	0.105	0.019
	0.5	0.055	0.004	0.086	0.004	0.071	0.005
	1	0.083	0.006	0.117		0.093	
Choline Buffer	1.5	0.090	0.002	0.147	0.015	0.122	0.008

[^{3}H]$E_2$17βG uptake in Rat Hepatoctyes

		Mean	SD			Mean	SD
	0.5	12.38524	2.170438	Ctrl	0.5	9.870482	0.142666
	1	15.09243	2.062472		1	14.65886	1.051743
	2.5	18.85566	2.330778	Rifamycin SV	0.5	2.193125	0.784988
Ctrl	5	25.16313	0.666116		1	2.091985	0.210735
	0.5	2.738443	0.306133	Glycyrrhizic Acid	0.5	2.048354	0.989725
	1	2.517903	0.020512		1	1.833771	0.575905
	2.5	2.974957	0.413613	Clonidine	0.5	9.474591	0.401928
Rifamycin SV	5	3.069813	0.049867		1	15.25649	0.246573
	0.5	3.030449	0.106825	Desipramine	0.5	11.57111	1.02265
	1	3.925705	1.97042		1	15.84401	0.574169
Glycyrrhizic	2.5	5.413246	3.861875	Ketoprofen	0.5	8.023864	1.358714
Acid	5	5.856332	3.890866		1	13.02364	2.307888
	0.5	9.970687	4.220903				
	1	13.37733	7.334079				
	2.5	19.26212	4.667984				
Clonidine	5	25.21137	1.654966				
	0.5	13.77704	1.291401				
	1	17.35233	0.133057				
	2.5	23.89008	5.098736				
Desipramine	5	23.95633	3.23873				
	0.5	11.56112	1.417318				
	1	14.39834	2.223683				
	2.5	17.15951	0.504023				
Ketoprofen	5	20.50233	0.154342				

[^{14}C]TEA uptake in Rat Hepatocytes

		Mean	SD			Mean	SD	Mean	SD
	1	19.62706	0.283542		0.5	15.67099	2.254442	12.38052	1.011012
	2.5	31.50644	0.37017		1	22.10304	1.308434	13.72543	0.775908
	5	36.35275	0.392576		2.5	33.46671	0.474105	30.90703	2.735914
	10	36.79896	11.79346	Ctrl	5	41.93236	1.737362	31.85378	
Ctrl	20	24.34477	1.191812		0.5	14.78319	0.470174	10.67335	1.141725
	1	40.62799	31.97156		1	18.64507	1.394285	11.58624	2.052951
	2.5	28.02024	7.60156	Rifamycin	2.5	26.53415	0.935913	21.92847	1.320568
	5	27.37999	0.059177	SV	5	34.22803	1.612172	18.77093	0.834149
	10	28.86343	1.771652		0.5	13.73598	1.010805	8.236493	4.587954
Rifamycin SV	20	19.60059	3.222042		1	16.47228	1.678505	9.00971	5.696714
	1	36.66742	37.57265	Glycyrrhizic	2.5	23.40738	3.486012	14.87233	11.29946
	2.5	16.32844	8.933144	Acid	5	28.95145	5.850027	12.69465	7.759001
	5	20.82923	9.205003		0.5	8.27905	1.356852	5.246362	0.948509
Glycyrrhizic	10	22.44201	10.85292		1	11.33615	4.136207	5.954638	0.644275
Acid	20	17.31598	0.008887		2.5	7.966801	0.188376	3.835009	1.58727
	1	9.881845	2.028322	Clonidine	5	9.24062	0.790033	6.439679	1.740032
	2.5	10.9993	1.370536		0.5	8.628189	0.166611	6.029467	1.770394
	5	10.98333	0.270778		1	73.3402	93.43815	5.538977	0.699209
	10	12.63309	0.122718		2.5	9.50094	1.428023	4.698821	0.415392
Clonidine	20	9.3659	0.480048	Desipramine	5	9.346783	0.610846	7.203302	0.830726
	1	15.675	9.92791		0.5	13.66023	0.066967	10.54654	0.295093
	2.5	10.45545	0.475845		1	15.64974	1.419428	12.08741	0.305804
	5	12.05765	0.049089		2.5	21.5592	1.950168	20.94596	0.584993
	10	12.15841	0.474319	Ketoprofen	5	26.74747	4.959626	23.02009	6.67613
Desipramine	20	14.0206	1.665536						
	1	22.63843	0.583946						
	2.5	28.0347	7.073127						
	5	42.96362	2.520017						
	10	38.40968	4.693135						
Ketoprofen	20	29.59863	0.648622						

^{99m}Tc-MEB uptake in Human Hepatocytes

		Mean	SD	Mean	SD
Ctrl	0.5	0.109	0.010	0.209	0.044
	1	0.145	0.015	0.292	0.043
Rifamycin SV	0.5	0.063	0.004	0.030	0.003
	1	0.079	0.003	0.034	0.004
Decynium 22	0.5	0.089	0.010	0.156	0.007
	1	0.120	0.011	0.238	0.021
Tetracycline	0.5	0.070	0.002	0.176	0.020
	1	0.087	0.008	0.267	0.025
Choline Buffer	0.5	0.101	0.005	0.170	0.004
	1	0.127	0.003	0.266	0.006

[^{3}H]$E_2$17βG uptake in Human Hepatoctyes

		Mean	SD	Mean	SD	Mean	SD
Ctrl	0.5	0.973357	0.246299	6.260282	1.451209	3.014948	0.226557
	1	1.150589	0.071566	6.690094	0.092808	4.390121	0.992107
Rifamycin SV	0.5	0.673821	0.048202	2.553705	0.043409	1.730216	0.096229
	1	0.756412	0.081221	2.578198	0.084623	2.094757	0.308152
Decynium 22	0.5	0.808107	0.310853	4.057475	0.456242	2.390392	0.042579
	1	1.057342	0.075733	5.292775	0.009627	3.783642	0.204595
Tetracycline	0.5	0.562734	0.123431	4.756897	0.196647	2.606126	0.270383
	1	0.619201	0.149388	5.806272	0.820912	3.738196	0.383336

[^{14}C]TEA uptake in Human Hepatocytes

		Mean	SD	Mean	SD	Mean	SD
Ctrl	1	16.41312	1.091486	10.83375	0.121054	5.425928	0.744333
	2.5	25.19218	0.546069	17.82554	0.811958	7.35569	0.158289
	5					8.181197	0.647109
Rifamycin SV	1	15.1858	1.263563	9.819604	0.789064	5.343774	0.568845
	2.5	22.43821	3.457341	17.9108	1.338277	6.495763	0.279994
	5					8.986862	0.156035
Decynium 22	1	6.48014	0.44253	11.62447	0.7526	5.407475	0.005449
	2.5	11.47248	0.615183	18.72718	0.382743	6.934536	0.244847
	5					8.226498	0.471793
Tetracycline	1	12.37583	1.201312	8.686384	0.773033	3.969133	0.176653
	2.5	20.0061	2.596266	9.160144	0.839768	4.741283	0.110022
	5					4.87555	0.064472

^{99m}Tc-MEB efflux in Sandwich-Culture Rat Hepatocytes

	5/20/2008		6/23/2008		8/4/2008		8/15/2008		Mean	SD
	Mean	**SD**	**Mean**	**SD**	**Mean**	**SD**	**Mean**	**SD**		
Basolateral & Apical Efflux	47.10	1.84	38.03	6.06	34.33	4.49	41.65	2.12	40.28	5.44
Basolateral & Apical Efflux with MK-571	38.90	0.99	33.93	1.83	31.26	1.81	41.15	2.85	36.31	4.52
Basolateral Efflux	27.68	5.70	17.20	3.91	22.44	1.38	32.67	0.47	25.00	6.67
Basolateral Efflux with MK-571	34.03	2.30	28.77	1.75	30.22	0.40	42.99	1.67	34.00	6.39
Apical Efflux	19.42		20.82		11.89		8.98		15.28	5.75
Apical Efflux with MK-571	4.86		5.16		1.04		-1.84		2.31	3.34
Total WT	47.10		38.03		34.33		41.65		40.28	5.44
Cells Only	48.78	1.49	61.97	6.06	65.67	4.49	58.35	2.12	58.69	7.25
	59.91	0.78	66.07	1.83	68.74	1.81	58.85	2.85	63.39	4.78
	70.15	7.10	82.80	3.91	77.56	1.38	67.33	0.47	74.46	7.04
Cells + Bile	64.38	2.01	71.23	1.75	69.78	0.40	57.01	1.67	65.60	6.44

^{99m}Tc-MEB efflux in Sandwich-Culture TR^{-} Rat Hepatocytes

	6/30/2008		9/22/2008		9/29/2008		Mean	SD
	Mean	SD	Mean	SD	Mean	SD		
Basolateral & Apical Efflux	33.67	2.01	22.55	6.01			28.11	7.86
Basolateral & Apical Efflux with MK-571	45.38	5.99	26.88	1.78			36.13	13.08
Basolateral Efflux	36.24	1.79	27.41	4.80			31.82	6.24
Basolateral Efflux with MK-571	46.74	1.34	34.85	3.71			40.80	8.41
Apical Efflux	-2.57		-4.86				-3.71	1.62
Apical Efflux with MK-571	-1.36		-7.96				-4.66	4.67
Total Efflux								
Cells Only	66.33	2.01	77.45	6.01	92.64	0.88	78.81	13.21
	54.62	5.99	73.12	1.78	92.23	0.66	73.32	18.81
	63.76	1.79	72.59	4.80	94.11	0.92	76.82	15.61
Cells + Bile	53.26	1.34	65.15	3.71	94.34	0.86	70.92	21.14

^{99m}Tc-MEB efflux in Sandwich-Culture Human Hepatocytes

	8/28/2009		8/31/2009			
	Mean	SD	Mean	SD	Mean	Range
Basolateral & Apical Efflux	68.08	0.88	56.76	0.98	62.42	8.00
Basolateral & Apical Efflux with MK-571	72.60	1.34	72.03	2.74	72.32	0.40
Basolateral Efflux	16.23	3.50	17.09	4.07	16.66	0.61
Basolateral Efflux with MK-571	39.71	4.59	40.32	1.05	40.02	0.43
Apical Efflux	51.84		39.67		45.76	8.61
Apical Efflux with MK-571	32.89		31.71		32.30	0.83
Total Efflux	68.08		56.76		62.42	8.00
Cells Only	31.92	0.88	43.24	0.98	37.58	8.00
	27.40	1.34	27.97	2.74	27.68	0.40
Cells + Bile	83.77	3.50	82.91	4.07	83.34	0.61
	60.29	4.59	59.68	1.05	59.98	0.43

^{99m}Tc-MIBI efflux in Sandwich-Culture Rat Hepatocytes

	5/20/2008		6/23/2008		8/4/2008		8/15/2008		Mean	SD
	Mean	**SD**	**Mean**	**SD**	**Mean**	**SD**	**Mean**	**SD**		
Basolateral & Apical Efflux	51.84	1.92	69.03	2.41	66.77	1.55	68.45	0.87	64.02	8.18
Basolateral & Apical Efflux with 20μM GF918	25.23	1.38	30.62	0.64	44.98	2.84	34.18	1.50	33.75	8.34
Basolateral Efflux	30.76	0.82	47.22	3.35	38.14	2.18	45.70	1.33	40.46	7.59
Basolateral Efflux with 20μM GF918	12.44	0.28	16.79	0.81	21.38	0.22	21.01	2.48	17.91	4.20
Apical Efflux	21.08		21.81		28.63		22.74		23.57	3.45
Apical Efflux with 20μM GF918	12.80		13.83		23.61		13.17		15.85	5.19
Total Efflux	51.84		69.03		66.77		68.45		64.02	8.18
	40.36	4.53	30.97	2.41	33.23	1.55	31.55	0.87	34.03	4.33
Cells Only	68.24	0.40	69.38	0.64	55.02	2.84	65.82	1.50	64.61	6.57
Cells + Bile	64.48	1.58	52.78	3.35	61.86	2.18	54.30	1.33	58.35	5.69
	85.17	0.41	83.21	0.81	78.62	0.22	78.99	2.48	81.50	3.22

^{99m}Tc-MIBI efflux in Sandwich-Culture TR^{-} Rat Hepatocytes

	6/30/2008		9/22/2008		9/29/2008		Mean	SD
	Mean	**SD**	**Mean**	**SD**	**Mean**	**SD**		
Basolateral & Apical Efflux	76.59	1.80	67.64	1.76	66.78	0.56	70.34	5.43
Basolateral & Apical Efflux with 20μM GF918	39.61	2.44	43.93	1.88	39.70	0.68	41.08	2.47
Basolateral Efflux	47.27	1.61	37.45	1.49	33.45	4.70	39.39	7.11
Basolateral Efflux with 20μM GF918	25.54	0.25	23.50	0.90	20.07	3.51	23.03	2.76
Apical Efflux	29.32		30.19		33.33		30.95	2.11
Apical Efflux with 20μM GF918	14.08		20.43		19.63		18.05	3.46
Total Efflux								
	23.41	1.80	32.36	1.76	33.22	0.56	29.66	5.43
Cells Only	60.39	2.44	56.07	1.88	60.30	0.68	58.92	2.47
	52.73	1.61	62.55	1.49	66.55	4.70	60.61	7.11
Cells + Bile	74.46	0.25	76.50	0.90	79.93	3.51	76.97	2.76

^{99m}Tc-MIBI efflux in Sandwich-Culture Human Hepatocytes

	8/28/2008		8/31/2008			
	Mean	**SD**	**Mean**	**SD**	**Mean**	**Range**
Basolateral & Apical Efflux	88.07	1.18	90.64	1.06	89.35	1.82
Basolateral & Apical Efflux with 20µM GF918	42.32	2.78	26.67	0.96	34.49	11.06
Basolateral Efflux	66.99	3.12	61.02	5.75	64.00	4.23
Basolateral Efflux with 20µM GF918	24.64	4.85	19.88	6.75	22.26	3.36
Apical Efflux	21.08		29.63		25.35	6.05
Apical Efflux with 20µM GF918	17.68		6.79		12.24	7.70
Total Efflux	88.07		90.64		89.35	1.82
	11.93	1.18	9.36	1.06	10.65	1.82
Cells Only	57.68	2.78	73.33	0.96	65.51	11.06
Cells + Bile	33.01	3.12	38.98	5.75	36.00	4.23
	75.36	4.85	80.12	6.75	77.74	3.36

^{99m}Tc-MIBI accumulation in Sandwich-Culture Rat Hepatocytes using RNAi

	WT 12-11-08				
	0.5µCi/mL	0.5µCi/mL + siNT	0.5µCi/mL + siNT+ 2 µM GF918	0.5µCi/mL + siBcrp	0.5µCi/mL + siBcrp+ 2 µM GF918
Accumulation Cells + Bile	2.82	3.55	6.29	3.41	4.78
SD	0.04	0.44	0.57	0.25	0.38
Accumulation Cells	1.94	2.31	6.40	2.47	5.13
SD	0.12	0.11	0.32	0.19	0.86
BEI	31.29	35.03	-1.89	27.59	-7.41

	WT 06-08-09				
	0.5µCi/mL	0.5µCi/mL + siNT	0.5µCi/mL + siNT + 2 µM GF918	0.5µCi/mL + siBcrp	0.5µCi/mL + siBcrp + 2 µM GF918
Accumulation Cells + Bile	1.99	1.90	2.69	1.93	2.64
SD	0.04	0.06	0.37	0.15	0.16
Accumulation Cells	1.56	1.5	3.2	1.39	3.1
SD	0.14	0.1	0.1	0.09	0.2
BEI	22.02	20.88	-18.82	27.90	-17.74

	WT 07-09-09				
	0.5µCi/mL	0.5µCi/mL + siNT	0.5µCi/mL + siNT + 2 µM GF918	0.5µCi/mL + siBcrp	0.5µCi/mL + siBcrp + 2 µM GF918
Accumulation Cells + Bile	2.84	2.74	3.75	2.70	3.83
SD	0.05	0.22	0.23	0.09	0.52
Accumulation Cells	2.21	1.97	4.4	2.1	4.6
SD	0.20	0.13	0.2	0.1	0.1
BEI	22.02	27.90	-17.74	20.88	-18.82

Chapter 5:

[^{14}C]Sorafenib uptake in Human Hepatocytes

		5/27/2009				7/15/2009			
		pmol taken up		pmol/mg		pmol taken up		pmol/mg	
		Mean	SD	Mean	SD	Mean	SD	Mean	SD
	0.5	6.185	1.902	52.142	14.706	5.134	0.996	36.784	5.542
	1.5	9.056	2.251	76.983	19.852	9.375	1.411	67.725	11.456
Ctrl	2.5	10.405	1.477	88.303	13.125	11.193	0.679	80.576	2.120
Rifamycin SV	0.5	5.876	1.450	48.901	12.059	4.309	3.833	30.962	28.577
	1.5	5.144	1.834	42.076	14.164	6.561	0.030	44.036	0.357
	2.5	6.540	3.360	53.936	26.264	6.420	1.046	44.322	7.327
	0.5	4.267	3.920	33.133	29.430	4.856	1.006	33.721	5.948
	1.5	9.690	0.379	74.781	6.725	9.205	0.984	64.090	5.035
Ketoprofen	2.5	6.929	2.586	52.801	17.345	11.407	0.719	79.509	3.371
	0.5	6.478	0.202	56.443	12.575	4.294	1.145	27.892	5.979
	1.5	5.784	0.447	52.427	18.503	7.550	1.421	49.887	12.004
Decynium 22	2.5	7.299	1.167	64.645	22.330	9.250	1.175	60.194	12.355
	0.5	5.875	2.736	63.597	26.126	4.799	0.696	46.202	8.791
	1.5	9.358	2.615	101.068	18.067	7.519	1.326	71.599	8.506
Choline Buffer	2.5	10.031	1.036	109.700	2.239	8.805	2.179	83.663	16.094
	0.5	3.177	0.395	23.169	1.659	2.558	2.212	18.163	16.184
	1.5	4.124	0.039	30.257	2.566	3.579	0.940	25.324	7.469
4°C	2.5	8.049	4.009	56.341	16.749	3.401	0.121	24.519	15.278

[^{14}C]Sorafenib uptake in CHO cells on 7-31-09 (data not graphed in dissertation)

	MOCK		MOCK (4C)		hOCT1		5mM MPP		5uM Decynium 22	
0.5	21.90	2.91	9.30	2.34	49.22	4.43	48.31	3.13	30.28	3.13
1	31.53	1.73	20.03	2.92	70.49	7.83	78.62	5.49	54.35	8.86
2	57.47	3.59	38.81	10.90	117.23	9.22	136.51	16.73	60.21	52.26
5	120.68	27.57	63.17	6.84	209.60	22.60	262.21	21.80	172.27	12.73
10	149.85	14.18	87.34	10.89	331.63	18.39	349.20	32.59	227.16	7.55
20	163.19	29.31	133.69	9.75	404.45	58.63	426.67	20.09	309.38	11.93
30	241.80	35.06	210.44	40.64	424.68	16.40	438.61	29.24	364.79	45.57

[^{14}C]Sorafenib uptake in CHO cells on 8-04-09

Time	**Mock**		**Mock + D22**		**OCT**		**OCT + D22**	
0.5	42.50062	7.226721	48.45512	3.086695	58.60809	4.697704	44.97996	4.589214
1	56.86105	3.977197	61.22597	0.222685	84.5143	10.43798	62.09995	3.583897
2	117.3075	9.950514	118.7676	4.392815	150.0874	31.3572	99.31056	5.502464
5	144.6614	13.60159	162.9711	5.404094	292.415	33.28804	197.7324	10.87009
10	229.0946	21.12277	247.0291	25.79778	385.2181	22.47608	287.7248	20.62574
20	271.3955	16.00803	273.2648	38.92738	488.141	37.779	345.8728	12.58161
30	319.4655	26.42162	343.8191	52.70886	529.1106	40.20235	398.7762	23.78705

Chapter 6:

^{99m}Tc-MEB in HCC+CPB Subject #01

Dose (µCi)	4818
Time (min)	**Blood (nCi/mL)**
2.5	486.80
5	no sample
7.5	548.61
10	405.09
20	311.83
40	182.43
60	170.59
80	122.31
100	104.84
120	105.70
140	90.13
165	76.66
180	74.87
Time (min)	**Urine (µCi)**
180	196.25

Time (min)	Activity (uCi)	Time (min)	Activity (uCi)	Time (min)	Activity (uCi)	Time (min)	Activity (uCi)	Time (min)	Activity (uCi)	Time (min)	Activity (uCi)	Time (min)	Activity (uCi)
2.0	548.2	30.0	1314.5	58.0	1114.6	86.0	1028.5	114.0	907.4	142.0	772.9	170.0	645.6
3.0	616.7	31.0	1342.3	59.0	1104.2	87.0	1003.3	115.0	841.1	143.0	759.3	171.0	642.0
4.0	686.8	32.0	1348.3	60.0	1090.5	88.0	992.6	116.0	837.7	144.0	762.0	172.0	620.5
5.0	756.1	33.0	1347.2	61.0	1073.5	89.0	989.3	117.0	817.2	145.0	769.1	173.0	612.2
6.0	812.1	34.0	1330.8	62.0	1077.7	90.0	986.8	118.0	841.5	146.0	698.8	174.0	589.4
7.0	873.0	35.0	1337.2	63.0	1078.1	91.0	966.0	119.0	843.2	147.0	715.5	175.0	629.3
8.0	932.3	36.0	1303.5	64.0	1059.7	92.0	939.1	120.0	852.5	148.0	709.0	176.0	613.4
9.0	977.4	37.0	1321.0	65.0	1087.0	93.0	928.9	121.0	824.9	149.0	722.1	177.0	614.0
10.0	1034.4	38.0	1293.1	66.0	1057.2	94.0	966.4	122.0	831.1	150.0	723.1	178.0	653.6
11.0	1080.0	39.0	1290.9	67.0	1063.9	95.0	939.3	123.0	803.2	151.0	730.8	179.0	626.4
12.0	1114.0	40.0	1270.5	68.0	1043.6	96.0	960.7	124.0	816.4	152.0	710.3	180.0	615.6
13.0	1153.1	41.0	1276.6	69.0	1076.5	97.0	943.6	125.0	820.5	153.0	717.6		
14.0	1185.8	42.0	1242.6	70.0	1108.2	98.0	942.4	126.0	845.3	154.0	698.6		
15.0	1228.3	43.0	1242.7	71.0	1108.1	99.0	934.7	127.0	812.3	155.0	708.5		
16.0	1265.8	44.0	1230.3	72.0	1111.6	100.0	951.3	128.0	787.7	156.0	634.8		
17.0	1289.4	45.0	1225.1	73.0	1119.2	101.0	924.6	129.0	786.7	157.0	654.1		
18.0	1307.3	46.0	1224.5	74.0	1099.4	102.0	886.8	130.0	785.8	158.0	624.0		
19.0	1325.5	47.0	1200.7	75.0	1093.4	103.0	869.3	131.0	789.0	159.0	641.9		
20.0	1355.9	48.0	1191.5	76.0	1087.9	104.0	915.4	132.0	833.0	160.0	683.3		
21.0	1366.5	49.0	1194.1	77.0	1132.3	105.0	918.4	133.0	819.2	161.0	695.2		
22.0	1372.8	50.0	1190.3	78.0	1143.5	106.0	930.3	134.0	811.2	162.0	697.6		
23.0	1376.2	51.0	1203.0	79.0	1123.4	107.0	917.9	135.0	803.8	163.0	705.7		
24.0	1356.8	52.0	1173.0	80.0	1102.9	108.0	916.3	136.0	832.0	164.0	704.3		
25.0	1362.6	53.0	1171.2	81.0	1055.8	109.0	922.3	137.0	827.2	165.0	693.3		
26.0	1340.1	54.0	1158.3	82.0	1020.8	110.0	915.9	138.0	774.5	166.0	684.2		
27.0	1342.6	55.0	1154.1	83.0	1052.3	111.0	883.7	139.0	777.6	167.0	689.1		
28.0	1323.4	56.0	1153.1	84.0	1022.7	112.0	939.9	140.0	787.9	168.0	698.2		
29.0	1317.2	57.0	1134.3	85.0	1021.0	113.0	928.9	141.0	783.7	169.0	677.2		

^{99m}Tc-MIBI in HCC+CPB Subject #01

Dose (µCi)	3860
Time (min)	**Blood (nCi/mL)**
1	0.94
2.5	2.36
5	4.72
7.5	7.08
10	9.43
20	18.87
40	37.74
80	75.47
100	no sample
120	113.21
140	no sample
165	no sample
180	169.81
Time (min)	**Urine (µCi)**
180	241.5

Time (min)	Activity (uCi)	Time (min)	Activity (uCi)	Time (min)	Activity (uCi)	Time (min)	Activity (uCi)	Time (min)	Activity (uCi)	Time (min)	Activity (uCi)	Time (min)	Activity (uCi)
2	652	30	715	58	587	86	525	114	472	142	526	170	443
3	712	31	720	59	567	87	537	115	516	143	527	171	431
4	760	32	680	60	572	88	538	116	465	144	489	172	428
5	760	33	680	61	572	89	514	117	505	145	512	173	488
6	793	34	674	62	551	90	534	118	491	146	529	174	456
7	805	35	658	63	568	91	526	119	464	147	535	175	483
8	792	36	661	64	622	92	518	120	512	148	476	176	455
9	798	37	676	65	533	93	547	121	544	149	535	177	412
10	826	38	651	66	539	94	543	122	478	150	495	178	483
11	795	39	674	67	571	95	518	123	505	151	456	179	429
12	828	40	655	68	543	96	536	124	517	152	505	180	492
13	806	41	630	69	591	97	538	125	500	153	505		
14	796	42	654	70	560	98	521	126	514	154	478		
15	829	43	646	71	556	99	530	127	524	155	528		
16	812	44	621	72	594	100	529	128	509	156	459		
17	771	45	622	73	549	101	524	129	500	157	481		
18	795	46	630	74	552	102	534	130	517	158	380		
19	791	47	598	75	566	103	537	131	506	159	454		
20	750	48	617	76	550	104	515	132	484	160	463		
21	772	49	609	77	545	105	532	133	497	161	437		
22	759	50	580	78	553	106	531	134	493	162	465		
23	747	51	615	79	555	107	516	135	488	163	432		
24	750	52	622	80	533	108	532	136	499	164	359		
25	754	53	591	81	554	109	433	137	457	165	339		
26	711	54	604	82	556	110	448	138	508	166	422		
27	725	55	597	83	539	111	499	139	487	167	351		
28	728	56	600	84	543	112	527	140	487	168	404		
29	694	57	596	85	539	113	512	141	475	169	393		